

**KERNFORSCHUNGSZENTRUM  
KARLSRUHE**

Mai 1975

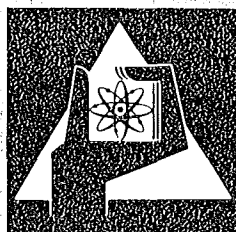
KFK 2046  
NEACRP-U-61  
NEANDC-U-98

Institut für Neutronenphysik und Reaktortechnik

**Neutron Capture in the keV Energy Range in  
Structural Materials for Fast Reactors**

Proceedings of a NEACRP/NEANDC Specialist Meeting,  
held in May 1973 at the Kernforschungszentrum Karlsruhe

B. Schatz, H. Küsters



**GESELLSCHAFT  
FÜR  
KERNFORSCHUNG M.B.H.  
KARLSRUHE**

Als Manuskript vervielfältigt

Für diesen Bericht behalten wir uns alle Rechte vor

GESELLSCHAFT FÜR KERNFORSCHUNG M. B. H.  
KARLSRUHE

KERNFORSCHUNGSZENTRUM KARLSRUHE

KFK 2046  
NEACRP-U-61  
NEANDC-U-98

Institut für Neutronenphysik und Reaktortechnik

Neutron Capture in the keV Energy Range in  
Structural Materials for Fast Reactors

Proceedings of a NEACRP/NEANDC  
Specialist Meeting, held in May 1973  
at the Kernforschungszentrum Karlsruhe

Edited by

B. Schatz and H. Küsters

Gesellschaft für Kernforschung mbH., Karlsruhe



## Summary

This report contains the contributions which were submitted to the NEACRP/NEANDC Specialist Meeting on neutron capture in structural materials for the energy range between about 1keV and 1MeV. The first chapter deals with experimental techniques and recent differential measurements for neutron capture cross sections of Cr, Fe, and Ni. One of the problems, which are not readily understood, is the proper detection of scattered neutrons, which may lead to discrepancies in experimental data of different groups by about 40 to 50 percent. The second chapter is devoted to recent evaluations for Fe and Ni, and it also discusses the differences of the recommended data in the nuclear Data files ENDF/B, UKNDL and KEDAK.

The user aspects are given in chapter 3. The required accuracy for the neutron capture cross section of stainless steel in the keV range is given to be  $\pm 10\%$ , mainly based on the target accuracy for the breeding gain of large LMFBR systems. The influence of neutron capture data uncertainties on physics quantities in zero power reactors is discussed. Data adjustment procedures seem to indicate that differential measurements on Fe, Ni and Cr are not fully consistent with results from integral experiments in critical facilities. Further work, especially on Fe-neutron capture data and testing, is required.

## Neutroneneinfang im keV-Bereich für Strukturmaterialien

### Schneller Reaktoren

#### Zusammenfassung

In diesem Bericht sind die schriftlichen Beiträge zu einem Spezialisten Treffen der NEACRP und NEANDC über Neutroneneinfangdaten in keV-Bereich für Strukturmaterialien schneller Reaktoren zusammengestellt.

Das erste Kapitel behandelt experimentelle Methoden und neuere Ergebnisse von Messungen der Einfangwirkungsquerschnitte für Cr, Fe und Ni.

Die existierenden Diskrepanzen zwischen verschiedenen Meßgruppen von bis zu 50 % können zum Teil dadurch verursacht sein, daß man eine genaue experimentelle Erfassung gestreuter Neutronen bisher nur unzureichend beherrscht.

In Kapitel 2 werden neue Auswertungen von Neutroneneinfangdaten für Fe und Ni vorgestellt. Außerdem sind die auf den Kerndatenbändern ENDF/B, UKNDL und KEDAK empfohlenen Daten miteinander verglichen.

Kapitel 3 beschreibt die Gesichtspunkte des Benutzers bei der Berechnung schneller Reaktoren. Für Edelstahl wird eine Genauigkeit der Einfangdaten von  $\pm 10$  % gefordert, welche hauptsächlich auf der erwarteten Genauigkeit für den Brutgewinn großer Reaktoren beruht. Weiterhin wird der Einfluß von Unsicherheiten der Einfangdaten auf physikalische Kenngrößen von Nulleistungsreaktoren diskutiert. Aus Anpassung der Daten an integrale Experimente scheint zu folgen, daß die differentiellen Meßergebnisse für Fe, Ni und Cr noch nicht genügend sicher sind. Weitere Untersuchungen, besonders hinsichtlich der Fe-Einfangdaten, sind erforderlich.

## Preface

These proceedings are issued very late. There are various serious reasons for this delay. Because the matter itself has not lost its actuality, I hope that in spite of the late issue this report will be, also in the near future, a helpful document for experimenters, evaluators, and users of neutron capture data in structural materials.

The meeting was attended by about 20 people out of three areas: differential measurements, evaluation, and reactor physics aspects. This combination I feel was a very effective one because most of all the relevant views thus could be given to the audience. After a "polite" discussion period at the beginning of the meeting, the interest to achieve at certain conclusions grew more and more, and in consequence very vivid discussions resulted. It was expressed by various participants that the meeting was fruitful because many impulses were given and at least some conclusions and recommendations could be drawn.

*A. Küsters*

## Contents

I. EXPERIMENTAL DATA	Page
F.H. Fröhner: Resonance capture measurements on structural materials with large liquid scintillators	1
C. Le Rigoleur, A. Arnaud: Fast neutron capture cross section facility at Cadarache	33
C. Le Rigoleur, A. Arnaud, J. Taste: Absolute capture cross section measurements on Au, Cr, Fe, Ni between 70 keV to 550 keV	51
R.L.Macklin: Neutron capture in Reactor structural materials. This report was distributed, but not presented at the meeting. Both papers were presented by C. Le Rigoleur	63
M. C. Moxon, D.B. Gayther and M.G. Sowerby: Some problems in capture cross section measurements. This paper was presented by M.C. Moxon	73
R.R. Spencer, H. Beer: Capture cross section measurements on reactor structural materials with a large liquid scintillator technique. The paper was presented by R.R. Spencer.	79
F.H. Fröhner: Conclusion	93

---

Zum Druck eingereicht am: 16.5.1975

	Page
II. EVALUATED DATA	98
T. Martinelli, E. Menapace, M. Motta and G.C. Panini: A comparison between single level and multilevel calculations of neutron cross sections in the resonance region. The paper was presented by M. Motta	99
M.C. Moxon: An evaluation of the neutron cross sections of natural nickel and its stable isotopes below 600 keV	156
S. Pearlstein: Thermal cross sections and resonance para- meters recommended in the new BNL 325, Vol.I, for Cr, Fe, Ni. The paper was distributed, but not presented at the meeting	190
B. Schatz: Comparison of the keV-capture cross sections for Cr, Fe, Ni on ENDF/B, UKNDL and KEDAK.	222
P. Ribon: Conclusion	251
III. USER ASPECTS	257
J.Y. Barré: Importance of the capture cross sections of structural materials for fast reactors	258
H. Häggblom: On the influence of the capture cross section of iron on the integral properties of some fast reactor critical assemblies.	276
M. Heindler: The reliability of calculated reactivity coefficients of structural materials; the sensitivity of Ni, Fe, Cr material worths to uncertainties in the cross section data	288

	Page
H. Takano, Y. Ishiguro: Comparison of effective capture cross sections and Doppler-Coefficients for structural materials calculated by three evaluated nuclear data files. The paper was presented by E. Kiefhaber, Kernforschungszentrum Karlsruhe.	317
H. Penkuhn: Sensitivity calculations in an iron shield with capture cross sections changed in the keV range	343
J.L. Rowlands: Capture cross sections of structural materials of importance in fast reactors. The paper was presented by J.S. Story.	349
H. Küsters: Conclusion	357
IV. APPENDIX	360
List of participants	361

TOPIC I

EXPERIMENTAL DATA

RESONANCE CAPTURE MEASUREMENTS ON STRUCTURAL  
MATERIALS WITH LARGE LIQUID SCINTILLATORS\*

F.H. Fröhner\*\*  
(NEA Centre de Compilation de Données  
Neutroniques, Saclay, France)

Abstract: The present status of neutron capture cross section data for structural materials is reviewed as far as they were measured with large liquid scintillator detectors until about 1972, mainly at RPI and KFK. New results from the analysis of KFK data on  $^{56}\text{Fe}$ ,  $^{58}\text{Ni}$ ,  $^{60}\text{Ni}$  and  $^{61}\text{Ni}$  for neutron energies between 7 and 220 keV are presented, in particular radiation widths and capture areas and also results on the correlation between neutron and radiation widths. Special attention is paid to the estimation of uncertainties.

---

\*) Paper presented at the Specialists' Panel on Capture Cross Sections of Structural Materials, Karlsruhe, 8-9.5.73, revised version.

\*\*) On leave from Kernforschungszentrum Karlsruhe, Germany.

## 1. Introduction

Neutron capture cross sections for the structural materials - Cr, Fe and Ni - are urgently needed in the keV neutron energy region for fast breeder core design. Nickel also plays a role as neutron reflector material for fast critical assemblies. Moreover, these capture cross sections are of considerable interest to astrophysicists: especially the nickel and iron isotopes play a key role in nucleosynthesis calculations based on the concept of the s (slow) process of element formation in stars whose temperatures correspond to about the same neutron energies as those encountered in fast breeders. A continuing effort is therefore under way in many laboratories to measure these cross sections. The present paper is restricted to a discussion of those measurements which were made with large liquid scintillator detectors. Much of the discussion will be devoted to the work with which the author is particularly familiar, namely that done at Karlsruhe until about 1972. More recent KFK results will be presented by R.R. Spencer et al.

Resonance capture measurements practically always employ the time-of-flight method, with detection of the prompt  $\gamma$  radiation emitted after each neutron capture event. For a given flight-time interval with flux  $\phi$  the observed count rate (corrected for dead-time and background) is given by

$$c = \phi y \epsilon \quad (1)$$

where  $y$  is the so-called capture yield, i.e. the probability that an incoming neutron is captured, and  $\epsilon$  is the efficiency of the  $\gamma$ -ray detector (plus associated electronics). The data reduction consists of stripping off  $\phi$  and  $\epsilon$  to get  $y$  and then to extract from  $y$  the capture cross section  $\sigma_\gamma$ .

The reduction of resonance capture data to capture cross sections is never easy, but the task is especially difficult for the structural materials due to

- the extreme smallness of the capture cross section relative to the scattering cross section: ratios of 1:100 or 1:1000 in the resonances are typical;
- the high neutron binding energies of the compound nuclei which imply inconveniently high capture  $\gamma$ -ray energies;

- the low-level densities and correspondingly low effective multiplicities of the capture  $\gamma$ -ray cascades.

The following sections deal with the resulting difficulties in a more general way.

## 2. Flux determination

The problem of neutron flux determination is usually by-passed by measuring the capture yield relative to a reference sample. One exposes the sample under study and the reference sample to the same flux and determines the ratio

$$\frac{c}{c_r} = \frac{y}{y_r} \frac{\epsilon}{\epsilon_r} \quad (2)$$

which does not contain the flux  $\phi$  but only the known yield  $y_r$  and the efficiency ratio  $\epsilon/\epsilon_r$ . The KFK results presented below were obtained with gold as reference material. Its capture cross section is known to about 5% near 30 keV (Refs. 1, 2, 3) and to about 8-10% near the lower and upper limits of the energy range considered here, 5-220 keV (Ref. 4).

It should be pointed out, however, that the recently reported structure near 23 keV in the total and capture cross section of gold (Ref. 5) casts some doubt on the absolute capture cross section values derived under the assumption of smooth average cross section behaviour from shell transmissions measured at 22.8 keV (Refs. 2, 6). Since the shell transmission method is only one of various methods used to normalize the capture cross section of gold, and not a very accurate method at that, no drastic change in the overall status of the gold capture cross section is to be expected. Nevertheless, the question cannot be considered as settled before the influence of the reported structure on the calibration point at 30 keV is studied in detail.

Another method to measure the flux is the "black resonance" technique: with a neutron detector of known energy dependence, e.g. a  $^{10}\text{B}$  slab viewed by NaI crystals, one determines the shape of the flux. The absolute value is obtained by replacing the capture sample with a sample having a suitable low-energy resonance, e.g. silver. This calibration sample is taken so thick that it appears black to neutrons with energies near the peak of the resonance.

At this energy the count rate is then given by Eq. (1) with  $\Gamma_\gamma/\Gamma < y < 1$ , the lower limit corresponding to the first-collision or primary yield, the upper limit to the case of negligible leakage of scattered neutrons out of the sample. If  $\Gamma_n \ll \Gamma$ , then  $\Gamma_\gamma/\Gamma \approx 1$  and  $y$  is known to good accuracy. This method is suitable for neutron sources with a spectrum going all the way down to the low eV region, such as linac sources. The RPI results discussed below were obtained with this method - the flux shape was determined with a B slab detector, the absolute calibration being based on the 5.19 eV resonance of silver. The accuracy of this method is probably as good as 2 percent near the calibration point, becoming worse with growing energy. Above 100 keV where the  $^{10}\text{B}(n,\alpha)$  cross section begins to deviate from a  $1/v$  behaviour the flux uncertainty is probably more like 5-10%.

### 3. Detector efficiency

The principal problem in capture detector design is the need for a detector which is insensitive to variations of the capture  $\gamma$ -ray spectrum with neutron energy. The probabilities for the many possible  $\gamma$ -ray cascade modes leading from the compound state to the ground state fluctuate violently from resonance to resonance. This is a consequence not only of the changing spins and parities but especially of the fact that the partial radiation widths for transitions to the various intermediate states are distributed according to Porter-Thomas distributions. Only the sum of all photon energies is the same for all cascades at a given neutron energy :

$$\sum_{i=1}^{\hat{i}} E_i = \sum_{j=1}^{\hat{j}} E_j = \dots = U \quad (3)$$

( $E_{\gamma i}$ ,  $E_{\gamma j}$ : photon energies,  $\hat{i}$ ,  $\hat{j}$ : cascade multiplicities,  $U$ : excitation energy).

The conceptionally simplest way to achieve insensitivity to the particular cascade modes is to build a detector capable of responding with 100% efficiency to each single photon in the capture spectrum. In order that this be true even for the ground state transition it is obvious that the detector must surround the sample in  $4\pi$  geometry and have a thickness such that the escape probability for the ground state transition photon is negligible. This is the principle of the large liquid scintillator detector.

Another possibility is to build a detector with an efficiency proportional to the photon energy,  $\epsilon = C \cdot E_{\gamma i}$ , and to make sure that only one photon per capture event interacts with the detector, e.g. by choosing the solid angle subtended by the detector as seen from the sample and its thickness sufficiently small. The probability for detection of either the 1st, or the 2nd, ... or the  $i$ -th photon of a cascade with multiplicity  $i$  is then

$$\epsilon = C(E_{\gamma 1} + E_{\gamma 2} + \dots + E_{\gamma i}) = CU. \quad (4)$$

This result is independent of the assumed cascade, i.e. the detector has the desired property. This is the principle of the Moxon-Rae detector. Proportionality is achieved by proper design. The same principle underlies the total-energy detector (sometimes called Maier-Leibnitz detector), where proportionality is achieved by appropriate weighting of the counts in the various pulse-height channels. Measurements with these two types of detector will be treated in other contributions to this meeting. The following discussion will therefore be restricted to experiments with large liquid scintillators.

### 3.1 Intrinsic efficiency

The ideal intrinsic efficiency (interaction probability) of 100% for even the most energetic photons is never reached in practice with large liquid scintillators. The size of the detector is usually limited by economic considerations and, even more important, by the background from cosmic rays and from natural radiation originating in the structure and the environment. This background is directly proportional to the detector volume. One is thus forced to compromise. Even the largest tanks in use today, the 4000 l modular device built by Haddad et al. at General Atomic (Ref. 7) or the 3500 l tank being tested by Fuketa at JAERI, still leave about 20% escape probability for 8 MeV photons. This is to be compared with the ground state transition energies of about 7-11 MeV of the structural materials. For the tanks employed in capture work on these nuclides, those at RPI (1100 l) and at Karlsruhe (800 l), the escape probability for 8 MeV photons is even higher - about 35%. Fig. 1 shows the intrinsic efficiency of the Karlsruhe detector as a function of total cascade energy, for ground state transitions (single photons) and for cascades consisting of two and three equal photons. The intrinsic efficiency is seen to approach unity fairly rapidly with increasing multiplicity.

For the reference material, gold, the level density and thus the average multiplicity is high (Ref. 8). Moreover, the instrumental resolution of the experiments reviewed here was such that only averages over many gold resonances are observed in each flight-time channel so that fluctuations are smeared out. This conclusion was confirmed experimentally by Kompe, who did not find any significant differences between the observed pulse height spectra taken at 50 and 150 keV neutron energy. Thus the intrinsic efficiency can be estimated easily as  $\epsilon_1^{\text{Au}} = (99 \pm 1)\%$ .

For the structural materials, on the other hand, the level density and thus the average multiplicity is low, and ground state transitions account for a large percentage of the compound state decays. Jackson and Strait (Ref. 9) derived from  $(\gamma, n)$  data partial radiation widths for the ground state transitions following neutron capture in  $^{52}\text{Cr}$ ,  $^{56}\text{Fe}$  and  $^{60}\text{Ni}$ . Comparison with the total radiation widths for the same compound states shows that for the s-wave compound levels up to about 25% of the decays can proceed directly to the ground state. For p-wave levels the ground state transitions are even stronger, accounting for no less than 50% of all decays for some levels (cf. Tables 2 and 4). Strong variations of the  $\gamma$ -ray spectrum and hence of the total radiation width must therefore be expected from level to level, and this is in fact what one finds.

At Karlsruhe the detector signals are usually stored in a two-dimensional array with 4096 time channels and 8 pulse-height channels. Fig. 2 shows examples of pulse-height spectra obtained for a number of  $^{56}\text{Fe}$  resonances. It is evident that the  $\gamma$ -ray spectra vary strongly, the sharply peaked ones indicating strong transitions to the ground (and other low-lying) states, the flat ones indicating higher multiplicity with fewer high-energy transitions.

These fluctuations clearly create a severe problem with respect to the intrinsic efficiency. One can use the curves of Fig. 1 and some plausible assumptions as to the cascade modes to calculate the intrinsic efficiencies for the various binding energies encountered. The resulting crude estimates of  $\epsilon_i/\epsilon_1^{\text{Au}}$  are shown in Table I for three assumed cases; (1) strong high-energy transitions, (2) a presumably more typical spectrum with moderately strong high-energy transitions, and (3) negligible high-energy transitions. The dispersion of the intrinsic-efficiency ratios is of the order of 10 percent.

If information on the pulse-height distribution for individual resonances is available the ratios of Table I can be used to correct the data. For example, the pulse-height distributions of Fig. 2 were divided into three categories - peaked, flat and intermediate - and the corresponding efficiency ratios from Table I were then applied to the data. This admittedly crude procedure is assumed to reduce the yield uncertainty caused by fluctuations of the intrinsic efficiency to about 5%.

### 3.2 Spectrum fraction

In order to reduce the cosmic-ray background one operates large liquid scintillator detectors with an electronic threshold just above the pulse height equivalent to the binding energy of the compound nucleus. A lower threshold is usually set at a pulse height corresponding to about 3 MeV so as to eliminate the 2.2 MeV  $\gamma$ -rays from neutron capture by the protons in the scintillator. Suppression of signals produced by neutrons which are scattered by the sample into the scintillator is extremely important for the structural materials where the scattering cross section is often 100 or 1000 times the capture cross section. The measures taken (liners containing  $^{10}\text{B}$  or  $^6\text{Li}$  between sample and scintillator, admixture of methyl borate to the scintillator) aim at having scattered neutrons absorbed by  $^{10}\text{B}$ , which emits only low-energy  $\gamma$ -rays, or by  $^6\text{Li}$ , which emits none at all. In this way one can achieve a detection efficiency for capture of scattered neutrons of only  $10^{-5}$  (Ref. 12). Nevertheless, a certain number of hydrogen capture signals must be eliminated by an appropriate lower threshold.

Fig. 2 shows the capture spectrum for gold as measured with the Karlsruhe 800 l detector. It is obvious that rejecting all pulses with pulse heights equivalent to less than 3 MeV one loses an appreciable fraction of all signals. This means that a corresponding correction must be applied to the observed part of the pulse-height spectrum, the so-called spectrum fraction  $\epsilon_D$ . The overall efficiency of the recording system is thus the product of spectrum fraction and intrinsic efficiency,  $\epsilon_i \epsilon_D$ .

For big tanks with carefully matched photomultipliers and good light collection properties the pulse-height distribution shows a more or less pronounced sum peak near the binding energy, and the resulting extrapolation to zero pulse height is possible with quite good accuracy. For the gold spectrum of Fig. 3 the result with the lower threshold at 3 MeV was  $\epsilon_D^{\text{Au}} = (64 \pm 3)\%$ . For the structural materials the uncertainties in  $\epsilon_D$  were somewhat larger - of the order of 8%. This yields an uncertainty of about

10% for the ratio  $\epsilon_b/\epsilon_b^{Au}$ , and of about 15% for the overall efficiency ratio  $(\epsilon_b \epsilon_i)/(\epsilon_b^{Au} \epsilon_i^{Au})$ .

#### 4. Scattered neutrons

In order to correct for the residual background from scattered neutrons which was observed in spite of the above-mentioned preventive measures, purely scattering samples (graphite) with about the same scattering properties as the sample under study and the gold reference sample were used at KFK to obtain the count rates  $c_s$  and  $c_s^{Au}$ . The capture yield was then calculated as

$$y = \frac{c - c_s}{c^{Au} - c_s^{Au}} \frac{\epsilon_i^{Au}}{\epsilon_i} \frac{\epsilon_b^{Au}}{\epsilon_b} y^{Au} \quad (5)$$

It is true that although the average scattering properties of capture sample and carbon scatterer were matched, the scattering is smooth for carbon and has resonance behaviour for the capture sample. However, the time required for scattered neutrons to be captured (e.g. 200 ns for 100 keV neutrons travelling 30 cm) is so much longer than the corresponding time for a photon (e.g. 2 ns for 60 cm) that practically all correlation with the resonances is destroyed and the resonance structure smeared out sufficiently. The fact that between resonances the corrected capture yield actually goes to zero confirms that the method works reasonably well. The uncertainty associated with the scattering corrections is estimated to be of the order of 1-3% at the lower energies where gaps between resonances allow a check on the background subtraction, and up to maybe 20% at higher energies where no such gaps are observed because of resonance overlap and resolution broadening.

#### 5. Data analysis

After correcting the data for scattered neutrons and estimating spectrum fraction and intrinsic efficiency ratios from the pulse height distributions one has to calculate  $y^{Au}$ . Because of the relatively large capture cross section of gold it is easy to use gold samples which are so thin in terms of neutron mean free paths that self-shielding and multiple-scattering effects are small, so that

$$y^{Au} = n^{Au} \sigma_{\gamma}^{Au}, \quad (n^{Au} \sigma_T^{Au} \ll 1) \quad (6)$$

where  $n^{Au}$  is the sample thickness (in nuclei/b) and  $\sigma_{\gamma}^{Au}$  is the gold capture cross section averaged over resonances. The sample thickness corrections for the 1 mm reference sample used at KFK were very small (a few percent): the associated uncertainty is estimated as 2%.

After this last step all the quantities on the right-hand side of Eq. (5) are known and  $y$  can be calculated. The next problem is the extraction of the capture cross section from the yield. For "thin" samples this is no problem (cf. Eq. (6)). For the sample thicknesses used at RPI and KFK, however, serious self-shielding and multiple scattering effects are encountered near and above the resonance energies, especially for the broad s-wave resonances. Correction for these effects depends on a fairly good knowledge of the scattering cross section, preferably in parametrized form. One difficulty is that for most of the resonances seen in the capture data no resonance parameters are known and that very often energy resolution and accuracy of the energy scale for existing transmission data is not quite good enough to correlate small resonances seen in transmission with one of the many capture peaks in a unique way. The strategy adopted at RPI and at KFK was therefore to determine the total as well as the capture cross section, if possible in the same experiment.

Resonance energies  $E_0$ , total widths  $\Gamma$  and - for odd isotopes - spin factors  $g$  are found from the transmission data with the help of area analysis or, more recently, of automatic shape-fitting codes. This works well for most s-wave levels and for the broadest p-wave levels. These parameters can then be used to find the radiation widths  $\Gamma_\gamma$  from the capture data by an area analysis programme. Narrow levels, however, are normally seen only in the capture data. The quantities which can then be extracted are the resonance energy  $E_0$  and the combination  $g\Gamma_n\Gamma_\gamma/\Gamma$  (if sample thickness effects are small, which is usually the case for narrow levels).

The assignment of parities is easy for broad levels with clearly identifiable interference dips in the total cross section for s-wave levels, and symmetric shapes for p-wave levels. Doppler broadening is of no importance for these broad peaks. For neutron widths smaller than the Doppler width (about 3 eV at 10 keV, 10 eV at 100 keV) or of the resolution width s- and p-wave resonance shapes become indistinguishable, and parity assignments are difficult in the absence of additional information such as the asymmetry values derivable from photoneutron experiments (Ref. 9).

Finally, after complete parametrization one can reconstruct the capture cross section, describing the levels with known  $E_0, \Gamma_n, \Gamma_\gamma, J^\pi$  by the same (R-matrix) formulae as used in the analysis, and the levels with known  $E_0$  and  $g\Gamma_n\Gamma_\gamma/\Gamma$  as  $2\pi^2\lambda_0^2(g\Gamma_n\Gamma_\gamma/\Gamma)\psi(x, \beta)$ , where  $2\pi\lambda_0$  is the neutron wave length corresponding to  $E_0$  and  $\psi(x, \beta)$  is the usual Doppler line shape function for  $x \equiv 2(E-E_0)/\Gamma$ ,  $\beta = 2\Delta/\Gamma \equiv (4/\Gamma)(E_0kT/A)^{1/2}$ .

It is difficult to assess the errors due to the resonance analysis method. The computer code for capture area analysis used at Karlsruhe (Ref. 10) describes all cross sections as sums of single-level Breit-Wigner terms. This is an adequate representation for the capture cross section where level-level interference effects for the many capture channels mutually cancel in good approximation. For the scattering cross section, which influences the multiple-scattering corrections, level-level interference is quite strong for the nuclides considered here and the single-level sum representation may lead to errors for the broad s-wave resonances. Apparently a version of the same code was used at RPI (Ref. 11). An uncertainty of 15% is tentatively assigned to the analysis procedure, but only a systematic investigation with a multi-level code can clarify this point.

If all sources of uncertainties are considered, including the statistical errors, it is found that the uncertainty of the capture yield is of the order 10-20%, which gives an error of about 15-25% for the radiation widths and  $g_n \Gamma_\gamma / \Gamma$  values.

#### 6. Resonance capture data from tank experiments

Resonance parameters including those determining the capture cross section ( $\Gamma_\gamma$  or  $g_n \Gamma_\gamma / \Gamma$ ) are listed in Tables 2, 3, 4 and 5 for the  $\gamma$  target nuclei  $^{56}\text{Fe}$ ,  $^{58}\text{Ni}$ ,  $^{60}\text{Ni}$  and  $^{61}\text{Ni}$ . They were taken from the published work of Hockenbury et al. (Ref. 12) and Stieglitz et al. (Ref. 13) at the RPI linac and from work of Rohr et al. (Ref. 14), Cho et al. (Ref. 15), Ernst et al. (Ref. 16) and Fröhner and Ernst (Ref. 17) at the KFK 3 MV Van de Graaff accelerator. For  $^{56}\text{Fe}$  and  $^{60}\text{Ni}$  the spin and parity quantum numbers and ground state transition area parameters  $g_n \Gamma_{\gamma 0} / \Gamma$  published by Jackson and Strait (Ref. 9) are included in the tables to give a feeling for the importance of the ground state transitions.

The data of Hockenbury et al. cover essentially the low keV energies up to about 30 keV. With the exception of the radiation width for the first strong s-wave resonance of  $^{56}\text{Fe}$  at 27.9 keV no radiation widths are given, but many capture area parameters ( $g_n \Gamma_\gamma / \Gamma$ ) for weak (presumably p-wave) levels. The paper by Stieglitz et al. reflects an improvement in instrumentation and data analysis. Many s-wave radiation widths are reported in addition to capture area parameters for weak levels up to about 160 keV. The KFK capture yield data cover the energy region from 7 keV up to about 220 keV; resonance parameters are given for essentially all resolved levels up to about the same energies as covered by Stieglitz et al.

The quality of the data is about the same for both laboratories, although the error estimates of the KFK group are somewhat more conservative. The overall agreement is remarkably good in view of the differences in experimental technique, data analysis and especially absolute calibration. In the majority of the cases where both groups report a value the discrepancy is smaller than the combined error. Nevertheless, for  $^{60}\text{Ni}$  where the RPI data are more complete than for the other isotopes listed, one can see that at about 50 keV the RPI capture area parameters begin to become systematically higher than the KFK values. This may be due to errors in the flux extrapolation by means of the  $^{10}\text{B}(n,\alpha)$  cross section to energies 10,000 times higher than the calibration energy (5.19 eV) at RPI, and/or to errors in the determination of the shape of the gold cross section at KFK.

Block et al. (Ref. 18) reported a significant positive correlation between neutron and radiation widths calculated from a composite sample of 27 s-wave levels belonging to  $^{50}\text{Cr}$ ,  $^{52}\text{Cr}$ ,  $^{53}\text{Cr}$ ,  $^{54}\text{Cr}$ , V and  $^{60}\text{Ni}$ . A similar calculation was performed for all the fully-parametrized s-wave levels of the isotopes included in the present paper, but without lumping the isotopes together. The results are given in Table 6. It will be seen that with the small sample sizes used the uncertainties of the correlation coefficients are large. The only significant value is that for  $^{60}\text{Ni}$ , obtained for a sample of nine resonances. Correlations between neutron widths and radiation widths do not seem to be a universal phenomenon for the structural materials, but the problem certainly needs further study when more radiation widths become available.

## 7. Conclusion

The good agreement between capture resonance parameters obtained by the groups at RPI and KFK using large liquid scintillator detectors is remarkable, especially in view of the different flux determination techniques employed. It is probably safe to state that at the present time the capture cross sections and capture resonance integrals can be calculated from these parameters with an accuracy of about 15-25% below about 100-150 keV for  $^{56}\text{Fe}$ ,  $^{58}\text{Ni}$  and  $^{60}\text{Ni}$ , and to about 50 keV for  $^{61}\text{Ni}$ . Above these energies the KFK yield data (available on request from the neutron data compilation centres) are practically unaffected by multiple scattering and self-shielding and represent the resolution-broadened cross section directly with about the same accuracy. Significant correlations between neutron and radiation widths were not found with the exception of  $^{60}\text{Ni+n}$ , where a correlation coefficient of  $0.8 \pm 0.3$  was calculated from a sample of nine s-wave resonances.

The most troublesome error sources are (1) the uncertainty of 5-10% of the gold reference cross section used at KFK and the probably somewhat smaller extrapolation uncertainty associated with the assumed  $1/v$  shape of the  $^{10}\text{B}(n,\alpha\gamma)$  cross section used at RPI; (2) the 10-15% uncertainty of intrinsic efficiencies and spectrum fractions caused by fluctuations of the  $\gamma$ -ray spectra; (3) uncertainties due to the resonance parameter determination methods; (4) background caused by scattered neutrons in the high-energy region where no gaps between resonances allow a check on the background subtraction.

As to point (1) adoption of the value of 649 mb at 30 keV recommended by Vaughn and Grench (Ref. 3) instead of 603 mb as used at KFK would raise the capture yields, radiation widths and capture area parameters reported by KFK by about 7.5%. In this context the influence of the gold cross section anomaly at 23 keV (Ref. 5) on shell transmission results used in the derivation of the 30 keV reference value should be investigated. The  $^{10}\text{B}(n,\alpha\gamma)$  cross section shape plays an analogous role for the RPI data.

Point (2) underlines the need for the acquisition of adequate pulse height data together with the time-of-flight data in tank experiments so that spectrum fluctuations can be corrected for. Measurements with other detector types that are insensitive to spectrum fluctuations, such as Moxon-Rae and total-energy detectors, will be extremely valuable in checking the fluctuation correction procedures used for tank data.

As to point (3) it should be investigated whether replacement of the single-level-sum description of the scattering cross section by a more correct multi-level description would increase the multiple-scattering corrections for broad s-wave levels. If so this could perhaps explain some of the observed correlations between neutron and radiation widths.

References

1. W.P. Pönitz et al., J. Nucl. Energy 22 (1968) 505
2. F.H. Fröhner, Proc. 2nd Int. Conf. on Nuclear Data for Reactors, Helsinki, 1970, vol. I, p. 197
3. V.J. Vaughn and H.A. Grench, Proc. 3rd Conf. on Neutron Cross Sections and Technology, Knoxville, 1971, vol. I, p. 430
4. D. Kompe, Nucl. Phys. A133 (1969) 513
5. E. Schneider, Karlsruhe Report KFK-1519 (1972)
6. T.T. Semler, J. Nucl. Energy 27 (1973) 185
7. E. Haddad et al., Nucl. Instr. Meth. 31 (1964) 125
8. J.E. Draper and T.E. Springer, Nucl. Phys. 16 (1960) 27
9. H.E. Jackson and E.N. Strait, Phys. Rev. C4 (1971) 1314
10. F.H. Fröhner, Report GA-6906 (1966)
11. N. Yamamuro, JAERI, private communication
12. R.W. Hockenbury et al., Phys. Rev. 178 (1969) 1746
13. R.G. Stieglitz et al., Nucl. Phys. A163 (1971) 592
14. G. Rohr et al., Proc. 1st Int. Conf. on Nuclear Data for Reactors, Paris, 1966, vol. I, p. 137
15. M. Cho et al., Proc. 2nd Int. Conf. on Nuclear Data for Reactors, Helsinki, 1970, vol. I, p. 619
16. A. Ernst et al., Proc. 2nd Int. Conf. on Nuclear Data for Reactors, Helsinki, 1970, vol. I, p. 633
17. F.H. Fröhner and A. Ernst, to be published
18. R.C. Block et al., Proc. 3rd Int. Conf. on Neutron Cross Sections and Technology, Knoxville, 1971, vol. II, p. 889
19. J.R. Stehn et al., BNL 325, 2nd Ed., Suppl. No. 2, (1964)

TABLE 1

Binding Energies and Crude Estimates of Intrinsic Efficiency Ratios for 800 l Detector

Reaction	Binding Energy (MeV)	$\epsilon_i/\epsilon_i^{\text{Au}}$ Estimated for contributions from high-energy transitions of		
		50%	10%	0%
$^{56}\text{Fe}+n$	7.646	0.81	0.91	0.98
$^{58}\text{Ni}+n$	8.999	0.79	0.90	0.97
$^{60}\text{Ni}+n$	7.819	0.81	0.91	0.98
$^{61}\text{Ni}+n$	10.596	0.77	0.89	0.95
$^{197}\text{Au}+n$	6.512	1	1	1

TABLE 2

Resonance Parameters for  $^{56}\text{Fe} + n$

Note: Brackets ( ) denote tentative or doubtful values, square brackets [ ] denote values and references from other labs.

$E_0$ (keV)	$g\Gamma_n$ (eV)	$\Gamma_\gamma$ (eV)	$g\Gamma_\gamma\Gamma_n/\Gamma$ (eV)	$g\Gamma_{\gamma 0}\Gamma_n/\Gamma$ (eV)	J	$\Pi$	Lab	Ref.
1.15		[0.6]	.08				RPI	12
2.35			.0004				RPI	12
11.2			.043 $\pm$ .007				RPI	12
22.7			.191 $\pm$ .020				RPI	12
22.79 $\pm$ .07			.16 $\pm$ .03		1/2	(-)	KFK	17
27.7		1.44 $\pm$ .14			1/2	+	RPI	12
27.68 $\pm$ .08	[1600 $\pm$ 10]	1.4 $\pm$ .2			1/2	+	KFK	16,[19]
34.1			.59 $\pm$ .07				RPI	12
34.25 $\pm$ .10			.62 $\pm$ .08	[.18 $\pm$ .04]		(-)	KFK	17,[9]
36.6			.30 $\pm$ .03				RPI	12
36.69 $\pm$ .11			.28 $\pm$ .04			(-)	KFK	17
38.3			.46 $\pm$ .05				RPI	12
38.38 $\pm$ .12			.34 $\pm$ .05			(-)	KFK	17
45.8			.32 $\pm$ .04				RPI	12
46.04 $\pm$ .14			.44 $\pm$ .06			(-)	KFK	17
51.9			.41 $\pm$ .05				RPI	12
52.20 $\pm$ .16			.58 $\pm$ .09			(-)	KFK	17

(Table 2,  $^{56}\text{Fe}+n$  cont.)

$E_0$ (keV)	$g\Gamma_n$ (eV)	$\Gamma_\gamma$ (eV)	$g\Gamma_\gamma\Gamma_n/\Gamma$ (eV)	$g\Gamma_\gamma\Gamma_n/\Gamma$ (eV)	J	$\Pi$	Lab	Ref.
53.3			.54±.06				RPI	12
53.60±.16			.48±.07			(-)	KFK	17
55.0			.14±.04				RPI	12
(55.3±.2)			(.08±.05)			(-)	KFK	17
59.0			.54±.06				RPI	12
59.25±.18			.72±.10	[.22±.04][1/2]	(-)		KFK	17,[9]
63.1							RPI	12
63.45±.19			.61±.09			(-)	KFK	17
72.6							RPI	12
(72.5 ±.5)						(-)	KFK	17
74.6							RPI	12
73.9 ±.5	539±42			[.08±.02]	1/2	+	KFK	14,[9]
76.7							RPI	12
76.9 ±.5	4.3±.3					(-)	KFK	17
80.4							RPI	12
80.8 ±.3	9±2		1.8±.3			(-)	KFK	17
83.6 ±.3	912±85	.9±.3			1/2	+	KFK	14,16
90.0							RPI	12
90.2 ±.3	70±15	1.2±.2			(1/2)	(+)	KFK	17
92.1							RPI	12
92.6 ±.3	3±1		1.6±.3			(-)	KFK	17

(Table 2,  $^{56}\text{Fe}+n$  cont.)

$E_0$ (keV)	$g\Gamma_n$ (eV)	$\Gamma_\gamma$ (eV)	$g\Gamma_\gamma\Gamma_n/\Gamma$ (eV)	$g\Gamma_{\gamma 0}\Gamma_n/\Gamma$ (eV)	J	$\Pi$	Lab	Ref.
95.9							RPI	12
96.1 ± .3	25 ± 4		2.2 ± .4			(-)	KFK	17
102							RPI	12
102.4 ± .3	35 ± 6		1.6 ± .3	[.04 ± .01]		(-)	KFK	17, [9]
105							RPI	12
105.8 ± .3	<2		1.4 ± .3			(-)	KFK	17
112							RPI	12
112.6 ± .3			1.1 ± .3			(-)	KFK	17
122.5 ± .4	65 ± 10	2.7 ± .6	2.6 ± .6	[.12 ± .02]	1/2	+	KFK	17, [9]
124							RPI	12
124.5 ± .4	13 ± 5					(+)	KFK	17
129							RPI	12
129.8 ± .4	380 ± 50			[.11 ± .02]	1/2	+	KFK	14, 17, [9]
140.3 ± .5	2460 ± 110			[.07 ± .02]	1/2	+	KFK	14, 17, [9]
151 ± 1						(-)	KFK	17
153 ± 1						(-)	KFK	17
163 ± 1						(-)	KFK	17
169 ± 1	870 ± 70			[.07 ± .02]	1/2	+	KFK	14, [9]
179.4 ± 1.2						(-)	KFK	17
180.7 ± 1.2						(-)	KFK	17

(Table 2,  $^{56}\text{Fe}+n$  cont.)

$E_0$ (keV)	$g\Gamma_n$ (eV)	$\Gamma_\gamma$ (eV)	$g\Gamma_\gamma\Gamma_n/\Gamma$ (eV)	$g\Gamma_{\gamma 0}\Gamma_n/\Gamma$ (eV)	J	$\pi$	Lab	Ref.
188 * 1	3430*270			[.42*.08]	1/2	+	KFK 14,	[9]
195.1*1.0	50*12					(-)	KFK 17	
201.1*1.0	71*18					(-)	KFK 17	
210 * 1	20*5					(-)	KFK 17	
220 * 1	1470*85			[.68*.13]	1/2	+	KFK 14,	[9]
225 * 1	200*50			[.13*.03]	1/2	(-)	KFK 17,	[9]
234 * 1	160*40			[.36*.07][3/2]		(-)	KFK 17,	[9]
245 * 1	630*40			[.38*.07]	1/2	+	KFK 14,	[9]
253 * 2				[.05*.01]		(-)	KFK 17,	[9]

TABLE 3

Resonance Parameters for  $^{58}\text{Ni}+n$

Note: Brackets ( ) denote tentative or doubtful values, square brackets [ ] denote values and references from other labs.

$E_0$ (keV)	$\Gamma_n$ (eV)	$\Gamma_\gamma$ (eV)	$g\Gamma_\gamma\Gamma_n/\Gamma$ (eV)	J	$\pi$	Lab	Ref.
6.89			.022±.002			RPI	12
12.6						RPI	12
13.3			.32±.03			RPI	12
13.34±.03			.49±.10		(-)	KFK	17
13.6			.52±.05			RPI	12
13.66±.04			.63±.12		(-)	KFK	17
14-16						RPI	12
15.4 ±.1	1200±150	2.1±.7		1/2	+	KFK	17
(16.5)						RPI	12
(17.2)						RPI	12
19.0			.063±.010			RPI	12
19.03±.05			.080±.020		(-)	KFK	17
20.0			.20±.02			RPI	12
20.04±.15			.24±.05		(-)	KFK	17
21.1			.56±.06			RPI	12
21.16±.05			.57±.11		(-)	KFK	17
26.08±.07			.25±.05		(-)	KFK	17

(Table 3,  $^{58}\text{Ni}+n$  cont.)

$E_0$ (keV)	$\Gamma_n$ (eV)	$\Gamma_\gamma$ (eV)	$g\Gamma_\gamma \Gamma_n / \Gamma$ (eV)	J	$\pi$	Lab	Ref.
26.6			.70±.07			RPI	12
26.67±.07			.73±.14	(1/2)	(+)	KFK	17
32.4			1.44±.15			RPI	12
32.36±.08			1.26±.25	(1/2)	(+)	KFK	17
34.2			.65±.08			RPI	12
34.24±.08			.69±.14		(-)	KFK	17
36.1			.86±.10			RPI	12
36.12±.09			1.01±.20	1/2	+	KFK	17
39.5						RPI	12
39.59±.10			.66±.13		(-)	KFK	17
47.9			1.58±.18			RPI	12
47.80±.15			.98±.20	(1/2)	(+)	KFK	17
52.1						RPI	12
52.00±.15			1.46±.30	(1/2)	(+)	KFK	17
54.8			.32±.10			RPI	12
54.70±.15			.28±.06		(-)	KFK	17
58.60±.15			.52±.10		(-)	KFK	17
60.1						RPI	12
60.10±.15			.44±.09		(-)	KFK	17
61.8						RPI	12
61.75±.15			.71±.14		(-)	KFK	17
63.0 ±.2	[3600±180]	3.2±.8		1/2	*	KFK	17,[19]
66.4						RPI	12
66.40±.15			.36±.07		(-)	KFK	17

(Table 3,  $^{58}\text{Ni}+n$  cont.)

$E_0$ (keV)	$\Gamma_n$ (eV)	$\Gamma_\gamma$ (eV)	$g\Gamma_\gamma\Gamma_n/\Gamma$ (eV)	J	$\Pi$	Lab	Ref.
68.75 $\pm$ .20			.24 $\pm$ .05		(-)	KFK	17
69.80 $\pm$ .20			.46 $\pm$ .09		(-)	KFK	17
78						RPI	12
77.95 $\pm$ .20			.12 $\pm$ .03		(-)	KFK	17
81.3						RPI	12
81.10 $\pm$ .20			.73 $\pm$ .15		(-)	KFK	17
83.0						RPI	12
83.10 $\pm$ .20	110 $\pm$ 40	3.5 $\pm$ .7		1/2	+	KFK	17
89.84			.45 $\pm$ .09		(-)	KFK	17
92.25 $\pm$ .20			.17 $\pm$ .04		(-)	KFK	17
94.45 $\pm$ .25			.9 $\pm$ .2		(-)	KFK	17
97.00 $\pm$ .25			.5 $\pm$ .1		(-)	KFK	17
101.10 $\pm$ .25			1.0 $\pm$ .4		(-)	KFK	17
105.3 $\pm$ .3			1.8 $\pm$ .4		(-)	KFK	17
107.7 $\pm$ .5	1500 $\pm$ 300	3.5 $\pm$ .8		1/2	+	KFK	17
110.7 $\pm$ .3			1.3 $\pm$ .3		(-)	KFK	17
117.5 $\pm$ .3			.8 $\pm$ .3		(-)	KFK	17
120.3 $\pm$ .3			3.3 $\pm$ .6	(1/2)	(+)	KFK	17
125.0 $\pm$ .5	750 $\pm$ 250	3.2 $\pm$ .6		1/2	+	KFK	17

TABLE 4

Resonance Parameters for  $^{60}\text{Ni}+n$

Note: Brackets ( ) denote tentative or doubtful values, square brackets [ ] denote values and references from other labs.

$E_0$ (keV)	$\Gamma_n$ (eV)	$\Gamma_\gamma$ (eV)	$g\Gamma_\gamma \Gamma_n / \Gamma$ (eV)	$g\Gamma_{\gamma 0} \Gamma_n / \Gamma$ (eV)	J	$\pi$	Lab	Ref.
1.292±.004			.0003±.0001			(-)	RPI	13
2.257±.009			.068±.011			(-)	RPI	13
5.53±.02			.056±.009			(-)	RPI	13
12.20±.04			.042±.007			(-)	RPI	13
12.23±.03			.09 ±.03			(-)	KFK	17
12.47±.06	2660±100	3.30±.30				1/2	+	RPI 13
12.5 ±.1	[2600±130]	3.4 ±.4		[.37±.07]	1/2	+	KFK	16,[19],[9]
13.60±.05			.090±.013			(-)	RPI	13
13.62±.03			.14 ±.03	[.04±.01]	1/2	(-)	KFK	17,[9]
23.8 ±.1			.92±.14			(-)	RPI	13
23.88±.06			.60±.12	[.02±.01]	[3/2]	(-)	KFK	17,[9]
28.47±.07			.08±.04			(-)	KFK	17
28.64±.10	800±50	1.1±.1				1/2	+	RPI 13
28.60±.10	[800±200]	1.2±.3				1/2	+	KFK 16,[19]
29.47±.08			.09±.03			(-)	KFK	17
30.1 ±.12			.32±.05			(-)	RPI	13
30.24±.08			.31±.06			(-)	KFK	17

(Table 4,  $^{60}\text{Ni}+n$  cont.)

$E_0$ (keV)	$\Gamma_n$ (eV)	$\Gamma_\gamma$ (eV)	$g\Gamma_\gamma\Gamma_n/\Gamma$ (eV)	$g\Gamma_{\gamma 0}\Gamma_n/\Gamma$ (eV)	J	$\Pi$	Lab	Ref.
32.90 $\pm$ .13			.351 $\pm$ .055			(-)	RPI	13
33.03 $\pm$ .08			.33 $\pm$ .07	[.02 $\pm$ .01]	[3/2]	(-)	KFK	17,[9]
33.30 $\pm$ .13			.19 $\pm$ .03			(-)	RPI	13
33.40 $\pm$ .08			.20 $\pm$ .05			(-)	KFK	17
39.40 $\pm$ .15			.57 $\pm$ .10			(-)	RPI	13
39.54 $\pm$ .10			.41 $\pm$ .08			(-)	KFK	17
43.08 $\pm$ .23	77 $\pm$ 15	1.73 $\pm$ .18				1/2	+	RPI 13
42.93 $\pm$ .11	120 $\pm$ 30	1.0 $\pm$ .2		[.02 $\pm$ .01]	1/2	+	KFK	17,[9]
47.40 $\pm$ .22			.86 $\pm$ .13			(-)	RPI	13
47.60 $\pm$ .12	(10)	1.0 $\pm$ .4	.78 $\pm$ .16	[.17 $\pm$ .03]	1/2	(+)	KFK	17,[9]
49.6 $\pm$ .25			.26 $\pm$ .04			(-)	RPI	13
49.8 $\pm$ .12			.27 $\pm$ .05			(-)	KFK	17
50.8 $\pm$ .26						(-)	RPI	13
50.99 $\pm$ .15			.11 $\pm$ .02			(-)	KFK	17
51.5 $\pm$ .26			.46 $\pm$ .08			(-)	RPI	13
51.64 $\pm$ .15			.38 $\pm$ .08	[.03 $\pm$ .01]	[3/2]	(-)	KFK	17,[9]
56.3 $\pm$ .28			.37 $\pm$ .06			(-)	RPI	13
56.00 $\pm$ .15			.15 $\pm$ .04			(-)	KFK	17
56.9 $\pm$ .29			.43 $\pm$ .07			(-)	RPI	13
56.74 $\pm$ .15			.45 $\pm$ .10			(-)	KFK	17
65.13 $\pm$ .40	390 $\pm$ 30	2.43 $\pm$ .25				1/2	+	RPI 13
65.42 $\pm$ .16	600 $\pm$ 150	2.2 $\pm$ .3				1/2	+	KFK 16,17
71.3 $\pm$ .45			.40 $\pm$ .07			(-)	RPI	13
71.51 $\pm$ .18			.33 $\pm$ .07			(-)	KFK	17

(Table 4,  $^{60}\text{Ni}+n$  cont.)

$E_0$ (keV)	$\Gamma_n$ (eV)	$\Gamma_\gamma$ (eV)	$g\Gamma_\gamma\Gamma_n/\Gamma$ (eV)	$g\Gamma_{\gamma 0}\Gamma_n/\Gamma$ (eV)	J	$\pi$	Lab	Ref.
71.3 ±.45			.40±.07			(-)	RPI	13
71.51±.18			.33±.07			(-)	KFK	17
73.2 ±.50			.61±.10			(-)	RPI	13
73.25±.18			.44±.09			(-)	KFK	17
78.2 ±.55			.31±.05			(-)	RPI	13
78.26±.20			.19±.04			(-)	KFK	17
79.9 ±.58			.45±.07			(-)	RPI	13
79.98±.20			.33±.07			(-)	KFK	17
81.95±.20			.22±.05			(-)	KFK	17
84.7 ±.59						(-)	RPI	13
84.94±.20			.41±.08	[.09±.02][3/2]		(-)	KFK	17,[9]
86.8 ±.6	330±25				1/2	+	RPI	13
86.33±.22	[300±45]	1.4±.3			1/2	+	KFK	17,[9]
87.6 ±.61						(-)	RPI	13
87.89±.22			.64±.13			(-)	KFK	17
89.93±.25			.17±.04			(-)	KFK	17
91.60±.25			.25±.05			(-)	KFK	17
93.3 ±.65						(-)	RPI	13
93.94±.25			.48±.10			(-)	KFK	17
98.1 ±.7	870±70				1/2	+	RPI	13
97.2 ±.3	]070±200	1.0±.2		[.10±.02]	1/2	+	KFK	17,[9]
99.24±.25			.92±.20			(-)	KFK	17

(table 4.  $^{60}\text{Ni}+n$  cont.)

$E_0$ (keV)	$\Gamma_n$ (eV)	$\Gamma_\gamma$ (eV)	$g\Gamma_\gamma\Gamma_n/\Gamma$ (eV)	$g\Gamma_{\gamma 0}\Gamma_n/\Gamma$ (eV)	J	$\pi$	Lab	Ref.
101.9 $\pm$ .3			0.10 $\pm$ .05			(-)	KFK	17
107.8 $\pm$ .75	610 $\pm$ 60				1/2	+	RPI	13
108.0 $\pm$ .25	700 $\pm$ 100	1.1 $\pm$ .3		[.21 $\pm$ .04]	1/2	+	KFK	17,[9]
111.3 $\pm$ 1.0			3.74 $\pm$ .80			(-)	RPI	13
111.6 $\pm$ .3			2.7 $\pm$ .6	[.42 $\pm$ .08]	[1/2]	(-)	KFK	17,[9]
123.8 $\pm$ 1.2						(-)	RPI	13
123.6 $\pm$ .3			.7 $\pm$ .2			(-)	KFK	17
129.7 $\pm$ 1.3						(-)	RPI	13
129.2 $\pm$ .3			1.0 $\pm$ .3			(-)	KFK	17
136.5 $\pm$ 1.4			4.3 $\pm$ .9			(-)	RPI	13
136.8 $\pm$ .5			3.1 $\pm$ .6			(-)	KFK	17
139.6 $\pm$ 1.4			4.0 $\pm$ .9			(-)	RPI	13
139.9 $\pm$ .6			3.0 $\pm$ .6			(-)	KFK	17
148.4 $\pm$ .4			1.2 $\pm$ .3			(-)	KFK	17
156.4 $\pm$ 1.2	440 $\pm$ 50				1/2	+	RPI	13
155.4 $\pm$ .4	[440 $\pm$ 50]	.8 $\pm$ .3			1/2	+	KFK	17,[13]
162.1 $\pm$ 1.3	1250 $\pm$ 130				1/2	+	RPI	13
161.7 $\pm$ .4	1400 $\pm$ 200	1.8 $\pm$ .5			1/2	+	KFK	17
167.0 $\pm$ .4			3.0 $\pm$ .8			(-)	KFK	17
173.7 $\pm$ .4			1.9 $\pm$ .5			(-)	KFK	17

TABLE 5

Resonance Parameters for  $^{61}\text{Ni}+n$

Note: Brackets ( ) denote tentative or doubtful values, square brackets [ ] denote values and references from other labs.

$E_0$ (keV)	$\Gamma_n$ (eV)	$\Gamma_\gamma$ (eV)	$g\Gamma_\gamma\Gamma_n/\Gamma$ (eV)	J	$\pi$	Lab	Ref.
1.354			.24±.03			RPI	12
2.35						RPI	12
3.14			.084±.018			RPI	12
3.3			.48±.06			RPI	12
6.47			.35±.10			RPI	12
7.12			.78±.12			RPI	12
7.152±.020	74±8	2.5±.5	.91±.15	1	-	KFK	15,16,17
7.53						RPI	12
7.545±.020	177±16	2.3±.6		2	-	KFK	15,16,17
8.71			.65±.13			RPI	12
8.745±.020	6±2	2.6±.8	1.13±.45	2	-	KFK	15,16
9.90						RPI	12
9.93 ±.02			.09±.03		(+)	KFK	17
10.2						RPI	12
10.18 ±.03			.19±.05		(+)	KFK	17
12.6						RPI	12
12.64 ±.03	75±4	1.7±.4		2	-	KFK	15,16,17

(Table 5,  $^{61}\text{Ni}+n$  cont.)

$E_0$ (keV)	$\Gamma_n$ (eV)	$\Gamma_\gamma$ (eV)	$g_\gamma \Gamma_n / \Gamma$ (eV)	J	$\pi$	Lab	Ref.
13.43 $\pm$ .03			.31 $\pm$ .08		(+)	KFK	17
13.63 $\pm$ .03	61 $\pm$ 4	1.6 $\pm$ .4		2	-	KFK	15,16
14.0 14.02 $\pm$ .03	17 $\pm$ 4	3.1 $\pm$ .5		1	-	RPI KFK	12 15,16
14.3 14.45 $\pm$ .04			.30 $\pm$ .08		(+)	RPI KFK	12 17
15.3 15.38 $\pm$ .04			.17 $\pm$ .04		(+)	RPI KFK	12 17
16.7 16.70 $\pm$ .05	817 $\pm$ 16	2.2 $\pm$ .4		1	-	RPI KFK	12 15,16
16.80 $\pm$ .05			.14 $\pm$ .04		(+)	KFK	17
17.8 17.86 $\pm$ .05	177 $\pm$ 8	1.6 $\pm$ .5		1	-	RPI KFK	12 15,16
19.0 18.87 $\pm$ .05	69 $\pm$ 4	.9 $\pm$ .3		2	-	RPI KFK	12 15,16
20.4 20.25 $\pm$ .05			.09 $\pm$ .03		(+)	RPI KFK	12 17
20.55 $\pm$ .05			.11 $\pm$ .03		(+)	KFK	17
21.40 $\pm$ .05			.88 $\pm$ .20		(+)	KFK	17
24.12 $\pm$ .05			.36 $\pm$ .09		(+)	KFK	17
24.8 24.62 $\pm$ .06	129 $\pm$ 10	1.4 $\pm$ .3	4.0 $\pm$ 1.3 .53 $\pm$ .10	1	-	RPI KFK	12 15,16

(Table 5,  $^{61}\text{Ni}+n$  cont.)

$E_0$ (keV)	$\Gamma_n$ (eV)	$\Gamma_\gamma$ (eV)	$g\Gamma_\gamma\Gamma_n/\Gamma$ (eV)	J	$\pi$	Lab	Ref.
25.12 $\pm$ .06			.25 $\pm$ .06		(+)	KFK	17
25.96 $\pm$ .06			.24 $\pm$ .06		(+)	KFK	17
26.45 $\pm$ .06			.18 $\pm$ .05		(+)	KFK	17
27.10 $\pm$ .07			.20 $\pm$ .05		(+)	KFK	17
27.6			1.74 $\pm$ .10			RPI	12
27.65 $\pm$ .07			.40 $\pm$ .10		(+)	KFK	17
28.21 $\pm$ .07	5 $\pm$ 4	3.0 $\pm$ 1.0		2	-	KFK	15,16
29.0						RPI	12
29.11 $\pm$ .07	409 $\pm$ 22	2.4 $\pm$ .4		1	-	KFK	15,16
30.8						RPI	12
30.64 $\pm$ .08	15 $\pm$ 8			2	-	KFK	15
31.13 $\pm$ .08	788 $\pm$ 28			1	-	KFK	15
31.7						RPI	12
31.83 $\pm$ .08	10 $\pm$ 6			2	-	KFK	15
32.70 $\pm$ .08	220 $\pm$ 10			2	-	KFK	15
33.8						RPI	12
33.68 $\pm$ .08	58 $\pm$ 10	2.8 $\pm$ .5		1	-	KFK	15,16
34.65 $\pm$ .10					(+)	KFK	17
36.02 $\pm$ .10					(+)	KFK	17
37.3						RPI	12
37.13 $\pm$ .09	133 $\pm$ 12	3.0 $\pm$ .5		2	-	KFK	15,16

TABLE 6

Correlations between Reduced Neutron Widths and Radiation Widths for s-wave Resonances:

Isotope	J	$\frac{\text{cov}[r_n^0, r_\gamma]}{\sqrt{\text{var}[r_n^0] \cdot \text{var}[r_\gamma]}}$	Sample size
<sup>56</sup> Fe+n	1/2	-0.32±0.47	4
<sup>58</sup> Ni+n	1/2	-0.46±1.04	5
<sup>60</sup> Ni+n	1/2	0.80±0.28	9
<sup>61</sup> Ni+n	1	-0.18±0.43	7
"	2	-0.09±0.46	7

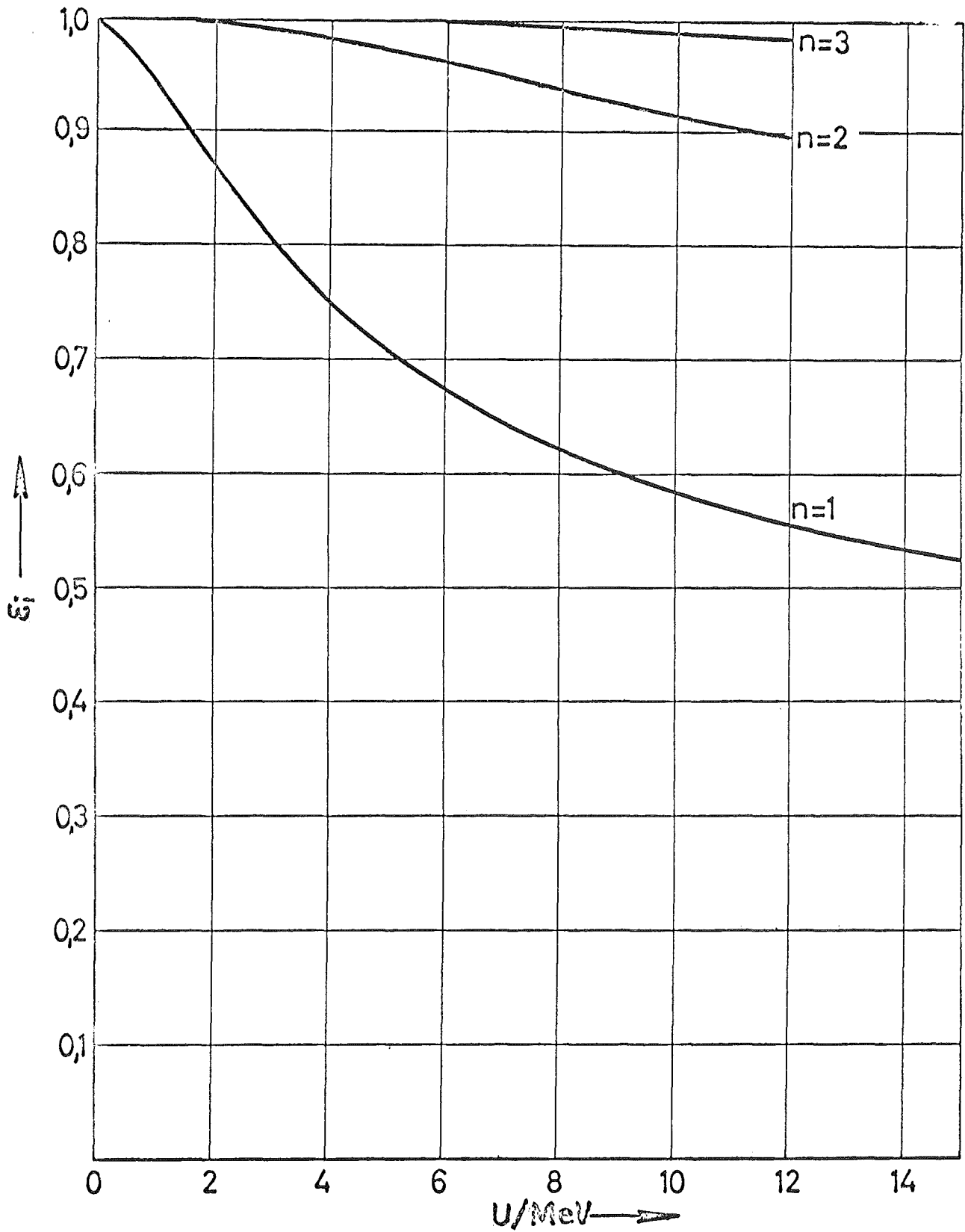


Fig. 1 - Intrinsic efficiency, i. e. probability of at least 1 interaction for photon cascades with total energy  $U$  and multiplicity  $n$ , calculated for the Karlsruhe 800 l scintillator tank.

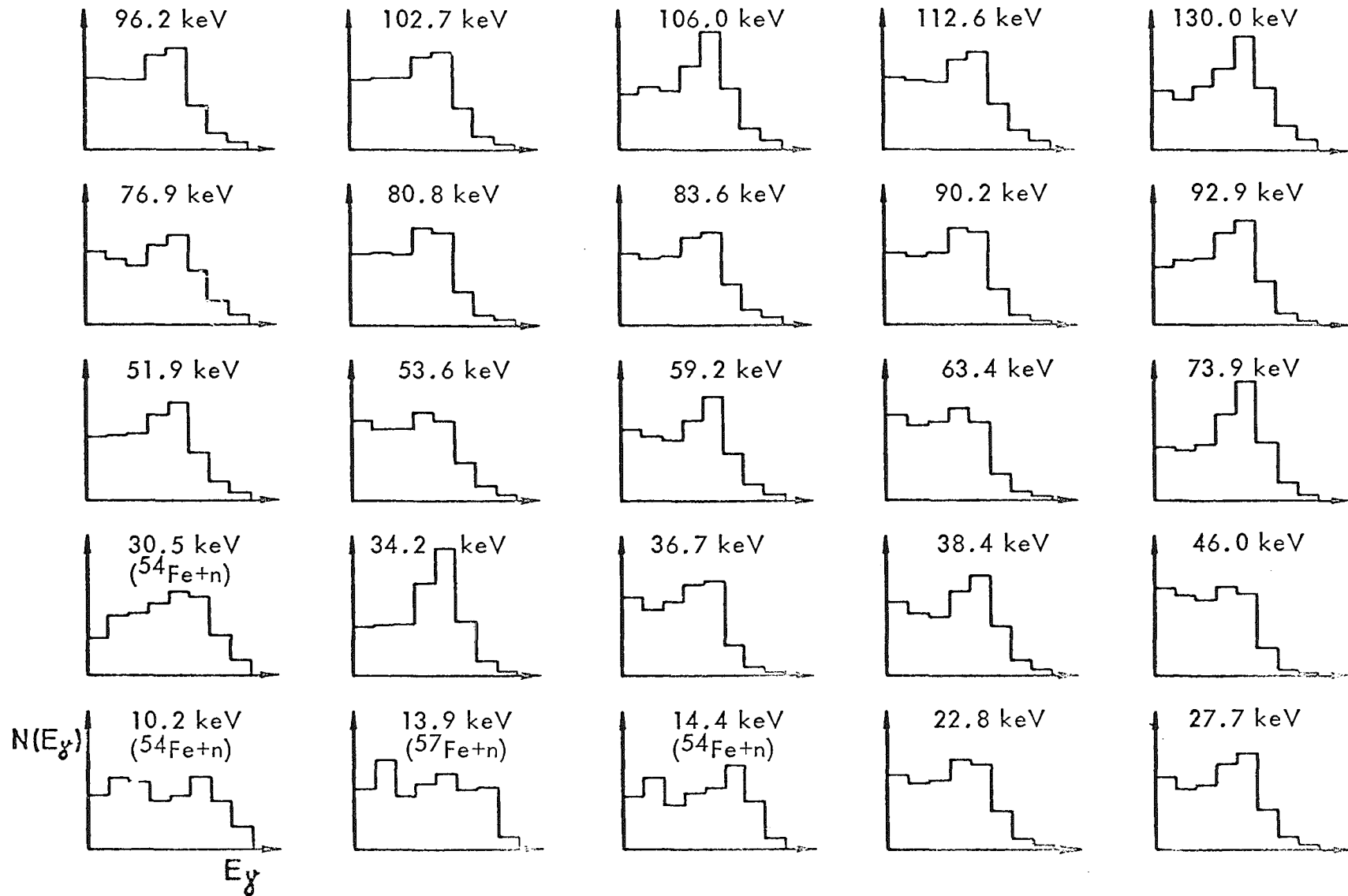


Fig. 2 - Pulse height distributions for levels of  $^{56}\text{Fe}+n$  (if not stated otherwise) obtained with the Karlsruhe 800 l scintillator tank.

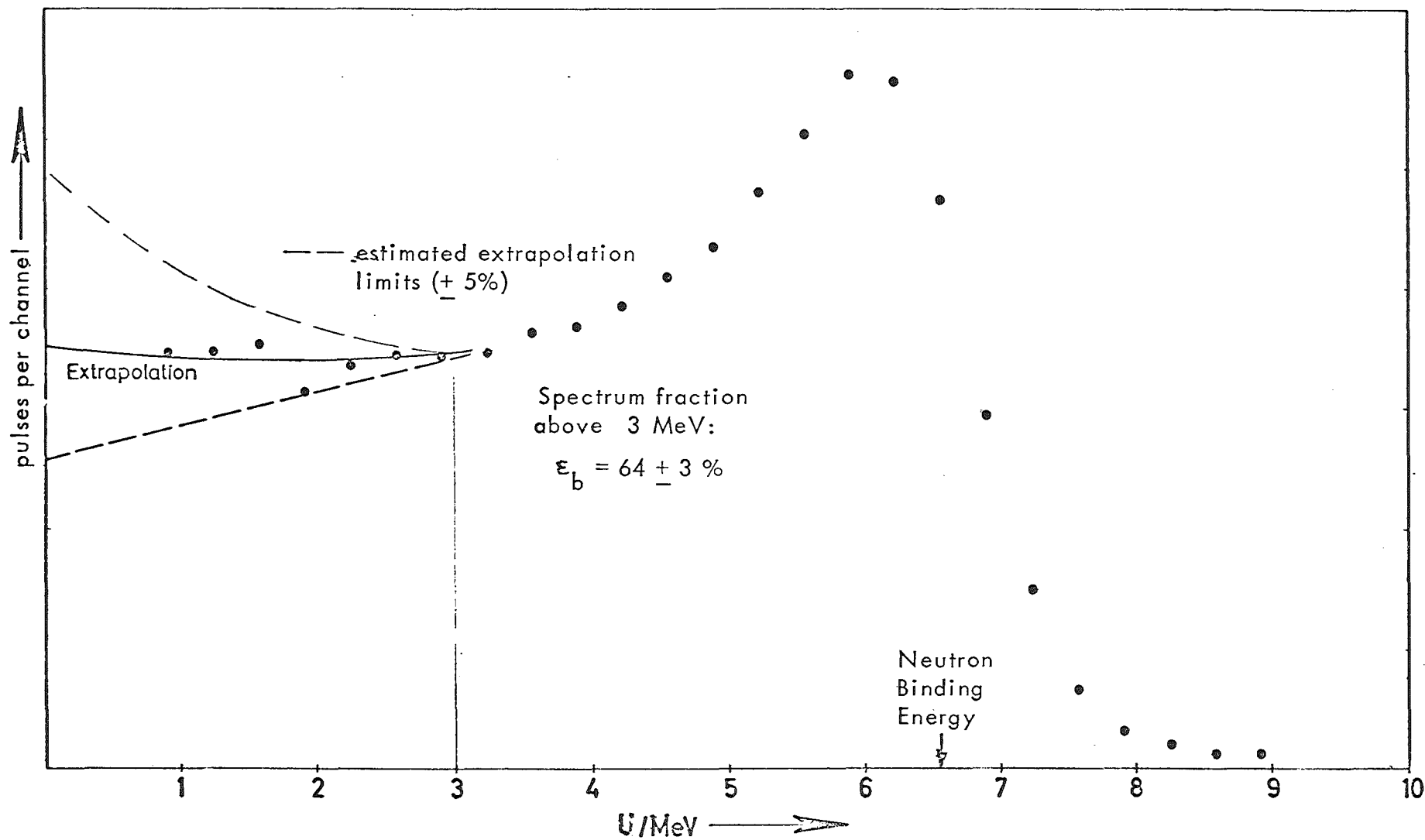


Fig. 3 - Pulse height distribution for gold capture obtained with the Karlsruhe 800 I tank

FAST NEUTRON CAPTURE CROSS SECTION

FACILITY AT CADARACHE

C. LE RIGOLEUR, A. ARNAUD

CONTRIBUTION TO THE MEETING

IN KARLSRUHE NUCLEAR RESEARCH CENTRE

May 8/9, 1973

A B S T R A C T

The total energy weighting technique has been applied to measure absolute fast neutron capture cross section at CADARACHE.

We use a non homogeneous liquid scintillator to detect the gamma from the cascade. The neutron flux is measured with a  $B^{10}$  INa(Tl) detector or  $Li^6$  glass scintillator of well known efficiency. Time of flight technique is used with on line digital computer data processing.

I - PRINCIPLE OF THE METHOD

We use at CADARACHE the total energy weighting technique proposed by MAIER-LEIBNITZ (réf. 1), first used by MACKLIN and GIBBONS (réf. 2 and 3) and then by CZIRR (réf. 4). The efficiency of the detector for capture  $\gamma$  rays is proportionnal to the total energy released that is neutron center of mass energy plus binding energy :

$$E_n + B_n = \sum_{i=1}^m E_{\gamma_i} \quad (I)$$

This way the efficiency of the detector is independant of wide variations in the capture gamma ray spectrum from nuclide to nuclide and from resonance to resonance. This is done by applying a weighting function  $W(I)$  to each pulse from the detector which is a function of pulse size only.

We define the weighting function  $W(I)$  such as :

$$\sum_{I=1}^N P(E_\gamma) S(I, E_\gamma) W(I) = E_\gamma \quad (II)$$

Where  $P(E_\gamma)$  is the probability of detection of a gamma of energy  $E_\gamma$  and  $S(I, E_\gamma)$  the probability to have a pulse of amplitude  $I$  if the gamma has been detected.

For the sake of convenience let us suppose that the cascade has only two gamma :

$$E_n + B_n = E_{\gamma_1} + E_{\gamma_2} = E_{\gamma_T} \quad (III)$$

The probability of detection of a capture is :

$$(1 - P(E_{\gamma_2})) P(E_{\gamma_1}) + (1 - P(E_{\gamma_1})) P(E_{\gamma_2}) + P(E_{\gamma_1}) P(E_{\gamma_2}) \quad (IV)$$

Where the first term is the probability of detection of  $\gamma_1$  only, the second  $\gamma_2$  only and the third the probability of detection in coincidence of  $\gamma_1$  and  $\gamma_2$

The calculated response of our detector for  $N$  captures is :

$$S_T = N \left[ (1 - P(E_{\gamma_2})) P(E_{\gamma_1}) \sum_{I=1}^{I_{max}} S(I, E_{\gamma_1}) W(I) + \right. \\ \left. (1 - P(E_{\gamma_1})) P(E_{\gamma_2}) \sum_{J=1}^{J_{max}} S(J, E_{\gamma_2}) W(J) + \right. \\ \left. P(E_{\gamma_1}) P(E_{\gamma_2}) \sum_{I=1}^{I_{max}} \sum_{J=1}^{J_{max}} S(I, E_{\gamma_1}) S(J, E_{\gamma_2}) W(I+J) \right] \quad (V)$$

introducing :

$$G(E_{\gamma}) = \sum_{I=1}^{I_{max}} S(I, E_{\gamma}) W(I)$$

$$G'(E_{\gamma_1}, E_{\gamma_2}) = \sum_{I=1}^{I_{max}} \sum_{J=1}^{J_{max}} S(I, E_{\gamma_1}) S(J, E_{\gamma_2}) W(I+J) \quad (VI)$$

if the expression II is fulfilled we get :

$$S_T = N \left[ E_{\gamma_1} + E_{\gamma_2} + P(E_{\gamma_1}) P(E_{\gamma_2}) \left( G'(E_{\gamma_1}, E_{\gamma_2}) - G(\bar{E}_{\gamma_1}) - G(\bar{E}_{\gamma_2}) \right) \right] \quad (VII)$$

if  $W(I)$  is linear the last term of VII is equal to zero and :

$$S_T = N (E_{\gamma_1} + E_{\gamma_2}) = N E_{\gamma T} \quad (VIII)$$

The calculated response is independant of individual energy  $E_{\gamma_i}$ .

Usually  $W(I)$  is not linear and a correction must be done to take account of the last term of VII.

Strickly the method is applicable to sample of separated isotopes or isolated resonances.

## II - DETERMINATION OF THE WEIGHTING FUNCTION $W(I)$

We have calculated with a MONTE CARLO code the pulse height response  $P(E_\gamma) S(I, E_\gamma)$  of our detector for different energies  $E_\gamma$ .

$W(I)$  is represented equal to :

$$W(I) = a_1 I + a_2 I^2 + a_3 I^3 + a_4 I^4 \quad (\text{IX})$$

Introducing  $W(I)$  in expression II we got with different energies  $E_\gamma$  an overdetermined system of linear equations that we solved by a least mean square method.

The validity of this theoretical weighting function  $W(I)$  has been checked through equation II with calibrated gamma sources. We were obliged to increase the theoretical efficiency of our detector by 4 % except in energy range 1 to 2 MeV.

The calculated energies through equation II for different calibrated gamma sources with this semi-theoretical weighting function are represented in figure II. The weighting function is represented in figure I.

Due to uncertainties on  $W(I)$  measurement of energy of a mono-energetic source of known activity through the equation II would lead to uncertainties of 1,2 % for energy below 1 MeV, 1,6 % to energy between 3 and 5 MeV, 2,4 % between 5 to 7 MeV, 4 % above 7 MeV.

These errors were estimated from the errors on calibrated gamma sources and uncertainties on gamma ray attenuation coefficients.

### III - EXPERIMENTAL SET UP (see figure III)

The data are obtained with time of flight techniques. Pulsed (3,5 MHz or 1,75 MHz), bunched protons ( 1,2 ns full width at half maximum FWHM) accelerated by the 5,5 MeV Van de Graaff at CADARACHE interacted with  $\text{Li}^7$  to produce 1,2 ns (FWHM) neutron pulses with a broad energy spectrum.

The neutrons at  $0^\circ$  were collimated by a channel through  $\text{HLi}^6$ ,  $\text{Li}_2\text{CO}_3$  plus paraffin, and lead.

Samples, 25 mm diameter or less, are exposed at the center of the prompt gamma ray detector at 85 cm from the target. The neutron beam covered a transverse area of 28 mm diameter.

The gamma detector is a non homogeneous liquid scintillator (1,441 liter of  $\text{C}_6\text{F}_6$ ) for low neutron sensitivity contained in a quartz cell.

The scintillator is viewed by two photomultiplier 56 DVPA.

The experimental time resolution is better than 1,8 ns.

The neutron flux is measured with either a  $\text{B}^{10}$ , Ina (Tl) detector or a  $\text{Li}^6$  glass scintillator. The experimental time resolution of these detectors is better than 2,5 ns.

The efficiency of these detectors has been measured by comparison with a flat detector of well known efficiency (1,8 %) (réf. 5). On figures 4, 5, 6 are represented the absolute efficiency of each neutron flux detector.

Time and pulse height parameters are digitized for each neutron event and transmitted to a CII 90 10 computer for on line processing.

Events are sorted according the identification of the  $\gamma$  detector or neutron flux detector and stored. For the event coming from the  $\gamma$  detector  $W(I)$  is store in the time spectrum of this detector where I is the amplitude of the pulse from the detector.

IV - ANALYSIS

Time of flight spectra are transformed in energy spectra with interval of energy  $\Delta E$ .

Non linearities in the time to digital conversion, photon flight time are taken into account. We get raw neutron radiative capture cross section in barns from :

$$\sigma_{nr}(E) = \frac{\Omega_2}{\Omega_1} \frac{1}{m} \frac{\mathcal{E}(E_n)}{N} \frac{S_T(E_n)}{E_n + B_n} \quad \begin{matrix} \times \\ (\cancel{X}) \end{matrix}$$

Where :

- $\Omega_2$  is the neutron flux detector solid angle subtended at  $\text{Li}^7$  target
- $\Omega_1$  is the capture sample solid angle subtended at  $\text{Li}^7$  target
- $n$  the thickness in nuclei/barn of the sample
- $\mathcal{E}(E_n)$  efficiency of the neutron flux detector at energy  $E_n + \frac{\Delta E_n}{2}$
- $N$  counting rate of the neutron flux detector in the energy range  $(E_n, E_n + \Delta E_n)$
- after correction of the few percent attenuation by the capture sample (calculated from the total cross section)
- $S_T(E_n)$  calculated counting rate of the detector in the energy range corrected for background measured with carbon sample.
- $B_n$  binding energy of the neutron in the nuclide

When natural elements are used which are no pure isotope the total energy released for incident center of mass energy  $E_n$  is :

$$E_{TOT} = E_n + \frac{\sum_{i=1}^n a_i \sigma_i(E_n) B_{ni}}{\sum_{i=1}^n a_i \sigma_i(E_n)} \quad (X)$$

Where  $a_i, \sigma_i, B_{ni}$  are the % abundance, relative capture cross section and  $B_{ni}$  binding energy of the nuclide  $Z^{A_i+1}$

Since  $\sigma_i$  is usually unknown we make the approximation that they are equal and the equation X gives :

$$E_{TOT} = E_n + \sum_{i=1}^n a_i B_{ni} \quad (XII)$$

Usually no error is introduced to take account of this approximation.

V - CORRECTIONS

Corrections are applied for different effects :

1 - Neutron scattering and resonance self shielding

Analytical calculations adjusted by Monte Carlo calculations at several energies are used (réf. 6).

2 - Gamma attenuation and non linearity of the weighting function

The corrections are connected with the capture gamma ray spectrum.

Following interaction inside the sample a capture gamma ray may disappear or interact with loss of energy.

A Monte Carlo code gives :

$$\int_0^{E_\gamma} h(E_{\gamma'}) E_{\gamma'} dE_{\gamma'} = E_{\gamma''} < E_\gamma \quad (\text{XIII})$$

The capture gamma ray detector measures  $E_{\gamma''}$  instead of  $E_\gamma$ . Our detector has a large efficiency (34% for 1 MeV gamma, 20% for 4,5 " gamma). The probability of detection in coincidence of two gamma of the cascade is important. Consequently to the shape of  $W(I)$  (figure 2) more weight is given to the sum of two pulses than to each pulse taken separately :

$$W(I + J) > W(I) + W(J) \quad (\text{XIV})$$

We may calculate the excess of weight for two gamma of energy  $E_{\gamma_1}$  and  $E_{\gamma_2}$ . It is equal to the last term of expression (VII)

Usually the capture gamma ray spectrum may have one, two or several gamma. In order to determine the excess of weight we use the capture gamma ray spectrum at thermal energy or theoretical spectrum.

From these spectra we deduce cascade and the excess of weight for each pair of gamma of the cascade, (Triple coincidence are neglected).

Drastic changes in the shape and multiplicity of capture gamma ray spectrum give the uncertainty of that correction. The excess of weight ranges from 3 % to 6 % and we estimate that we have to introduce an additional error of 1,6 %.

3 - Some other minor corrections are applied

Correction for scattering of neutron in air,  $\gamma$  rays from inelastically scattered neutrons on capture sample.

VI - CONCLUSION

On table I are listed the contributions to the final error of the cross section at the present time and in the future.

- TABLE I -

SOURCE OF ERROR	PRESENT ERROR	ERROR EXPECTED IN THE FUTURE
Mass sample, solid angle	0,2 %	0,2 %
Neutron flux measurement including transmission correction	2,5 %	2 %
Weighting function	1,2 % to 3 % according the sample	1 % to 1,5 % according the sample
Non linearity of the weighting function	1,6 %	< 1 %
Multiple scattering and self protection	1,5 %	< 1 %
TOTAL ERROR	3,6 % to 4,5 %	2,7 % to 3 %

The total error does not include statistical error and is only valid for monoisotopic nuclide.

We have recorded in energy bins the amplitude response of the gamma detector. From these responses we expect to get a good idea of the capture gamma ray spectrum and this way to calculate with a good accuracy the correction due to the non linearity of weighting function.

The total energy weighting technique first used by MACKLIN and GIBBONS (réf. 2) offers good efficiency, good time resolution and low background. Strickly the method is only valid for single isotopes or isolated resonances but only low quantities of material are needed (less than 7 g )

The method requires for time of flight work either a two parameters experiment or on line digital computer data processing.

At CADARACHE the smallest capture cross sections we could measure should be 1 to 2 *mb* below 200 KeV and 0,5 *mb* above. Our measurements are absolute capture cross sections measurements.

R E F E R E N C E S

- [1] H. MAIER-LEIBNITZ (Private communication to  
R.L. MACKLIN and J.H. GIBBONS)
- [2] R.L. MACKLIN and J.H. GIBBONS  
Phys. Rev. 159 (1967) 1007
- [3] R.L. MACKLIN and B.J. ALLEN  
Nuclear Inst. and Methods Vol 91 (1971) n°4 - 565
- [4] J.B. CZIRR  
Nuclear Instruments and Methods Vol 72 (1969) 23-28
- [5] J.L. LEROY et alii  
Conference Proceedings HELSINKI 1970  
Communication CN 26/70
- [6] J. TASTE  
to be published

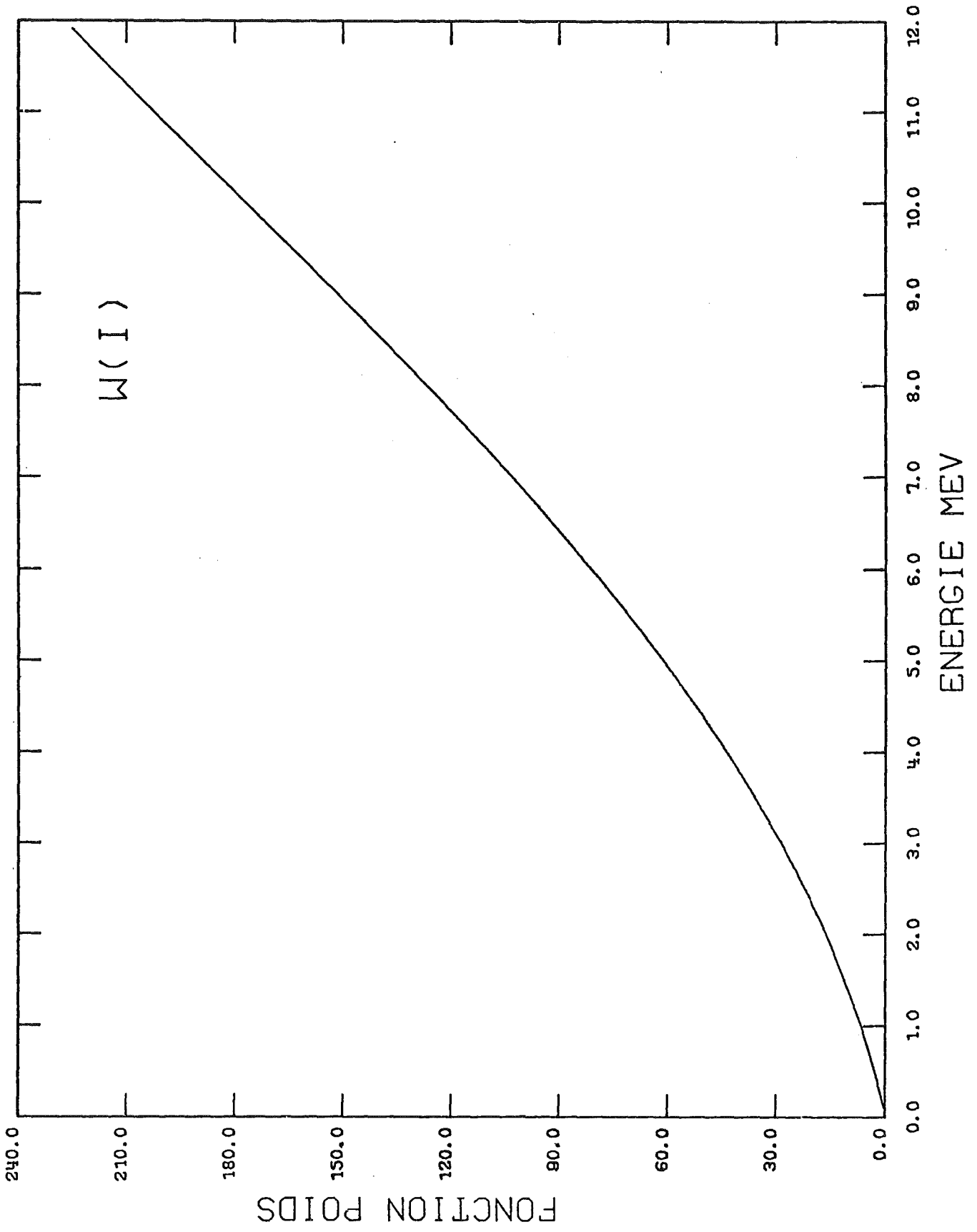


FIG 1

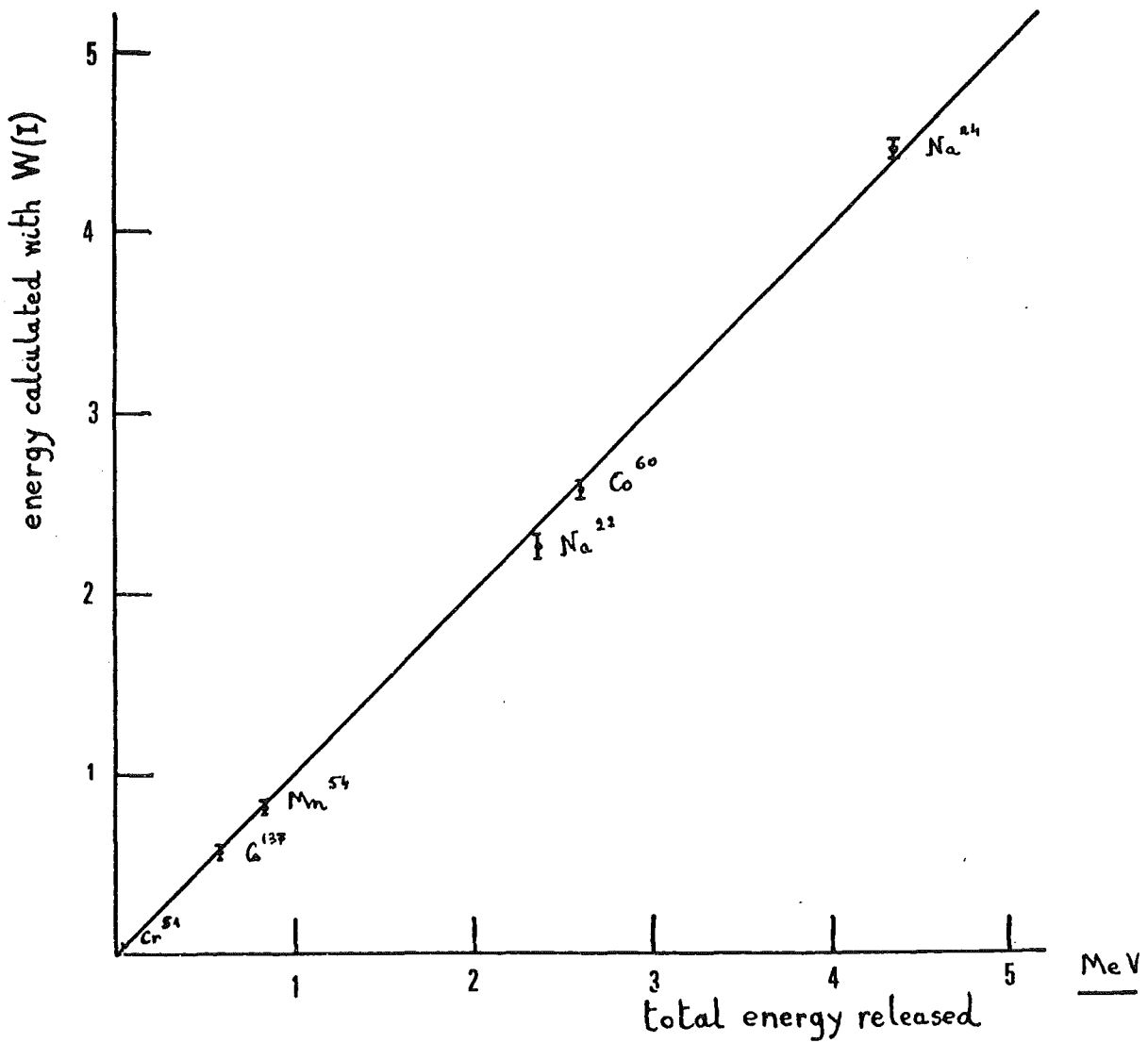
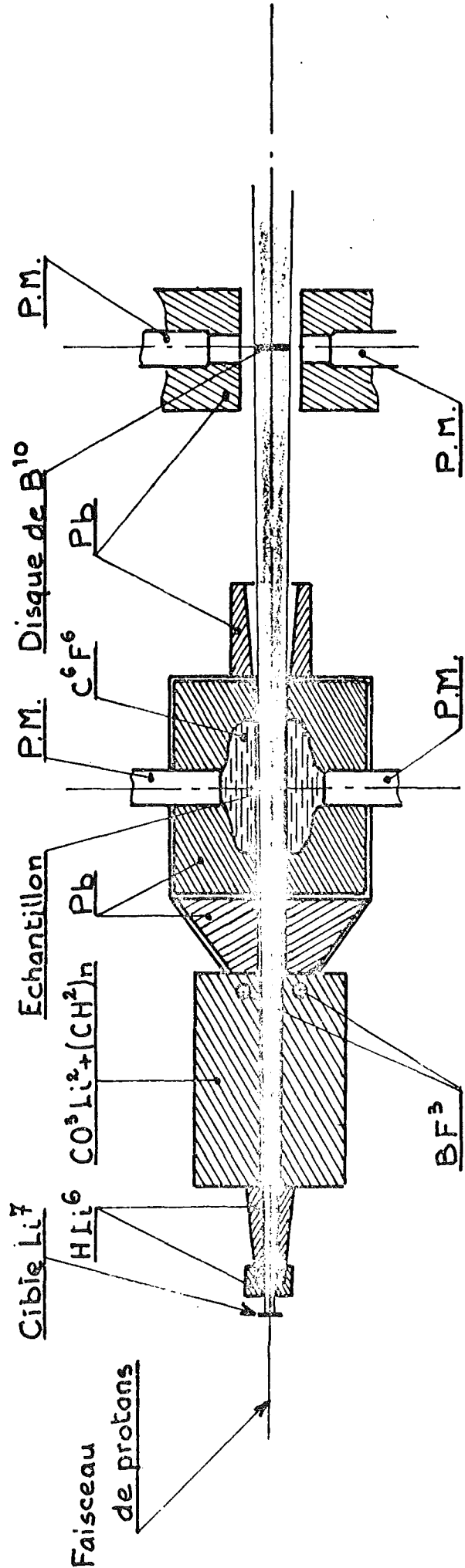


FIG 2



DISPOSITIF EXPERIMENTAL

FIG 3

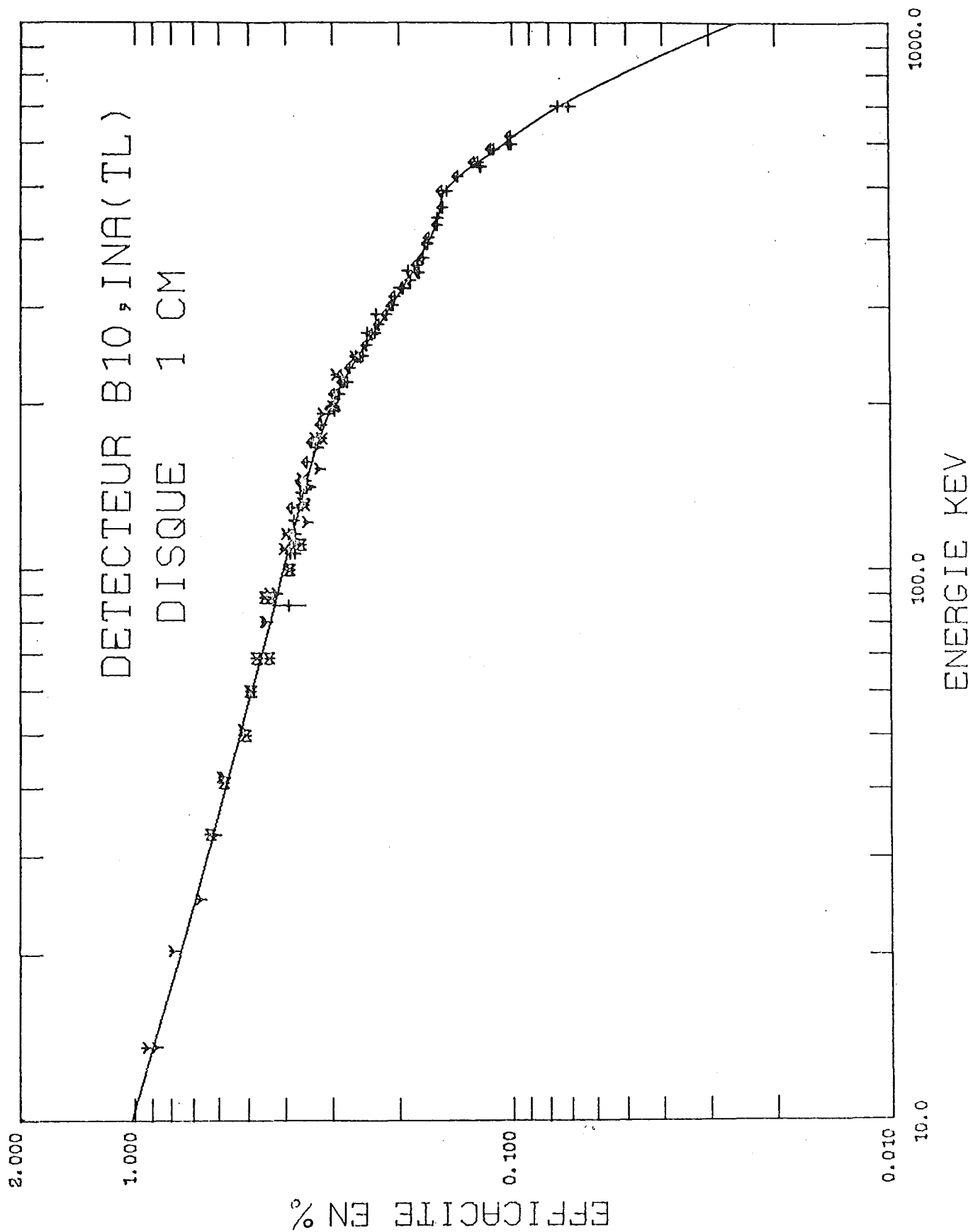


FIG4

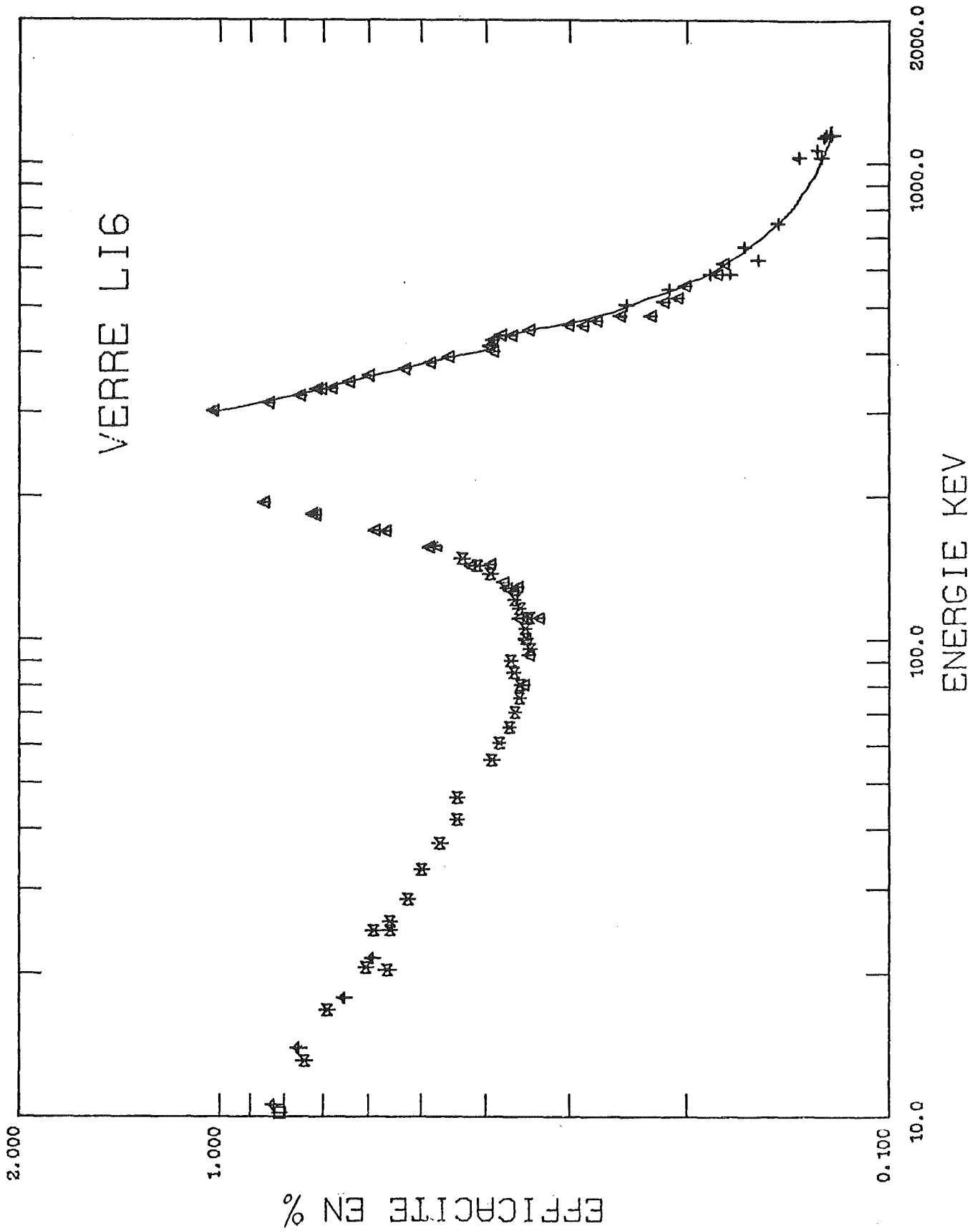


FIG 5

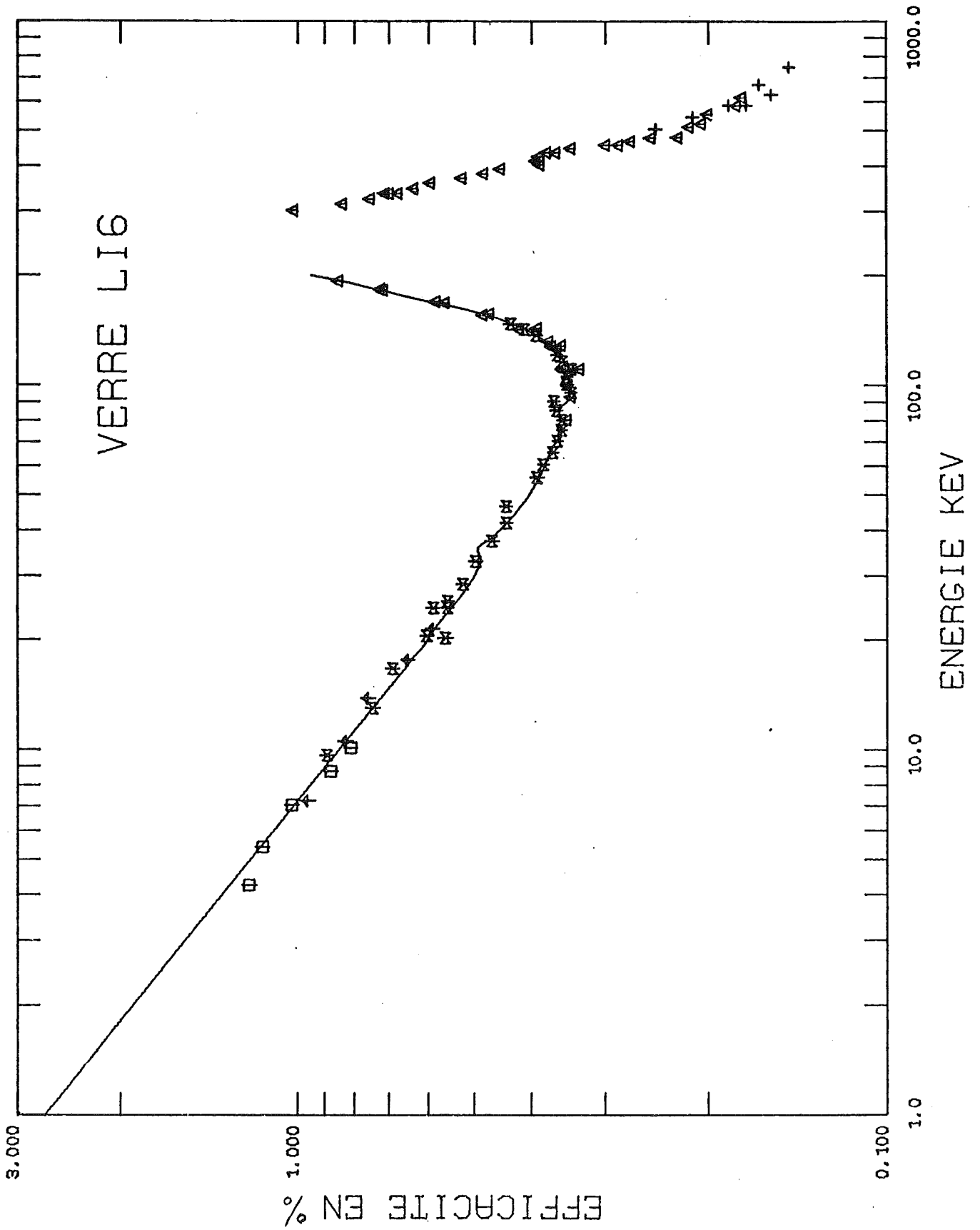


FIG 6

ABSOLUTE CAPTURE CROSS SECTION  
MEASUREMENTS OF Au, Cr, Fe, Ni  
BETWEEN 70 KeV TO 550 KeV

C. LE RIGOLEUR, A. ARNAUD, J. TASTE

CONTRIBUTION TO THE MEETING  
IN KARLSRUHE NUCLEAR RESEARCH CENTRE

May 8/9, 1973

A B S T R A C T

Total energy weighting technique was used to measure absolute radiative capture cross sections of elemental Cr, Fe, Ni and Au for neutrons of energy 70 to 550 KeV. A comparison with other data is done.

We have presented in an other contribution to this meeting the absolute capture measurement technique we use at CADARACHE.

We present here the results of our measurements on Cr, Fe, Ni and Au.

The sample characteristics are listed in table I.

TABLE I

	Thickness in nuclei/barn
CHROMIUM	$18.2 \cdot 10^{-3}, 34.91 \cdot 10^{-3}$
IRON	$8.244 \cdot 10^{-3}, 16.642 \cdot 10^{-3}, 24.89 \cdot 10^{-3}$
NICKEL	$9.233 \cdot 10^{-3}, 18.499 \cdot 10^{-3}, 27.793 \cdot 10^{-3}$
GOLD	$2.911 \cdot 10^{-3}, 5.836 \cdot 10^{-3}$

As we used natural samples the total energy released after a capture is equal to :

$$E_{TOT} = E_n + \frac{\sum_{i=1}^m a_i \sigma_i B_i}{\sum_{i=1}^m a_i \sigma_i} \quad (I)$$

Where  $E_n$  is the incident neutron center of mass energy,  $a_i, \sigma_i, B_i$  are fractional abundance, relative capture cross section and neutron binding energy of the nuclide  $Z^{A_i+1}$  and  $m$  the number of isotopes of elemental mixture.

Since the relative capture cross sections  $\sigma_i$  are generally not known we make the approximation that they are equal and equation (I) reduces to :

$$E_{TOT} = E_n + \sum_{i=1}^m a_i B_i \quad (II)$$

No error is introduced by this approximation. The contributions to final error of different sources of error are listed in table II.

TABLE II

SOURCE OF ERROR	Cr	Fe	Ni	Au
Mass sample, solid angles	0,2 %	0,16 %	0,16 %	0,16 %
Neutron flux measurement including transmission correction	2,5 %	2,5 %	2,5 %	2,5 %
Uncertainties on the weighting function	2,5 %	2,4 %	2,8 %	1,4 %
Multiple scattering and self protection	1,5 %	1,5 %	1,5 %	0,5 % to 1 %
Non linearity of the weighting function	1,6 %	1,1 %	1,5 %	1,6 %

CHROMIUM (figure 1)

Between 90 KeV and 160 KeV we get higher cross sections than most of other experimental results. The agreement is better between 200 to 600 KeV.

Recently R.G. STIEGLITZ and alii (Réf. 2) have measured capture cross sections of chromium isotopes. The average cross sections obtained by these measurements are compared with our results in table III and the agreement is good.

TABLE III

ENERGY RANGE KEV	R.G. STIEGLITZ and alii (réf.2)	THIS WORK
90 - 100	$18.8 \pm 3.5$	$20.8 \pm 1.$
100 - 150	$8.8 \pm 2.$	$9.96 \pm 0,45$

The results of STIEGLITZ and alii (réf. 2) are not shown in figure 1.

With their results we calculate the average energy released with equation (I) without incident neutron center of mass energy and in table IV we compare with the value calculated from equation II

TABLE IV

ENERGY RANGE KEV	AVERAGE Bn EQUATION I	Bn CALCULATED FROM EQUATION II
90 - 100	7.99 MeV	8.12 MeV
100 - 150	7.96 MeV	8.12 MeV

It appears that our average results should be decreased by 1,8 %.

The approximation of equation II seems reasonable.

#### IRON (fig. II)

The general trend of our results is also to find higher values. It seems from the curves of ERNST and alii (réf.3) that the agreement is good. Their results are not shown on figure II.

#### NICKEL (fig. III)

The agreement is better than for iron and chromium.

#### GOLD (fig. IV)

The agreement with the results of POENITZ (réf. 12) is quite good (1 % to 2 %).

#### CONCLUSION

For Cr, Fe, Ni we find higher value than most of the other measurements. Our results seem to prove the high values of capture cross sections measured these last years.

We got the values of references from C C D N (réf. 17).

R E F E R E N C E S

- [1] ISAKOV  
ZET 38 989 Mar 60  
Transl in Soviet Phys. JETP 11, 712 (60)
- [2] R.G. STIEGLITZ AND ALII  
N.P. VOL A 163 (1971) N°2
- [3] A. ERNST AND ALII  
Conference proceedings HELSINKI (1970)  
Communication CN 26/11
- [4] BLOCK (68)  
Communication privée au CCDN  
R.W. HOCKEMBURY and alii  
Physical review vol. 178 N° 4 p 1746
- [5] DIVEN  
P.R. 120 556 oct. 60
- [6] L.M. SPITZ et alii  
M.P. A 121 655 déc. 68
- [7] STAVISSKI  
A.E. 12 514 June 62  
Transl in Sov. J. AC En 12, 545 (62)
- [8] BELANOVA  
ZET 34 574 mar 68  
Transl in Sov J At En 10, 255 (62)

- [ 9 ] STAVISSKI  
AE 10 264 Mar 61  
Transl. in Soviet J At En 10, 255 (62)
- [ 10 ] MALYSHEV  
AE 17 508 Dec 64  
Transl in soviet AT En 17, 1277 et J Nuc En  
19, 918 (1965)
- [ 11 ] BELANOVA  
AE 8 - 549 June 60  
Transl in soviet J AT En 8, 462 (1961)
- [ 12 ] R.L. MACKLIN AND J.H. GIBBONS  
The physical review vol 159 n°4 1007-1012
- [ 13 ] F.J. VAUGHN AND J. A. GRECH  
BNL 50 298 - NCSAC 38  
EANDC (US) 156 - U INDC (USA) 30 U
- [ 14 ] W.P. POENITZ et alii  
J. Nucl energy 22 505 (1968)
- [ 15 ] M.P. FRICKE et alii  
Nuclear data for reactors  
Conference proceedings, HELSINKI 1970  
CN 26/43 AIEA
- [ 16 ] W.P. POENITZ  
J Nucl Energy 20.825 (1966)
- [ 17 ] M. ALOIS SCHETT  
Private communication

FIG 1

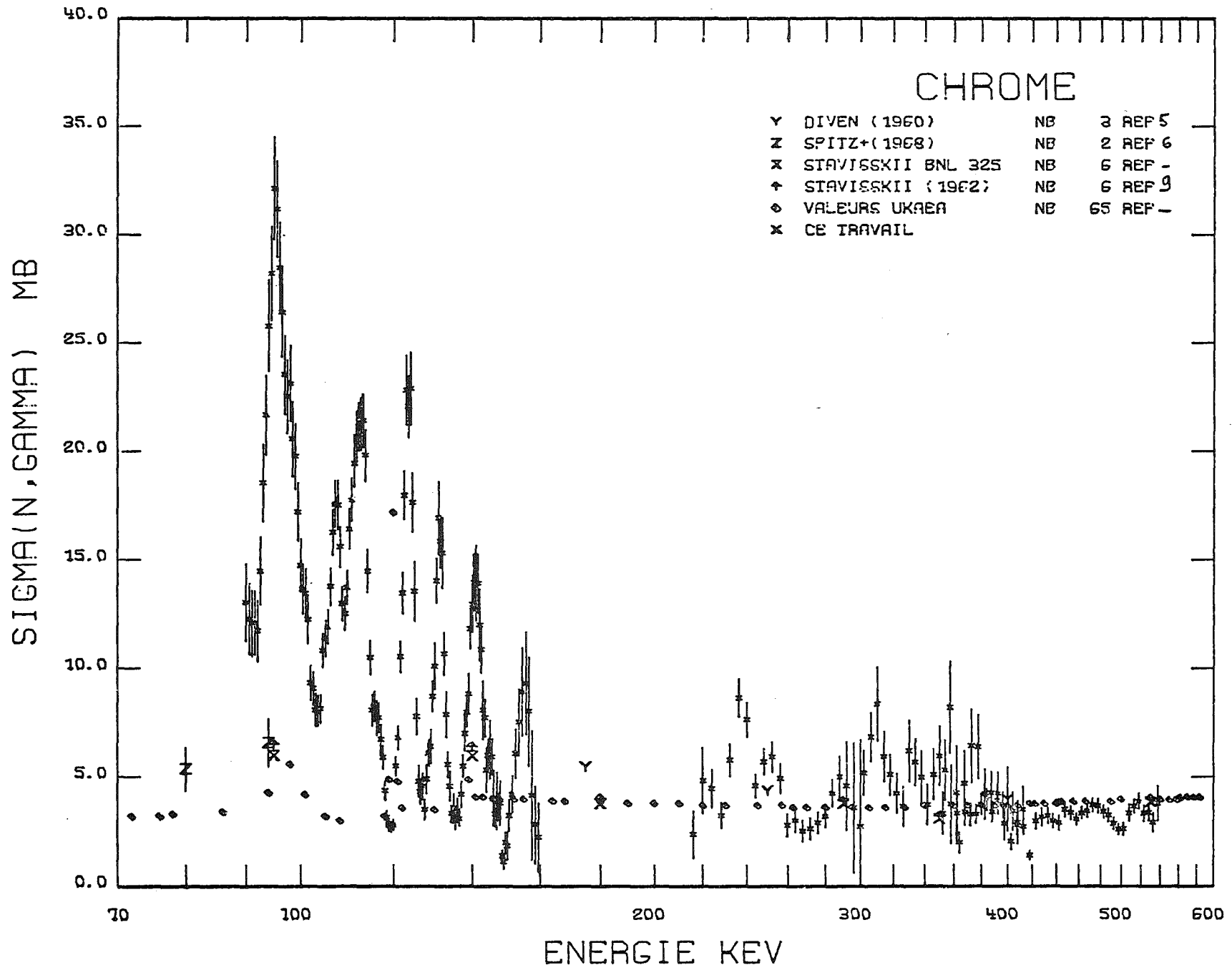


FIG 2

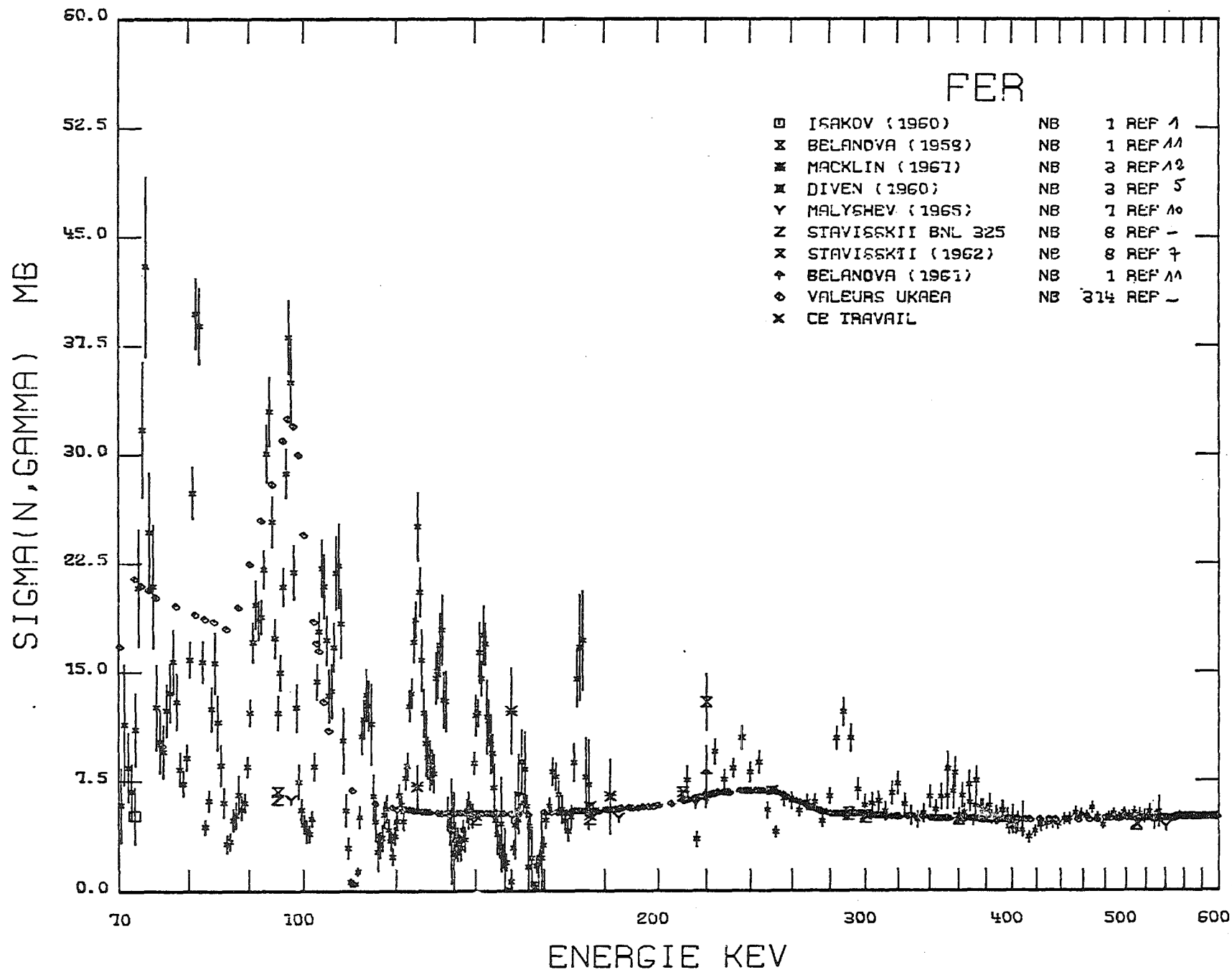


FIG 3

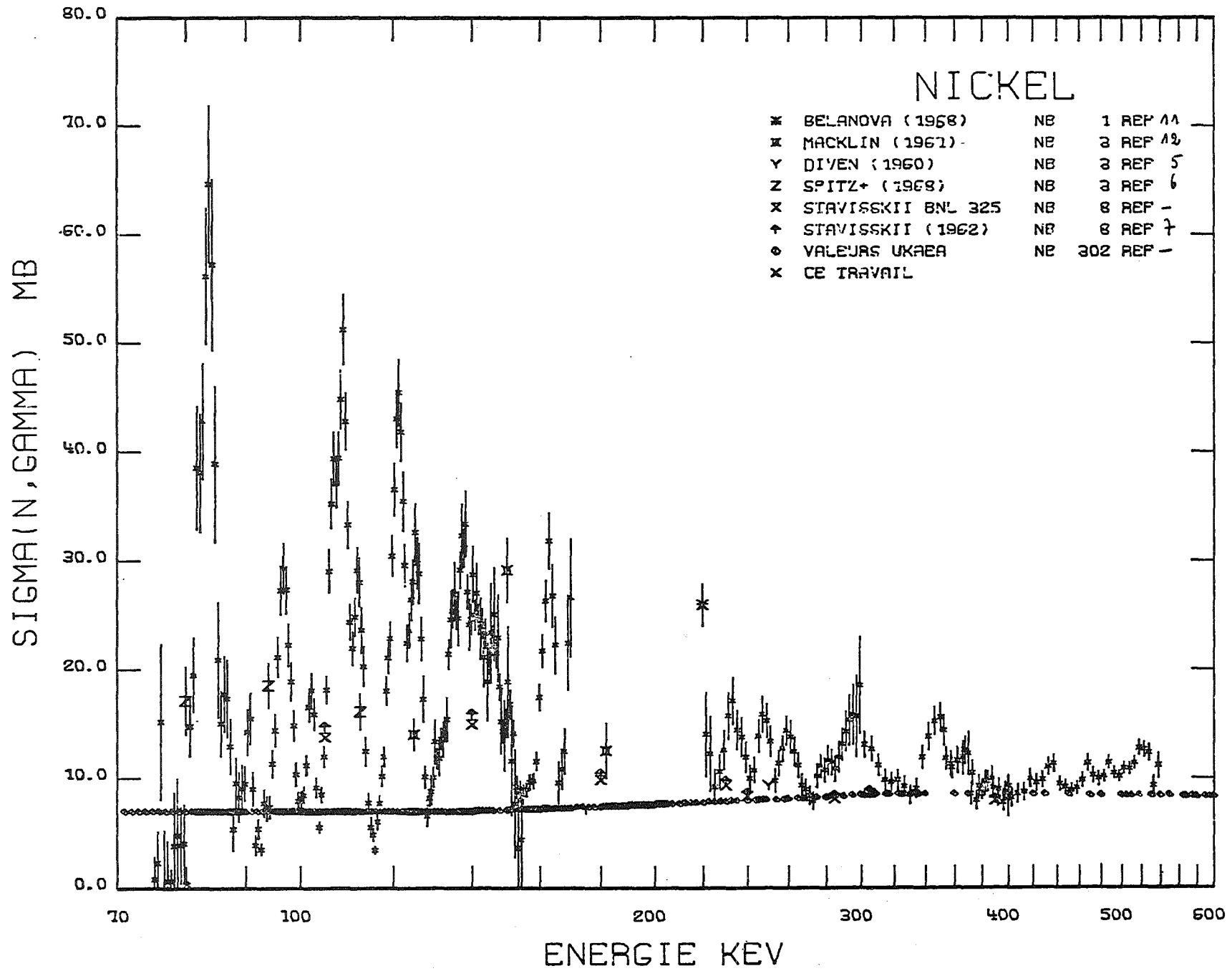
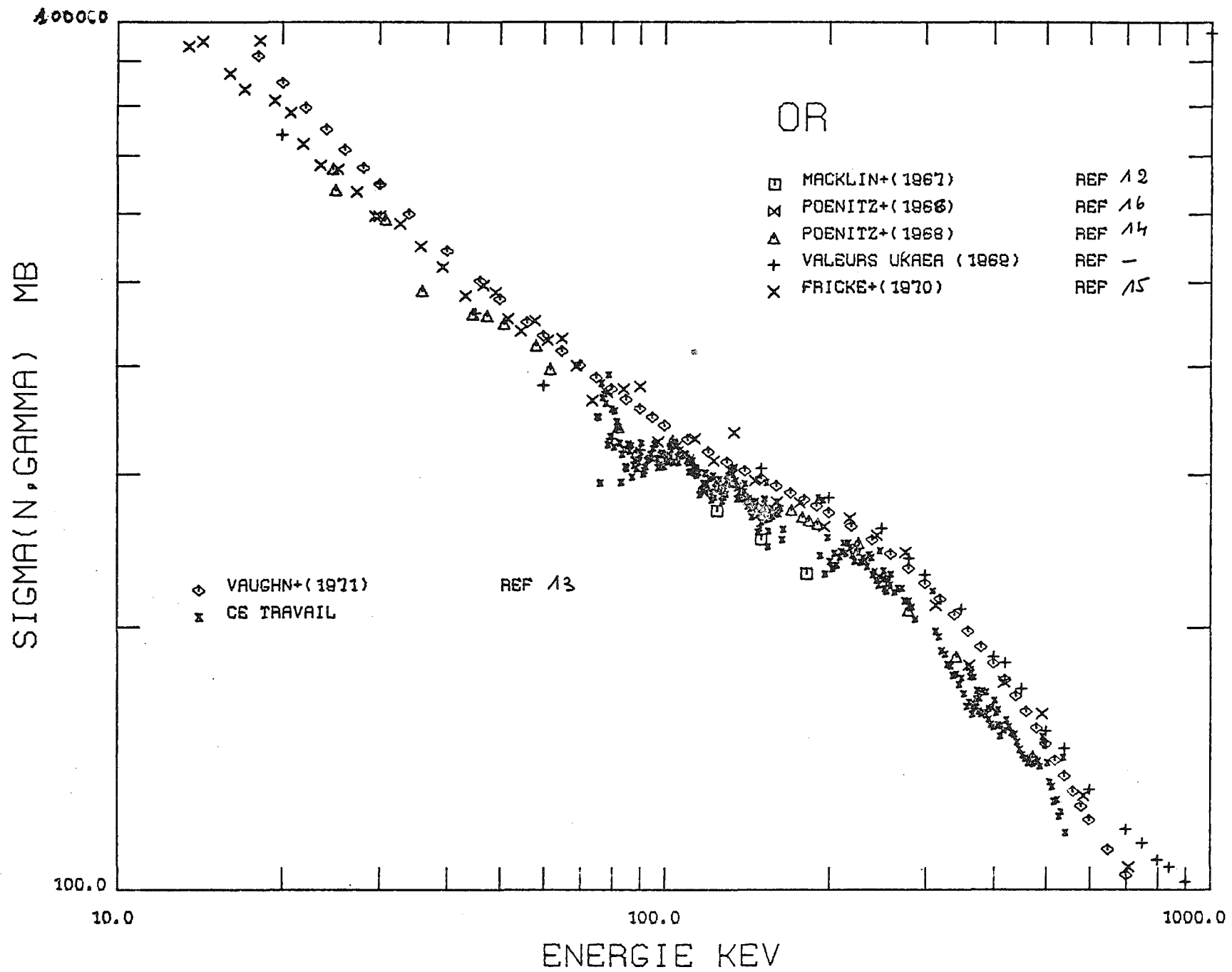


FIG 4



NEUTRON CAPTURE IN REACTOR STRUCTURAL MATERIALS  
by  
R.L. Macklin

A EACRP-EANDC meeting on the above topic, stressing Ni, Fe and Cr, is scheduled for May 8-9, 1973, at Karlsruhe. Written comments and contributions under various topics have been solicited.

I. At the Oak Ridge Electron Linear Accelerator (ORELA) there are indeed capture and transmission measurements under way. Time-of-flight transmission work at 18, 50, 80 and 200 meters is carried on by J. A. Harvey, N. W. Hill, W. M. Good, C. H. Johnson, J. L. Fowler, F. G. Perey, T. A. Love, W. E. Kinney, and visiting scientists from Idaho Falls, Savannah River, Brookhaven, Taiwan, and various US universities. The last group also includes undergraduate students on summer assignments and in alternating work-study programs. Transmission measurements on  $^{16}\text{O}$ ,  $^{23}\text{Na}$ ,  $^{27}\text{Al}$ ,  $^6\text{Li}$ , stable isotopes of calcium, silicon, sulfur, titanium, zirconium, and lead,  $^{242}\text{Pu}$ ,  $^{248}\text{Cm}$  and particularly  $^{54,56,57}\text{Fe}$  near the  $^{56}\text{Fe}$  windows are of current interest.

Capture cross section measurements on  $^{238}\text{U}$  and  $^{235}\text{U}$  have been made by G. de Saussure, R. W. Ingle, E. G. Silver, and R. B. Perez at 40 meters with a large liquid scintillation tank. An extensive program on enriched stable isotope capture is also being conducted (R. L. Macklin and J. Halperin) using small non-hydrogenous liquid scintillators and on-line pulse height weighting to give a response like an ideal Moxon-Rae detector.<sup>1)</sup> Resonance capture in silicon (reported at the Asilomar Conference on Photonuclear Reactions),  $^{93}\text{Nb}$ ,  $^{59}\text{Co}$ ,  $^{103}\text{Rh}$ ,  $^{139}\text{La}$ ,  $^{45}\text{Sc}$  and p-wave capture in  $^{56}\text{Fe}$  above 100 keV are of current interest. Measurements on capture by  $^{92}\text{Mo}$ ,  $^{111}\text{Cd}$ ,  $^{19}\text{F}$ ,  $^{27}\text{Al}$ ,  $^{205}\text{Tl}$ , and stable isotopes of Sr, Zr, Ca, Cr<sup>2)</sup>, Ti, Te, Ba, and Pb are in various

stages of analysis. Most of the work on resonance capture analysis and publication must be done in collaboration with visiting scientists from other laboratories and universities (B. J. Allen and co-workers at Lucas Heights, AAEC, G. Vanpraet (Belgium), D. Earle (Chalk River, Canada), O. A. Wasson (Brookhaven National Laboratory), and R. R. Winters (Denison University, Ohio).

## II. Background, Resolution, Corrections, Normalization and Analysis

We enjoy a very clean pulsed beam at ORELA both in terms of sharp collimation and off-energy neutron contamination. Neutrons whose energy does not correspond to flight time directly from the moderator are under 1% of the direct beam up to at least 1 MeV.<sup>(3)</sup>

The sharp definition of the beam has permitted our capture detectors to be placed close to the sample position with only an allowance of a few millimeters for penumbra, alignment and vacuum window.<sup>4)</sup> While a uranium target would provide a few times more neutron intensity than our present tantalum target<sup>3)</sup> it would also introduce a sample dependent background from delayed fission neutrons.

Corrections of a few percent are made to the gamma energy yield data (deadtime, room background, sample scattered neutron background and particularly resonance self-protection). As the enriched samples are rare and expensive we try to use just one sample thickness in the general case. This leads to substantial (up to a factor of 2 or so) resonance self-protection corrections at the lower end of our energy range (2.5 keV) and sparse statistics up near 1 MeV. As several other laboratories are well equipped to measure capture up to several keV, we have generally avoided taking data below 2.5 keV.

Our present choice of flux standardization is based on the saturated resonance technique (4.9 eV Au, 0.005 cm thickness) and the thin  ${}^6\text{Li}$  glass scintillation monitor.<sup>5)</sup> The first seems clearly preferable to thermal cross section normalization as one relies on the literature only for the 2% or so (backscatter) correction rather than the entire standard thermal cross section. By use of a re-entrant or cup shaped sample the backscatter correction could be reduced still further if desirable. (Of course, it is nice to check the thermal value against the saturated resonance capture, but the experimental setup may need to be substantially modified to deal carefully with the thermal energy range.) The present accuracy of the  ${}^6\text{Li}(n,\alpha)$  cross section at and above the 0.25 MeV resonance is not entirely satisfactory. Experiments currently underway, particularly time-of-flight ratio measurements of  ${}^6\text{Li}$  glass and fast plastic scintillators, should help.

As to analysis of data, I remember a wise dictum of Eric Lynn in response to a question at Antwerp in 1965. He had spoken on the strong interference effects of fission resonances but advised the experimentalist to continue to use the traditional isolated resonance parameter description, leaving the theoretician to reinterpret the results with more elaborate formalisms. Beyond this one still has use for Occam's razor when describing capture where resonances are unresolved. Prescriptions like  $D_J\pi = D_0(2J+1)$ ,  $\Gamma_\gamma = \bar{\Gamma}_\gamma$  independent of  $J$ ,  $\pi$ ,  $\ell$ , serve to reduce the ambiguity of description. I feel they should continue to be used except where shown to be inadequate.

### III. Gamma Detectors for Neutron Capture Cross Sections

As the history of this subject is quite familiar, I confine myself to advantages and limitations of detectors in recent or current use for prompt

gamma cascade measurement. These range from the large (2 meter diameter) liquid scintillator tank, to small scintillators (such as NaI(Tl) 10.2 x 12.7 cm and  $C_6F_6$  4 x 10.2 cm) and converter-scintillator combinations developed from the original Moxon Rae detector.<sup>6)</sup>

Typical capture gamma cascades give 4.8 to over 10 MeV of total gamma ray energy per neutron captured. While cascades of 4 to 5 gamma rays with average energies of 1-2 MeV are usual, cases where a single gamma ray (near 7 MeV) is prominent are known and such rarities often lead to added interest in the data.

In the large tank detectors most of the volume is needed to raise the efficiency for the rare high energy gamma rays<sup>7)</sup> but contributes heavily to the background.

To override background pileup, bias levels of 3 MeV are not uncommon and the necessary extrapolation to zero pulse height is unsupported by observation below 1 MeV. As the "spectrum fraction" so estimated is typically 0.5-0.6, it is clear that undetected systematic errors might approach several percent. Half tank coincidence methods to reduce background, in principle re-introduce a strong dependence on cascade multiplicity, though for the important case of  $^{238}U(n,\gamma)$  it does not appear significant.

In the small detectors, independence of cascade details is achieved through the method, first put forward by Rae, of making the average detector response proportional to the energy of each gamma ray detected. In the original work<sup>6)</sup> this was approximately achieved by counting with a thin plastic scintillator the electrons emerging from a gamma converter plate. Material and geometric modifications of this approach to achieve higher

efficiency have originated in many laboratories. With such detectors enhanced escape of high energy gamma rays is directly compensated by increased efficiency. At the same time environmental backgrounds are modest and pileup not a problem. The converter plate inevitably absorbs low energy gamma rays so that the linearity of the efficiency vs  $E_\gamma$  relation cannot be maintained below about 0.5 MeV. As the abundance of prompt cascade gamma rays below this energy falls rapidly (with few if any below 0.1 MeV or so) their unobservability is of less potential significance than for the large liquid scintillator.

The Moxon-Rae average response characteristic can also be achieved for most detectors by assigning an importance (or "weight") to each event which is a monotonic increasing function of the pulse height.<sup>8)</sup> This allows considerable freedom in optimizing other characteristics such as sensitivity to sample scattered neutrons, gamma ray stopping power and solid angle.

Swedish laboratories have used this approach with sodium iodide<sup>9)</sup>, Livermore with a deuterated liquid scintillator<sup>10)</sup> and ourselves with fluorocarbon liquid scintillators. The sodium iodide provides greater gamma ray stopping power, but somewhat poorer timing capability and a formidable scattered neutron sensitivity through neutron capture in the iodine. This last requires a neutron shield such as  $^6\text{LiH}$  when a "white" neutron source is used and we have not been successful in trying to measure the angular distribution of capture gamma rays with this detector at ORELA. The fluorocarbon scintillator we use (NE-226) has good timing, fair gamma ray stopping power (density  $1.6 \text{ gm/cm}^3$ ) and little sensitivity to sample scattered neutrons. Thus no neutron shield is required and pulse heights down to 150 keV can be used. This provides a "spectrum fraction" typically over

99% for the weighted response (see Fig. 4 of reference 4) and of course no sensitivity to the decreased stopping power for high energy gamma rays. The deuterated liquid scintillator has good timing, somewhat less gamma ray stopping power (density  $0.945 \text{ gm/cm}^3$ ) and even less probability of neutron capture than for fluorocarbons. Although neutron thermalization and subsequent capture in the surroundings may need to be guarded against, this is probably the detector of choice for neutron capture cross section measurements. With hydrogenous scintillators of modest size, neutron thermalization and capture is generally considered unacceptably large for this application. (In large liquid scintillators the effect is generally suppressed by a few centimeters of  $^6\text{LiH}$  as a liner and the addition of trimethyl borate<sup>11)</sup> to compete (via  $^{10}\text{B}(n,\alpha)$ 's 478 keV gamma ray) with the 2.2 MeV  $\text{H}(n,\gamma)$  reaction.)

Another consideration in the shape of gamma ray detectors is their sensitivity to non-isotropic angular distributions. This is particularly significant for  $\sigma(n,n')\gamma$  measurements<sup>12)</sup> where a single gamma ray is produced for neutron energies between the first and second excited state thresholds. The angular distribution can be described in terms of Legendre Polynomials and is proportional to  $(1 + aP_2(\cos \theta) + b P_4(\cos \theta))$  for quadrupole radiation. The coefficient  $b$  is zero for dipole radiation (and  $-1 \leq a \leq 2$ ). The change in total efficiency for a number of detector materials and geometries has recently been calculated using an 860 keV gamma ray energy as a test case. In general it is possible to completely cancel the sensitivity to  $P_2$  distortion for simple geometries without much sacrifice of efficiency or increase of volume. The sensitivity to  $P_4$  distortion was typically small and negative for the geometries studies.

Finally, let me suggest a next-generation capture detector incorporating many of the good features of existing systems. As mentioned above, deuterated liquid scintillator seems the best choice for freedom from scattered neutron sensitivity. The first resonance is near 150 keV in  $^{13}\text{C}$  (a 1.1% isotope in natural carbon) and no more are known below 1.75 MeV. There is the possibility of neutron recoil rejection by pulse shape discrimination, as well as good timing down to less than a nanosecond.<sup>10)</sup> Much better timing would be of little value in neutron time-of-flight work because of the neutron flight time uncertainty introduced by typical finite target, moderator and sample thicknesses.

A small cylindrical volume provides reasonable efficiency in utilization of the scintillator with ease of fabrication. A central cylindrical duct of 8 cm or so will accommodate typical samples, including enriched isotopes, as well as a modest  $^6\text{Li}$  liner if needed. Calculations (see the Figure) show total efficiencies of over 65% (for  $E_\gamma = 860$  keV) with cancellation of  $P_2$  sensitivity, for volumes of 30 and 64 liters. The importance function for pulse height weighting has not been worked out for these cases but is expected to increase somewhat more steeply than linearly as for the plastic scintillator case (Fig. 4, reference 8). While it might be possible following Czirr and Bowman to linearize the weight function using filters, it is probably best to follow the suggestion of R. C. Block to divide the cylinder into a few separate sections to avoid significant coincidence summing. Quadrants would probably be quite sufficient for this and allow placement of a photomultiplier<sup>13)</sup> at each end of each quadrant. Adding the signals from the two phototubes at the end of a quadrant is a good way to even out the light collection efficiency and make the pulse height more uniform as a function of source position.<sup>14)</sup>

REFERENCES

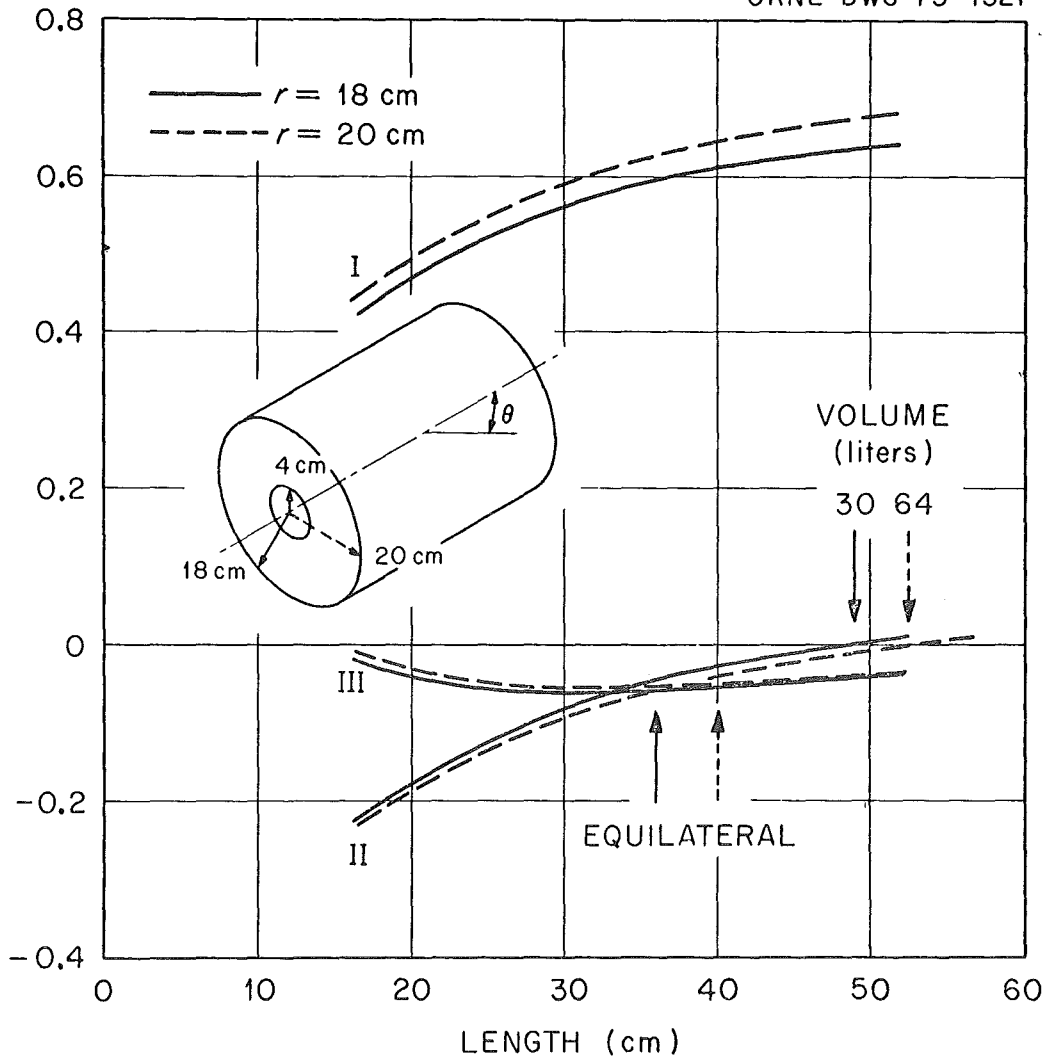
1. L. W. Weston and J. H. Todd have used similar detectors and pulse height weighting for  $\eta$  measurements.
2. Three years ago we considered concentrating on the Fe, Cr, Ni of your conference. The extensive RPI work on capture in these elements, however, led us to check quickly on the chromium isotopes. Substantial agreement with the RPI resonance structure in this case led us to defer further work on those elements. Recent high resolution transmission data on Fe showing many p-wave resonance in  $^{56}\text{Fe}$  above 100 keV have led to a specific request for capture measurements on them. A suitable enriched sample has been procured for this and data taking is expected in Spring '73.
3. R. L. Macklin, Nucl. Instr. and Meth. 91, 79 (1971).
4. R. L. Macklin and B. J. Allen, Nucl. Instr. and Meth. 91, 565 (1971).
5. R. L. Macklin, N. W. Hill and B. J. Allen, Nucl. Instr. and Meth. 96, 509 (1971).
6. M. C. Moxon and E. R. Rae in Neutron Time of Flight Methods, J. Spaepen ed. (European Atomic Energy Community, Brussels, 1961).
7. Some 15% of 7 MeV gamma rays escape from even a very large liquid scintillator (2 meter diameter, 20 cm central duct) for example.
8. This powerful technique was originally pointed out to me by H. Maier-Leibnitz and is described and applied in R. L. Macklin and J. H. Gibbons, Phys. Rev. 159, 1007 (1967).
9. G. Nystrom, B. Lundberg and I. Bergqvist, Physica Scripta 4, 95 (1971).
10. J. B. Czirr and J. S. Lindsey, Nucl. Sci. & Eng. 41, 56 (1970).
11. J. H. Gibbons, R. L. Macklin, P. D. Miller, and J. H. Neiler, Phys. Rev. 122, 182 (1961).
12. F. G. Perey, W. E. Kinney and R. L. Macklin, Proc. Third Conf. Neutron Cross Sections and Technology 191 (1971) ed. R. L. Macklin, USAEC Report CONF-710301.
13. The RCA-4522 Photomultiplier has been used satisfactorily here.
14. E. Haddad et al., Nucl. Instr. and Meth. 31, 125 (1964).

FIGURE CAPTION

Total Efficiency and distortions for an 860 keV gamma source centered in hollow cylinders of  $C_6D_6$ .

- I. Efficiency for an isotropic source as a function of the length of the detector for two outer detector diameters.
- II. Fractional reduction in efficiency for equal  $P_2(\cos \theta)$  distortion of the source angular distribution (i.e.  $1 + P_2(\cos \theta)$  distribution).
- III. Fractional reduction in efficiency for equal  $P_4(\cos \theta)$  distortion of the source angular distribution (i.e.  $1 + P_4(\cos \theta)$  distribution).

ORNL-DWG 73-1321



Some Problem Areas in Capture Cross-section Measurements

M. C. Moxon, D. B. Gayther and M. G. Sowerby

U.K.A.E.A., A.E.R.E., Harwell, Didcot, Berks., U.K.

1. Introduction

This paper outlines some of the problems that have been encountered and are envisaged in the measurement and evaluation of capture cross-sections. Particular emphasis is placed on the cross-sections of the structural materials used in fast reactors. The topics considered are the influence of scattered neutrons, the determination of background, sample thickness corrections, and the theoretical representation of resonance parameters.

2. The Detection of Scattered Neutrons in Capture Detectors

One of the most severe problems in determining the capture cross-sections of Fe, Ni and Cr lies in assessing the relative sensitivity of capture detectors to scattered neutrons. For s-wave resonances at keV energies, the average values of the neutron and capture widths in these elements differ by a factor of  $\sim 10^3$  ( $\bar{\Gamma}_n \approx 1$  keV,  $\bar{\Gamma}_\gamma \approx 1$  eV). Hence if accurate measurements are to be made, detector efficiencies for scattered neutrons ( $\epsilon_n$ ) must be a factor of  $\sim 10^5$  smaller than their efficiencies for capture events ( $\epsilon_\gamma$ ). A number of facts suggest that for many practical detectors this condition may not apply:

- (a) Values of  $\bar{\Gamma}_\gamma$  for p-wave resonances are generally found to be 2-3 times smaller than for s-wave resonances, and this could be due merely to the relative unimportance of scattered neutrons in the p-wave measurements. For example, in Fe-56 for the p-wave resonance at 1.167 keV,  $\bar{\Gamma}_\gamma = 0.67$  eV and  $\bar{\Gamma}_n = 0.056$  eV, while for the 27.9 keV s-wave resonance,  $\bar{\Gamma}_\gamma = 1.44$  eV and  $\bar{\Gamma}_n = 1.67$  keV.
- (b) Capture cross-sections measured with the lead slowing-down time spectrometer, a device with very low sensitivity to scattered neutrons, are generally found to be lower than other values. For example, the Ni data of Kapchigashev and Popov (Atomnaya Energiya 15, 120 (1963)) at 20 keV are a factor of  $\sim 100$  lower than other measurements in the region of the 12 and 16 keV s-wave resonances.
- (c) Activation measurements frequently give relatively low capture cross-sections. For example, the activation data of Grench (Phys. Rev. 140, B1277 (1965)) on Ni-64 from 0.2 to 2 MeV are considerably lower than

the values obtained for natural Ni and Ni-60 by Stieglitz et al (Nuc. Phys. A163, 592 (1971)) using a large liquid scintillator on a linac. Divan et al (Phys. Rev. 120, 556 (1960)) using a large liquid scintillator, however, obtained low cross-sections, although this could be explained by their use of monoenergetic neutrons and time-of-flight measurements which in principle allows separation of scattered neutrons from the prompt gamma-rays.

In contradiction to these arguments, other evidence suggests that  $\Gamma_\gamma$  for s-waves could be considerably larger than 1 eV and the higher measured cross-sections could therefore be correct. In order to explain the well-known thermal capture cross-section of Fe,  $\Gamma_\gamma$  values as high as 2 eV are required for the negative energy resonances which are assumed to be responsible. As another example, Ni-62 has a wide level spacing ( $\bar{D}_0 = 40$  keV) and its high thermal capture cross-section of 14.2 b probably arises mainly from the resonance at 4.6 keV. This resonance has a neutron width of 2.075 keV which would require a  $\Gamma_\gamma$  of 2.31 eV to account for the thermal value.

It should also be mentioned that there are some theoretical grounds for supporting small p-wave radiation widths in this mass region. The main reason arises from the fact that the first levels of opposite parity to the compound nucleus ground state generally occur at excitation energies of  $\sim 2$  MeV. As a result, the initial E1 de-excitation gamma-rays of states formed by s-wave capture can reach compound nucleus states below 2 MeV, while similar transitions for p-wave capture must generally go to states above this energy. The  $E_\gamma^3$  dependence of E1 transition probabilities consequently implies that  $\Gamma_\gamma$  for p-wave capture should be a factor  $\sim 3$  smaller than for s-wave capture. This would not be the case, however, if there was some enhancement of the M1 transitions for p-wave resonances. The radiation widths for d-waves should be similar to those for s-waves, but with a reduction due to the possible higher spins of the resonances by a factor somewhat less than 3.

A number of experimentalists have attempted to determine the ratio  $\epsilon_n/\epsilon_\gamma$  for their capture detectors. Allen and Macklin (Phys. Rev. C3, 1737 (1971)) using a small non-hydrogenous liquid scintillator obtained a value of  $\sim 10^{-4}$  for this ratio while Hockenbury et al (Phys. Rev. 178, 1746 (1969)) obtained a value of  $\sim 10^{-5}$  for their large liquid scintillator\*. Moxon (Thesis HL68/3739 (1968)) estimates the value of  $\epsilon_n/\epsilon_\gamma$  for his Moxon-Rae detector to be  $\sim 1.5 \times 10^{-4}$ .

---

\* Allen and Macklin point out that the resonance parameters originally assumed by Hockenbury et al have been revised and as a consequence the value of  $\epsilon_n/\epsilon_\gamma$  was underestimated by a factor of  $\sim 6$ .

The experimental determinations of  $\epsilon_n/\epsilon_\gamma$  often rely on comparing the measured thick sample capture area of a resonance for which  $\tau_\gamma \ll \tau_n$  (e.g. 85 keV in Mg) with the value obtained when the sample is backed with a thick graphite scatterer. This method is generally inaccurate because  $\tau_\gamma/\tau_n$  is poorly known and corrections for neutrons scattered in the graphite and interacting in the capture sample have not been applied. The multiple scattering correction clearly requires a Monté Carlo treatment.

The determination of  $\epsilon_n/\epsilon_\gamma$  at a particular energy does not necessarily apply at other energies. A thick boron or lithium liner is frequently used between the sample and the capture detector and this must attenuate scattered neutrons by an energy-dependent factor. Another energy-dependent error can occur because the scattered neutrons are not all detected promptly by the capture detector. The backgrounds in linac time-of-flight measurements are often determined with "black" resonance filters, a technique which cannot identify as background prompt pulses from scattered neutrons. The time spread of the "black" resonance dips in the observed spectrum depends on the neutron energy, and consequently delayed pulses from scattered neutrons may be correctly identified as background at high energies, but considered as prompt signal at low energies where the time spread of the resonance dips is large. Fortunately, this and the effect of the liner tend to compensate one another.

One must conclude from this discussion that the efficiency of capture detectors for scattered neutrons is not adequately known. There is a tendency for some experimentalists to tacitly ignore this problem, which must be solved if capture cross-sections for the structural materials are to be measured and evaluated to the requested accuracy of  $\sim \pm 10\%$ .

### 3. Background Measurements

The determination of background occupies an important role in the measurement of small cross-sections. However, in the resolved resonance region, the data are analysed in terms of resonance parameters and the background is frequently determined simply from the counts between resonances. It would be preferable if good background measurements were attempted in order to check that no small smooth capture cross-section underlies the resonance structure. This becomes of increasing importance at energies where the experimental resolution only reveals the presence of large resonances. It is well-known in the case of iron, for example, that the cross-section between resonances calculated from the known parameters is much lower than the directly measured value.

Background measurements in capture cross-section measurements are often difficult and we have a number of comments on the techniques. First, however, it is worth noting that even where the capture cross-sections are relatively large as in U-238 and Pu-239, for example, it has not been possible to make measurements to better than  $\pm 5\%$  to  $\pm 10\%$ . Some of this uncertainty must be due to background problems.

When linac or similar neutron sources and the time-of-flight technique are employed, backgrounds are usually measured by using the "black" resonance filter technique. If no permanent high energy filter is used, then it is imperative that measurements should be made for a number of filter thicknesses, and the measured backgrounds corrected to give the values at zero filter thickness. Some experimenters use the counts from a lead sample to determine the background shape. This technique gives smooth background shapes which can be fitted to the values at the resonance dips. This method cannot be exact because the background must depend on the cross-sections of the capture sample.

Measurements made with Van de Graaff accelerators have a potential advantage if "mono-energetic" neutron sources are used with the time-of-flight technique, as it is possible to virtually eliminate the backgrounds due to directly scattered and room return neutrons. However, in practice the existence of structure in the cross-section can create severe problems when the measurements are made at a limited number of neutron energies.

#### 4. Multiple Scattering and Self-screening Corrections

Large corrections are normally required in capture measurements in structural materials in order to allow for the effects of multiple scattering and self-screening. The corrections are not small because count rate considerations usually make it necessary to use relatively thick samples. Figure 1 shows the results of some Monte Carlo calculations made by Moxon (Nuclear Data for Reactors, 2, 815, IAEA Vienna (1970)) on capture in vanadium. The area under the calculated capture yield curve is plotted as a function of sample thickness and compared with the area for the neutrons captured on their initial collision in the sample. In most measurements the samples normally have a thickness of  $\sim 0.01$  atoms/barn and it can be seen that under these conditions the capture area is  $\sim 50\%$  greater than that for zero sample thickness. It can also be seen that measuring the capture area as a function of sample thickness and then extrapolating to zero thickness does not necessarily give the correct value.

Calculation of the corrections needs accurate representation of the total cross-section, particularly in the energy range below 100 keV. This requires

accurate high resolution total cross-section data which are not always available. Monte Carlo calculations are necessary when the corrections are large, as no other technique appears to have sufficient accuracy and reliability.

#### 5. Resonance Representation

It is necessary in the measurement and evaluation of the structural material cross-sections to represent the data by resonance parameters. Though single level parameters are quite satisfactory for representing the data and can be used to calculate doppler coefficients and self-screened data, they are physically not significant and should not be used as a basis for evaluating average parameters in the unresolved resonance region. R-matrix fits are to be preferred particularly when all the partial cross-sections have not been determined (if, for example, only total cross-section data are available). In this situation s-matrix fits are not satisfactory as the formalism does not ensure that the partial cross-sections sum to the total cross-section.

#### 6. Conclusion

In this paper we have selected for discussion four problem areas in the measurement and evaluation of the capture cross-sections of structural materials. The experimental problems of scattered neutron detection and background determination are not readily resolved and require more attention if the requested accuracy of  $\pm 10\%$  is to be achieved. The interpretation of the data in the form of resonance parameters and the sample thickness corrections, in principle, should not present serious difficulties with available techniques.

The problem of designing a detector with an efficiency for capture events which is independent of the form of the gamma-ray cascade is well understood. The solution of this problem, however, should not be considered in isolation and in particular the sensitivity of the detector to scattered neutrons must remain of paramount importance.

It would be of great assistance to the evaluators of capture cross-sections if experimenters always estimated for their systems, the ratio of the detection efficiency for scattered neutrons to that for capture events.

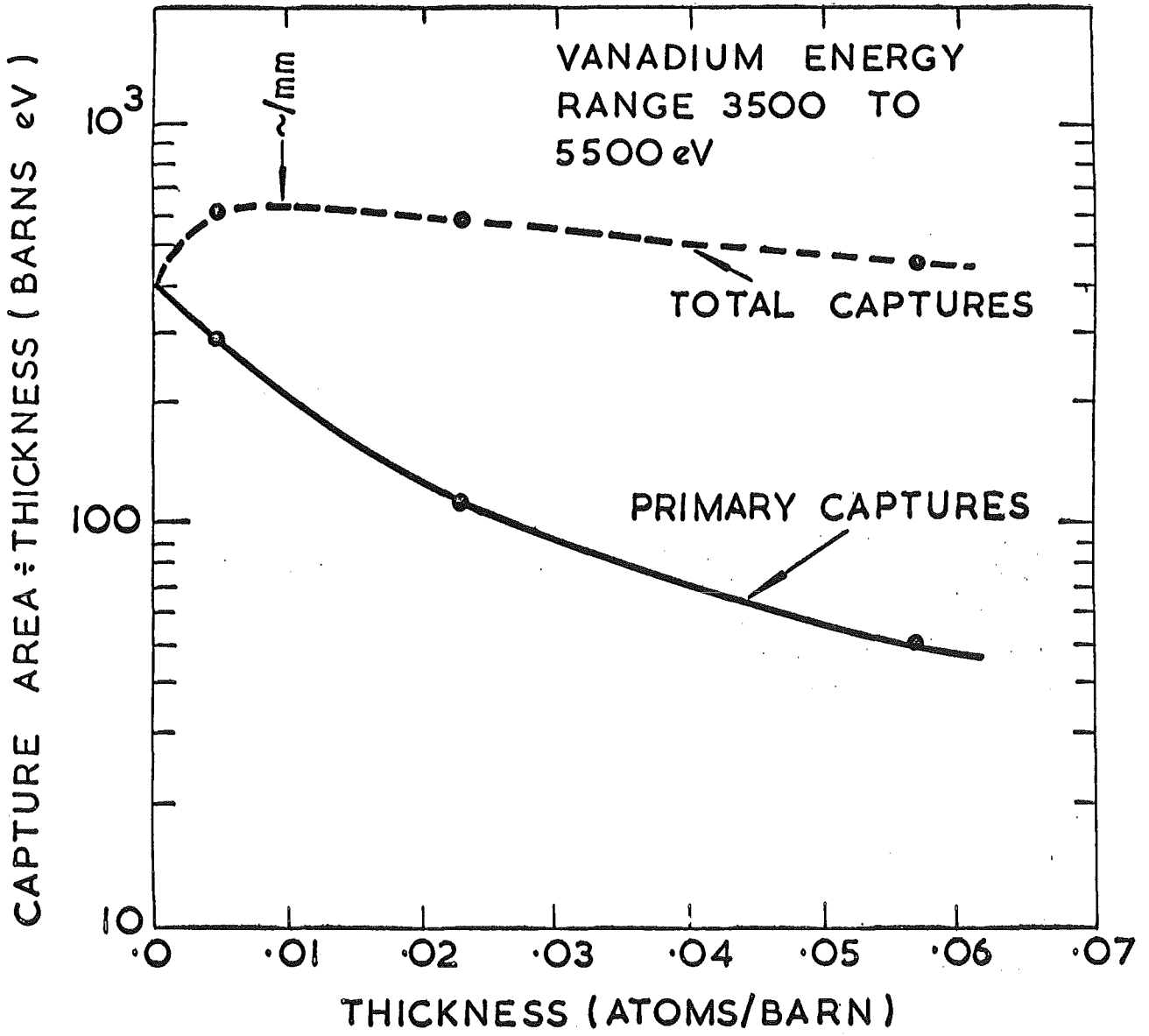


FIG. 1

CAPTURE CROSS SECTION MEASUREMENTS  
ON REACTOR STRUCTURAL MATERIALS WITH A  
LARGE LIQUID SCINTILLATOR DETECTOR

R.R. Spencer, H. Beer  
Kernforschungszentrum Karlsruhe  
Institute für Angewandte Kernphysik

ABSTRACT

A brief, general outline is given of the use of the large liquid scintillator for measurement of the capture cross sections of medium weight nuclei in the resolved resonance region. The method of data reduction and some examples of the results on  $^{50}\text{Cr}$  and  $^{54}\text{Fe}$  are shown.

## 1. INTRODUCTION

A large portion of the applied physics effort of the Kernforschungszentrum Karlsruhe, Van-de-Graaff-group over the past several years has been devoted to the measurement of the capture cross sections of reactor structural materials in the keV neutron energy region (i.e. 10 - 200 keV).

For the materials chromium, iron and nickel 11 isotopes have been measured.

This covers all the stable isotopes of these three elements except

$^{54}\text{Cr}$  and  $^{58}\text{Fe}$ . Emphasis has been placed on the determination of the

resonance parameters for the individual isotopes, hence the restriction

to energies less than 200 keV where individual resonances can be resolved.

The purpose of this paper is to give a brief description of the measurements

and the resulting analysis with particular regard to factors which signi-

ficantly affect the precision of the results. Since the experimental

details and the data analysis leading to the derived resonance parameters

are necessarily complex, and since the experimenters present are

generally familiar with these details, the following outline is directed

toward those users and evaluators unfamiliar with the use of the large

scintillator tank for capture measurements.

## 2. EXPERIMENTAL ARRANGEMENTS

Neutrons for the capture measurements were produced by means of the  $^7\text{Li}(p,n)^7\text{Be}$  reaction. Proton pulses 1 ns in width and at a 500 kHz repetition rate are incident on a relatively thick (150 keV) lithium target. The resulting neutrons then traverse a 2 meter flight path to the sample and prompt capture gamma-rays are detected in the scintillator tank. The Karlsruhe tank<sup>(1)</sup> is shown in the first slide. It is approximately 1.1 meter diameter, contains approximately 800 liters of NE 224 liquid scintillator<sup>+</sup> and has a 10 cm diameter through hole for placement of the sample at the tank center. The scintillator is viewed by 12 60 DVP photo-multiplier tubes, the outputs of which are matched in both pulse height and time and then summed. This

---

<sup>+</sup> Nuclear Enterprises Limited

system results in relatively good pulse height resolution ( $\approx 16\%$  for the 2.5 MeV  $^{60}\text{Co}$  sum peak) and excellent time resolution (4-5 ns).

Three important properties of this detector result from its large size:

- 1.) The large volume insures a high detection efficiency. The interaction probability for a single gamma ray of 8 MeV is over 60 % and for a cascade of multiplicity 3 or more the interaction probability has been estimated to be  $0.97 \pm 0.03$   $\sqrt{1}$ .
- 2.) The  $4\pi$  geometry eliminates any consideration of non-isotropic gamma ray distributions.
- 3.) The large volume also insures a large background counting rate and large amounts of shielding consequently.

The samples, which for these measurements consisted of powdered oxides or powdered metal, were contained in 8 cm diameter, bronze, thin walled holders. The neutron beam was carefully collimated to fall within the sample area. The sample, a carbon scatterer, and a 1 mm thick gold "standard" were cycled into the detector, cycling intervals being determined by a proton beam current integrator. This procedure averages out fluctuations in neutron intensity.

The thickness of the carbon scatterer is chosen to give a scattering intensity equivalent to the "hard sphere" scattering of the sample. This matching of the carbon to the sample scattering can never be exact in practice and the resulting mismatch leads to a possible systematic error that is important primarily in the regions between resonances and which can be of the order of .5 mb.

The data, which consist of all gamma ray events between about 3 MeV and an energy well above the neutron binding energy, are stored by an on-line computer for each sample position into an 8 x 512 channel, pulse height vs. time array. The lower threshold of 3 MeV is set in order to avoid any effect due to the 2.2 MeV gamma ray resulting from capture of scattered neutrons in the hydrogen of the scintillator. This type of background is reduced considerably by addition of tri-methyl borate to the scintillator, but is still a problem as scattering events in the sample are of the order of 1000 times more probable than capture events.

### 3. REDUCTION OF DATA

Values of capture yield per sample thickness are computed from the counts per channel data after summing the appropriate pulse height channels by means of the following formula:

$$"σ_{\gamma}" = \frac{(C_X - C_{SX})}{(C_A - C_{SA})} \cdot \frac{N_A}{N_X} \cdot \frac{\epsilon_A}{\epsilon_X} \cdot \sigma_{\gamma A}$$

where  $C_X, C_A$  are counts per channel for the sample and gold standard, respectively

$N_X, N_A$  are thicknesses for sample and gold

$\epsilon_X, \epsilon_A$  are the spectrum fractions for sample and gold

$C_{SX}, C_{SA}$  are backgrounds

and  $\sigma_{\gamma A}$  is the gold capture cross section.

Energies corresponding to each time of flight channel are computed from the measured flight path and the time of each channel relative to the position of the "prompt"  $\gamma$ -ray peak from the lithium target (corrected for the photon time of flight and for non-linearity of the time analyzer). The spectrum fractions used are in general an average for each sample and result from the lack of data below our 3 MeV pulse height threshold. Since the shape of this spectrum below threshold is unknown an assumption as to its shape must be made and a liberal error, usually of the order of 10 %, is assigned to these values.

The overall error of the capture yield which includes statistical error, error in the gold cross section, and error in the spectrum fraction, is computed for each channel.

The results to this point are shown for  $^{50}\text{Cr}$  and  $^{54}\text{Fe}$  in slides 2 through 5. These slides also show the corresponding total cross sections of each isotope computed from fits to transmission measurements. The complexity of the capture curves are somewhat startling in comparison to the total cross section plots and suggest that the capture cross sections of some of the less abundant isotopes should be considered in computations of the

capture for the natural material. It also is apparent that p-wave and perhaps higher l-wave capture is an important effect.

The last phase of data reduction consists of area analysis of the resolved resonances. Integrated capture yields are determined for each resonance. For ideal thin targets these areas are equal to

$$A = 2 N \pi^2 \lambda_0^2 g \Gamma_n \Gamma_\gamma / \Gamma$$

where

N	is target thickness
$\lambda_0$	is the neutron wave length at resonance
g	is the statistical factor
$\Gamma_n, \Gamma_\gamma, \Gamma$	are the neutron, gamma and total widths, respectively.

This result is essentially independent of resolution. Although the samples in the present experiments were thin as far as capture is concerned, they are not thin for scattering, particularly in the large s-wave resonances. Therefore corrections must be made for multiple scattering and resonance self-protection effects. These corrections are carried out by a Monte-Carlo-calculation using the FORTRAN IV program TACASI<sup>(2)</sup>. When values of g and  $\Gamma_n$  are available from transmission measurements  $\Gamma_\gamma$  may be computed. Otherwise the analysis results in values of  $g \Gamma_n \Gamma_\gamma / \Gamma$ . Tables I thru IV show our results for <sup>50</sup>Cr and <sup>54</sup>Fe. The data are complete and available also for <sup>52</sup>Cr, <sup>53</sup>Cr, <sup>57</sup>Fe, <sup>62</sup>Ni and <sup>64</sup>Ni.

When considered along with the data of Ernst, et al.<sup>(3)</sup> and Stieglitz et al.<sup>(4)</sup> capture measurements on enriched samples of all the stable isotopes of chromium, iron, and nickel have been made with the exception of <sup>58</sup>Fe, which has a very low abundance (0.33 %).

REFERENCES

- (1) D. KOMPE, Nucl. Phys. A 133 (1969) 513.
- (2) F.H. FRÖHNER, General Atomic Report GA-6906 (1966).
- (3) A. ERNST, F.H. FRÖHNER, D. KOMPE, Second Int. Conf on Nucl. Data for Reactors, Paper CN-26/11 (IAEA, Vienna 1970).
- (4) R.G. STIEGLITZ, R.W. HOCKENBURY and R.C. BLOCK, Nucl. Phys. A 163 (1971) 592.

TABLE I      The s-wave resonances of  $^{50}\text{Cr}$

$E_0$ (keV)	$\Gamma_n$ (keV)	$\Gamma_\gamma$ (eV)	% Multiple Scattering
$28.43 \pm 0.09$	$0.415 \pm 0.010$	$0.47 \pm 0.09$	10
$37.32 \pm 0.12$	$2.24 \pm 0.03$	$1.97 \pm 0.30$	25
$54.99 \pm 0.18$	$0.281 \pm 0.017$	$0.69 \pm 0.13$	2
$64.8 \pm 0.2$	$0.043 \pm 0.020$		
$94.75 \pm 0.4$	$1.67 \pm 0.05$	$0.65 \pm 0.14$	6
$114.8 \pm 0.5$	$0.12 \pm 0.05$		
$129.0 \pm 0.6$	$0.54 \pm 0.08$	$1.48 \pm 0.30$	2
$156.6 \pm 0.7$	$1.23 \pm 0.11$		
$162.45 \pm 0.8$	$0.75 \pm 0.10$		
$185.2 \pm 0.9$	$3.52 \pm 0.14$		
$218.3 \pm 1.2$	$0.17 \pm 0.13$		
$231.6 \pm 1.2$	$0.94 \pm 0.15$		
$245.6 \pm 1.4$	$0.20 \pm 0.15$		
$276.6 \pm 1.5$	$1.9 \pm 0.2$		
289.8      -	3.7		

TABLE II      The  $l > 0$  resonances of  $^{50}\text{Cr}$

$E_0$ (keV)	$g\Gamma_n$ (keV)	$g\Gamma_n \Gamma_\gamma / \Gamma$ (eV)	$g\Gamma_\gamma$ (eV)
18.60 ± 0.07		0.57 ± 0.09	
19.18 ± 0.07		0.46 ± 0.08	
24.08 ± 0.10		0.08 ± 0.02	
24.84 ± 0.11		0.31 ± 0.06	
33.45 ± 0.18		0.85 ± 0.12	
35.4 ± 0.2		1.51 ± 0.21	
40.6 ± 0.2		0.86 ± 0.13	
46.7 ± 0.3		0.69 ± 0.10	
50.0 ± 0.3		0.56 ± 0.10	
53.4 ± 0.3		0.68 ± 0.12	
59.1 ± 0.4		1.05 ± 0.16	
63.5 ± 0.4			
65.6 ± 0.5			
70.2 ± 0.5			

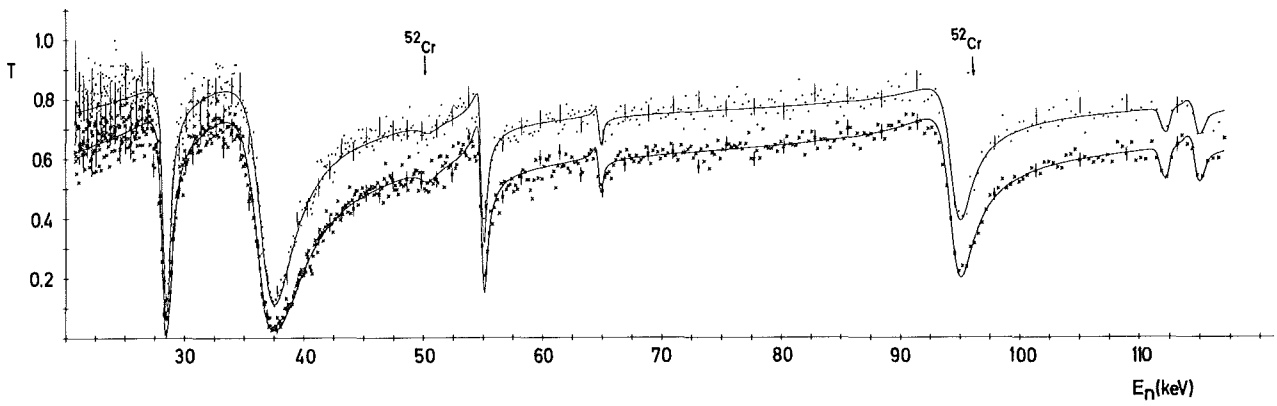
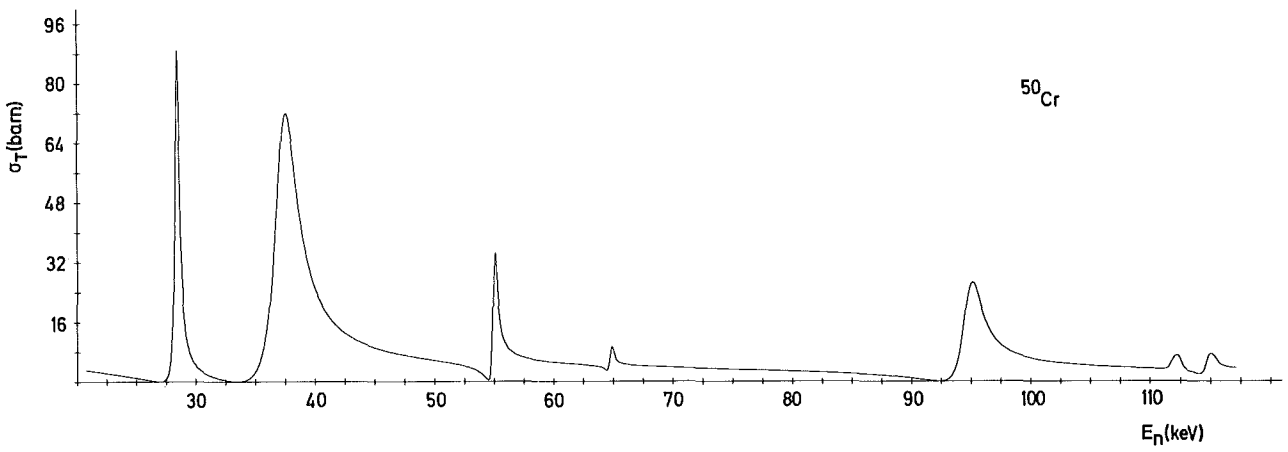
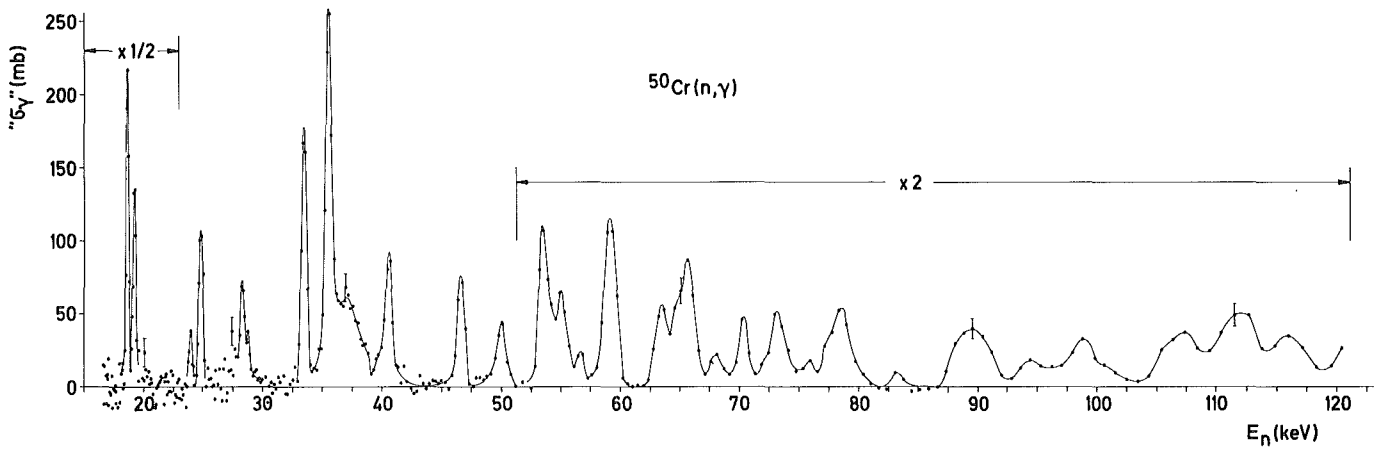
TABLE III      The s-wave resonances of  $^{54}\text{Fe}$

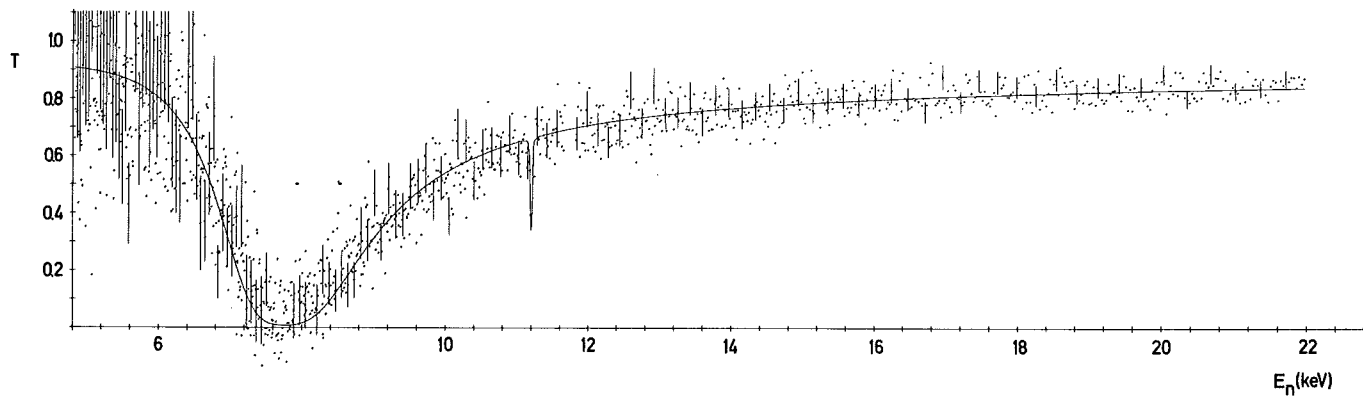
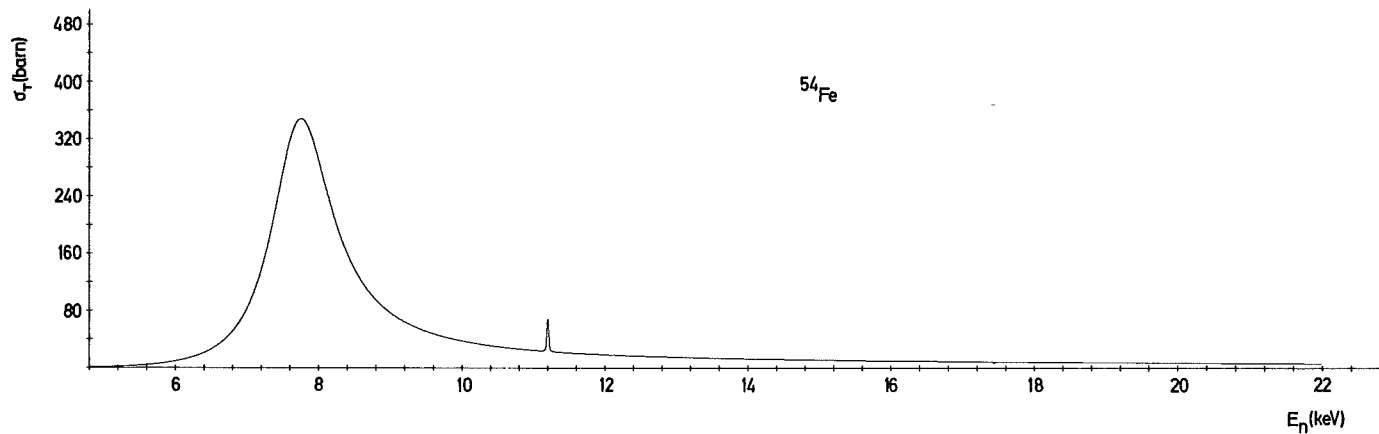
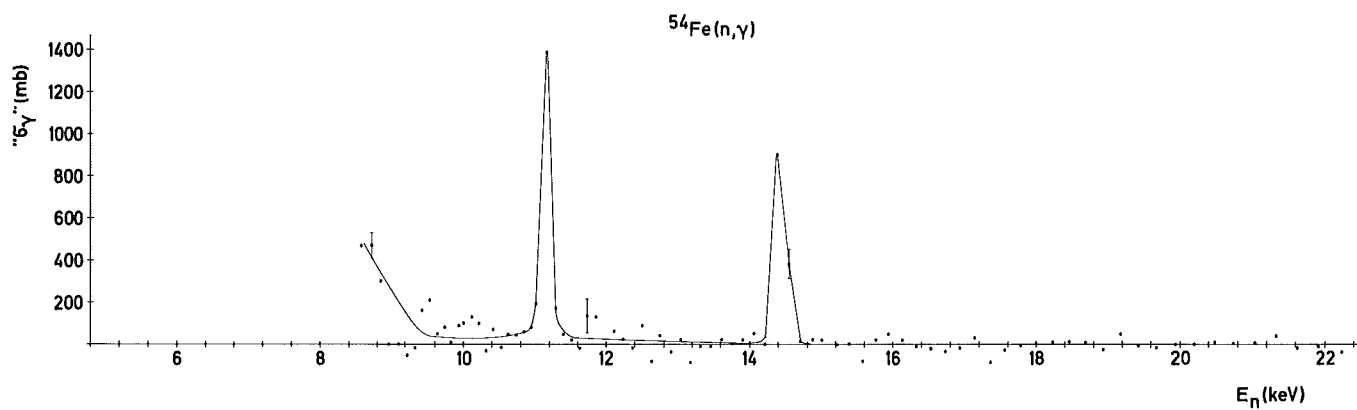
$E_0$ (keV)	$\Gamma_n$ (keV)	$\Gamma_\gamma$ (eV)	% Multiple Scattering
$7.67 \pm 0.02$	$1.01 \pm 0.01$		
$52.78 \pm 0.18$	$2.16 \pm 0.02$	$1.8 \pm 0.3$	23
$71.86 \pm 0.25$	$1.77 \pm 0.03$	$0.8 \pm 0.2$	12
$98.5 \pm 0.4$	$0.51 \pm 0.05$	$3.2 \pm 0.5$	11
$129.6 \pm 0.5$	$3.00 \pm 0.09$	$3.0 \pm 0.6$	9
$147.1 \pm 0.7$	$2.75 \pm 0.11$	$3.0 \pm 0.6$	5
$159.0 \pm 0.8$	$0.18 \pm 0.09$	$3.9 \pm 0.8$	1
$173.9 \pm 0.8$	$2.8 \pm 0.1$	$2.4 \pm 0.5$	2
$191.2 \pm 1.0$	$42.4 \pm 0.5$		
$222.8 \pm 1.2$	$1.57 \pm 0.14$		
$230.2 \pm 1.2$	$0.26 \pm 0.14$		
$245.7 \pm 1.3$	$24.6 \pm 0.6$		

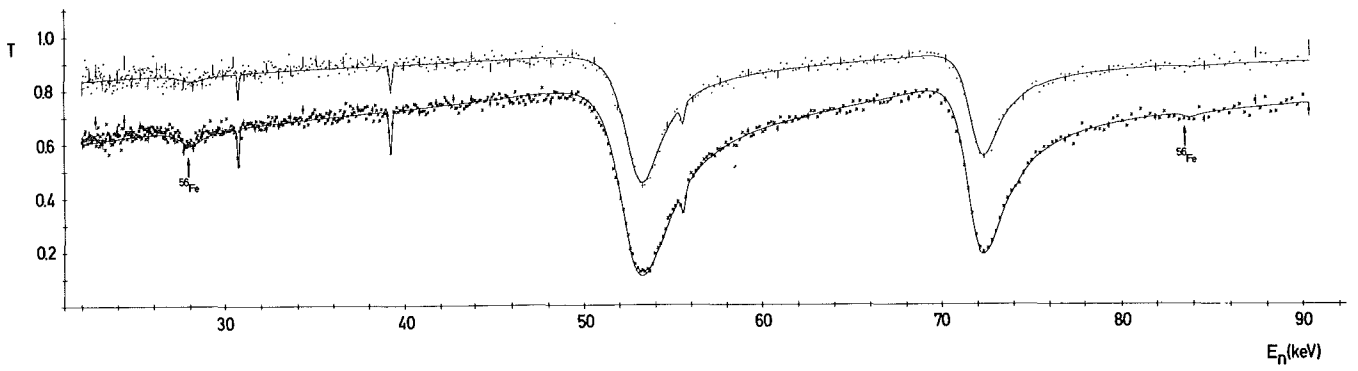
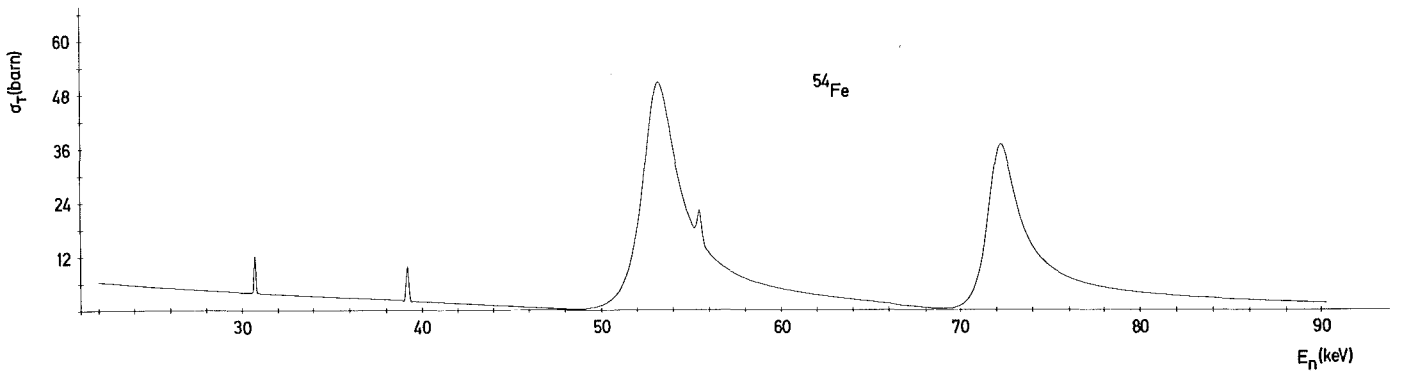
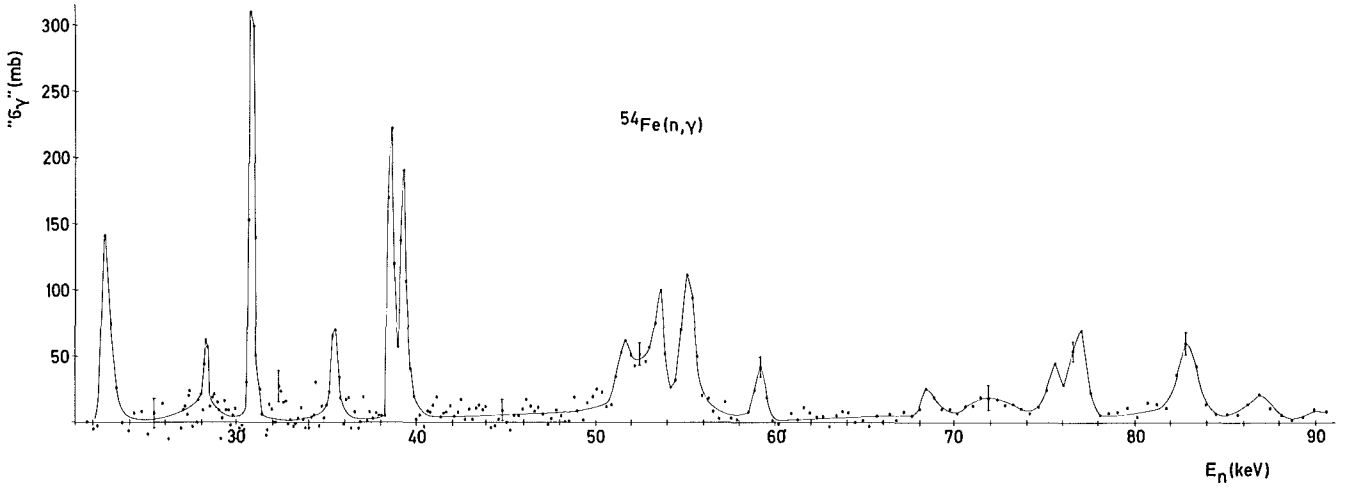
TABLE IV

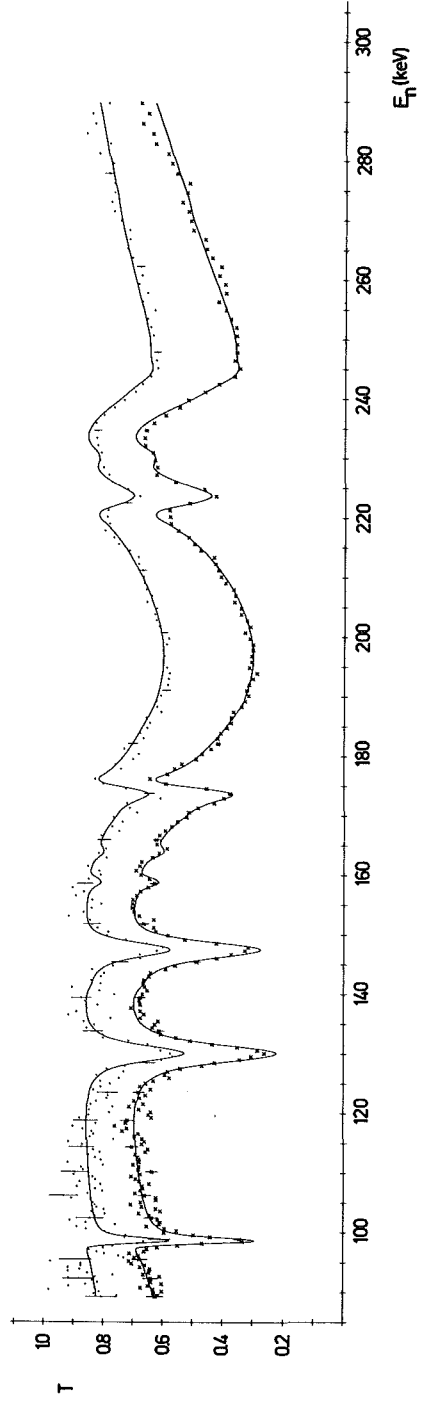
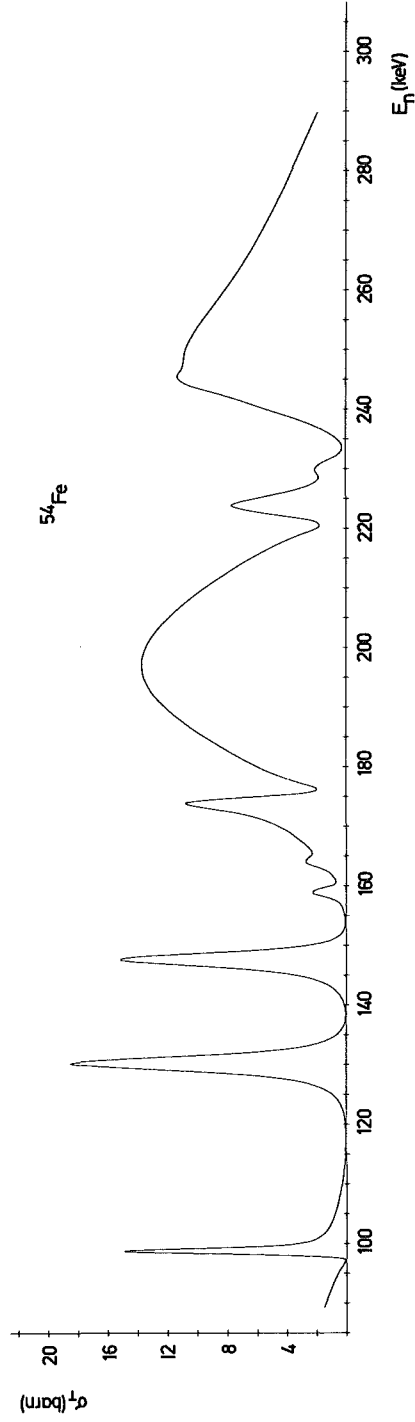
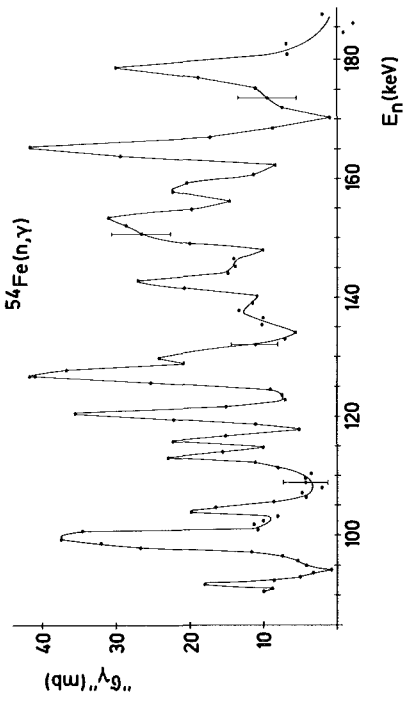
The  $\ell > 0$  resonances of  $^{54}\text{Fe}$

$E_0$ (keV)	$g\Gamma_n$ (keV)	$g\Gamma_n \Gamma_\gamma / \Gamma$ (eV)	$g\Gamma_\gamma$ (eV)
11.19 ± 0.03	≈0.007	0.80 ± 0.16	≈0.9
14.44 ± 0.08		0.92 ± 0.16	
22.97 ± 0.16		0.57 ± 0.11	
28.24 ± 0.10		0.16 ± 0.06	
30.70 ± 0.10	≈0.010	1.07 ± 0.16	≈1.2
35.31 ± 0.15		0.33 ± 0.07	
38.5 ± 0.2		1.00 ± 0.15	
39.18 ± 0.12	≈0.015	1.31 ± 0.19	≈1.4
51.7 ± 0.3		0.40 ± 0.08	
53.7 ± 0.4		0.76 ± 0.11	
55.46 ± 0.19	0.03 ± 0.02	0.90 ± 0.13	0.9 ± 0.7
59.3 ± 0.3		0.46 ± 0.08	
68.8 ± 0.4		0.5 ± 0.1	
75.9 ± 0.5		1.0 ± 0.2	
77.4 ± 0.5		1.5 ± 0.3	
83.4 ± 0.5		≈1.7	
87.4 ± 0.6		0.8 ± 0.2	
104.3 ± 1.0		1.1 ± 0.2	
113.0 ± 0.8		1.5 ± 0.3	
115.7 ± 0.8		1.3 ± 0.2	
120.3 ± 0.8		2.6 ± 0.4	
126.3 ± 1.0		2.3 ± 0.3	
142.4 ± 1.2			
152 ± 2			
165 ± 1.5			









SUMMARY ON TOPIC I : EXPERIMENTAL DATA

F. H. Fröhner\*

(NEA Centre de Compilation de Donnees  
Neutroniques, Saclay, France)

1. New Capture Data

New experimental results were reported by the groups at Karlsruhe and at Cadarache.

The Karlsruhe group measured capture yields with a large liquid scintillator detector and transmissions and derived resonance parameter sets for  $^{56}\text{Fe}$ ,  $^{58}\text{Ni}$ ,  $^{60}\text{Ni}$ ,  $^{61}\text{Ni}$  (Ref. 1) and for  $^{50}\text{Cr}$ ,  $^{52}\text{Cr}$ ,  $^{53}\text{Cr}$ ,  $^{54}\text{Fe}$ ,  $^{57}\text{Fe}$ ,  $^{62}\text{Ni}$ ,  $^{64}\text{Ni}$  (Ref. 2). Where previously published parameters exist the agreement is reasonably good - especially with the results of the RPI group (Refs. 3, 4). These parameter sets reproduce the capture cross sections with an estimated accuracy of 15-25% up to about 100 keV for the even, to about 30 keV for the odd isotopes - at least within the limits of the experimental resolution. Unresolved doublets or other unresolved structures do not influence calculated group cross sections or resonance integrals very much. They can, however, influence level-statistical conclusions. Parity assignments should always be regarded as tentative except for the broad s-wave levels.

Above the rather completely parametrized energy region of resolved resonances sample thickness effects, i. e. self-protection and multiple scattering, are practically negligible in the Karlsruhe data. The capture yield divided by the sample thickness (in nuclei/b) can therefore be directly equated to the capture cross section. In this region, on the other hand, no gaps exist normally between resonance peaks where background subtraction can be checked directly. This causes uncertainties of perhaps 15-30% for the capture yields and cross sections.

The Cadarache group reports capture cross sections obtained with a total-energy detector at somewhat higher energies: 70-550 keV (Refs. 5, 6). The error estimates of the authors imply accuracies of roughly 5% for gold and somewhat higher errors for the natural elements chromium, iron and nickel. Even if one would assign more liberal errors to e. g. the flux determination, capture detector efficiency calibration and sample

---

\*) On leave from Kernforschungszentrum Karlsruhe, Germany

thickness corrections the accuracy of the method is impressive: 5-10% overall error in the capture cross section. One drawback is the difficulty to measure capture cross sections of isotopic mixtures with widely differing binding energies of the components - a difficulty which also exists for the Moxon-Rae detector.

It is interesting to note that the Cadarache data appear to confirm the higher capture cross sections for chromium, iron and nickel obtained during the past years, whereas for the monotope gold the values of Pönitz (Ref. 7) are confirmed rather than the higher evaluated values of Vaughn and Grench (Ref. 8).

## 2. Error Sources

A recurring topic during the session were error sources, treated for example in a contribution from Harwell (Ref. 9). The following conclusions were reached:

### 2.1. Scattered and then promptly captured neutrons:

It was agreed that one of the most serious problems is the sensitivity of capture detectors to scattered neutrons. A constant background is relatively easy to subtract, but the time-dependent background produced by scattered and subsequently captured neutrons is a source of serious difficulties in time-of-flight measurements. The usual method of measuring this time-dependent background by replacing the sample with a carbon or lead scatterer may work adequately when scattered neutrons cannot be captured very close to the sample and the scattering properties of sample and scatterer are matched well. This means that sample containers must be as light as possible if they cannot be avoided completely, so that neutrons scattered in a resonance cannot be captured close to the sample but reach the detector or other capturing material only long after the capture photons from the sample have been registered. It means also that the energy range of the neutron spectrum should be limited (e. g. not contain the thermal region), so that the average scattering cross sections of sample and scatterer can be matched over the whole range. Because of the shorter time scale and the mode of neutron production both conditions are easier to fulfill at pulsed Van de Graaff accelerators than with linac sources.

Where resonances are well resolved the gaps between widely separated peaks can be used to check on the background subtraction, so the resulting uncertainty of e. g. resonance areas can be quite small (a few percent). At higher energies such gaps do not normally exist and uncertainties will be higher (10-20%, say).

It was recommended (in Ref. 9) to check the effect of scattered and promptly captured neutrons by using a carbon sample with a black-resonance filter in front of it as described in Ref. 3.

Another check on the relative efficiency of the capture detector for neutrons and photons is possible with monoenergetic neutrons by means of purely scattering samples and samples with known ratio of capture to scattering cross section.

Le Rigoleur proposed a third method which is feasible at the Cadarache installation, namely to place the neutron-producing  $^7\text{Li}$  target in the middle of the capture detector.

## 2.2. Sample thickness corrections:

Corrections for self-protection and multiple scattering are quite important for the structural materials, especially for the heavily scattering broad s-wave resonances. Monte Carlo codes exist for area analysis of resonances which can be described by (sums of) single-level cross section formulae. Most of the published radiation widths of the structural materials were extracted by means of such codes. The fact that a positive correlation was found between the neutron and radiation widths for many chromium isotopes and for  $^{60}\text{Ni}$  caused some suspicion that the analysis methods could be at fault, in particular the description of the scattering cross sections of these nuclides by essentially single-level expressions. Moxon reported that he tried both single-level and multi-level cross section representations for the first broad s-wave resonance of  $^{58}\text{Ni}$  and obtained essentially the same result. Another hint that the single-level representation used in area analysis codes is not the cause of the observed correlations is the fact that the Karlsruhe group found correlations for some isotopes but not for others where exactly the same analysis methods were employed.

The errors due to the analysis methods, in particular the self-protection and multiple-scattering corrections, were estimated as relatively small (a few percent)

## 2.3. Efficiency calibration:

The efficiency of the capture gamma ray detector is another source of uncertainty. The total-energy detector at Cadarache was calibrated with gamma ray sources of known intensity. The combined error for the weighting function and its linearity is estimated as of order 2-4%.

The efficiency of the liquid-scintillator tank at Karlsruhe is determined by a measurement of the gold cross section, which is known to about 5% near 30 keV and to 10% at the lowest and highest energies used

(7 and 250 keV). The RPI group, on the other hand, used the  $^{10}\text{B}(n, \alpha)$  cross section to determine the neutron spectrum shape and the black-resonance technique for absolute calibration, which yields probably an accuracy of 3% near the calibration point in the eV region and 5-10% at keV energies.

#### 2.4. Capture spectrum fluctuations:

The fact that the strength of the ground-state and other high-energy transitions varies from resonance to resonance and its implications for tank measurements on structural materials was discussed in Ref. 1. It was stated that the capture cross section uncertainty caused by this effect is about 5-15% and can be reduced somewhat with the help of pulse height data for individual resonances. Moxon-Rae detector measurements, on the other hand, are not affected. Total-energy detector measurements are slightly afflicted; the estimated error for the Cadarache detector is less than 2%.

### 3. Recommendations

The following recommendations were made:

- (1) Supplementary measurements should be undertaken to determine the detector sensitivity to scattered and promptly captured neutrons - at Karlsruhe with scatterer plus resonance filter, at Cadarache with the neutron source at the sample position in the centre of the capture detector - with utilisation of monoenergetic neutrons in both laboratories, as explained in Sect. 2.1.
- (2) Barre recommended that the capture cross section of stainless steel be measured directly. This would best be done at Karlsruhe, since the large liquid scintillator detector is not afflicted by the difficulties which beset the Moxon-Rae detector and the total-energy detector with regard to isotopic mixtures.
- (3) Natural samples of chromium and nickel should be measured below 70 keV so that consistency with the already measured capture cross sections of the individual isotopes can be checked - again at Karlsruhe.

References

1. F. H. Fröhner, contribution to this panel;
2. R. R. Spencer and H. Beer, contribution to this panel;
3. R. W. Hockenbury et al., Phys. Rev. 178(1969)1746;
4. R. G. Stieglitz et al., Nucl. Phys. A163(1971)592;
5. C. Le Rigoleur and A. Arnaud, contribution to this panel;
6. C. Le Rigoleur et al., contribution to this panel;
7. W. P. Pönitz et al., J. Nucl. En- 22(1968)505
8. F. J. Vaughn and J. A. Grench, Proc. 3rd Conf. on Neutron Cross Sections and Technology, Knoxville, 1971, p. 430
9. M. C. Moxon et al., contribution to this panel.

TOPIC II

EVALUATED DATA

A COMPARISON BETWEEN SINGLE LEVEL AND MULTILEVEL CALCULATIONS  
OF NEUTRON CROSS SECTIONS IN THE RESONANCE REGION (\*)

T. Martinelli, E. Menapace, M. Motta and G.C. Panini  
Centro di Calcolo del CNEN, Bologna, Italy

SUMMARY

The aim of the present paper is a comparison of cross sections and deduced group averaged values resulting from the application of single level and multilevel formulas to the same multilevel resonance parameters. The parameters were partly taken from Karlsruhe Centre's publications and communications and partly from ENDF/B-III. They refer to isotopes or elements of great importance, owing to their utilizations as structural material in the reactor construction.

(\*) Paper presented at the meeting on  
"The keV Capture of the Structural Materials Ni, Fe, Cr"  
held in Karlsruhe 8-9 May 1973.

## INTRODUCTION

The aim of the present paper is the comparison of neutron cross sections and their group averaged values in resonance region, calculated by means of single level and multilevel formalisms, respectively.

Following a suggestion of Karlsruhe Nuclear Centre's people who have also kindly furnished the set of multilevel resonance parameters, the nuclides of structural materials, such as  $\text{Cr}^{50}$ ,  $\text{Cr}^{52}$ ,  $\text{Ni}^{62}$  and  $\text{Ni}^{64}$  have been considered [1]. For more completeness, the same calculations have been performed on the nuclides of the ENDF/B-III list, for which the multilevel parameters are given.

The codes for reactor physics calculation generally utilize cross section libraries which are compiled through the application in the resonance region of single level Breit-Wigner formula, even if the experimentalists give a multilevel set of resonance parameters. In such a case the usual single level calculations might generate non negligible differences in the cross sections and, consequently, in their group averaged values.

In order to examine the amount of such possible differences, some calculations here presented were performed through the multilevel formalism described in Feshbach, Porter and Weisskopf's well known paper on the "Model for Nuclear Reactions with Neutrons" [2].

No fissile materials have been considered, so that the multilevel formalism has to be applied only to the elastic scattering cross section for which the assumption of a single reaction exit channel may be an acceptable approximation. For the capture reaction, the large number of open channels makes the interferential effects to vanish, due to the random distribution of signs for the reduced amplitude widths; then the capture reaction can be treated by the single level formalism, and the differences between multilevel and single level calculations can here be attributed to the elastic cross section.

THE FORMALISM

The multilevel formula in the Feshbach approximation is a hermitean form which will be here written more conveniently using a matrix formalism, by generalization of the procedure illustrated in ref. [3] for non elastic reactions.

The main advantage of the matrix representation lies first in the separation of energy dependent quantities from the constant quantities which characterize the set of resonances, the last being all included in a central matrix. In second place, if elastic reaction is considered, a better evidence is given to the terms which are responsible for the interferences of either the resonance scattering or the resonance to potential scattering interaction.

Then, the expression for the multilevel, one exit channel cross section for reaction of type  $x$ , can be written as

$$\sigma_x(E) = (\pi\lambda^2) \times M_{jk} z^j \bar{z}^k$$

where Einstein's convention for summation is adopted and the bar indicates complex conjugate element. Calling  $M$  the square symmetric matrix with elements  $M_{jk}$  and  $z$  the column vector with elements  $z^k$ , the above expression in matrix form becomes

$$\sigma_x(E) = (\pi\lambda^2) \times z^+ M z$$

being  $z^+$  the adjoint vector of  $z$ .

If the number of levels is "N" and the maximum value of the  $\ell$  quantum number is "L" the vector  $z$  and matrix  $M$  are so defined:

a) The matrix  $M$  is square, symmetric of order  $(L+N)$  and can be partitioned in submatrix A, B, C, as follows

$$M = \begin{array}{c} \left. \begin{array}{cc} \overbrace{\quad\quad}^L & \overbrace{\quad\quad}^N \\ \left[ \begin{array}{cc} A & B \\ \hline \tilde{B} & C \end{array} \right] \end{array} \right\} \begin{array}{l} L \\ N \end{array} \end{array}$$

For non elastic reactions, the matrices A and B are zero. For the elastic reaction the submatrix A refers to the potential scattering, C to the resonance reaction and B to the interference between potential and resonance scattering ( $\tilde{B}$  is the B transposed matrix).

The matrix A is diagonal with real elements (numbered from index zero, for the sake of simplicity)

$$a_{\ell k} = (2\ell+1)\delta_{\ell k} \quad (\ell = 0,1,\dots,L)$$

$\ell$  being the quantum number and row index simultaneously.

b) The matrix C is real symmetric, expressed by

$$c_{jk} = u_j \times u_k \quad (j,k = L+1,\dots,L+N)$$

being

$$u_j = \left[ g \frac{\Gamma_n \Gamma_x}{P_\ell(E_j)} \right]_j^{\frac{1}{2}}$$

where  $g$  is the statistical factor,  $P_\ell(E_j)$  the penetration factor,  $\Gamma_n$  the neutron width of the entrance channel and  $\Gamma_x$  the width of the exit channel for the examined decay process. It will be  $\Gamma_x = \Gamma_n / P_\ell(E_j)$  in the case of the elastic reaction. The  $j$ -label means that all the quantities are those of the corresponding level at the energy  $E_j$ .

Every diagonal  $j$ -element of C gives rise to the single level Breit-Wigner formula for each  $j$ -level, while the non diagonal terms  $jk$  refer to the interference between the levels of index  $j$  and  $k$  of the same spin and parity. In any other case the non diagonal elements must be put equal to zero.

c) The elements of rectangular real matrix B (dimension  $L \times N$ ) will not be zero only in the places where the row index is equal to the quantum number  $\ell$  of the  $j$ -resonance. In such a case they are

$$b_{\ell j} = g_j^{\frac{1}{2}} u_j \quad (\ell = 0,1,\dots,L) \\ (j = L+1,\dots,L+N)$$

The energy dependent vector  $z$  can be partitioned in two subvectors with  $L$  real (i.e. imaginary part always equal to zero) and  $N$  complex elements respectively, given by:

$$z^{\ell}(E) = 2 \sin \phi_{\ell}(E) \quad (\ell=0, 1, \dots, L)$$

$$z^j(E) = \frac{P_{\ell}^{\alpha}(E)}{e^{i\phi_{\ell}} \left[ (E_j - E) + i \frac{\Gamma_j}{2} \right]} \quad (j=L+1, \dots, L+N)$$

with the exponent  $\alpha=2$  for the elastic reactions and  $\alpha=1$  for any other reaction.  $i$  is the imaginary unit.

$\phi_{\ell}$  is the phase shift at energy  $E$  for  $\ell$  wave resonances,  $\Gamma_j$  the total width of the  $j$ -level and  $P_{\ell}(E)$  is the neutron  $\ell$ -wave penetrability at energy  $E$ , being the  $j$ -level related to  $\ell$ -wave neutrons.

The first  $L$  elements of the  $z$  vector can be put zero in the case of non elastic reactions; they correspond, in the product for  $\sigma(E)$ , to the elements of the submatrices  $A$  and  $B$ .

From the above matrix formalism, it can be easily understood that accidental negative values of elastic cross section may result from the single level calculation. In fact, in such a treatment all the non diagonal elements of the matrix  $C$  are put equal to zero, while the non zero elements of matrix  $B$  are conserved and contribute to the final value. By this way, only a part of interferences coming from the mixed terms of the positive definite matrix  $M$  is suppressed with the consequence that negative values for the elastic cross section may appear in some energy points.

Looking at the elements  $c_{jk}$  of the  $C$  matrix it must also be observed that no uncertainty of sign can arise from the square root operation on  $\Gamma_n$ , when elastic cross section is considered; in fact,  $\Gamma_x = \Gamma_n / P_{\ell}(E_j)$  and the plus sign is only possible for the  $u_j u_k$  products. Consequently, a unique curve exists for the multilevel elastic cross section with interference.

## CALCULATIONS AND COMMENTS

The performed calculations include:

- 1) Tabulated list of capture, elastic and total cross sections, obtained from the set of multilevel parameters and with both the single level and multilevel formalisms for elastic and total cross sections.
- 2) The vector of the differences between the multilevel and single level values in every energy point of the grid.

- 3) The group averaged cross sections in the ABBN scheme (Russian library), with a  $1/E$  weighting flux (infinite dilution), calculated from the multilevel and single level tabulated list. For some isotopes the calculations were repeated with constant weighting flux.
- 4) The ratios, the differences and the percent differences of the group averaged elastic cross sections.

The following codes of the CNEN Nuclear Data Laboratory in Bologna have been used:

- 1) CRESO, which generates cross sections in the resolved and unresolved energy region from the Breit-Wigner, Reich-Moore and Adler-Adler formalisms. Doppler broadening and plotting options are included [4].
- 2) FOUR ACES, which calculates group averaged cross sections taking the data directly from UKNDL, ENDF/B and KEDAK tapes. Up to 256 energy groups and arbitrary weighting function can be given in input. All the above mentioned resonance formalisms are included [5].
- 3) PIUME, which calculates single level and multilevel cross sections with the Feshbach approximation. All the possible signs, plus or minus, can be assigned to the  $u_j u_k$  products and the corresponding cross sections are calculated [6]. A linked routine performs the group integration.

The examined isotopes and elements are:

- $\text{Cu}^{63}$ ,  $\text{Cu}^{65}$ , natural Cu,  $\text{Co}^{59}$  and natural Fe, with multilevel parameters from ENDF/B-III.
- $\text{Cr}^{50}$ ,  $\text{Cr}^{52}$ ,  $\text{Ni}^{62}$  and  $\text{Ni}^{64}$  with the multilevel parameters in the energy region 10-300 keV from ref. [1]. For each isotope the set of parameters was completed as follows:
  - i) some J attributions were deduced from ref. [7];
  - ii) everywhere uncertainty remained between two possible J values the statistical factor  $g_J$  was adopted, which gives equal probability to both values;
  - iii) a constant  $\Gamma_\gamma$  value was assumed for resonances of equal  $\ell$ -number. In particular,  $\Gamma_\gamma$  widths for  $\text{Cr}^{50}$  and  $\text{Cr}^{52}$  were deduced from ref. [8] by averaging procedure and those for  $\text{Ni}^{62}$  and  $\text{Ni}^{64}$  from ENDF/B-III.

The complete set of parameters is given in tables 1 to 4 where ENDF/B symbols and units are used.

For the same isotopes, the group averaged elastic cross sections, obtained through the single level and multilevel formulas, are compared in table 5. The constant and  $1/E$  weighting fluxes were considered.

It can be observed that:

- for each isotope both negative and positive differences may appear in the groups;
- the percent differences may overcome values as large as 50%;
- if negative values of the microscopic single level cross section are set to zero in the integration, the highest percent differences are greatly reduced.

The values given in table 5 were obtained from the microscopic elastic cross sections plotted in the last pages of this paper together with the absolute differences in barns.

As concerns the materials of ENDF/B-III analogous comparison is shown in tables 6 to 10. The cross sections have been averaged following the ABBN scheme. The highest differences in these tables can be observed for  $\text{Co}^{59}$  and natural Fe, even though the relative differences never reach 50%. For more completeness, the total, elastic and capture cross sections of the natural iron from the ENDF/B-III parameters in the resolved region, are plotted at the end of this paper. Both the multi-level and single level curves appear in the figures.

#### ACKNOWLEDGEMENTS

The authors are greatly indebted to Dr. H. Beer for discussions and suggestions on the matter.

Thanks are due to Mr. M. Vaccari for his contribution in calculating and running the machine codes.

REFERENCES

- [1] R.R. Spencer, H. Beer and P.H. Fröhner: KFK1517 (1972) and private communication.
- [2] H. Feshbach, C.E. Porter and V.F. Weisskopf: Phys. Rev. 96, 448 (1954).
- [3] M. Motta: CNEN Report RT/FI(70)38 (1970).
- [4] C.G. Panini: to be published.
- [5] G.C. Panini: in press.
- [6] T. Martinelli, M. Motta: CNEN Report RT/FI(72)50 (1972).
- [7] H.E. Jackson, E.N. Strait: Phys. Rev. C 4, 1314 (1971).
- [8] R.G. Stieglitz, R.W. Hockenbury and R.C. Block: Nucl. Phys. A163, 592 (1971).

\*CRESO RUN FOR MAT 2450

CHROMIUM-50

NIS 1  
ISOTOPE 1 ZAI= 24050. ABN= 1.000 LFW= 0 NER= 1  
RANGE 1 EL= 10000.0000 EH= 300000.0 LRU= 1 LRF= 2 SPI= 0.0 AP= 0.445000 NLS= 2  
L-STATE 1 AWRI= 49.5165 AM= 0.0 L= 0 NRS= 15

	ER	AJ	GT	GN	GG	GF
1	2.84300E+04	5.00000E-01	4.15850E+02	4.15000E+02	8.50000E-01	0.0
2	3.73200E+04	5.00000E-01	2.24085E+03	2.24000E+03	8.50000E-01	0.0
3	5.49900E+04	5.00000E-01	2.81850E+02	2.81000E+02	8.50000E-01	0.0
4	6.48000E+04	5.00000E-01	4.38500E+01	4.30000E+01	8.50000E-01	0.0
5	9.47500E+04	5.00000E-01	1.67085E+03	1.67000E+03	8.50000E-01	0.0
6	1.14800E+05	5.00000E-01	1.20850E+02	1.20000E+02	8.50000E-01	0.0
7	1.29000E+05	5.00000E-01	5.40850E+02	5.40000E+02	8.50000E-01	0.0
8	1.56600E+05	5.00000E-01	1.23085E+03	1.23000E+03	8.50000E-01	0.0
9	1.62450E+05	5.00000E-01	7.50850E+02	7.50000E+02	8.50000E-01	0.0
10	1.85200E+05	5.00000E-01	3.52085E+03	3.52000E+03	8.50000E-01	0.0
11	2.18300E+05	5.00000E-01	1.70850E+02	1.70000E+02	8.50000E-01	0.0
12	2.31600E+05	5.00000E-01	9.40850E+02	9.40000E+02	8.50000E-01	0.0
13	2.45600E+05	5.00000E-01	2.00850E+02	2.00000E+02	8.50000E-01	0.0
14	2.76600E+05	5.00000E-01	1.90085E+03	1.90000E+03	8.50000E-01	0.0
15	2.89800E+05	5.00000E-01	3.70085E+03	3.70000E+03	8.50000E-01	0.0

MULTI-LEVEL BREIT-WIGNER FORMULA REQUIRED

Table 1a

\*CRESO RUN FOR MAT 2450

CHROMIUM-50

NIS 1  
ISOTOPE 1 ZAI= 24050. ABN= 1.000 LFW= 0 NER= 1  
RANGE 1 EL= 10000.0000 EH= 300000.0 LRU= 1 LRF= 2 SPI= 0.0 AP= 0.445000 NLS= 2  
L-STATE 2 AWRI= 49.5165 AM= 0.0 L= 1 NRS= 1

ER AJ GT GN GG GF  
1 1.11800E+05 1.00000E+00 6.08500E+01 6.00000E+01 8.50000E-01 0.0  
MULTI-LEVEL BREIT-WIGNER FORMULA REQUIRED

Table 1b

\*CRESD RUN FOR MAT 2452

CHROMIUM-52

NIS 1  
ISOTOPE 1 ZAI= 24052. ABN= 1.000 LFW= 0 NER= 1  
RANGE 1 EL= 10000.0000 EH= 300000.0 LRU= 1 LRF= 2 SPI= 0.0 AP= 0.445000 NLS= 2  
L-STATE 1 AWRI= 51.4938 AM= 0.0 L= 0 NRS= 8

	ER	AJ	GT	GN	GG	GF
1	3.16200E+04	5.00000E-01	1.65794E+01	1.50000E+01	1.57940E+00	0.0
2	5.01900E+04	5.00000E-01	1.71158E+03	1.71000E+03	1.57940E+00	0.0
3	9.62000E+04	5.00000E-01	6.40158E+03	6.40000E+03	1.57940E+00	0.0
4	1.18100E+05	5.00000E-01	3.15794E+01	3.00000E+01	1.57940E+00	0.0
5	1.21400E+05	5.00000E-01	6.11579E+02	6.10000E+02	1.57940E+00	0.0
6	1.39700E+05	5.00000E-01	5.40158E+03	5.40000E+03	1.57940E+00	0.0
7	1.41300E+05	5.00000E-01	7.01579E+02	7.00000E+02	1.57940E+00	0.0
8	2.49300E+05	5.00000E-01	5.51579E+02	5.50000E+02	1.57940E+00	0.0

MULTI-LEVEL BREIT-WIGNER FORMULA REQUIRED

Table 2a

\*CRESO RUN FOR MAT 2452

CHROMIUM-52

NIS 1  
ISOTOPE 1 ZAI= 24052. ABN= 1.000 LFW= 0 NER= 1  
RANGE 1 EL= 10000.0000 EH= 300000.0 LRU= 1 LRF= 2 SPI= 0.0 AP= 0.445000 NLS= 2  
L-STATE 2 AWRI= 51.4938 AM= 0.0 L= 1 NRS= 11

	ER	AJ	GT	GN	GG	GF
1	2.29200E+04	5.00000E-01	5.54700E+00	5.00000E+00	5.47000E-01	0.0
2	5.76000E+04	5.00000E-01	7.95470E+01	7.90000E+01	5.47000E-01	0.0
3	1.06000E+05	1.50000E+00	3.05470E+01	3.00000E+01	5.47000E-01	0.0
4	1.11600E+05	1.50000E+00	3.05470E+01	3.00000E+01	5.47000E-01	0.0
5	1.30100E+05	1.50000E+00	1.10547E+02	1.10000E+02	5.47000E-01	0.0
6	2.34000E+05	1.00000E+00	2.00547E+02	2.00000E+02	5.47000E-01	0.0
7	2.35800E+05	5.00000E-01	1.10055E+03	1.10000E+03	5.47000E-01	0.0
8	2.42600E+05	5.00000E-01	2.20547E+02	2.20000E+02	5.47000E-01	0.0
9	2.46300E+05	1.00000E+00	6.73880E+02	6.73330E+02	5.47000E-01	0.0
10	2.56700E+05	1.00000E+00	2.07214E+02	2.06660E+02	5.47000E-01	0.0
11	2.81900E+05	1.50000E+00	2.75547E+02	2.75000E+02	5.47000E-01	0.0

MULTI-LEVEL BREIT-WIGNER FORMULA REQUIRED

Table 2b

\*CRESO RUN FOR MAT 2862

NICKEL-62

NIS 1  
ISOTOPE 1 ZAI= 28062. ABN= 1.000 LFW= 0 NER= 1  
RANGE 1 EL= 10000.0000 EH= 300000.0 LRU= 1 LRF= 2 SPI= 0.0 AP= 0.600000 NLS= 2  
L-STATE 1 AWRI= 61.3958 AM= 0.0 L= 0 NRS= 11

	ER	AJ	GT	GN	GG	GF
1	4.28700E+04	5.00000E-01	3.42140E+02	3.40000E+02	2.14000E+00	0.0
2	7.72000E+04	5.00000E-01	7.21400E+01	7.00000E+01	2.14000E+00	0.0
3	9.47000E+04	5.00000E-01	2.50214E+03	2.50000E+03	2.14000E+00	0.0
4	1.05600E+05	5.00000E-01	4.60214E+03	4.60000E+03	2.14000E+00	0.0
5	1.49300E+05	5.00000E-01	1.42140E+02	1.40000E+02	2.14000E+00	0.0
6	1.88200E+05	5.00000E-01	9.21400E+01	9.00000E+01	2.14000E+00	0.0
7	2.14700E+05	5.00000E-01	1.92140E+02	1.90000E+02	2.14000E+00	0.0
8	2.29500E+05	5.00000E-01	6.18214E+03	6.18000E+03	2.14000E+00	0.0
9	2.43200E+05	5.00000E-01	7.82140E+02	7.80000E+02	2.14000E+00	0.0
10	2.81100E+05	5.00000E-01	4.80214E+03	4.80000E+03	2.14000E+00	0.0
11	2.88000E+05	5.00000E-01	1.00214E+03	1.00000E+03	2.14000E+00	0.0

MULTI-LEVEL BREIT-WIGNER FORMULA REQUIRED

Table 3a

\*CRESD RUN FOR MAT 2862

NICKEL-62

NIS 1  
ISOTOPE 1 ZAI= 28062. ABN= 1.000 LFW= 0 NER= 1  
RANGE 1 EL= 10000.0000 EH= 300000.0 LRU= 1 LRF= 2 SPI= 0.0 AP= 0.600000 NLS= 2  
L-STATE 2 AWRI= 61.3958 AM= 0.0 L= 1 NRS= 2

	ER	AJ	GT	GN	GG	GF
1	5.69100E+04	1.50000E+00	3.94700E+01	3.73300E+01	2.14000E+00	0.0
2	7.84000E+04	1.50000E+00	3.54700E+01	3.33300E+01	2.14000E+00	0.0

MULTI-LEVEL BREIT-WIGNER FORMULA REQUIRED

Table 3b

\*CRESD RUN FOR MAT 2864

NICKEL-64

NIS 1  
ISOTOPE 1 ZAI= 28064. ABN= 1.000 LFW= 0 NER= 1  
RANGE 1 EL= 10000.0000 EH= 300000.0 LRU= 1 LRF= 2 SPI= 0.0 AP= 0.600000 NLS= 2  
L-STATE 1 AWRI= 63.3782 AM= 0.0 L= 0 NRS= 13

	ER	AJ	GT	GN	GG	GF
1	1.43000E+04	5.00000E-01	2.90214E+03	2.90000E+03	2.14000E+00	0.0
2	3.38200E+04	5.00000E-01	8.90214E+03	8.90000E+03	2.14000E+00	0.0
3	1.29300E+05	5.00000E-01	1.34214E+03	1.34000E+03	2.14000E+00	0.0
4	1.48800E+05	5.00000E-01	8.21400E+01	8.00000E+01	2.14000E+00	0.0
5	1.55000E+05	5.00000E-01	3.90214E+03	3.90000E+03	2.14000E+00	0.0
6	1.63200E+05	5.00000E-01	1.42140E+02	1.40000E+02	2.14000E+00	0.0
7	1.77700E+05	5.00000E-01	4.72140E+02	4.70000E+02	2.14000E+00	0.0
8	2.05300E+05	5.00000E-01	6.21400E+01	6.00000E+01	2.14000E+00	0.0
9	2.19800E+05	5.00000E-01	3.21400E+01	3.00000E+01	2.14000E+00	0.0
10	2.26900E+05	5.00000E-01	1.22140E+02	1.20000E+02	2.14000E+00	0.0
11	2.31900E+05	5.00000E-01	3.77214E+03	3.77000E+03	2.14000E+00	0.0
12	2.69700E+05	5.00000E-01	2.20214E+03	2.20000E+03	2.14000E+00	0.0
13	2.83500E+05	5.00000E-01	3.52140E+02	3.50000E+02	2.14000E+00	0.0

MULTI-LEVEL BREIT-WIGNER FORMULA REQUIRED

Table 4a

\*CRESO RUN FOR MAT 2864

NICKEL-64

NIS 1  
ISOTOPE 1 ZAI= 28064. ABN= 1.000 LFW= 0 NER= 1  
RANGE 1 EL= 10000.0000 EH= 300000.0 LRU= 1 LRF= 2 SPI= 0.0 AP= 0.600000 NLS= 2  
L-STATE 2 AWRI= 63.3782 AM= 0.0 L= 1 NRS= 6

	ER	AJ	GT	GN	GG	GF
1	1.06500E+05	1.00000E+00	7.39300E+01	7.33300E+01	6.00000E-01	0.0
2	1.42000E+05	1.00000E+00	1.13930E+02	1.13330E+02	6.00000E-01	0.0
3	1.91500E+05	1.00000E+00	1.07260E+02	1.06660E+02	6.00000E-01	0.0
4	2.14700E+05	1.00000E+00	5.39300E+01	5.33300E+01	6.00000E-01	0.0
5	2.37900E+05	1.00000E+00	2.13930E+02	2.13330E+02	6.00000E-01	0.0
6	2.55700E+05	1.00000E+00	1.13930E+02	1.13330E+02	6.00000E-01	0.0

MULTI-LEVEL BREIT-WIGNER FORMULA REQUIRED

Table 4b

Table 5

Comparison of group averaged elastic cross sections (SL  $\equiv$  single level formulas, ML  $\equiv$  multilevel formulas)

Isotope	Group Index (ABBN)	A	B	C	A-C (b)	$\frac{A-C}{C} \times 10^2$	$\frac{B-C}{C} \times 10^2$	A	B	C	A-C (b)	$\frac{A-C}{C} \times 10^2$	$\frac{B-C}{C} \times 10^2$
		$\sigma_{el.}^{SL} (b)$ $\Phi=1/E$	( $^\circ$ )	$\sigma_{el.}^{ML} (b)$ $\Phi=1/E$				$\sigma_{el.}^{SL} (b)$ $\Phi=const$	( $^\circ$ )	$\sigma_{el.}^{ML} (b)$ $\Phi=const$			
Cr <sup>50</sup>	7	3.313		3.345	- 0.032	- 0.96		3.326		3.371	- 0.045	- 1.33	
	8	3.526		3.423	0.103	3.01		3.641		3.540	0.101	2.85	
	9	4.225		4.044	0.181	4.48		4.225		4.068	0.157	3.86	
	10	10.920	(11.415)	11.030	- 0.110	- 1.00	3.49	12.435	(12.822)	12.372	0.063	0.51	4.12
	11	0.179	(0.241)	0.605	- 0.426	- 70.4	- 60.2	0.114	(0.198)	0.566	- 0.452	- 79.9	- 65.0
Cr <sup>52</sup>	7	3.380		3.423	- 0.043	- 1.26		3.284		3.323	- 0.039	- 1.17	
	8	6.608		6.893	- 0.285	- 4.13		6.353		6.751	- 0.398	- 5.90	
	9	6.299	(6.365)	6.187	0.112	1.81	2.88	6.065	(6.120)	5.975	0.090	1.51	2.43
	10	0.291	(0.474)	0.753	- 0.462	- 61.4	- 37.1	0.148	(0.395)	0.668	- 0.52	- 77.8	- 40.9
	11	0.937		1.121	- 0.184	- 16.4		0.918		1.107	- 0.189	- 17.1	
Ni <sup>62</sup>	7	4.989		5.039	- 0.050	- 1.00		5.082		5.153	- 0.071	- 1.38	
	8	7.027		6.936	0.091	1.31		6.408		6.333	0.075	1.18	
	9	2.861	(3.059)	3.160	- 0.299	- 9.46	- 3.20	2.946	(3.203)	3.274	- 0.328	- 10.0	- 2.17
	10	3.366	(3.401)	3.546	- 0.180	- 5.08	- 4.09	3.636	(3.680)	3.815	- 0.179	- 4.69	- 3.54
	11	3.018		3.117	- 0.159	- 5.00		3.003		3.104	- 0.101	- 3.25	
Ni <sup>64</sup>	7	6.012		6.113	- 0.101	- 1.65		5.891		6.098	- 0.207	- 3.39	
	8	7.034		6.883	0.151	2.19		7.148		7.040	0.108	1.53	
	9	12.742		13.195	- 0.453	- 3.43		11.768		12.098	- 0.330	- 2.73	
	10	38.100		34.161	3.939	11.53		40.554		38.139	2.415	6.33	
	11	59.987		61.883	- 1.896	- 3.06		60.525		58.531	1.994	3.41	

( $^\circ$ ) The averaged cross sections into parenthesis have been obtained by truncation of negative values of the single level microscopic cross section.

\*\*\*\*FOUR ACES\*\*\*\*

GROUP CONSTANTS  
(ABBN SCHEME)

GROUP	ENERGY BOUNDS (MEV)		ENERGY WIDTH	LETHARGY WIDTH	FISSION SPECTRUM	WEIGHTING FUNCTION
	LOWER	UPPER				
1	6.5000E+00	- 1.0500E+01	4.0000E+00	0.47957	0.01598	3.4711E-02
2	4.0000E+00	- 6.5000E+00	2.5000E+00	0.48551	0.08819	1.9157E-01
3	2.5000E+00	- 4.0000E+00	1.5000E+00	0.47000	0.18325	3.9805E-01
4	1.4000E+00	- 2.5000E+00	1.1000E+00	0.57982	0.26986	5.7982E-01
5	8.0000E-01	- 1.4000E+00	6.0000E-01	0.55962	0.20228	5.5962E-01
6	4.0000E-01	- 8.0000E-01	4.0000E-01	0.69315	0.14056	6.9315E-01
7	2.0000E-01	- 4.0000E-01	2.0000E-01	0.69315	0.06102	6.9315E-01
8	1.0000E-01	- 2.0000E-01	1.0000E-01	0.69315	0.02388	6.9315E-01
9	4.6416E-02	- 1.0000E-01	5.3584E-02	0.76753	0.00940	7.6753E-01
10	2.1544E-02	- 4.6416E-02	2.4872E-02	0.76753	0.00305	7.6753E-01
11	1.0000E-02	- 2.1544E-02	1.1544E-02	0.76753	0.00098	7.6753E-01
12	4.6416E-03	- 1.0000E-02	5.3584E-03	0.76753	0.00031	7.6753E-01
13	2.1544E-03	- 4.6416E-03	2.4872E-03	0.76753	0.00010	7.6753E-01
14	1.0000E-03	- 2.1544E-03	1.1544E-03	0.76753	0.00003	7.6753E-01
15	4.6416E-04	- 1.0000E-03	5.3584E-04	0.76753	0.00001	7.6753E-01
16	2.1544E-04	- 4.6416E-04	2.4872E-04	0.76753	0.00000	7.6753E-01
17	1.0000E-04	- 2.1544E-04	1.1544E-04	0.76753	0.00000	7.6753E-01
18	4.6416E-05	- 1.0000E-04	5.3584E-05	0.76753	0.00000	7.6753E-01
19	2.1544E-05	- 4.6416E-05	2.4872E-05	0.76753	0.00000	7.6753E-01
20	1.0000E-05	- 2.1544E-05	1.1544E-05	0.76753	0.00000	7.6753E-01
21	4.6416E-06	- 1.0000E-05	5.3584E-06	0.76753	0.00000	7.6753E-01
22	2.1544E-06	- 4.6416E-06	2.4872E-06	0.76753	0.00000	7.6753E-01
23	1.0000E-06	- 2.1544E-06	1.1544E-06	0.76753	0.00000	7.6753E-01
24	4.6416E-07	- 1.0000E-06	5.3584E-07	0.76753	0.00000	7.6753E-01
25	2.1544E-07	- 4.6416E-07	2.4872E-07	0.76753	0.00000	7.6753E-01

WEIGHTING FUNCTION IS SO DEFINED.....

- | ENERGY RANGE (MEV)          | NORM. FACT. | FUNCTION         |
|-----------------------------|-------------|------------------|
| 1) 2.1544E-07 TO 2.5000E+00 | 1.0000E+00  | 1/E              |
| 2) 2.5000E+00 TO 1.0500E+01 | 2.1722E+00  | FISSION SPECTRUM |

MAT 1085,COPPER-63

ELASTIC

GROUP	A=SINGLE LEVEL	B=MULTI LEVEL	A/B	A-B	(A-B)/B
1	2.1578E+00	2.1578E+00	1.0000E+00	0.0	0.0
2	2.1333E+00	2.1333E+00	1.0000E+00	0.0	0.0
3	1.8867E+00	1.8867E+00	1.0000E+00	0.0	0.0
4	2.2482E+00	2.2482E+00	1.0000E+00	0.0	0.0
5	3.1881E+00	3.1881E+00	1.0000E+00	0.0	0.0
6	4.1559E+00	4.1559E+00	1.0000E+00	0.0	0.0
7	4.7980E+00	4.7980E+00	1.0000E+00	0.0	0.0
8	4.6177E+00	4.6177E+00	1.0000E+00	0.0	0.0
9	6.8600E+00	6.8600E+00	1.0000E+00	0.0	0.0
10	1.1557E+01	1.1550E+01	1.0006E+00	7.0000E-03	0.1
11	1.4048E+01	1.4126E+01	9.9448E-01	-7.8000E-02	-0.6
12	1.7131E+01	1.7235E+01	9.9397E-01	-1.0400E-01	-0.6
13	9.0572E+00	9.0025E+00	1.0061E+00	5.4701E-02	0.6
14	1.9728E+01	2.0403E+01	9.6692E-01	-6.7500E-01	-3.3
15	9.2314E+00	9.4373E+00	9.7818E-01	-2.0590E-01	-2.2
16	4.2821E+00	4.4055E+00	9.7199E-01	-1.2340E-01	-2.8
17	4.7584E+00	4.8097E+00	9.8933E-01	-5.1300E-02	-1.1
18	5.0940E+00	5.0930E+00	1.0002E+00	9.9945E-04	0.0
19	5.4532E+00	5.3930E+00	1.0112E+00	6.0201E-02	1.1
20	5.8378E+00	5.7107E+00	1.0223E+00	1.2710E-01	2.2
21	5.5206E+00	5.5206E+00	1.0000E+00	0.0	0.0
22	5.5457E+00	5.5457E+00	1.0000E+00	0.0	0.0
23	5.5619E+00	5.5619E+00	1.0000E+00	0.0	0.0
24	5.5703E+00	5.5703E+00	1.0000E+00	0.0	0.0
25	5.5745E+00	5.5745E+00	1.0000E+00	0.0	0.0

Table 6

MAT 1086,COPPER-65

ELASTIC

GROUP	A=SINGLE LEVEL	B=MULTI LEVEL	A/B	A-B	(A-B)/B
1	2.1578E+00	2.1578E+00	1.0000E+00	0.0	0.0
2	2.1333E+00	2.1333E+00	1.0000E+00	0.0	0.0
3	1.8867E+00	1.8867E+00	1.0000E+00	0.0	0.0
4	2.2482E+00	2.2482E+00	1.0000E+00	0.0	0.0
5	3.1881E+00	3.1881E+00	1.0000E+00	0.0	0.0
6	4.1559E+00	4.1559E+00	1.0000E+00	0.0	0.0
7	4.7980E+00	4.7980E+00	1.0000E+00	0.0	0.0
8	4.6177E+00	4.6177E+00	1.0000E+00	0.0	0.0
9	6.9010E+00	6.9010E+00	1.0000E+00	0.0	0.0
10	1.0254E+01	1.0265E+01	9.9893E-01	-1.1001E-02	-0.1
11	1.2315E+01	1.2114E+01	1.0166E+00	2.0100E-01	1.7
12	1.3788E+01	1.3539E+01	1.0184E+00	2.4900E-01	1.8
13	2.0391E+01	2.0125E+01	1.0132E+00	2.6601E-01	1.3
14	7.6819E+00	7.0885E+00	1.0837E+00	5.9340E-01	8.4
15	1.0627E+01	9.8344E+00	1.0806E+00	7.9260E-01	8.1
16	1.3276E+01	1.2280E+01	1.0811E+00	9.9600E-01	8.1
17	1.4902E+01	1.3709E+01	1.0870E+00	1.1930E+00	8.7
18	1.5711E+01	1.4475E+01	1.0854E+00	1.2360E+00	8.5
19	1.6227E+01	1.4954E+01	1.0851E+00	1.2730E+00	8.5
20	1.6761E+01	1.5449E+01	1.0849E+00	1.3120E+00	8.5
21	1.5300E+01	1.5300E+01	1.0000E+00	0.0	0.0
22	1.5352E+01	1.5352E+01	1.0000E+00	0.0	0.0
23	1.5385E+01	1.5385E+01	1.0000E+00	0.0	0.0
24	1.5403E+01	1.5403E+01	1.0000E+00	0.0	0.0
25	1.5408E+01	1.5408E+01	1.0000E+00	0.0	0.0

Table 7

MAT 1087, NATURAL COPPER

ELASTIC

GROUP	A=SINGLE LEVEL	B=MULTI LEVEL	A/B	A-B	(A-B)/B
1	2.1578E+00	2.1578E+00	1.0000E+00	0.0	0.0
2	2.1333E+00	2.1333E+00	1.0000E+00	0.0	0.0
3	1.8867E+00	1.8867E+00	1.0000E+00	0.0	0.0
4	2.2482E+00	2.2482E+00	1.0000E+00	0.0	0.0
5	3.1881E+00	3.1881E+00	1.0000E+00	0.0	0.0
6	4.1559E+00	4.1559E+00	1.0000E+00	0.0	0.0
7	4.7980E+00	4.7980E+00	1.0000E+00	0.0	0.0
8	4.6177E+00	4.6177E+00	1.0000E+00	0.0	0.0
9	6.8948E+00	6.8948E+00	1.0000E+00	0.0	0.0
10	1.1150E+01	1.1141E+01	1.0008E+00	8.9998E-03	0.1
11	1.3537E+01	1.3481E+01	1.0042E+00	5.6000E-02	0.4
12	1.6105E+01	1.6029E+01	1.0047E+00	7.5989E-02	0.5
13	1.2593E+01	1.2471E+01	1.0098E+00	1.2200E-01	1.0
14	1.5924E+01	1.6194E+01	9.8333E-01	-2.7000E-01	-1.7
15	9.6815E+00	9.5722E+00	1.0114E+00	1.0930E-01	1.1
16	7.0872E+00	6.8611E+00	1.0330E+00	2.2610E-01	3.3
17	8.1131E+00	7.7399E+00	1.0482E+00	3.7320E-01	4.8
18	8.5938E+00	8.1699E+00	1.0519E+00	4.2390E-01	5.2
19	8.9187E+00	8.4566E+00	1.0546E+00	4.6210E-01	5.5
20	9.2558E+00	8.7534E+00	1.0574E+00	5.0240E-01	5.7
21	7.7000E+00	7.7000E+00	1.0000E+00	0.0	0.0
22	7.7000E+00	7.7000E+00	1.0000E+00	0.0	0.0
23	7.7000E+00	7.7000E+00	1.0000E+00	0.0	0.0
24	7.7000E+00	7.7000E+00	1.0000E+00	0.0	0.0
25	7.7000E+00	7.7000E+00	1.0000E+00	0.0	0.0

Table 8

MAT 1118, COBALT-59

ELASTIC

GROUP	A=SINGLE LEVEL	B=MULTI LEVEL	A/B	A-B	(A-B)/B
1	2.0311E+00	2.0311E+00	1.0000E+00	0.0	0.0
2	2.1257E+00	2.1257E+00	1.0000E+00	0.0	0.0
3	2.2535E+00	2.2535E+00	1.0000E+00	0.0	0.0
4	2.9383E+00	2.9383E+00	1.0000E+00	0.0	0.0
5	3.6499E+00	3.6499E+00	1.0000E+00	0.0	0.0
6	4.0220E+00	4.0220E+00	1.0000E+00	0.0	0.0
7	4.2385E+00	4.2385E+00	1.0000E+00	0.0	0.0
8	5.3408E+00	5.3408E+00	1.0000E+00	0.0	0.0
9	6.3484E+00	6.3484E+00	1.0000E+00	0.0	0.0
10	1.5351E+01	1.5163E+01	1.0124E+00	1.8800E-01	1.2
11	8.7953E+00	8.2869E+00	1.0613E+00	5.0840E-01	6.1
12	5.8607E+01	5.6372E+01	1.0396E+00	2.2350E+00	4.0
13	2.4451E+01	2.6281E+01	9.3037E-01	-1.8300E+00	-7.0
14	2.7081E+00	2.2396E+00	1.2092E+00	4.6850E-01	20.9
15	6.1310E+00	4.1461E+00	1.4787E+00	1.9849E+00	47.9
16	1.5314E+01	1.0832E+01	1.4138E+00	4.4820E+00	41.4
17	7.7975E+02	7.7504E+02	1.0061E+00	4.7100E+00	0.6
18	1.8677E+01	1.9149E+01	9.7535E-01	-4.7200E-01	-2.5
19	9.4594E+00	7.4643E+00	1.2673E+00	1.9951E+00	26.7
20	9.2887E+00	6.6018E+00	1.4070E+00	2.6869E+00	40.7
21	9.3990E+00	6.4618E+00	1.4545E+00	2.9372E+00	45.5
22	9.4171E+00	6.4592E+00	1.4579E+00	2.9579E+00	45.8
23	9.4303E+00	6.4609E+00	1.4596E+00	2.9694E+00	46.0
24	9.4438E+00	6.4623E+00	1.4614E+00	2.9815E+00	46.1
25	9.4569E+00	6.4592E+00	1.4641E+00	2.9977E+00	46.4

Table 9

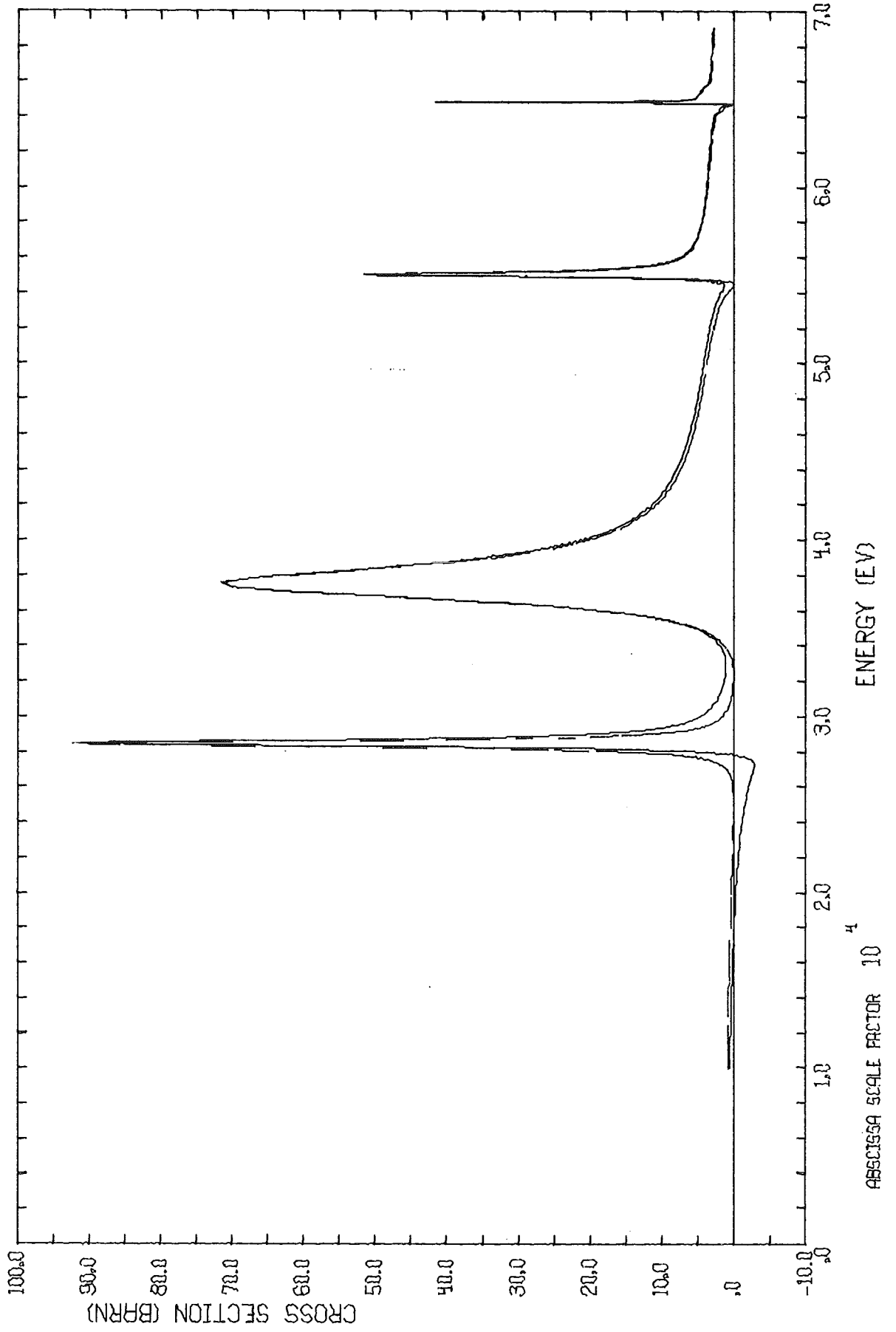
MAT 1180,NATURAL IRON

ELASTIC

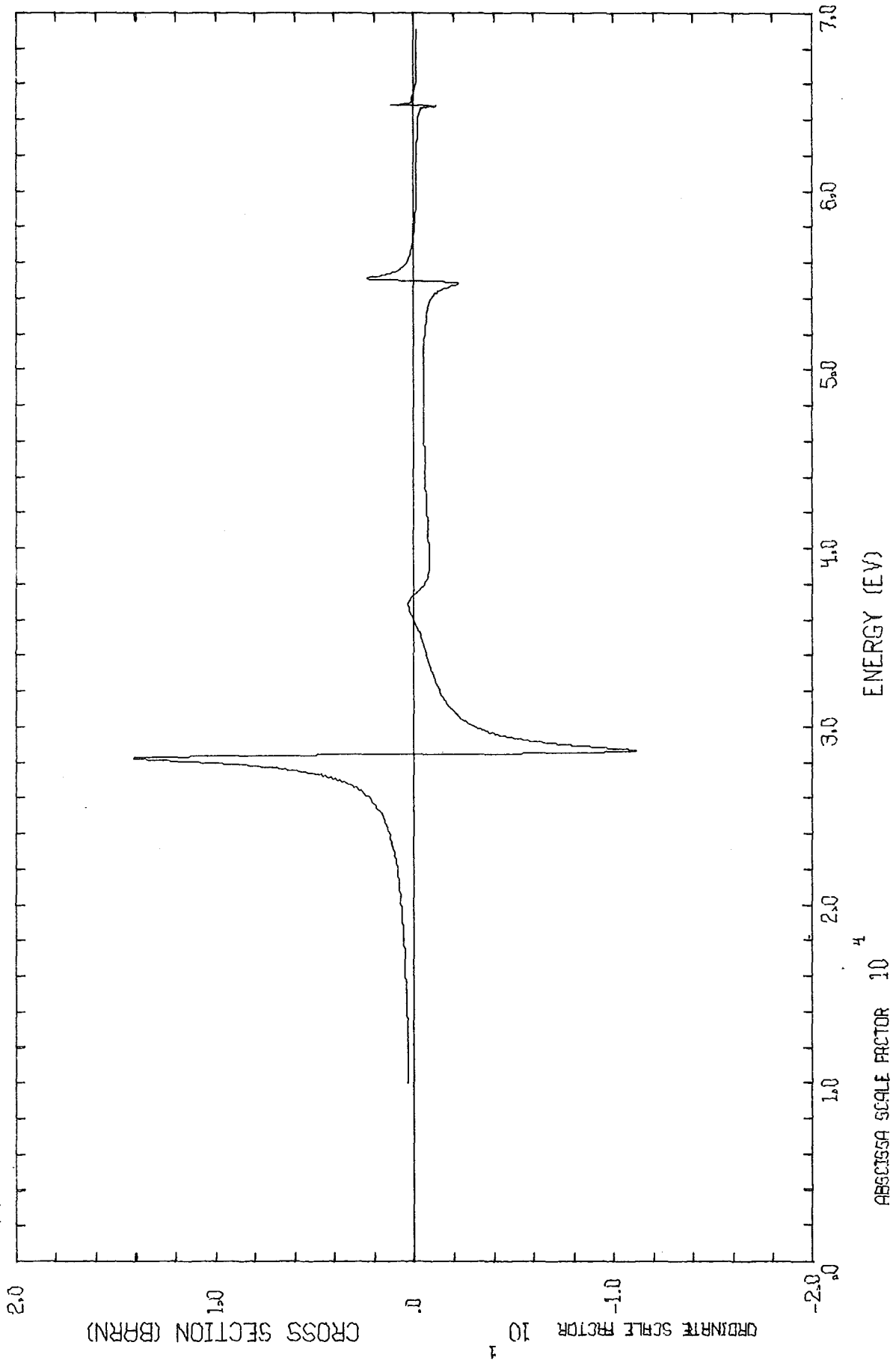
GROUP	A=SINGLE LEVEL	B=MULTI LEVEL	A/B	A-B	(A-B)/B
1	1.9711E+00	1.9711E+00	1.0000E+00	0.0	0.0
2	2.2664E+00	2.2664E+00	1.0000E+00	0.0	0.0
3	2.3632E+00	2.3632E+00	1.0000E+00	0.0	0.0
4	2.3683E+00	2.3683E+00	1.0000E+00	0.0	0.0
5	2.2010E+00	2.2010E+00	1.0000E+00	0.0	0.0
6	3.0868E+00	3.0868E+00	1.0000E+00	0.0	0.0
7	2.9226E+00	2.9226E+00	1.0000E+00	0.0	0.0
8	3.6882E+00	3.6882E+00	1.0000E+00	0.0	0.0
9	5.2640E+00	5.3000E+00	9.9321E-01	-3.6000E-02	-0.7
10	1.3787E+01	1.3481E+01	1.0227E+00	3.0600E-01	2.3
11	3.5103E+00	2.7999E+00	1.2537E+00	7.1040E-01	25.4
12	1.0713E+01	1.0080E+01	1.0628E+00	6.3300E-01	6.3
13	7.5902E+00	6.8361E+00	1.1103E+00	7.5410E-01	11.0
14	9.4346E+00	8.5916E+00	1.0981E+00	8.4300E-01	9.8
15	9.8900E+00	9.8900E+00	1.0000E+00	0.0	0.0
16	1.0949E+01	1.0949E+01	1.0000E+00	0.0	0.0
17	1.1339E+01	1.1339E+01	1.0000E+00	0.0	0.0
18	1.1400E+01	1.1400E+01	1.0000E+00	0.0	0.0
19	1.1400E+01	1.1400E+01	1.0000E+00	0.0	0.0
20	1.1400E+01	1.1400E+01	1.0000E+00	0.0	0.0
21	1.1400E+01	1.1400E+01	1.0000E+00	0.0	0.0
22	1.1400E+01	1.1400E+01	1.0000E+00	0.0	0.0
23	1.1400E+01	1.1400E+01	1.0000E+00	0.0	0.0
24	1.1400E+01	1.1400E+01	1.0000E+00	0.0	0.0
25	1.1400E+01	1.1400E+01	1.0000E+00	0.0	0.0

Table 10

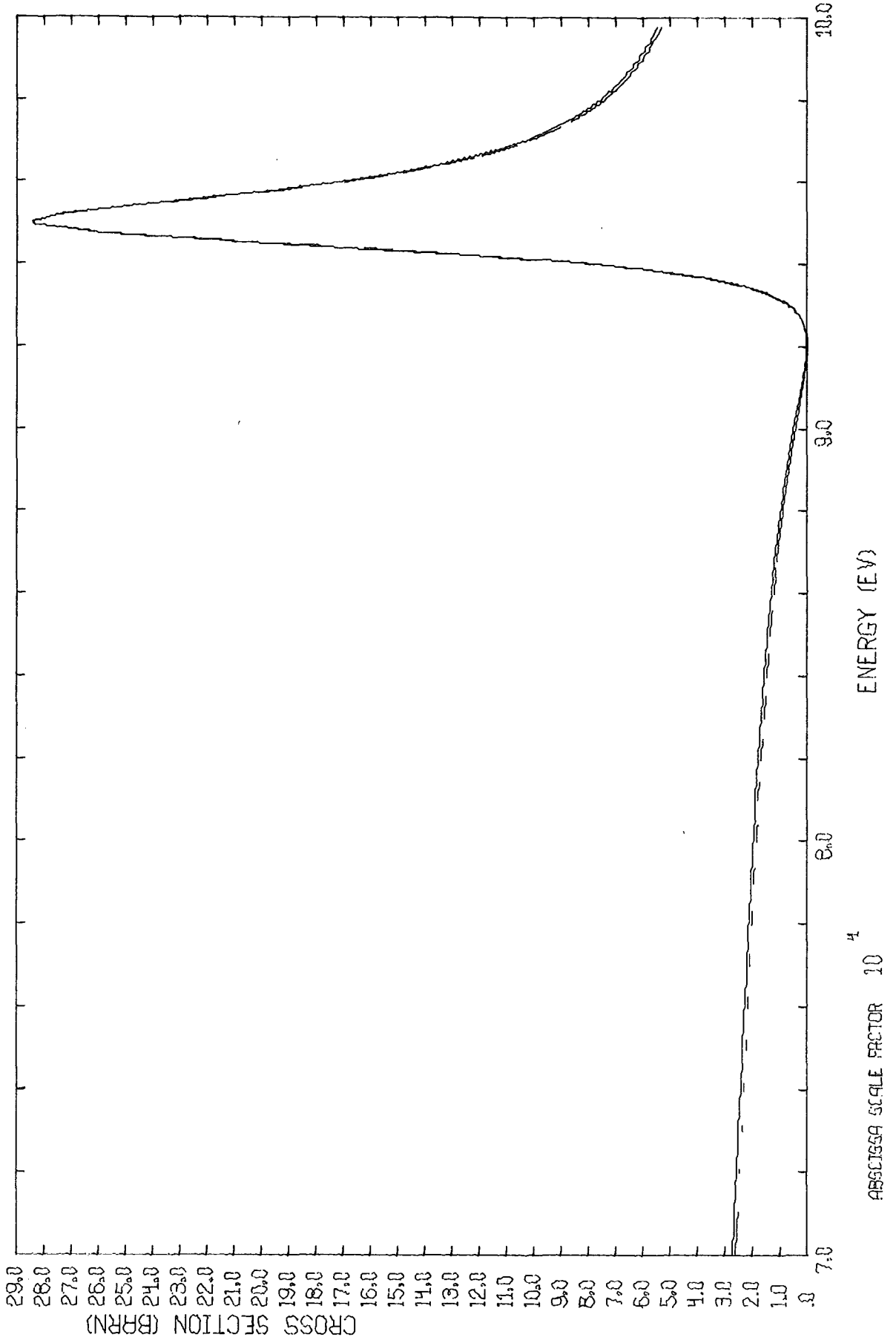
ELASTIC CR 50



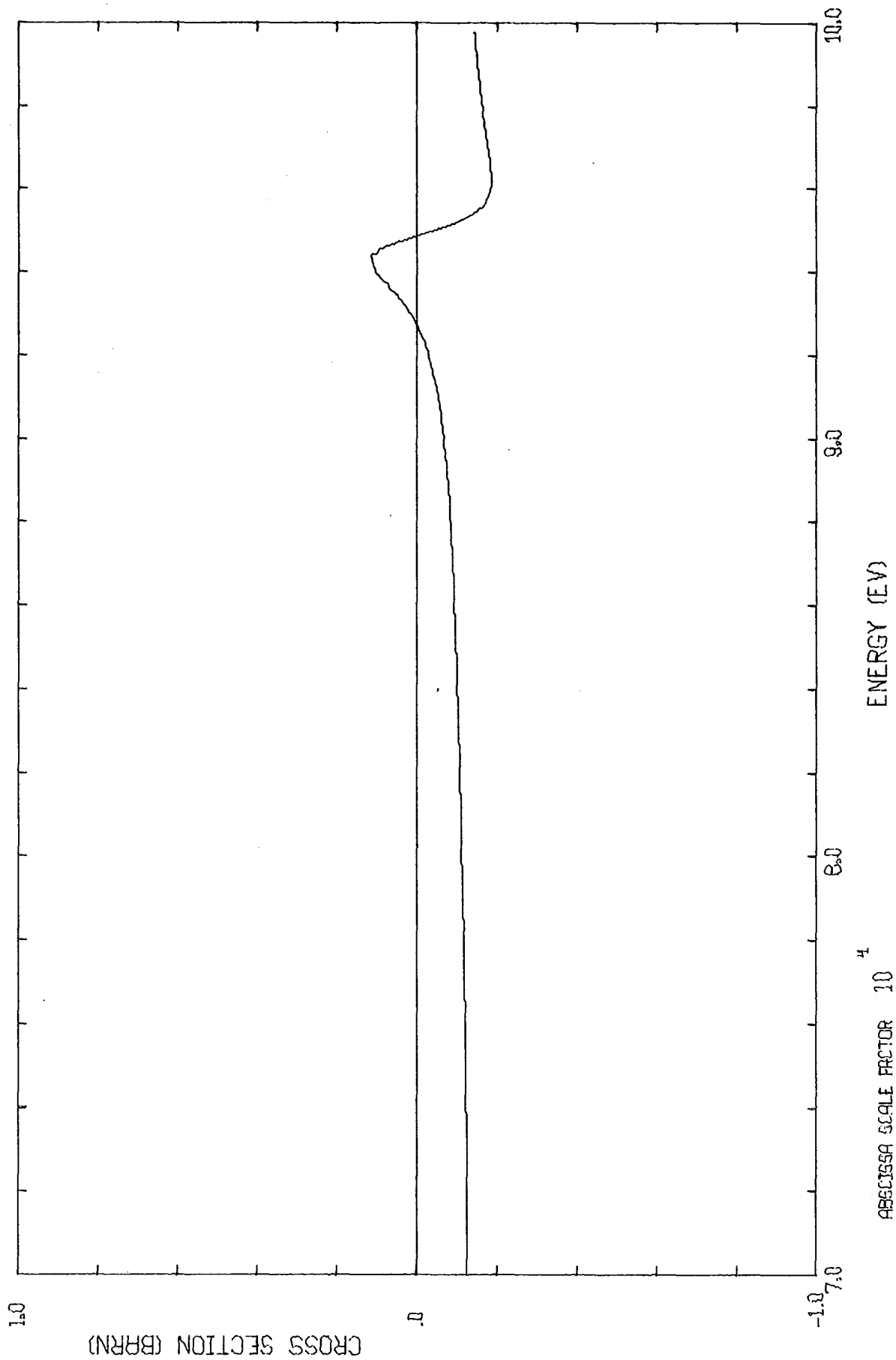
ELASTIC CR 50 DIFFERENCE ML-SL



ELASTIC CR 50



ELASTIC CR 50 DIFFERENCE ML-SL



CROSS SECTION (BARN)

ABSCISSA SCALE FACTOR 10<sup>4</sup>

ENERGY (EV)

1.0

0

-1.0

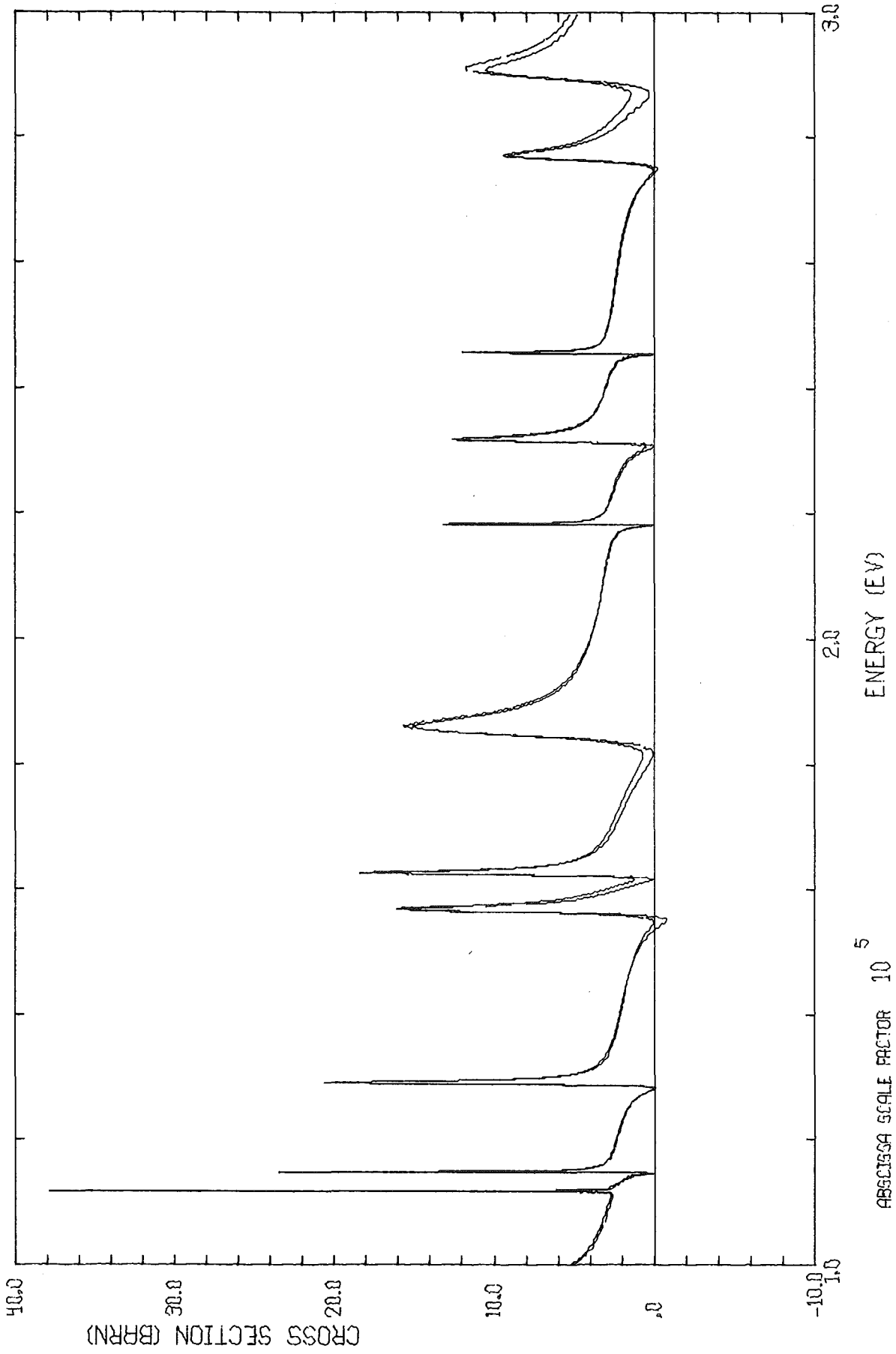
7.0

8.0

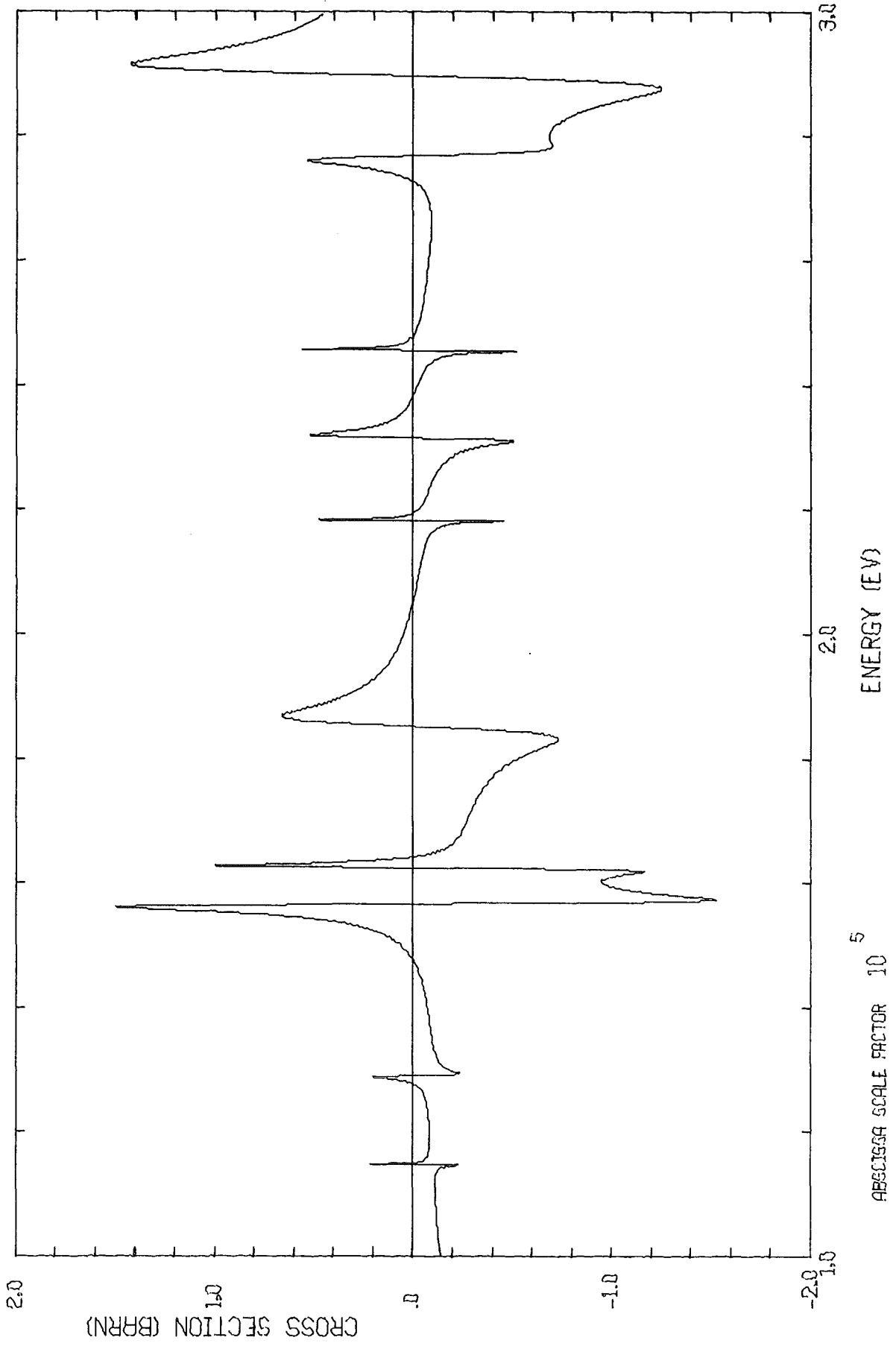
9.0

10.0

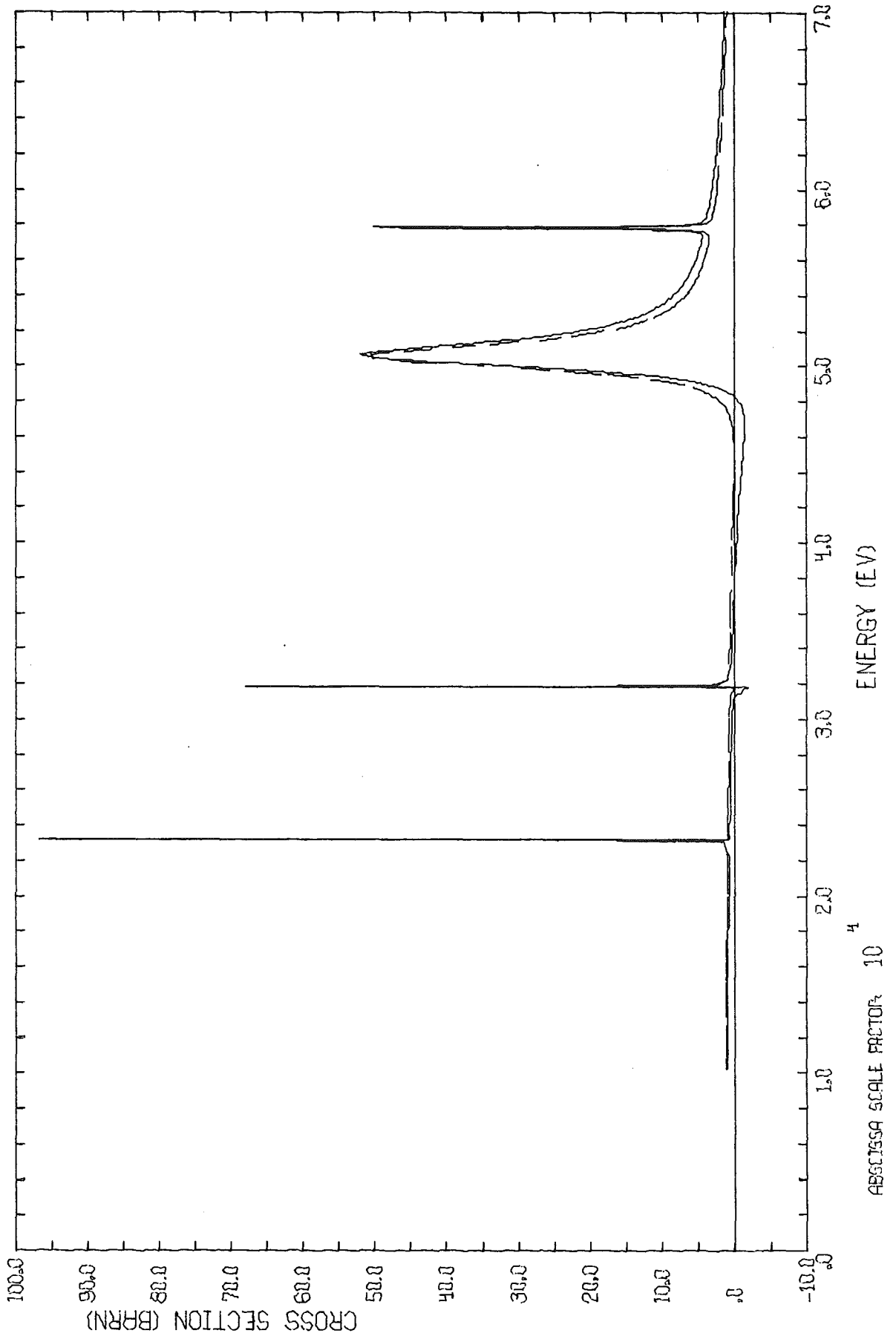
ELASTIC CR 50



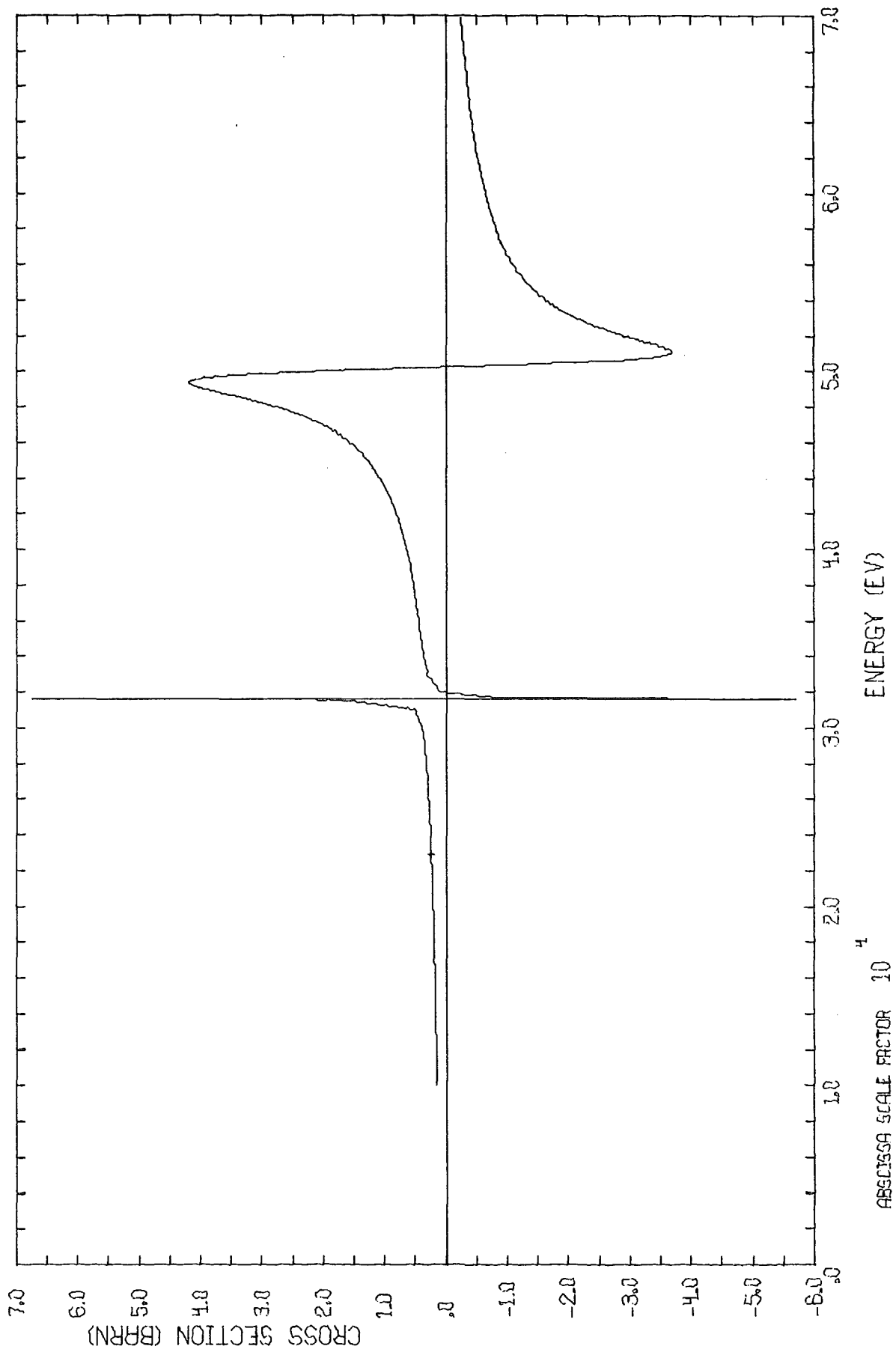
ELASTIC CR 50 DIFFERENCE ML-SL



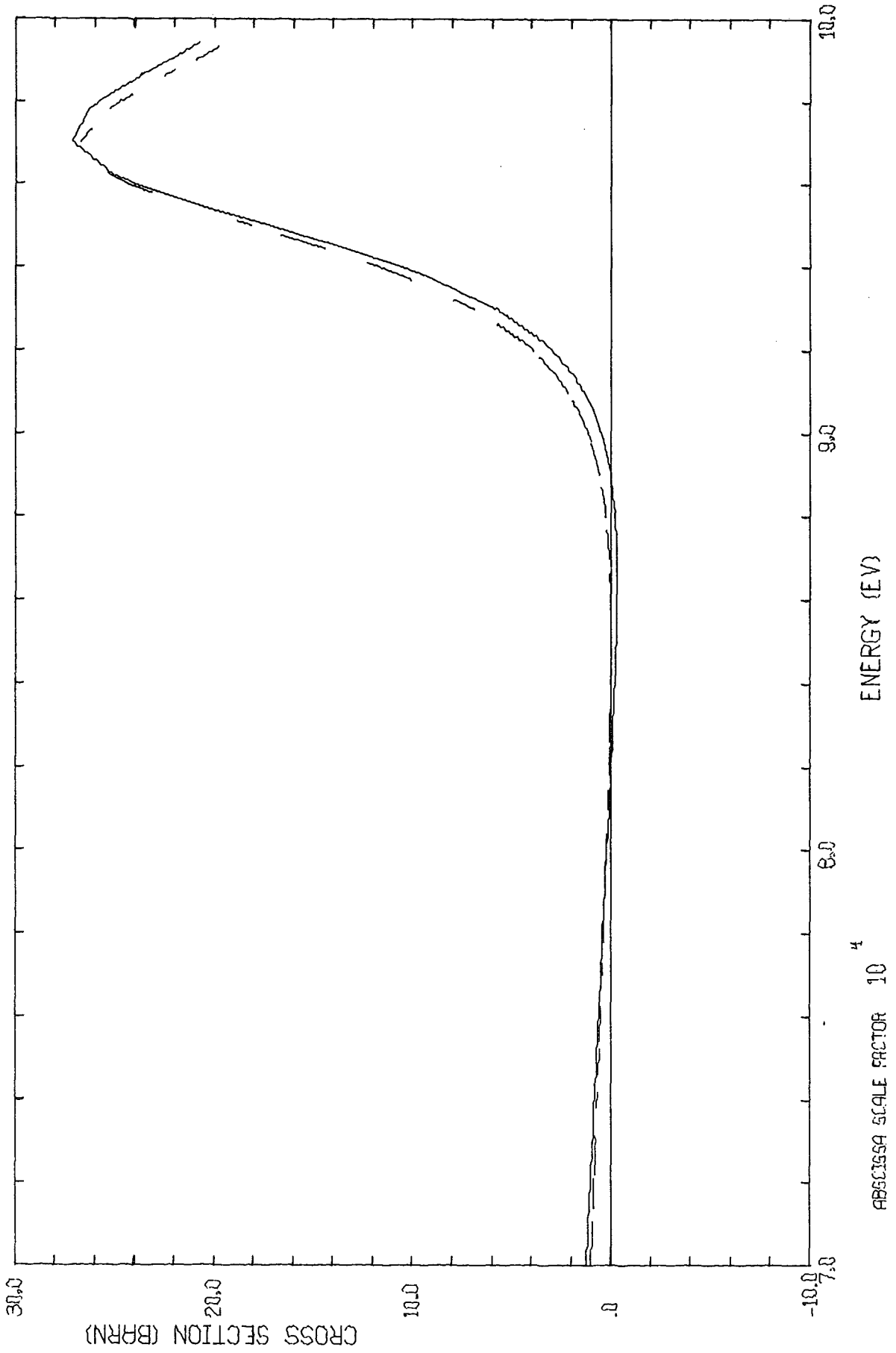
ELASTIC CR 52



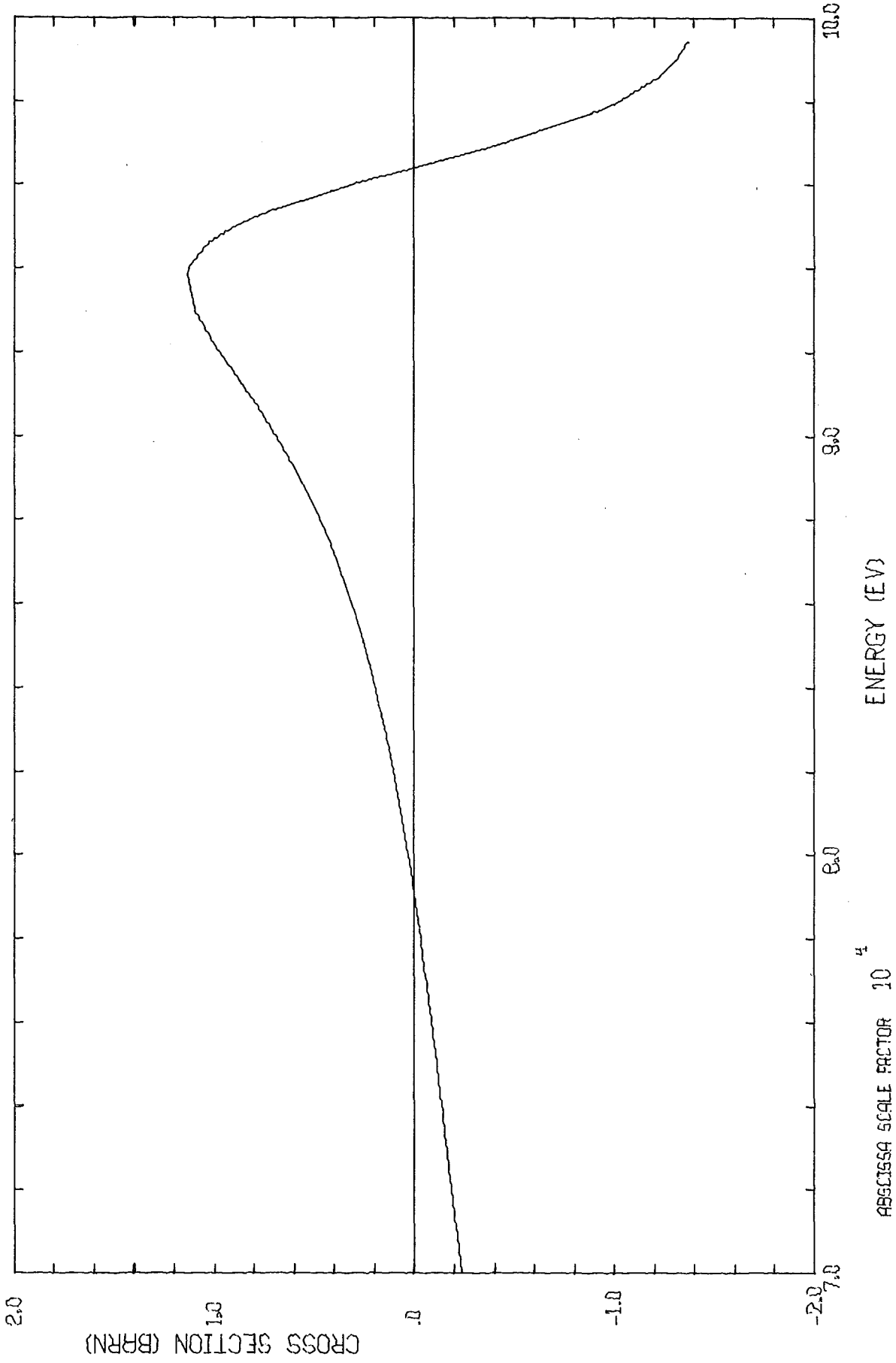
ELASTIC CR 52 DIFFERENCE ML-SL



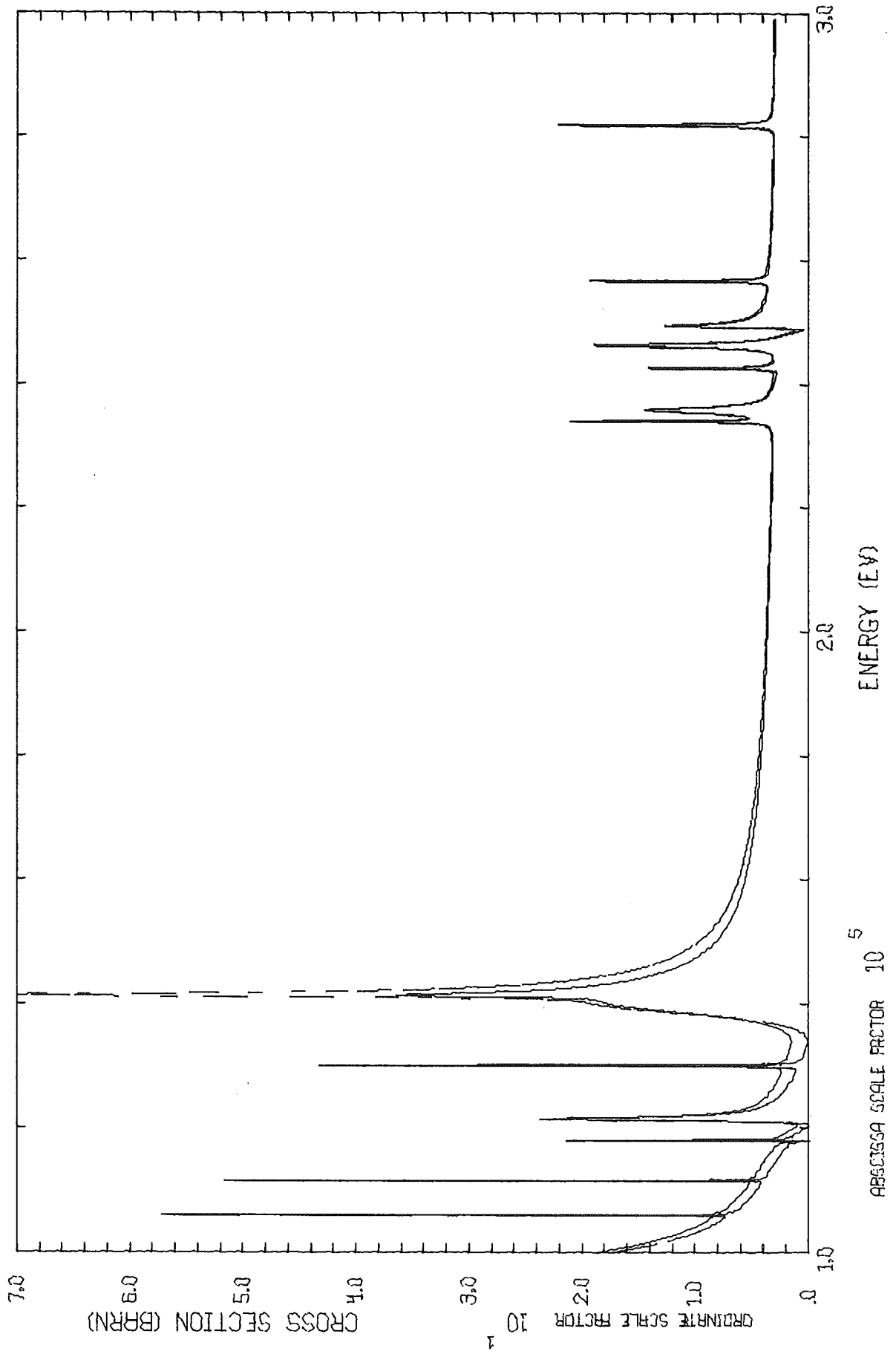
ELASTIC CR 52



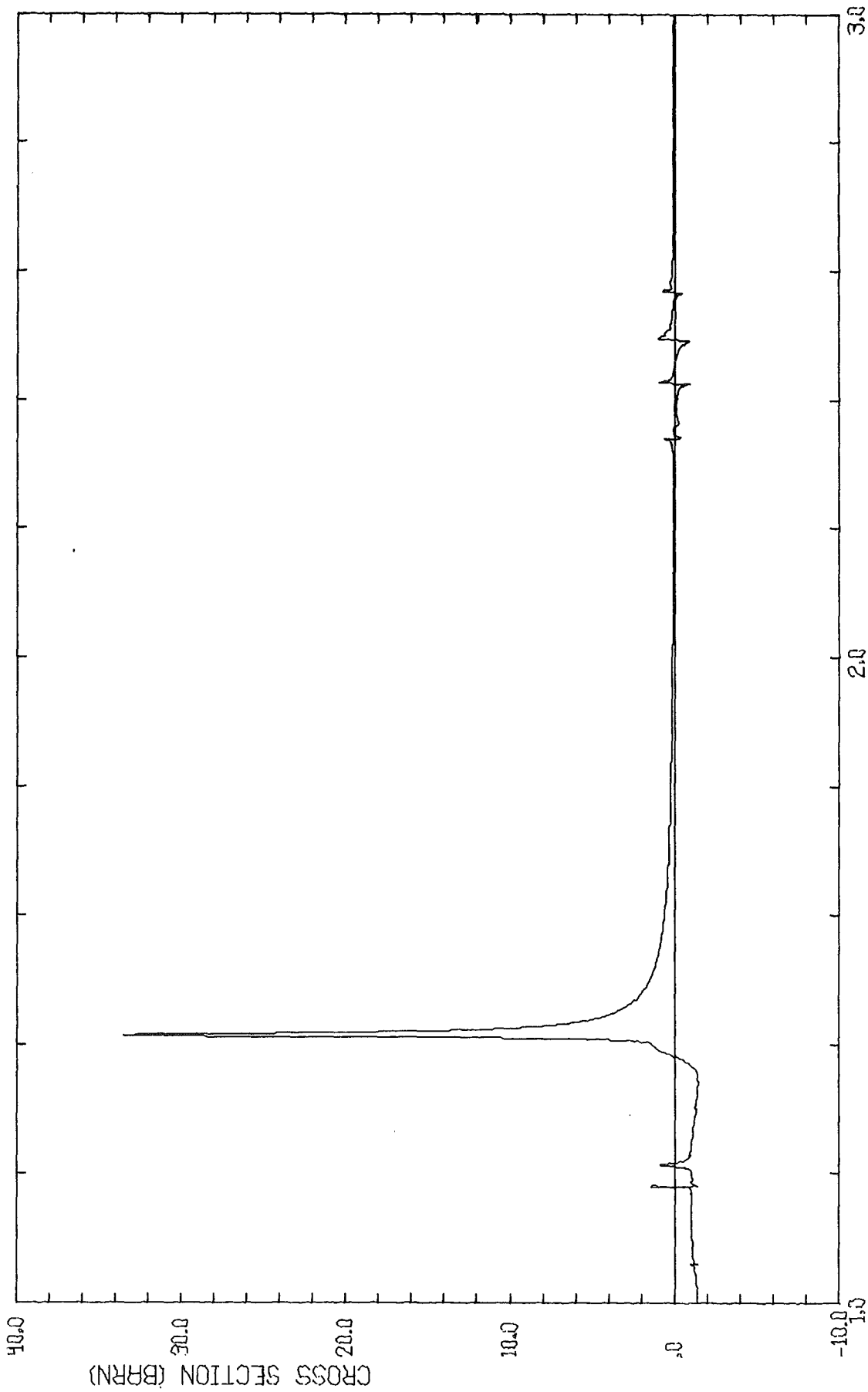
ELASTIC CR 52 DIFFERENCE ML-SL



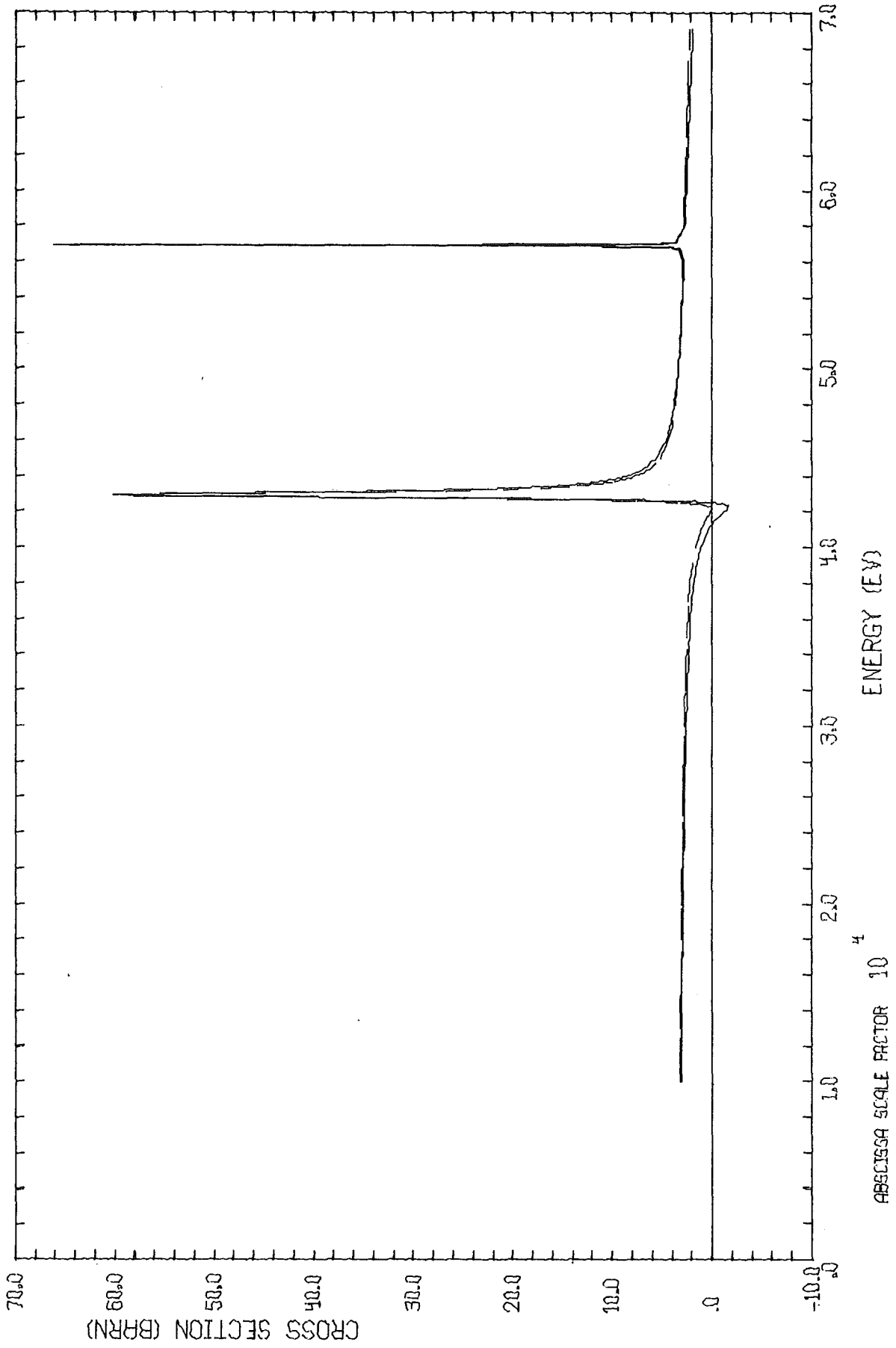
ELASTIC CR 52



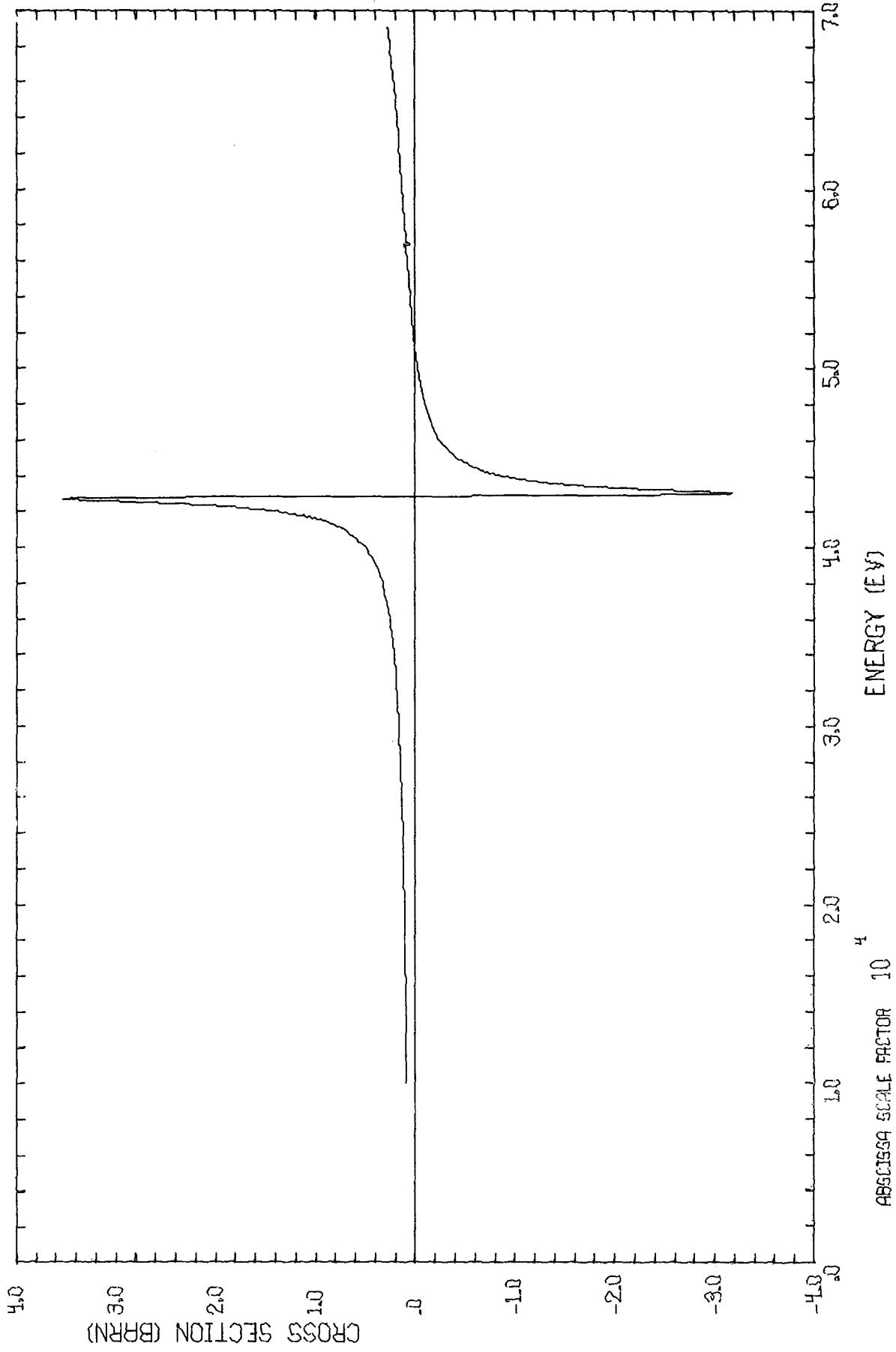
ELASTIC CR 52 DIFFERENCE ML-SL



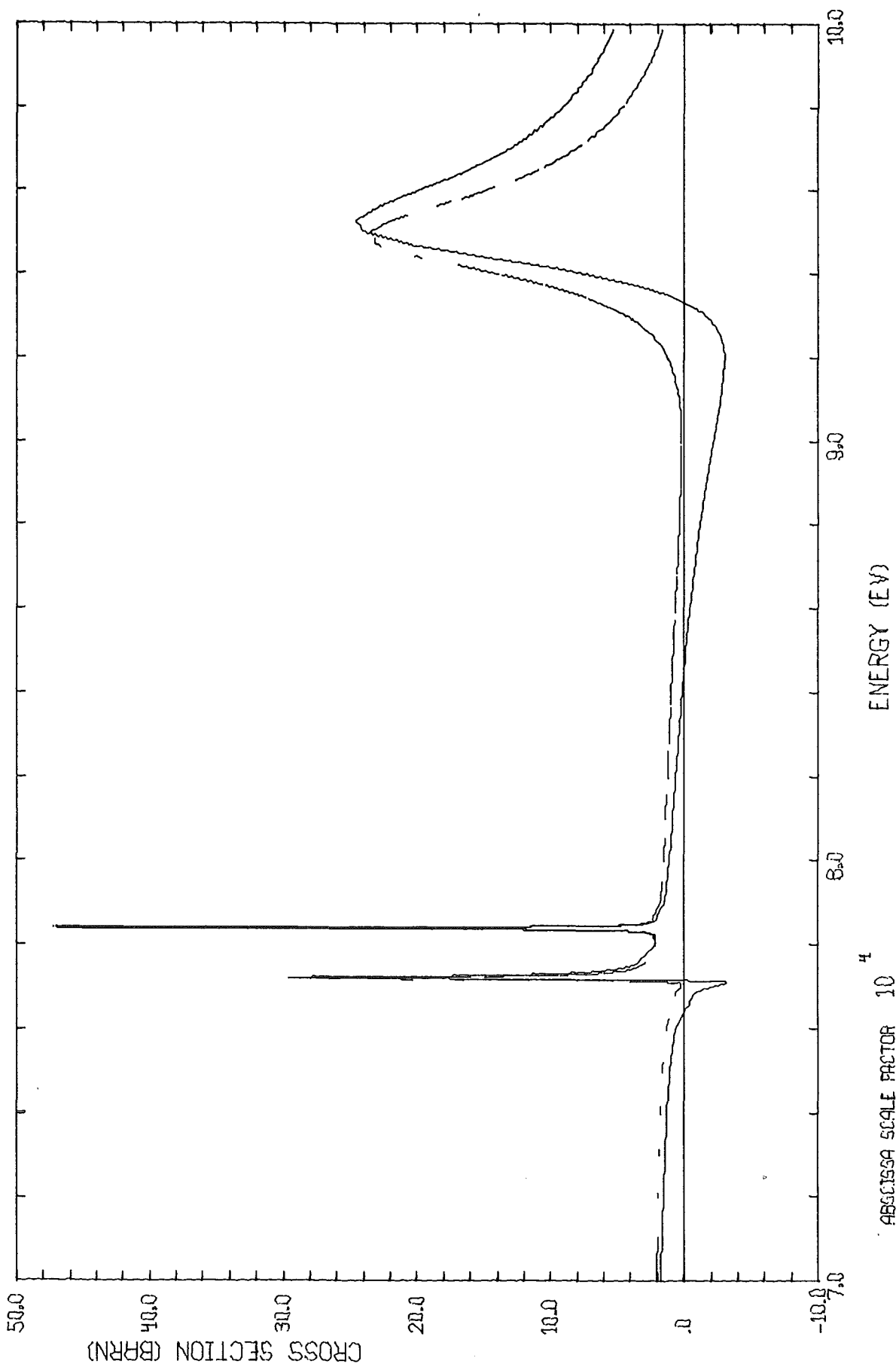
ELASTIC NI 62



ELASTIC NI 62 DIFFERENCE ML-SL

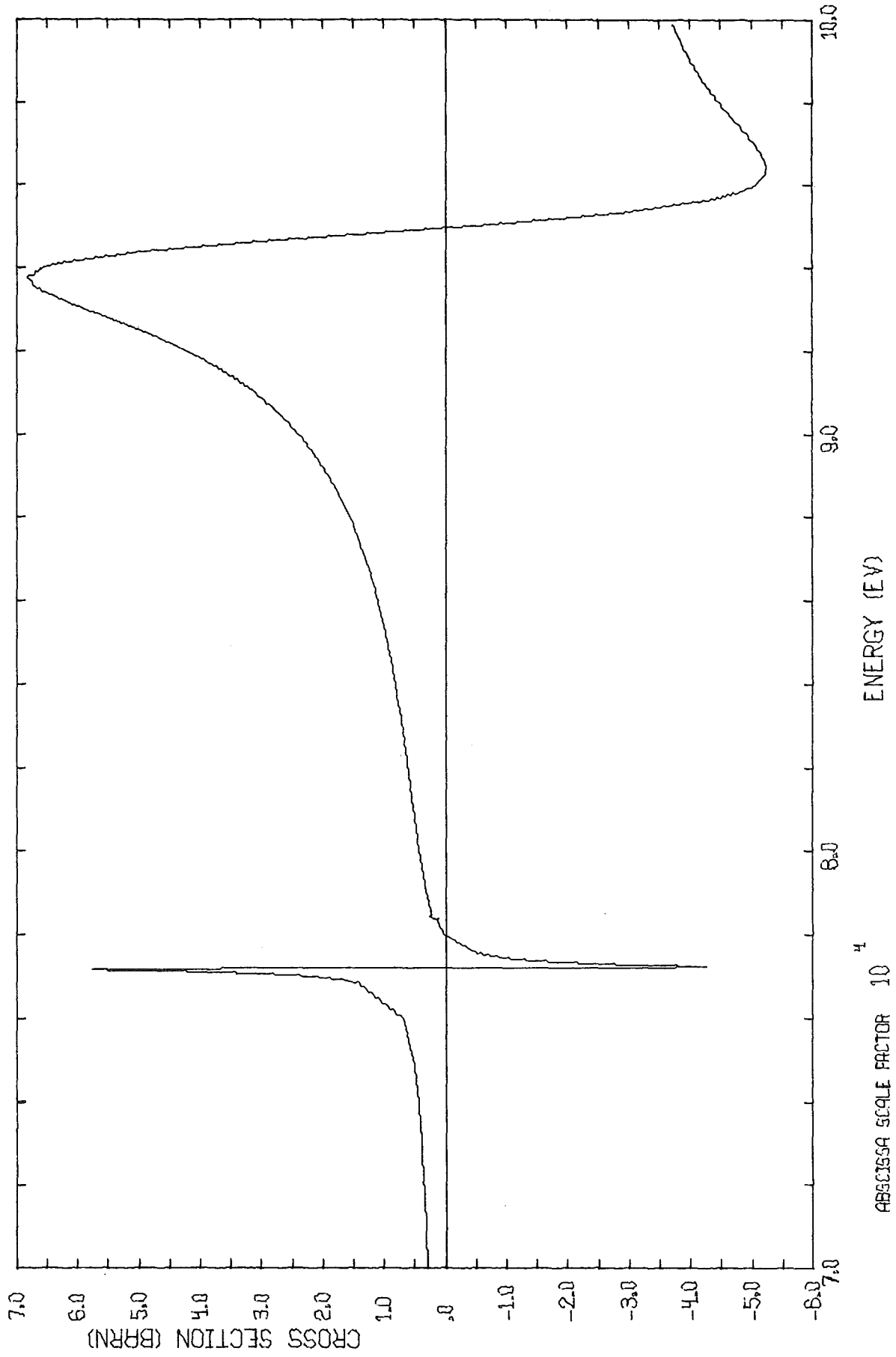


ELASTIC NI 62

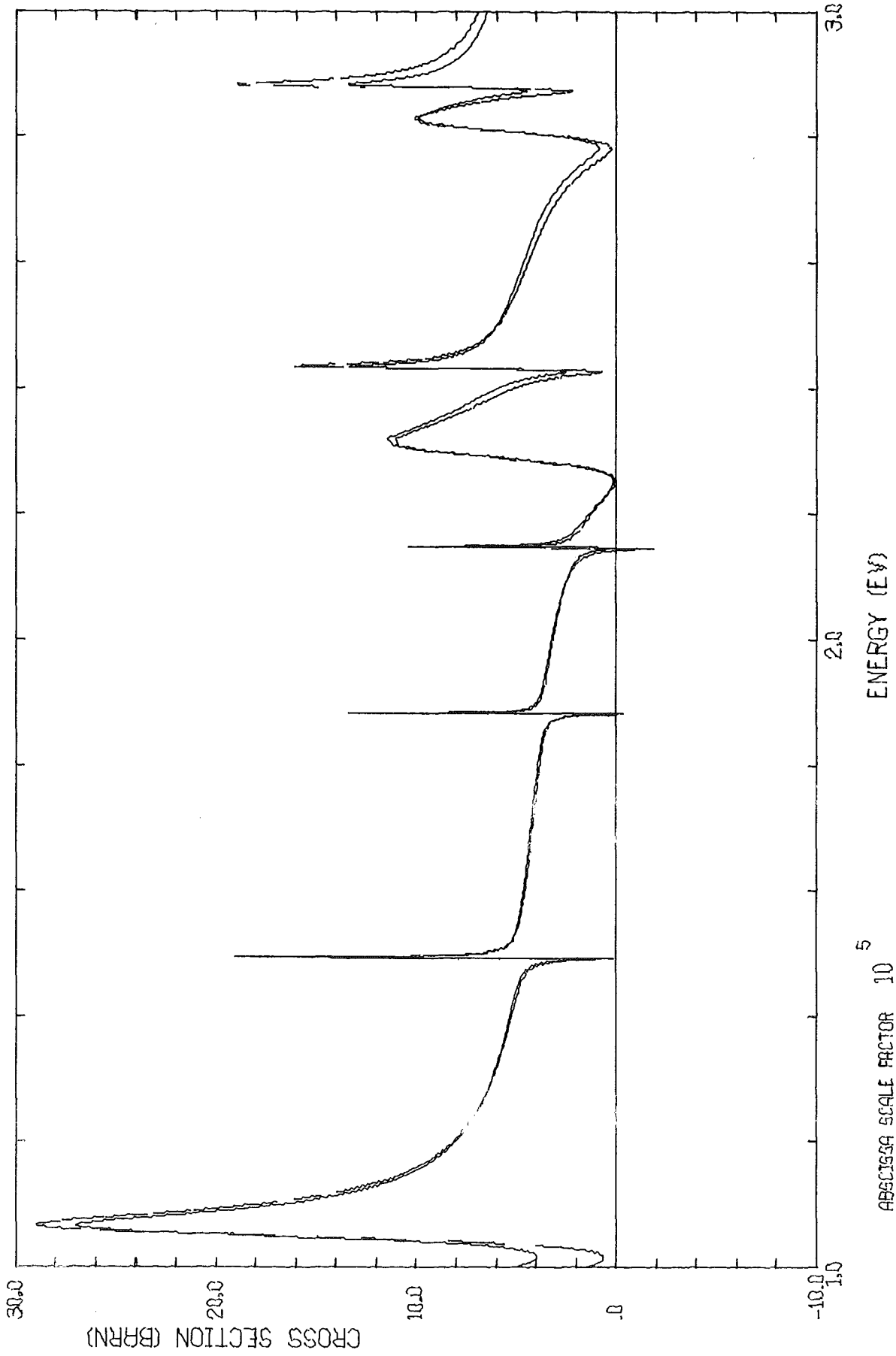


ABSCISSA SCALE FACTOR 10<sup>4</sup>

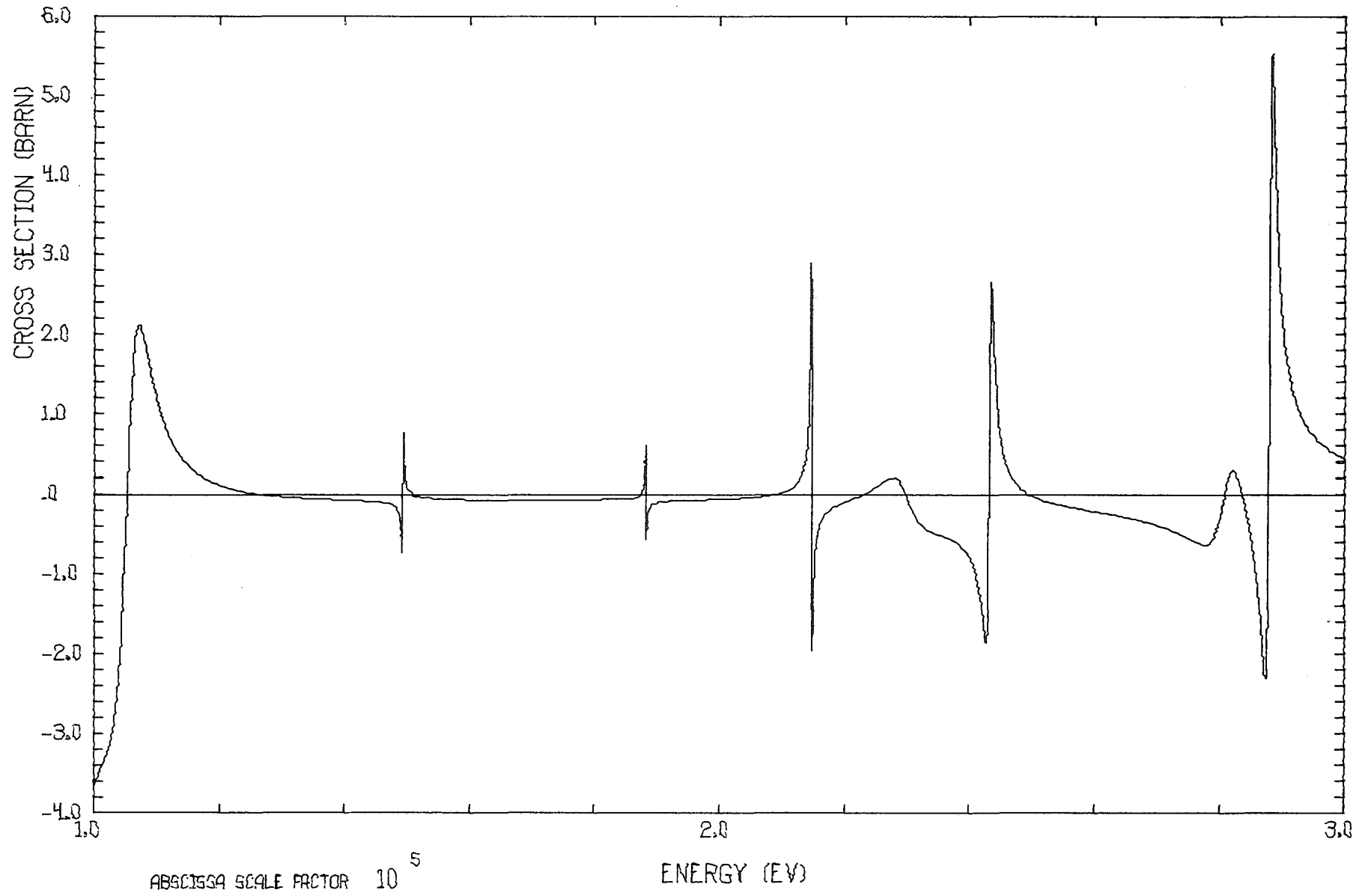
ELASTIC NI 62 DIFFERENCE ML-SL



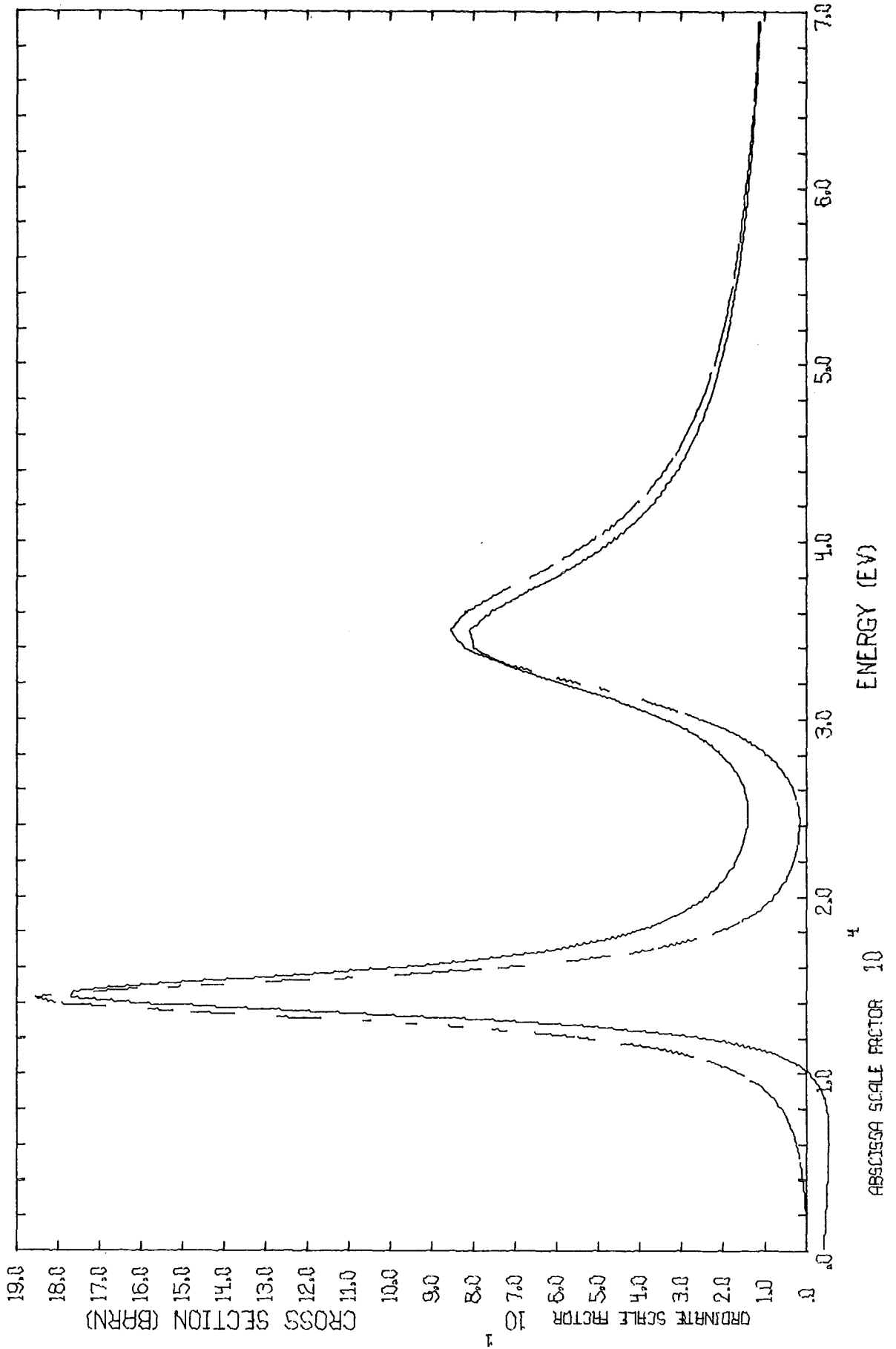
ELASTIC NI 62



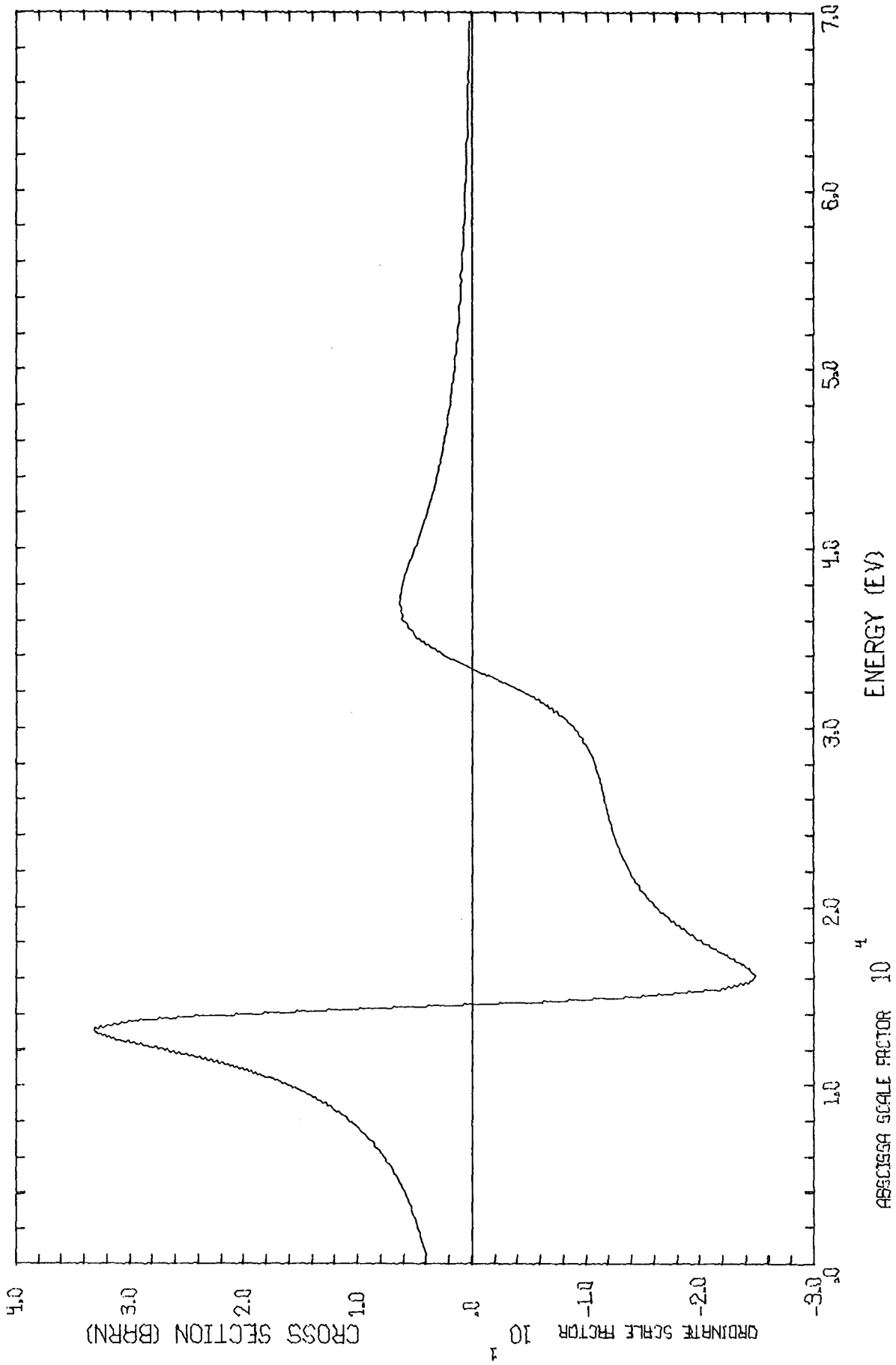
ELASTIC NI 62 DIFFERENCE ML-SL



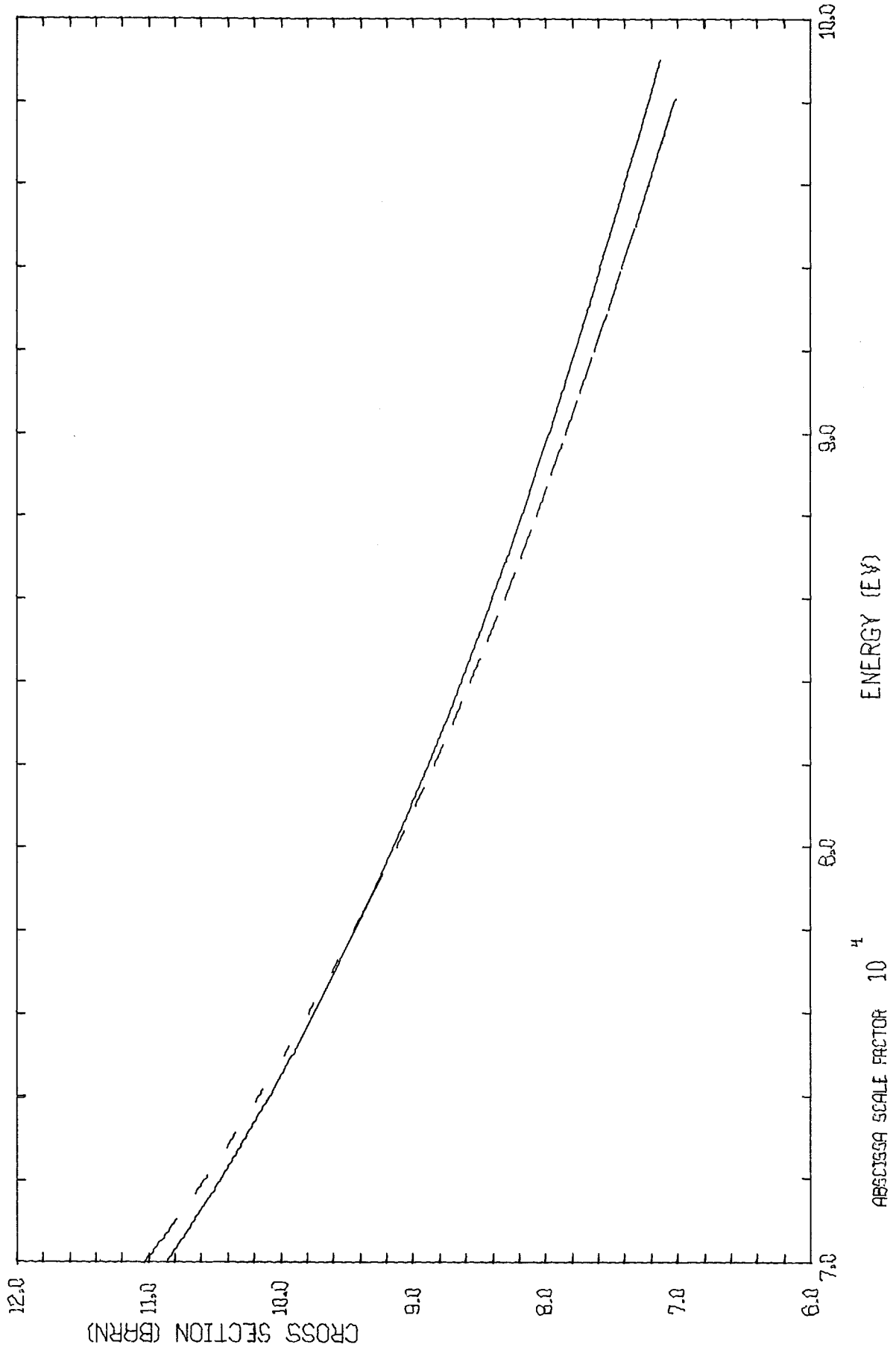
ELASTIC NI 64



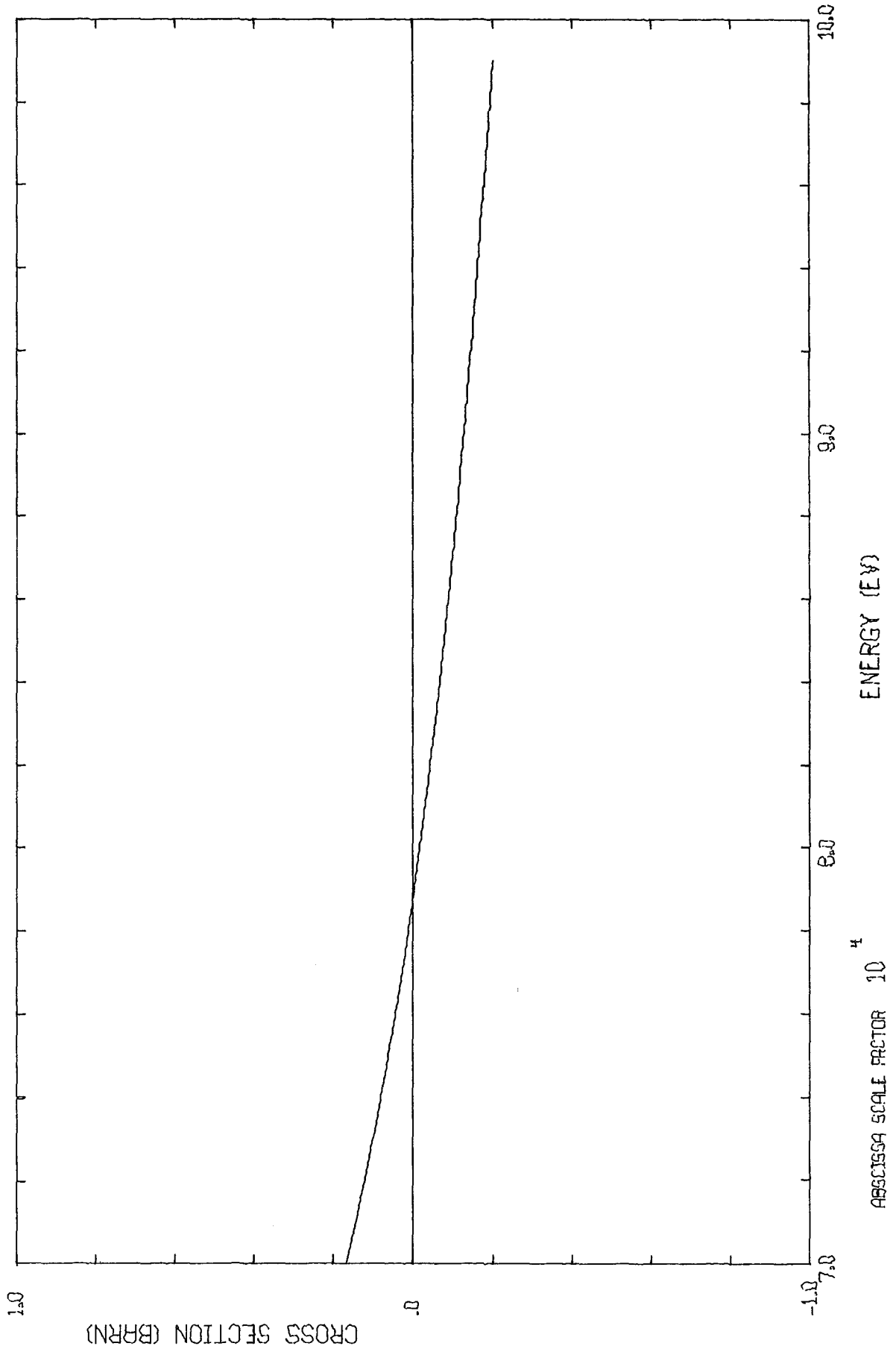
ELASTIC NI 64 DIFFERENCE ML-SL



ELASTIC NI 64

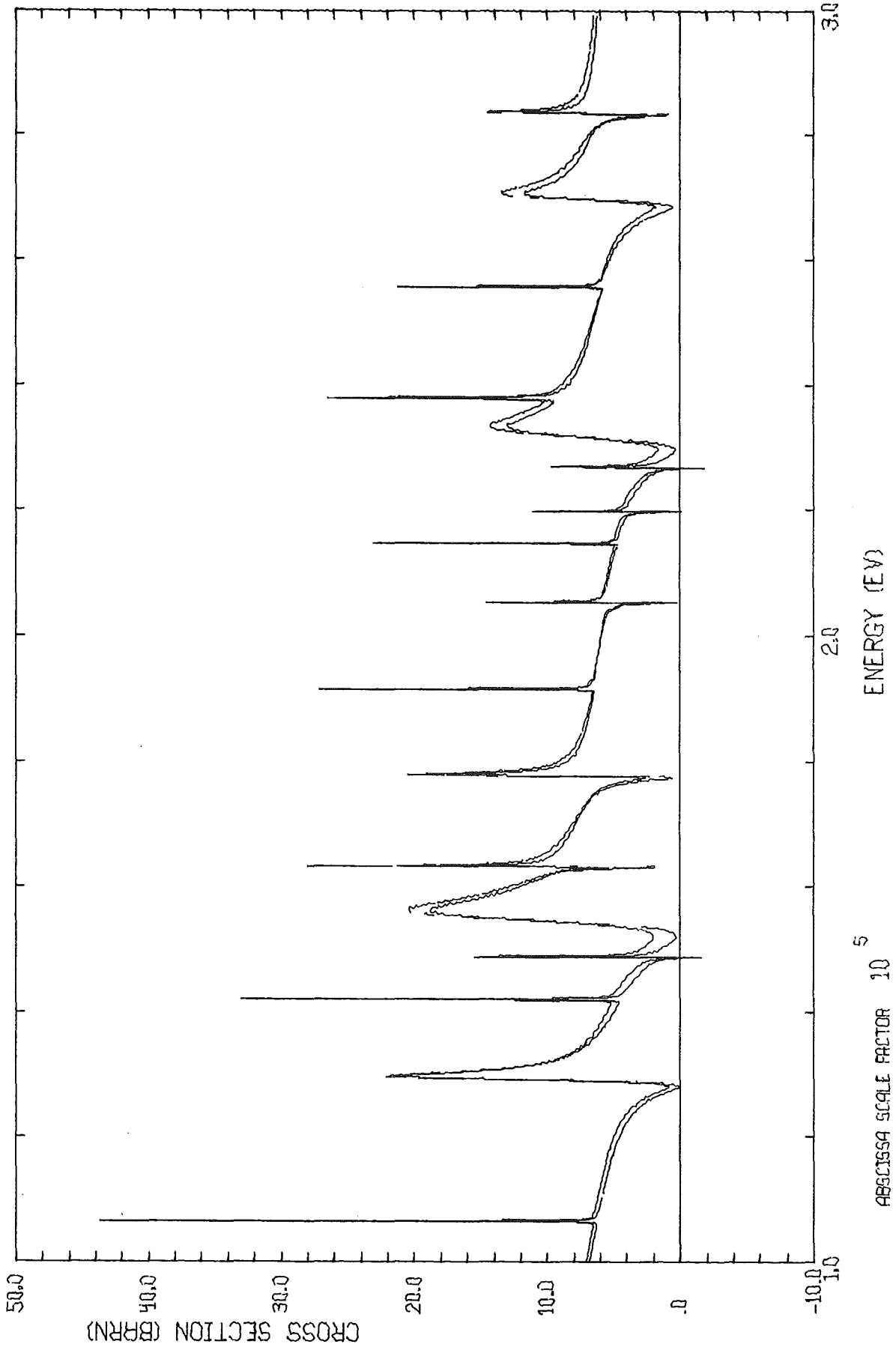


ELASTIC NI 64 DIFFERENCE ML-SL

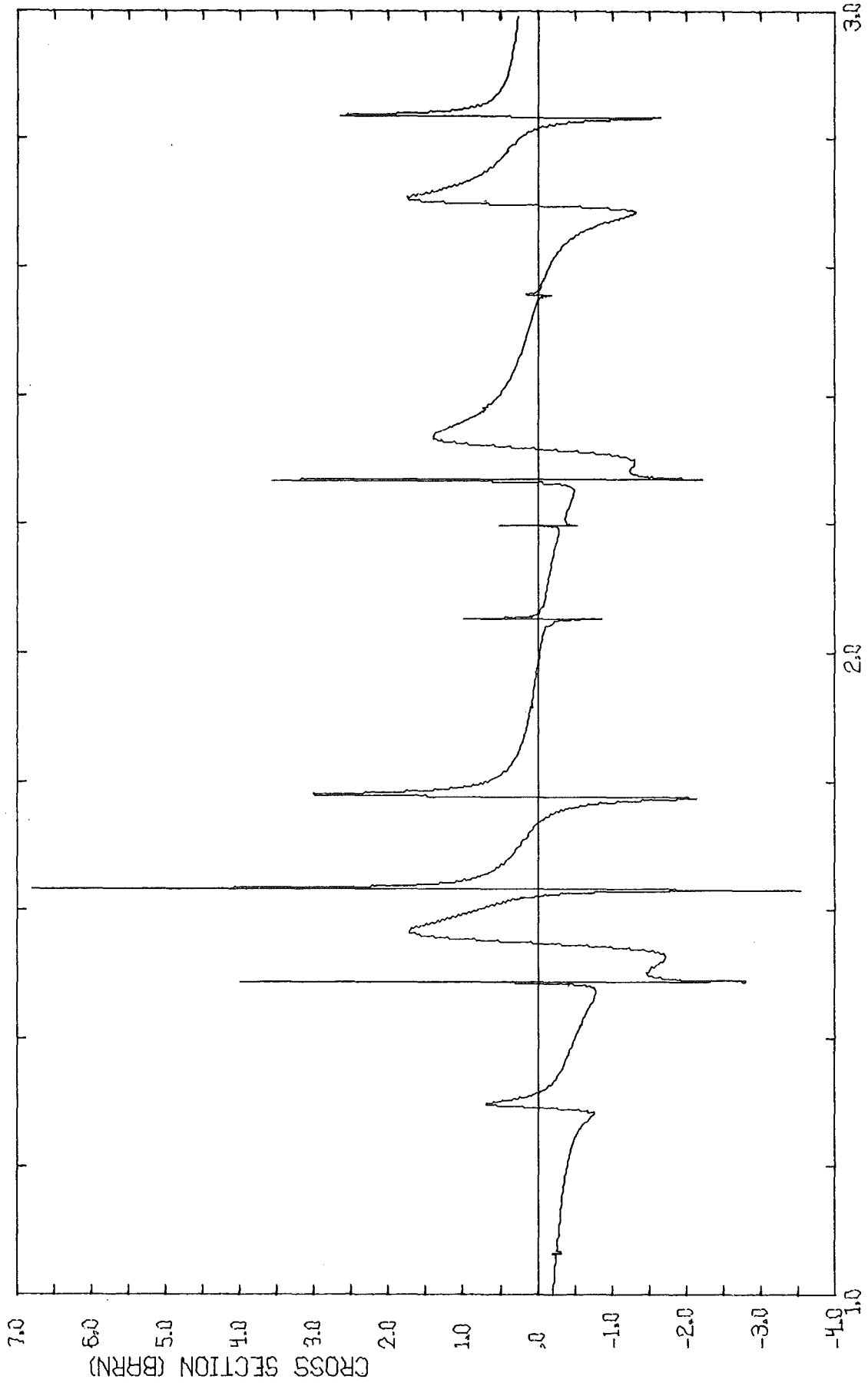


ABSCISSA SCALE FACTOR 10<sup>4</sup>

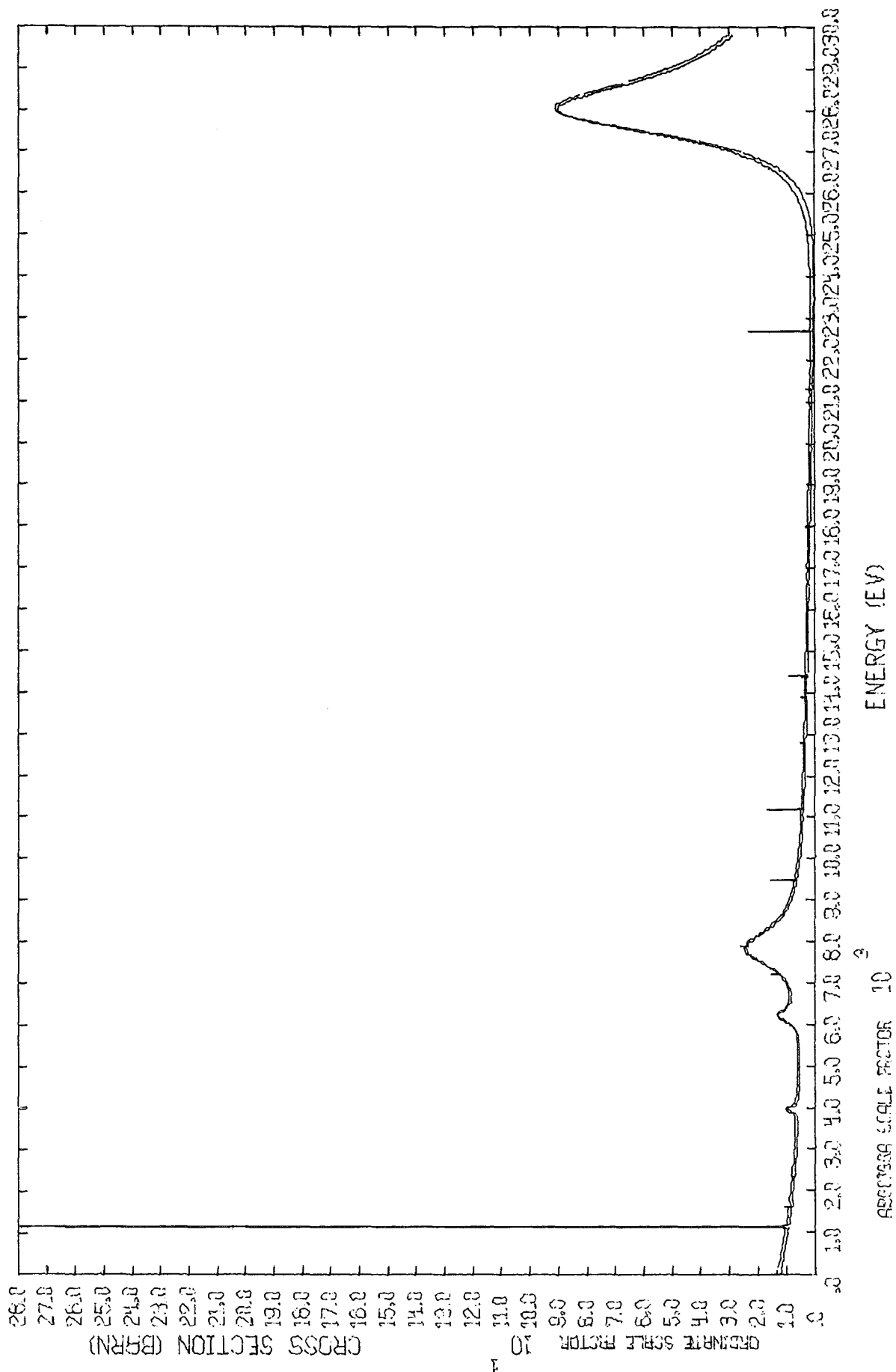
ELASTIC NI 64



ELASTIC NI 64 DIFFERENCE ML-SL



TOTAL FE

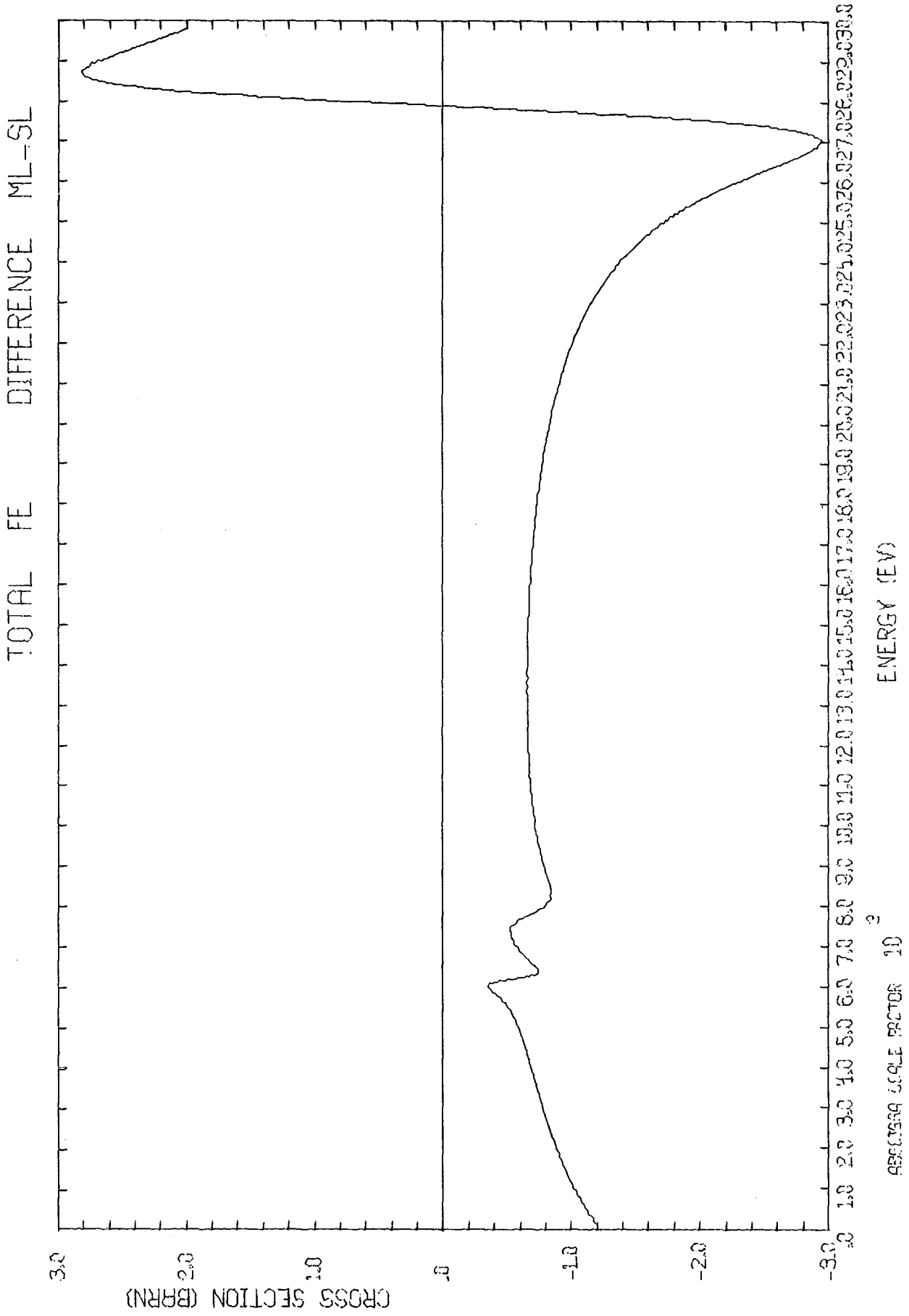


ENERGY (eV)

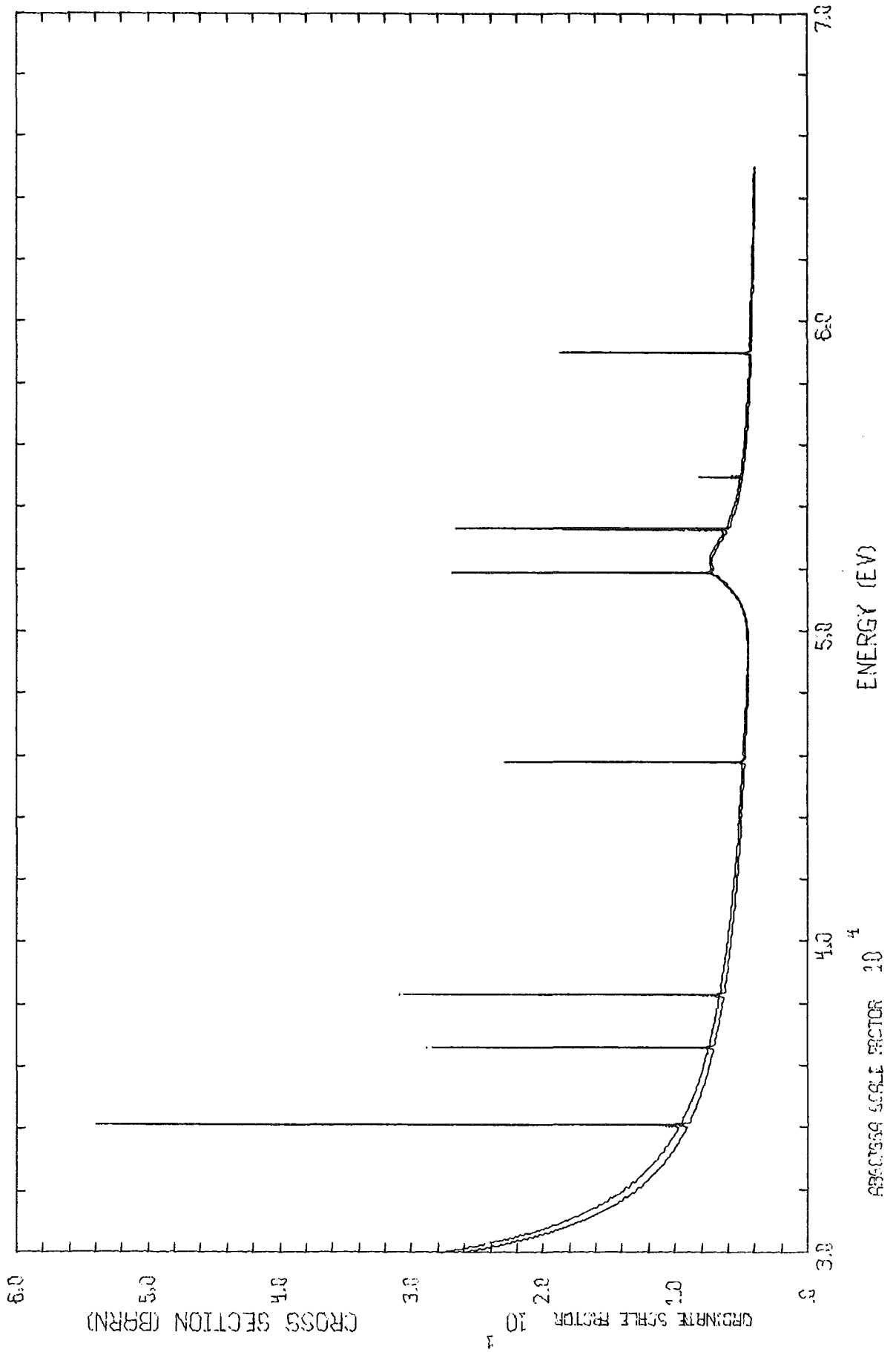
ABSCISSA SCALE FACTOR 10<sup>3</sup>

CROSS SECTION (BBRN)

28.0  
27.0  
26.0  
25.0  
24.0  
23.0  
22.0  
21.0  
20.0  
19.0  
18.0  
17.0  
16.0  
15.0  
14.0  
13.0  
12.0  
11.0  
10.0  
9.0  
8.0  
7.0  
6.0  
5.0  
4.0  
3.0  
2.0  
1.0  
0



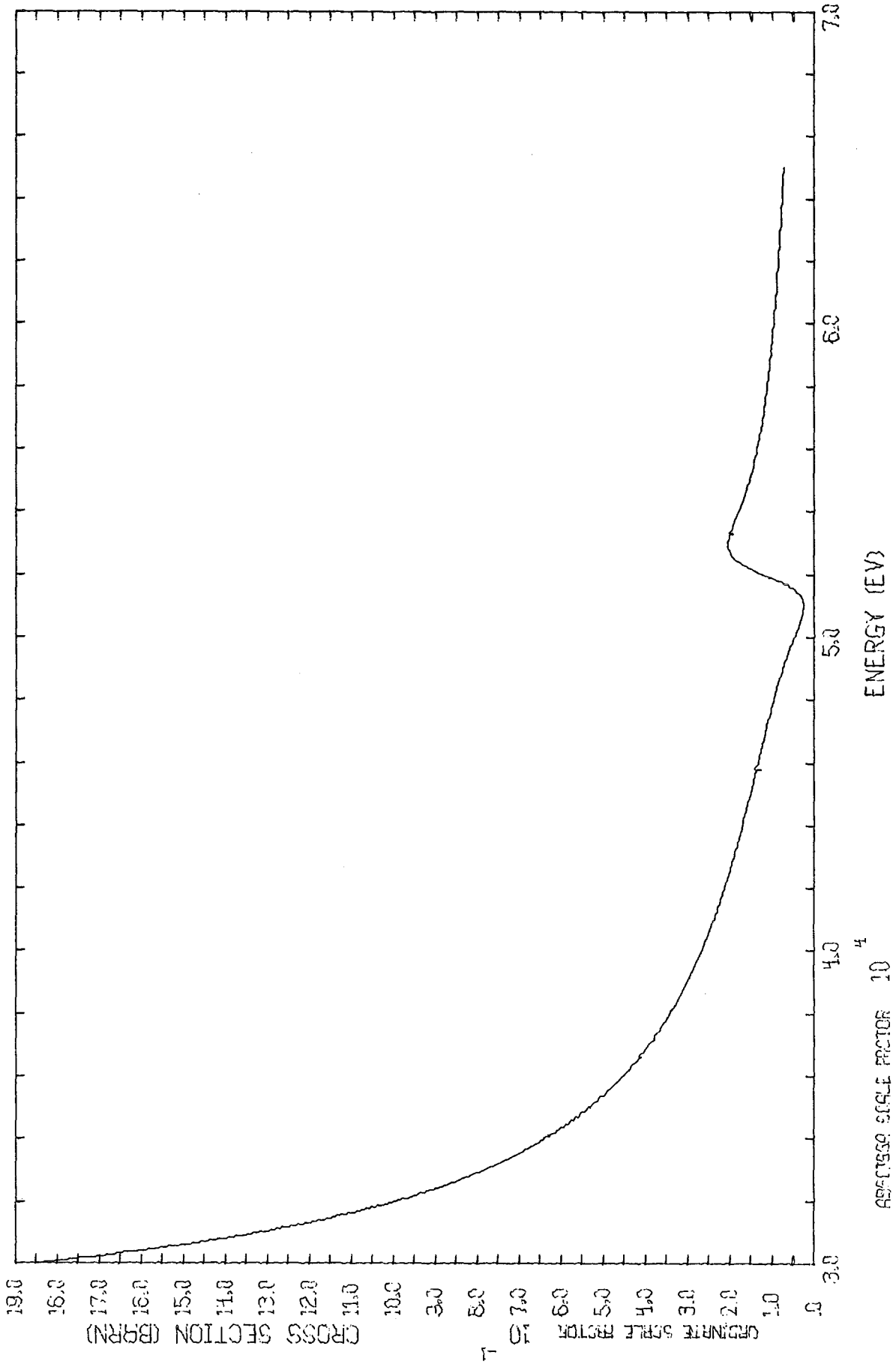
TOTAL FE



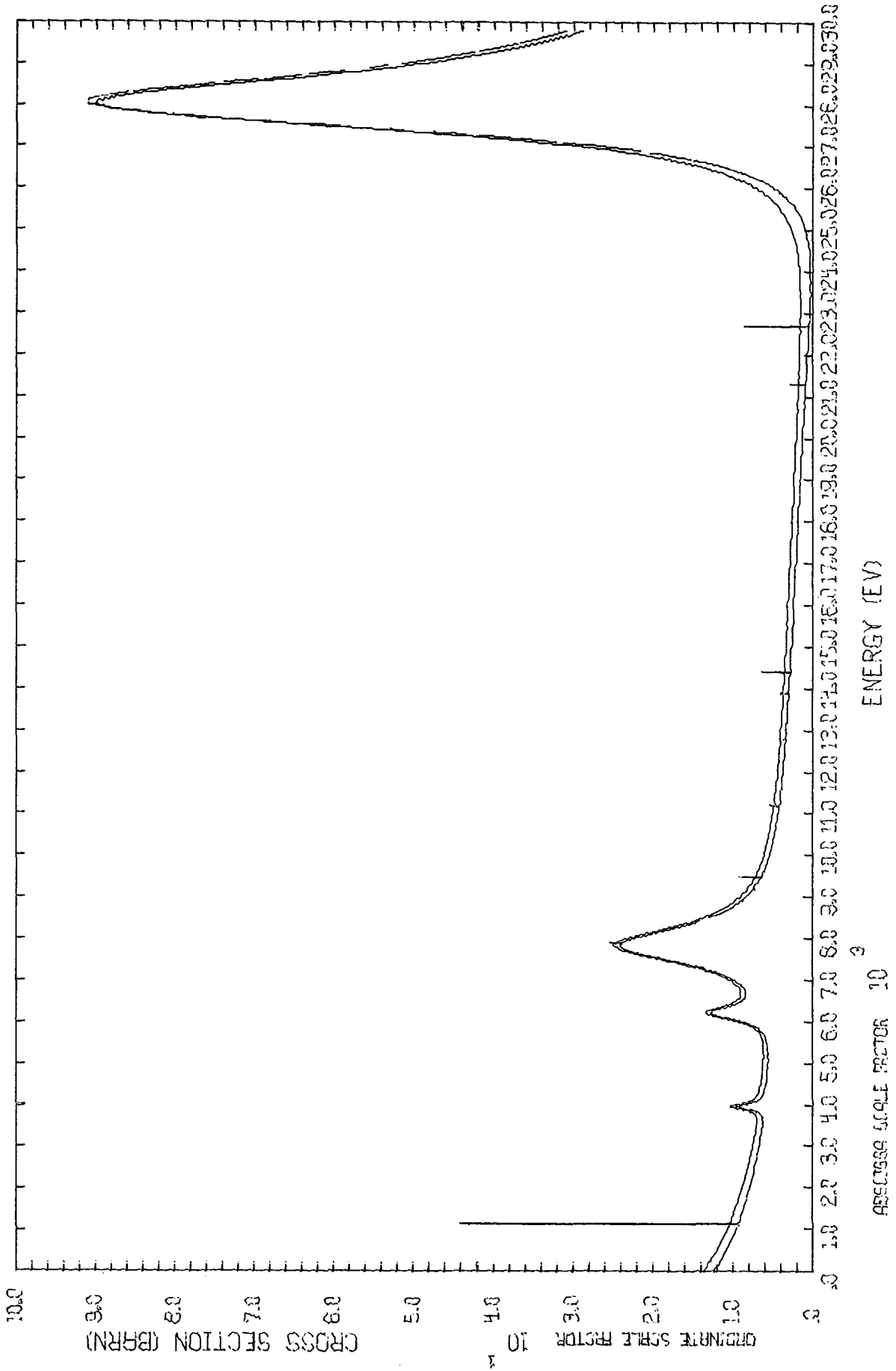
ABSCISSA SCALE FACTOR 10<sup>4</sup>  
ENERGY (EV)

CROSS SECTION (BRRN)  
GROUND STATE FACTOR 10<sup>4</sup>

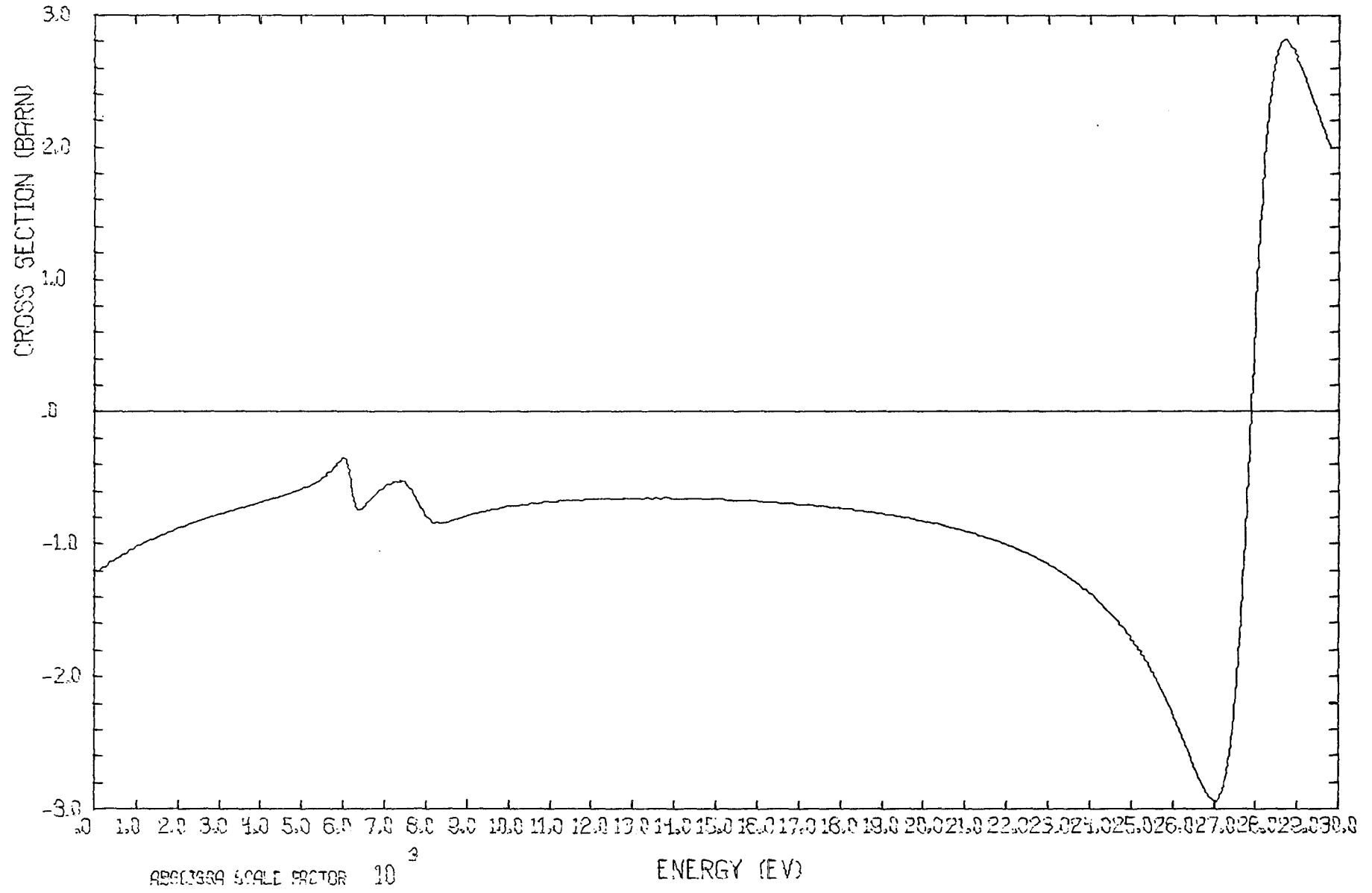
TOTAL FE DIFFERENCE ML-SL



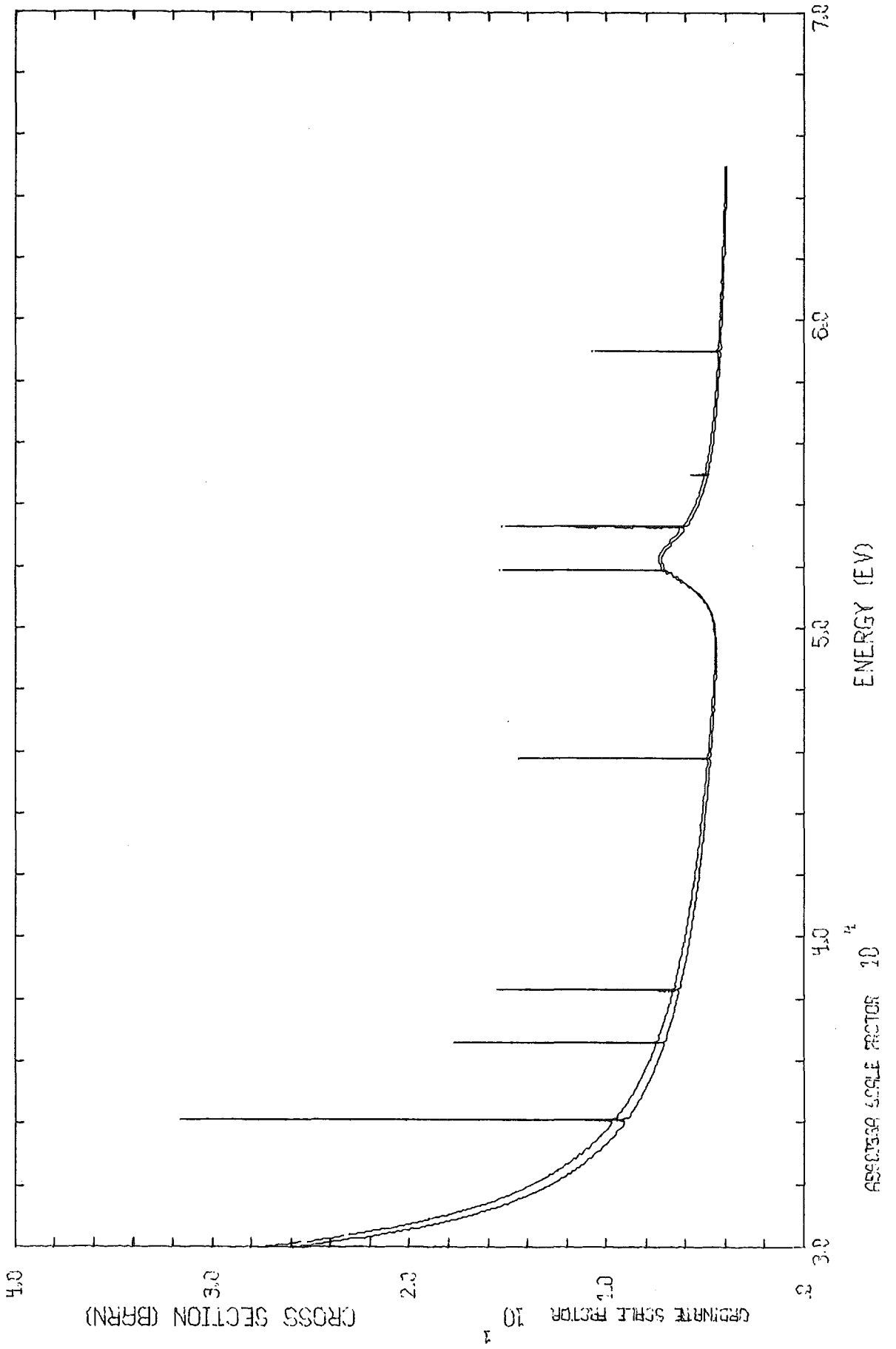
ELASTIC FE



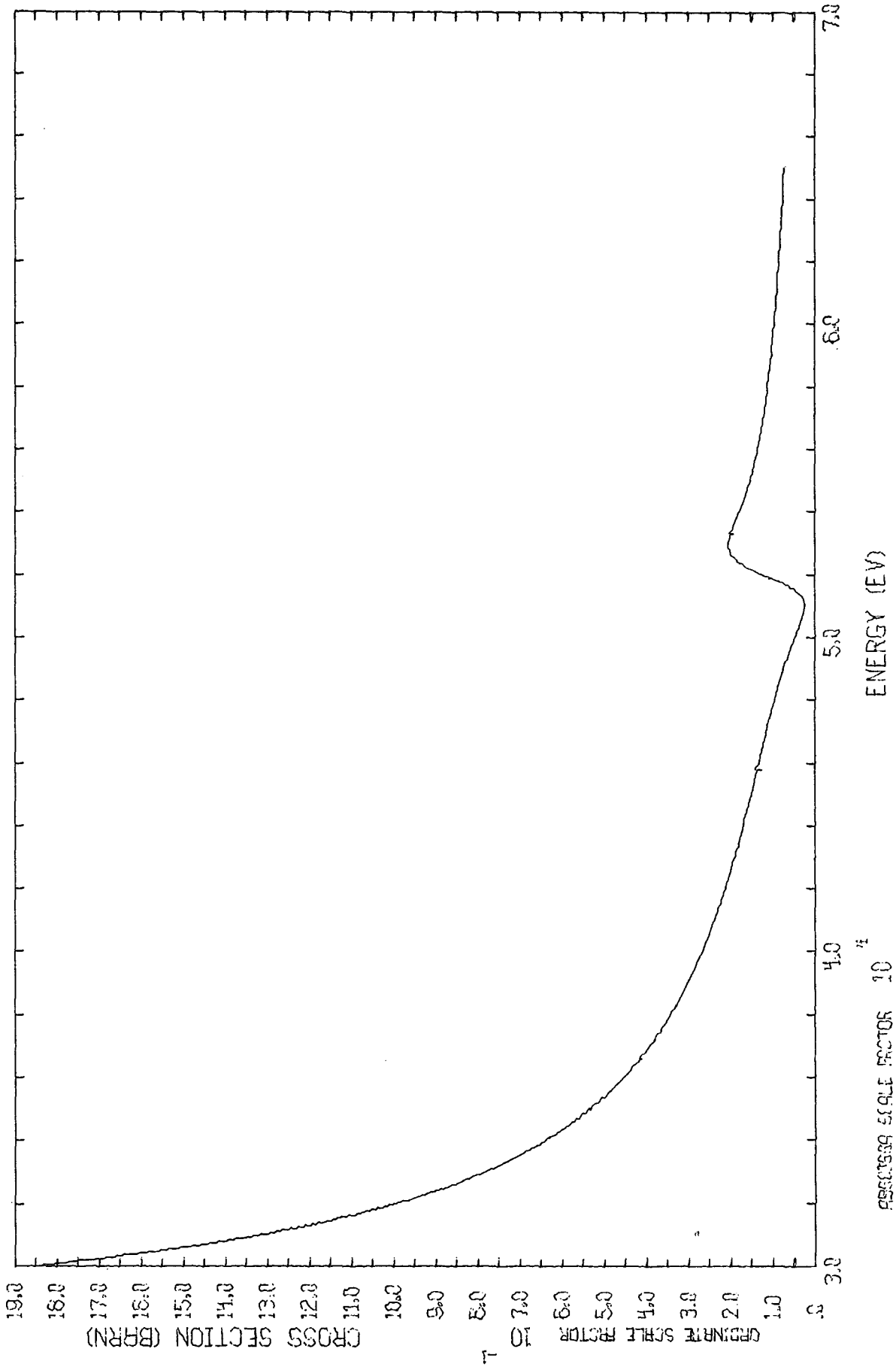
ELASTIC FE DIFFERENCE ML-SL



ELASTIC FE

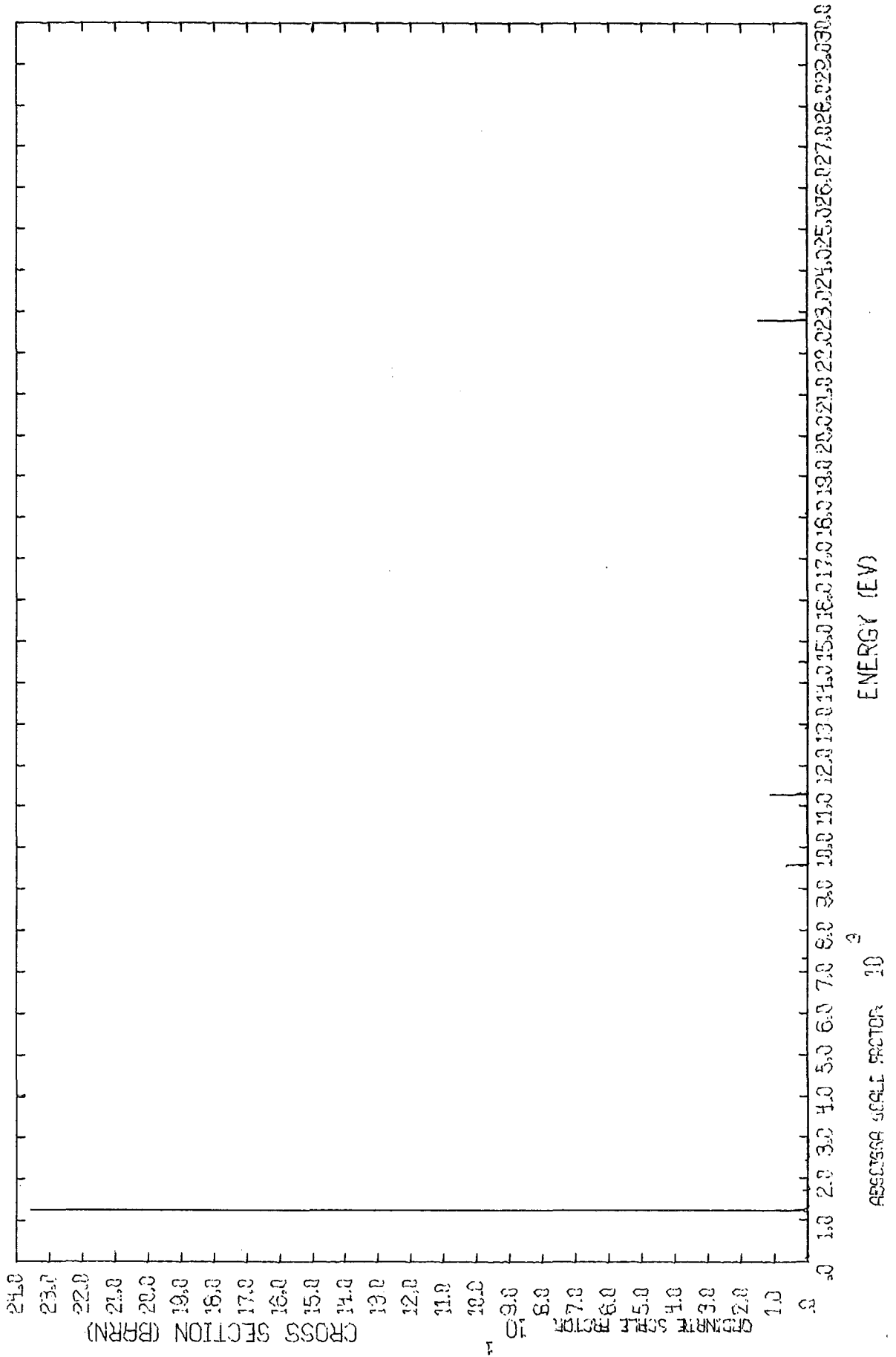


ELASTIC FE DIFFERENCE ML-SL

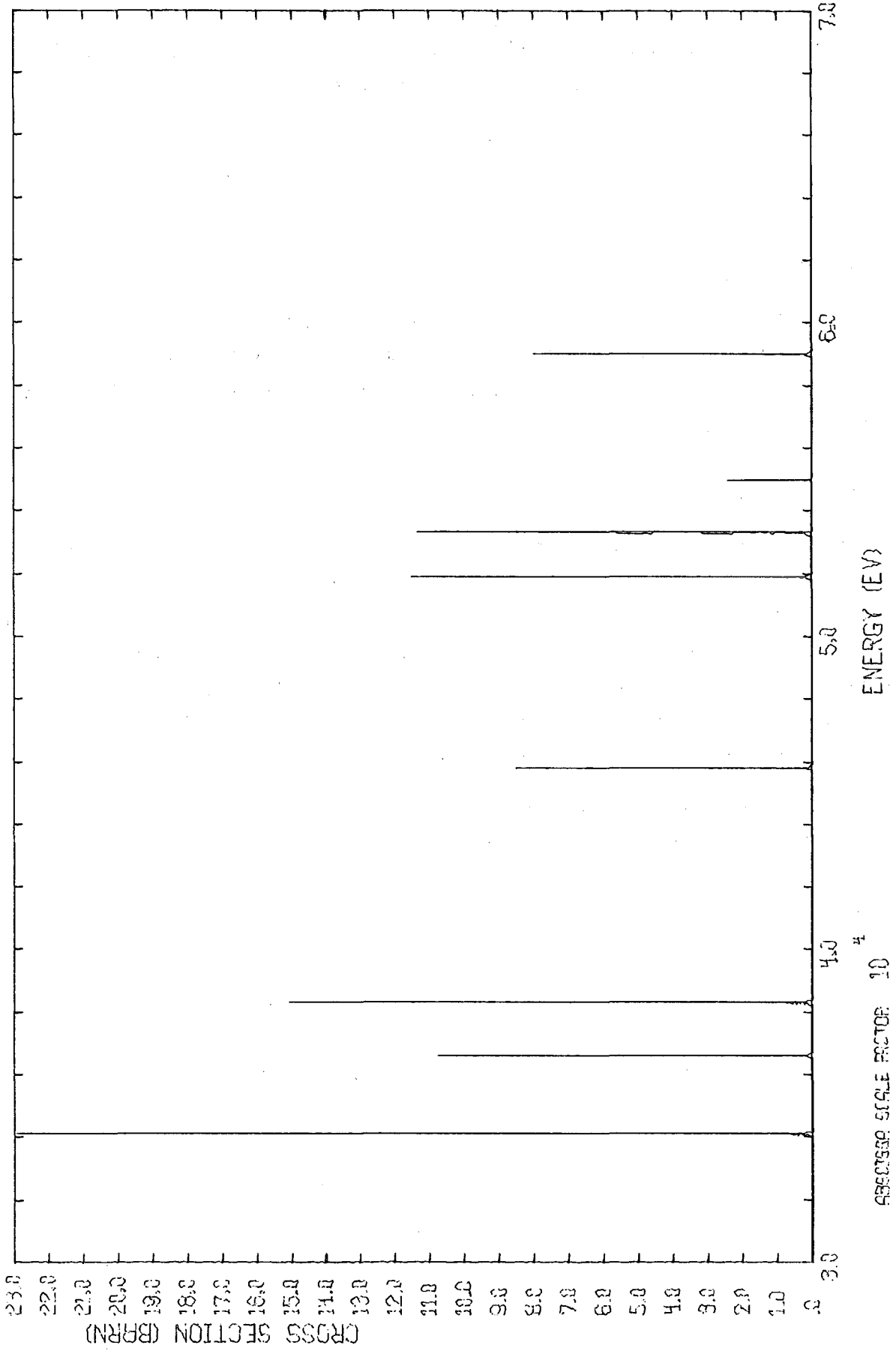


ASSOCIATED SCALE FACTOR 10<sup>-1</sup>

CAPTURE FE



CAPTURE FE



An evaluation of the neutron cross-sections of natural nickel and its stable isotopes below 600 keV

M. C. Moxon

U.K.A.E.A., A.E.R.E., Harwell, Didcot, Berks., U.K.

1. Introduction

This is a summary of a forthcoming Harwell Report. It includes much of the experimental data collected by S. A. Cox<sup>(1)</sup>. Additional data and results given in progress reports up to January 1972 have been included. The list of references is complete.

2. General data

The recommended atomic abundances and masses for the nickel isotopes are given in Table 1. The exact masses are taken from the compilation of Mapples et al<sup>(6)</sup>. Table 2 gives the Q values for neutron reaction producing charged particles. The positive Q values show that some n,p and n, $\alpha$  reactions are energetically possible with zero energy neutrons. However, the coulomb barrier is sufficiently high that the cross-sections for charged particle emission are negligible for most purposes below 600 keV.

Table 3 lists the level schemes for the stable nickel isotopes up to 3 MeV as given in reference 7. Only Ni-61 has excited states below 600 keV and as this isotope occurs at 1.19% abundance, inelastic scattering can be neglected in the present evaluation.

The weighted mean value of the published values of the thermal capture cross-section of natural nickel is  $4.390 \pm 0.049$  b, with a chi-squared value of 30.8 for 8 degrees of freedom. Therefore a value of  $4.40 \pm 0.1$  b is recommended. Few measurements have been made on separated isotopes and the recommended values are given in Table 4.

There is much disagreement in the measurement of the resonance integral for natural nickel, values varying from 2.0 to 0.06 b. The recommended values given in Table 4 are those calculated from the resonance parameters in this report. Note that they do not include the absorption due to charged particle emission.

The potential scattering cross-section  $\sigma_{pot}$  can be expressed as

$$\sigma_{pot} = 4\pi R^2$$

where  $R'$  is the effective nuclear radius in the energy region being considered. Assuming that all resonances near to the energy region being considered have been taken into account,  $R'$  can be written in terms of the nuclear radius  $a' = 1.35 A^{1/3}$  fm and a constant component  $R_\infty$  to take into account far away levels

$$R' = 1.35 A^{1/3} (1 - R_\infty)$$

Bilpuch et al<sup>(43)</sup> derive values for  $R'$  of  $7.5 \pm 0.5$  fm ( $R_\infty = 0.317 \pm 0.067$ ) and  $6.5 \pm 0.5$  fm ( $R_\infty = -0.186 \pm 0.077$ ) for the isotopes 58 and 60 respectively from their total cross-section measurements in the energy range  $\sim 20$  to 600 keV. Since the slow neutron scattering by the even isotopes is wholly coherent, their 'free atom' scattering cross-section may be derived from measurements of their bound coherent scattering lengths and conversely, in Table 5 the recommended parameters are given.

### 3. Resonance parameters

Table 6 lists the published data that give some information about the resonance parameters of the nickel isotopes. The first section of the table gives the reports that specifically give the parameters while the latter section lists the reports that give either average cross-sections or have too poor an energy resolution to separate individual resonances but from which average resonance data can be deduced.

Tables 7-11 list recommended values of the resonance parameters for each isotope. Where several sets of data exist there is general agreement. The energies published by Bilpuch et al<sup>(43)</sup> and Farrell et al<sup>(44)</sup> have been increased by 1.24 keV to bring them into line with the energies obtained by the time of flight measurements of Garg et al<sup>(45)</sup>. The parameters of negative energy resonances have been adjusted so that the calculated cross-sections at low energies are in agreement with the recommended values given in this report.

Figures 1 and 2 show respectively the measured total cross-section data and the calculated cross-section using the recommended parameters up to a neutron energy of 100 keV. The agreement is good in the energy region below  $\sim 20$  keV and in the region of the large s-wave resonances when the resolution effects are taken into account, but in the region between these resonances the calculated cross-section tends to be higher than the measured one. This suggests that either some of the resonance parameters need adjustment or that there is an energy dependent term in the potential cross-sections. To change either of these set

parameters is not a trivial matter and at present the quality of the data does not warrant the effort required to get a better fit to the measurements.

Farrell et al<sup>(44)</sup> used shape techniques to distinguish between the s-wave and higher orbital angular momentum resonances above neutron energies of 100 keV. In the energy region below 100 keV, capture measurements (refs. 46, 47, 48, 49) are more sensitive than the transmission measurements in detecting the small resonances due to p-wave and higher orbital angular momentum neutrons. Capture measurements on natural nickel carried out at RPI<sup>(48)</sup> were analysed with the area technique and for the narrow resonances this gives  $g \Gamma_n \Gamma_\gamma / \Gamma$ . Some measurements carried out on Ni-58 and Ni-60 at Karlsruhe<sup>(46)</sup> give similar results. The level spacing determined from the Karlsruhe<sup>(46)</sup> data indicates that if the level spacing follows the (2J+1) rule, and is independent of parity, then about 30% of the resonances between 20 keV and 60 keV must be attributed to d-wave neutrons, as expected if the d-wave strength function is nearly the same as the s-wave one.

#### 4. Radiation widths

The measured values of the radiation widths are given where possible. For the isotopes 60 and 61 several widths have been measured<sup>(46,50)</sup>. In the case of the isotope 58 there are no published values of  $\Gamma_\gamma$  and for Ni-62 and Ni-64 there is only one uncertain value of  $\Gamma_\gamma$  for each isotope. A comparison of measurements of the capture cross-section and that calculated from the parameters given in the report are shown in figures 3 and 4.

Values of  $g \Gamma_n \Gamma_\gamma / \Gamma$  are published<sup>(44,46,48,50)</sup> for the narrow resonances seen in capture measurements. As the neutron widths of these resonances are small, the values of the capture cross-section obtained from the published data tend to be independent of the radiation width used in the calculation, but to calculate Doppler effects a value of the total width (i.e.  $\Gamma_n + \Gamma_\gamma$ ) of the resonances is required. As there are no published values, estimates of the radiation width have to be obtained from the average capture cross-sections in the energy region 20 to 200 keV. Assuming the d-wave strength function is the same as the s-wave one, i.e.  $\sim 2.5 \times 10^{-4}$ , and the p-wave strength function is  $\sim 0.075 \times 10^{-4}$  and a level spacing the same as for the s-wave resonances, then in the case of Ni-60 and Ni-64 the p- and d-wave radiation widths obtained from the average data from ref. (50) and (54) are estimated to be  $\sim 0.7$  eV and  $\sim 0.3$  eV respectively. These values are smaller than the s-wave values of 2.28 eV (4 resonances in Ni-60) and 1.73 eV (1 resonance in Ni-64).

In the case of Ni-60 there appears to be some evidence of a correlation between the neutron and radiation width for the s-wave resonance from the data obtained with the large liquid scintillators<sup>(46,48)</sup> and Moxon-Rae detectors<sup>(47,49)</sup>.

parameters is not a trivial matter and at present the quality of the data does not warrant the effort required to get a better fit to the measurements.

Farrell et al<sup>(44)</sup> used shape techniques to distinguish between the s-wave and higher orbital angular momentum resonances above neutron energies of 100 keV. In the energy region below 100 keV, capture measurements (refs. 46, 47, 48, 49) are more sensitive than the transmission measurements in detecting the small resonances due to p-wave and higher orbital angular momentum neutrons. Capture measurements on natural nickel carried out at RPI<sup>(48)</sup> were analysed with the area technique and for the narrow resonances this gives  $g \Gamma_n \Gamma_\gamma / \Gamma$ . Some measurements carried out on Ni-58 and Ni-60 at Karlsruhe<sup>(46)</sup> give similar results. The level spacing determined from the Karlsruhe<sup>(46)</sup> data indicates that if the level spacing follows the (2J+1) rule, and is independent of parity, then about 30% of the resonances between 20 keV and 60 keV must be attributed to d-wave neutrons, as expected if the d-wave strength function is nearly the same as the s-wave one.

#### 4. Radiation widths

The measured values of the radiation widths are given where possible. For the isotopes 60 and 61 several widths have been measured<sup>(46,50)</sup>. In the case of the isotope 58 there are no published values of  $\Gamma_\gamma$  and for Ni-62 and Ni-64 there is only one uncertain value of  $\Gamma_\gamma$  for each isotope. A comparison of measurements of the capture cross-section and that calculated from the parameters given in the report are shown in figures 3 and 4.

Values of  $g \Gamma_n \Gamma_\gamma / \Gamma$  are published<sup>(44,46,48,50)</sup> for the narrow resonances seen in capture measurements. As the neutron widths of these resonances are small, the values of the capture cross-section obtained from the published data tend to be independent of the radiation width used in the calculation, but to calculate Doppler effects a value of the total width (i.e.  $\Gamma_n + \Gamma_\gamma$ ) of the resonances is required. As there are no published values, estimates of the radiation width have to be obtained from the average capture cross-sections in the energy region 20 to 200 keV. Assuming the d-wave strength function is the same as the s-wave one, i.e.  $\sim 2.5 \times 10^{-4}$ , and the p-wave strength function is  $\sim 0.075 \times 10^{-4}$  and a level spacing the same as for the s-wave resonances, then in the case of Ni-60 and Ni-64 the p- and d-wave radiation widths obtained from the average data from ref. (50) and (54) are estimated to be  $\sim 0.7$  eV and  $\sim 0.3$  eV respectively. These values are smaller than the s-wave values of 2.28 eV (4 resonances in Ni-60) and 1.73 eV (1 resonance in Ni-64).

In the case of Ni-60 there appears to be some evidence of a correlation between the neutron and radiation width for the s-wave resonance from the data obtained with the large liquid scintillators<sup>(46,48)</sup> and Moxon-Rae detectors<sup>(47,49)</sup>

The lower data points from the lead slowing down spectrometer<sup>(55)</sup> and the smaller average value of  $\Gamma_\gamma$  required to fit the average cross-section region for p- and d-wave neutrons suggest that it may be an experimental effect.

There are some theoretical grounds for supposing that the radiation widths for odd parity resonances should be less than for the even parity ones, the main argument being that the first levels of opposite parity to the ground state in the compound nucleus occur at an excitation energy of between 2 and 3 MeV (see nuclear data sheets, reference (7)). As a large fraction of the s-wave capture goes to states in the compound nucleus below 2 MeV via E1 transitions, the  $E_\gamma^3$  dependence of E1 transition probability would indicate a reduction in  $\Gamma_\gamma$  for p-wave capture by a factor of  $\sim 3$ , unless there was some enhancement of the M1 transitions for the p-wave resonances. In the case of d-wave resonances one would expect similar radiation widths as for s-wave, with some reduction due to the possible higher spins of the resonances, but not as much as a factor of  $\sim 3$ .

One of the main experimental problems associated with the measurement of capture cross-section of the light nuclei is the relative efficiency of detecting scattered neutrons to that of detecting the neutrons captured in the sample. Several experimenters<sup>(47,48)</sup> have tried to measure this quantity and estimates for various detectors are in the region of  $10^{-4}$ . The capture to scattering ratios for the nickel s-wave resonances are  $\lesssim 10^{-3}$ , so even a small underestimate of the neutron detecting efficiency could produce too large a value of the radiation width and an apparent correlation between the neutron and radiation widths. It should be noted that in the case of the lead slowing down spectrometer, the scattered neutrons will have little effect on the detector since it is in the neutron flux, but may cause an additional effect due to perturbation of the neutron flux in the spectrometer. Diven et al<sup>(59)</sup> in their measurements above 100 keV used a large liquid scintillator and fast time of flight equipment to reduce the background and may have greatly reduced the effect of the scattered neutrons on their data.

Another problem arises in correcting the measured yields for multiple scattering and self screening. To obtain the true capture cross-section even for thin samples, corrections often exceeding factors of 2 have to be made to the observed data in the regions of the large s-wave resonances. These corrections are much easier to calculate for the time of flight data where a parallel neutron beam at normal incidence is used, than in the case of the lead slowing down spectrometers where the samples are in an isotropic neutron flux and have a much poorer energy resolution.

In measuring the small capture cross-section of such elements as nickel, the measurement of the background is very important and erroneous assumptions about the

effect of filters etc. on the background can lead to large systematic errors. The most easily measured background is that due to cosmic rays, local long lived activities, and that due to the neutron source and sample holder, all of which can be measured simply by removing the sample. In time of flight experiments the background, caused by the scattered neutrons from the sample which are subsequently captured in the surrounding materials at times greater than the resolving time of the spectrometer, is very difficult to measure. The form of this background will not only depend on the sample, its nuclear mass and its scattering cross-section, but also on the surrounding materials. The use of resonance filters gives only the background at a limited number of spot points and if the background does not vary smoothly with time of flight, these effects may be missed or underestimated. Samples of lead or carbon do not reproduce the scattering structure of the samples and have to be physically much thicker than the samples themselves to obtain the same  $n\sigma_s$  as occur in the peaks of s-wave resonances in the keV region and these data have to be normalised and adjusted to reproduce the scattering effects of the sample.

For the lead slowing down spectrometers the background is measured by carrying out a run without the sample. The presence of a sample containing a large scattering resonance in the block of lead and near to the gamma ray detector will perturb the neutron flux, and this could have two effects: (a) the background which is caused by capture of neutrons in the detector and nearby lead will not be the same with and without the sample, and (b) the energy dependence of the neutron flux incident on the sample will be altered by the sample. Bergman et al.<sup>(56)</sup> in their original paper mention corrections at low energies for the depression of the flux due to absorption of the neutrons in low energy resonances but no remarks are made about the effects of large scattering resonances for light nuclei. Both these effects could result in the lowering of the observed capture cross-section in the region of the large s-wave scattering resonances, but should have little effect where the scattering and the capture cross-sections are smoothly varying functions of neutron energy.

For these reasons I think that there is justification for ignoring the capture data from the lead slowing down spectrometer measurements<sup>(55)</sup> above a few keV for the light and intermediate nuclei, and should consider the s-wave radiation widths so far produced by the time-of-flight measurements as upper limits only.

Thus a value of  $2 \pm 1$  eV for the radiation width is recommended for s-wave resonances in nickel where no measurements exist and is based on only published capture data and systematics in this mass region. This large uncertainty on the value of  $\Gamma_\gamma$  will result in an uncertainty of  $\pm 50\%$  in the s-wave contribution to the capture cross-section. A radiation width of  $1.0 \pm 0.5$  eV is the recommended

value for p-wave and higher l value resonances observed in the isotopes of nickel. The large uncertainty will not result in a corresponding uncertainty in the capture cross-section for energies below 100 keV for the main isotopes 58 and 60 where most of the resonance areas are proportional only to  $g \Gamma_n$  as  $\Gamma_n \ll \Gamma_\gamma$ . In the case of the isotopes 61, 62 and 64 where there are few observed narrow resonances, there may be a corresponding uncertainty of  $\sim \pm 50\%$  to their contribution to the average capture cross-section of nickel due to uncertainties in the strength function. It is not known what effect this large uncertainty on the radiation width will have on the Doppler calculation.

## 5. Average resonance parameters, statistics and cross-sections

### (1) Resonance parameters

The observed values of the s-wave strength function and mean spacings are given in Table 12. The data for the even isotopes are mainly based on the results of Farrell et al<sup>(44)</sup>, which covers a much wider energy range than the other data.

Farrell et al<sup>(44)</sup> in the energy region above 100 keV assumed that resonances in which resonance-potential and resonance-resonance interference effects were not present had angular momentum  $>0$ . This technique is difficult to use on resonances that have widths smaller than the energy resolution of the experiment. Hence as the energy resolution used in these experiments was  $\sim 1$  keV we must cast some doubt on the allocation of the resonances with widths less than 1 keV and so cannot obtain any meaningful values of average parameters for p or higher orbital angular momentum neutrons from these data.

As already stated, the capture measurements<sup>(46,47,48)</sup> clearly indicate the presence of many small resonances in the energy region below 100 keV. The authors have assumed these resonances to be p-wave but some of the resonances are probably d-wave, especially in the energy region above 40 keV.

In the case of Ni-60, if it is assumed that all the narrow resonances are p-wave, a value of  $0.075 \times 10^{-4}$  is obtained for the p-wave strength function and a value of 3.8 keV for the level spacing, i.e.  $D_0 = 22.8$  keV. This value is lower than the s-wave one of 32.4 keV, whereas one would expect a higher value as small resonances can easily be missed, hence increasing the observed level spacing. The conclusion that can be drawn from this is that either the level spacing depends on the l value or that if the level spacing follows the  $(2J + 1)$  rule and is independent of parity then about 30% of the resonance between 20 and 60 keV must be attributed to "d"-wave neutrons. There appears to be no means at present of checking which of these assumptions is correct. If the level spacing of the p-wave resonances is consistent with  $D_0 = 22.8$  keV, then the mean radiation width obtained

from the average capture data is reduced to  $\sim 0.5$  eV, and is then further removed from the s-wave value of  $\sim 2$  eV. Values for the p- and d-wave strength functions of  $\lesssim 0.05 \times 10^{-4}$  and  $\gtrsim 3 \times 10^{-4}$  fit the observed data. The recommended values of the average parameters are given in Table 12 and as there are few observed values, the recommended ones are determined mainly by the systematics in this nuclear mass region.

(ii) Average cross-sections

Here we are mainly concerned with the capture cross-section data since the total cross-section in the energy range of interest, i.e. up to  $\sim 600$  keV is reasonably represented by the resonance parameters given in Tables 7 to 10.

The capture data from the three time of flight experiments<sup>(47,48,49)</sup> are in reasonable agreement both in shape and magnitude when resolution effects are taken into account. These data are also in agreement over the common energy range with those of Diven et al<sup>(59)</sup> and Stavisskii and Shapar<sup>(60)</sup>. Difficulties of comparing the capture measurements made at spot energy points<sup>(58,62)</sup> arising from lack of knowledge of the exact energy and energy resolution, may explain the differences between these measurements and the time of flight data.

There is one capture measurement on Ni-60 carried out at RPI<sup>(50)</sup> giving average capture cross-sections up to 200 keV. These data were used to fit the p- and d-wave radiation widths and are shown in figure 5.

The activation measurement by Grench<sup>(54)</sup> on Ni-64 in the energy region 0.2 to 2 MeV indicates a much lower average capture cross-section for this isotope than indicated for Ni-60 by the RPI data or from the measurements on natural nickel. In fact fits to these data give a value of 0.34 eV for the average radiation width of the  $1/2^+$  resonances in Ni-64 + n.

6. Recommendations and further experimental work required

(i) Capture cross-section

(a) 0 to 40 keV

The resonance parameters given in Tables 7-11 are used in calculating the cross-sections from 0 to 40 keV. The uncertainties in the capture cross-section vary from  $\sim 5\%$  in the  $1/v$  part to  $\sim 50\%$  in the contribution due to the s-wave resonances. In this energy range all the large s-wave resonances have been observed and it can be assumed that below 40 keV for Ni-58 and Ni-60 all the major p- and d-wave resonances have been seen, but none for Ni-62 and Ni-64 and only those below 7 keV for Ni-61. To take into account these missed levels it is suggested that  $1.0 \pm 0.4$  mb be added to the capture cross-section in the region 7.5 to 40 keV. The total cross-section requires no correction for these resonances as they will have very little effect on the average cross-section.

(b) 40 keV to 200 keV

In this energy region it is suggested that the cross-section due to the s-wave resonances is used and the high l values are taken into account by their average cross-sections given in Table 13(a).

(c) Energy greater than 200 keV

Here average cross-sections will have to be used for the capture cross-section and the recommended values are given in Table 13(b).

(ii) Total cross-section

The recommended resonance parameters given in Tables 7-11 and the values of "a" and "R" given in Table 5 give a reasonable representation of the total cross-section in the energy region up to 400 keV when using the R-matrix formulation. The uncertainties vary from  $\sim \pm 0.5$  b in the region below 10 keV to  $\sim \pm 1$  b in the region between the large s-wave resonances above this energy. The resonance contribution is an added uncertainty caused by the errors in the total width. Where the data are based on the measurement of Farrell et al, the resonance energies have been increased by 1.24 keV to bring them more into line with the time of flight results.

(iii) Further experimental work

As can be gathered from this report, the neutron cross-section data on nickel are scant and often of poor quality. The recommendations for further work are:-

- (1) Accurate measurements of the total cross-section for all the isotopes, especially Ni-58 and Ni-60 from 1 eV to several hundred keV and its analysis in terms of the resonance parameters.
- (2) The measurement of the capture cross-section for separated isotopes in the range 1 to hundreds of keV and analysis of the data in terms of resonance parameters and average radiation widths for p- and d-wave neutrons.
- (3) Attempts should be made to measure the total width of some of the narrow resonances observed in the capture measurements to try to confirm the radiation width required to fit the average capture cross-section above 50 keV. This may involve the use of cooled samples to reduce the Doppler effects.

The identification of the spin and parities of these narrow resonances may be helped by measurement of the capture gamma-ray spectra or the angular distribution of the scattered neutrons, and, in the case of Ni-60 measurement, of the angular distribution of the neutrons from the ( $\gamma$ , n) reaction on Ni-61 at gamma-ray energies just above the neutron threshold.

References

- (1) Cox S. A., private communication (1970).
- (2) Ewald H., Zeits Phys. 122, 686 (1944).
- (3) Ingham M. G. and Hess D. C., ANL-4120 (1948).
- (4) White J. R. and Cameron A. E., Phys. Rev. 74, 991 (1948).
- (5) Mattraw H. C. and Pachucki C. F., AECU-1903 (1952).
- (6) Maples C., Goth G. W. and Cerry J., Nuclear Data A2, 429 (1967).
- (7) Nuclear Data (Academic Press) Vol. 2, No. 3 (1967); Vol. 2, No. 5 (1968); Vol. 3, No. 3 (1970) and Vol. 3, No. 4 (1970).
- (8) Faraggi H., Bernas R. and Bonnet A., Comptes Rendus 235, 425 (1952).
- (9) Story J. S., private communication (1970).
- (10) Abramov A. I., Atomnaya Energiya 12, 62 (1962).
- (11) Bendt P. J. and Ruderman I. W., Phys. Rev. 77, 575 (1950).
- (12) Colmer F. C. W. and Littler D. J., Proc. Phys. Soc. 63A, 1175 (1950).
- (13) Harris S. P., Muchlhaise C. O., Rasmussen S., Schroeder H. P. and Thomas G. E., Phys. Rev. 80, 342 (1950).
- (14) Pomerance H., Phys. Rev. 83, 641 (1951).
- (15) Grineland B., Hellstrand E. and Wetter F., Comptes Rendus 232, 2089 (1951).
- (16) Jowitt D., Pattenden S. K., Rose H., Somall V. G. and Tattersell R. B., AERE R/R 2516 (1958) and Geneva Conference 16, 34 (1958).
- (17) Anno J., Res. Reactor J., 1, 15 (1961).
- (18) Vidal R., EANDC(E)66U, 200 (February 1966).
- (19) Malik S. S., Binnhant G., Shore F. J. and Sailor V. L., Nuc. Inst. and Methods 86, 83 (1970).
- (20) Pomerance H., Phys. Rev. 88, 412 (1952).
- (21) Dailnitsya E. Ya., INDSWG - 120E (1965).
- (22) Sims G. H. E. and Juhnke D. G., J. Inorg. Chem. 32, 2839 (1970).
- (23) Barnes I. L., Garfinkel S. B. and Mann W. B., Int. J. of Applied Radiation and Isotopes, 22, 777 (1971).
- (24) McMuller C. C., Pate D. D., Tomlinson R. H. and Yaffe L., Can. J. Chem. 34, 1742 (1956).
- (25) Harrockes D. L. and Harkness A. L., Phys. Rev. 125, 1619 (1962).
- (26) Seren L., Friedlander H. N. and Tuskel S. H., Phys. Rev. 72, 888 (1947).
- (27) Overman R. T., Fry L. M., Jones J. W., Baldwin W. D., Lamb E. and Savolainier J. E., ORNL 4 (1948).
- (28) Hughes D. J., Spatz W. B. and Goldstein N., Phys. Rev. 75, 1181 (1949).
- (29) Lyon W. S., Nuc. Sci. Eng. 8, 378 (1960).
- (30) Macklin R. L. and Pomerance H. S., Geneva Conf. 5, 16 (1956).
- (31) Prokherov Ju. A., Dissertation  $\frac{1}{2}$  EI (1951).
- (32) Klimentov V. B. and Gryazev V. M., Atomnaya Energiya 3, 507 (1957).
- (33) Tattersell R. B., Rose H., Pattenden S. K. and Jowitt D., J. Nuc. Eng. A12, 32 (1960).

- (34) Kapchigashev S. V. and Popov Yu. P., *Atomnaya Energiya* 15, 120 (1963).
- (35) Sunyar A. W. and Goldhaber M., *Phys. Rev.* 76, 189 (1949).
- (36) Bandt F. J. and Ruderman I. W., *Phys. Rev.* 77, 577 (1950).
- (37) Skull C. G. and Wollan E. O., *Phys. Rev.* 81, 527 (1951).
- (38) Goldberg M. D. and Harvey J. A., *Phys. Rev.* 91, 451 (1953).
- (39) Allen R. G., Stephenson T. E., Standford C. P. and Bernstein S., *Phys. Rev.* 96, 1297 (1954).
- (40) Rayburn L. A. and Wollan E. O., *Nuc. Phys.* 61, 381 (1965).
- (41) Sidhu S. S. and Anderson K. D., *Phys. Rev.* 156, 1225 (1967).
- (42) Bernstein S., Borst L. B., Standford C. P., Stephenson T. E. and Dial J. B., *Phys. Rev.* 87, 487 (1952).
- (43) Bilpuch E. G., Seth K. K., Bowman C. D., Tabony R. H., Smith R. C. and Newson H. W., *Ann. Phys.* 14, 387 (1961).
- (44) Farrell J. A., Bilpuch E. G. and Newson H. W., *Ann. Phys.* 37, 367 (1966).
- (45) Garg J. B., Rainwater J. and Havens W. W. Jr., *Columbia NAL-2* (1971).
- (46) Ernst A., Frohner F. H. and Komple D., *IAEA Helsinki Conf. 1970*, paper CN-26/11.
- (47) Moxon M. C., preliminary data on natural nickel and Ni-58 (1972).
- (48) Hockenbury R. W., Bartolome E. M., Tararezuk J. R., Moyer W. R. and Block R. C., *Phys. Rev.* 178, 1746 (1969).
- (49) Spitz L. M., Barnard E. and Brooks F. D., *Nuc. Phys.* A121, 655 (1968).
- (50) Stieglitz R. G., Hockenbury R. W. and Block R. C., *Nuc. Phys.* A163, 592 (1971).
- (51) Cho M., Frohner F. H., Kazerouni M., Muller K. N. and Rohr G., *UAEA Helsinki Conf. 1970*, paper CN-26/127.
- (52) Good W. H., Paya D., Wagner R. and Tamura T., *Phys. Rev.* 151, 912 (1966).
- (53) Pawlick G. W., Smith E. C. and Thurlow P. E. F., *ORNL-1620*, 42 (1953).
- (54) Grench H. A., *Phys. Rev. B*, 140, 1277 (1965).
- (55) Kapchigashev S. V. and Popov Yu. P., *Atomnaya Energiya* 15, 120 (1963).
- (56) Bergman A., Isakov A. I., Murin I. D., Shapiro F. L., Shtranikh I. V. and Kazarnovskii M. V., *Proc. of the First Int. Conf. on the Peaceful Uses of Atomic Energy, Geneva 1956*, IV, P-642.
- (57) Manero F. and Wigon M. A., *Nuc. Phys.*, A119, 356 (1968).
- (58) Gibbons J. H., Macklin R. L., Miller P. S. and Neiler J. H., *Phys. Rev.* 122, 182 (1960).
- (59) Diven B. C., Terrell J. and Hemmendinger A., *Phys. Rev.* 120, 556 (1960).
- (60) Staviskii Yu. Ya. and Shapar A. V., *Atomnaya Energiya* 10, 264 (1961) and *Atomnaya Energiya* 12, 514 (1962).
- (61) Schmitt H. W. and Cook C. W., *Nuc. Phys.* 20, 202 (1960).
- (62) Sowerby M. G., Patrick B. H., Uttley C. A. and Diment K. M., *J. Nuc. Energy* 24, 323 (1970).
- (63) Belanova T. S., *Zh. Eksp. Teor. Fiz.* 34, 574 (1958).
- (64) Seth K. K., *Ann. Phys.* 8, 223 (1959).
- (65) Spencer R. R., Beer M. and Frohner F. H., *KFK-1517* (1972) and private communication (1972).
- (66) Merrison A. W. and Wiblin E. R., *Proc. Roy. Soc.* A215, 278 (1952).
- (67) Carre J. C. and Vidal R., *Proc. Nuclear Data for Reactors, Paris 1966*, I,479

Table 1	The abundances and exact atomic masses of the stable nickel isotopes.
Table 2	Q values for some neutron reactions.
Table 3	Level schemes for stable nickel isotopes up to 3 MeV.
Table 4	Thermal capture cross-section and resonance integrals.
Table 5	Slow neutron scattering data for nickel and its stable isotopes.
Table 6	Comments on experimental measurements.
Table 7	Recommended resonance parameters for Ni-58.
Table 8	Recommended resonance parameters for Ni-60.
Table 9	Recommended resonance parameters for Ni-61.
Table 10	Recommended resonance parameters for Ni-62.
Table 11	Recommended resonance parameters for Ni-64.
Table 12	Assumed average parameter for nickel isotopes.
Table 13	The average capture cross-section to be added to that calculated from the resonance parameters as explained in the text.

TABLE 1

The abundances and exact atomic masses of the stable  
nickel isotopes

	58	60	61	62	64
Abundance %	67.86 $\pm 0.22$	26.21 $\pm 0.51$	1.19 $\pm 0.07$	3.66 $\pm 0.01$	1.08 $\pm 0.2$
Masses A.M.U.	57.9353389 60.9310531 63.9279546				
Atomic weight of natural nickel 58.7049 A.M.U.					

TABLE 2

Q values for some neutron reactions  
(Q in MeV)

Isotope	(n, $\gamma$ )	(n,2n)	(n,p)	(n,d)	(n,t)	(n,He <sup>3</sup> )	(n,He <sup>4</sup> )
58	9.0013 $\pm 0.0024$	-12.1997 $\pm 0.0093$	+0.3963 $\pm 0.0055$	-5.954	-11.076	-6.483	+2.8928 $\pm 0.0047$
60	7.8174 $\pm 0.0029$	-11.3874 $\pm 0.0046$	-2.0395 $\pm 0.0043$	-7.303	-11.511	-9.184	+1.3519 $\pm 0.0053$
61	10.5997 $\pm 0.0031$	-7.8173 $\pm 0.0046$	-0.5213 $\pm 0.0183$	-7.633	-8.866	-10.420	+3.5747 $\pm 0.0059$
62	6.8357 $\pm 0.0028$	-10.5997 $\pm 0.0045$	-4.4373 $\pm 0.0300$	-8.883	-11.975	-12.097	-0.4408 $\pm 0.0045$
64	6.0990 $\pm 0.0050$	-9.7570 $\pm 0.0071$	-6.9010 -	-10.250	-12.457	-10.3	-2.4370 $\pm 0.0450$

TABLE 3

Level schemes for stable nickel isotopes up to 3 MeV

Isotope	Energy MeV	Spin and Parity	Isotope	Energy MeV	Spin and Parity	
58	0	0 <sup>+</sup>	61	0	3/2 <sup>-</sup>	
	1.4540	2 <sup>+</sup>		0.06740	5/2 <sup>-</sup>	
	2.4591	4 <sup>+</sup>		0.2829	1/2 <sup>-</sup>	
	2.7753	2 <sup>+</sup>		0.6560	3/2 <sup>-</sup>	
	2.9017	(1 <sup>+</sup> )		0.9086	5/2 <sup>-</sup>	
	2.9424	(0 <sup>+</sup> )		1.019	1/2 <sup>-</sup> , 7/2 <sup>-</sup>	
60	0	0 <sup>+</sup>		1.1001	3/2 <sup>-</sup>	
	1.33252	2 <sup>+</sup>		1.1325	5/2 <sup>-</sup>	
	2.158	2 <sup>+</sup>		1.1860	3/2 <sup>-</sup>	
	2.286	0 <sup>+</sup>		1.457	7/2 <sup>-</sup>	
	2.50575	4 <sup>+</sup>		1.611	(5/2 <sup>-</sup> )	
	2.625	3 <sup>+</sup>		1.7304	1/2 <sup>-</sup> , 3/2 <sup>-</sup>	
62	0	0 <sup>+</sup>		1.812	1.990	
	1.1717	2 <sup>+</sup>		1.997	1/2, 5/2	
	2.0471	0 <sup>+</sup>		2.020		
	2.293	2 <sup>+</sup>		2.114	9/2 <sup>+</sup>	
	2.336	4 <sup>+</sup>		2.1224	(1/2 <sup>-</sup> )	
	2.890	-		2.412		
64	0	0 <sup>+</sup>		2.470	(5/2 <sup>-</sup> )	
	1.348	2 <sup>+</sup>		2.532		
	2.272	0 <sup>+</sup>		2.598		
	2.605	4 <sup>+</sup>	2.645	1/2 <sup>-</sup> , 3/2 <sup>-</sup>		
	2.863	2 <sup>+</sup>	2.708	3/2 <sup>+</sup> , 5/2 <sup>+</sup>		
	2.968	-	2.778	1/2 <sup>-</sup> , 3/2 <sup>-</sup>		
			2.803	5/2 <sup>-</sup> , 7/2 <sup>-</sup>		
			2.865	1/2 <sup>-</sup> , 3/2 <sup>-</sup>		
		2.890				
		2.910	7/2 <sup>-</sup>			

TABLE 4

Thermal capture and resonance integrals

	58	60	61	62	64	Nat
Thermal cross-section (b)	4.56 $\pm 0.37$	2.76 $\pm 0.22$	2.47 $\pm 0.71$	14.2 $\pm 0.2$	1.61 $\pm 0.24$	4.40 $\pm 0.10$
Resonance integral (b)	0.13	0.24	$\geq 1.3$	$\sim 0.5$	$\sim 0.2$	0.19 $\pm 0.07$

TABLE 5

Slow neutron scattering data for nickel and its stable isotopes

Isotope	$R_{\infty}$ (fm)	$\sigma_{\text{free}}$ (barns)	$\sigma_{\text{bound}}$ (barns)	$\sigma_{\text{b coh}}$ (barns)	$\sigma_{\text{b incoh}}$ (barns)	$b_{\text{coh}}$ (fm)
Ni (nat)	-	17.43±0.05	-	13.13±0.21	4.90	+10.22±0.08
Ni-58	-0.417	24.61±0.096	-	25.47±0.1	Nil	+14.24±0.028
Ni-60	-0.553	1.01±0.12	-	1.04±0.12	Nil	+ 2.88±0.16
Ni-61	J=1,-0.23 J=2,+0.12	9.6 ±2.0	-	-	-	+ 7.6 ±0.06
Ni-62	-0.505	9.2 ±0.39	-	-	Nil	- 8.7± 0.18
Ni-64	+0.029	1.45±0.4	-	1.50±0.41	Nil	-0.353±0.04

Year and Reference	Authors and Laboratory	Cross-section and isotopes	Energy Range (keV)	Neutron Source	Detectors and analysis	Remarks
1961 43	Bilpuch et al., Duke University	$\sigma_T$	58 60	2 - 200	Collimated neutron beam from p,n reaction using a 4 MeV D.C. Van de Graaff	BF <sub>3</sub> counters. Area analysis. The neutron energy depends on the kinematics of the reaction and the resolution may be overestimated. There may also be some errors due to the fact that the neutron source, sample and detector are very close together. Resonance energies increased by 1.24 keV to give agreement with the time of flight data of Garg et al.
1966 44	Farrell et al., Duke University	$\sigma_T$	58 60 62 64	90 - 650 50 - 650 ~20 - 650 50 650	Collimated neutron beam from the Duke 3 MeV Van de Graaff which had better energy stability than the 4 MeV one	BF <sub>3</sub> counters. Area and shape analysis to determine the l value. Experimental technique is similar to that for ref. 43. Only one sample of each isotope was used and the statistical accuracy is poor at the lower energies. The resonance energies are increased by 1.24 keV to give agreement with the time of flight data of Garg et al.
1971 45	Garg et al. Columbia University	$\sigma_T$	Natural	2 - ~200	Time of flight using the neutron target on the Nevis synchro-cyclotron	<sup>10</sup> B-NaI detector. Area and shape analysis. Only natural nickel samples were used. The isotopic assignment given by Farrell et al. was used in the analysis. This work was carried out several years ago and only published recently. The resonance energies are on average 1.24 keV higher than the Van de Graaff data and in the regions below 200 keV were used as standards for the major isotopes.
1970 46	Ernst et al., Karlsruhe	$\sigma_\gamma$	58 60 61	12 - 220 7 - 220 7 - 220	Fast time of flight using a pulsed Van de Graaff	Large liquid scintillator. Measurements relative to Au cross-section. Area analysis used to get the resonance parameters. The gold is possibly not a good standard as it is not well known and there appears to be some structure in the region below 100 keV. They have tried to reduce the effect of variation of the $\gamma$ -ray cascade following neutron capture by taking pulse height spectra distribution, but this effect on the efficiency for detecting neutron capture events may not be entirely eliminated. As the capture to scattering ratio is very small the effect of scattered neutrons may not have been eliminated and would tend to give a high value of the capture cross-section especially in the region of the resonances with large neutron widths. No values of the radiation widths for Ni-58 have been published to date.

TABLE 6(2)

-174-

Year and Reference	Authors and Laboratory	Cross-section and isotopes	Energy Range (keV)	Neutron Source	Detectors and analysis	Remarks	
1972 47	Moxon, AERE Harwell	$\sigma_Y$	Natural 58	.005 - 100 .005 - 100	Time of flight using the booster target of the Harwell electron linac	Moxon-Rae capture $\gamma$ -ray detector. Capture measurements relative to $^{10}\text{B}(n,\alpha\gamma)$	The capture yields may be increased due to the effects of scattered neutrons.
		$\sigma_T$	Natural 58	$\sim 1\text{eV} - 50\text{keV}$ $\sim 1\text{eV} - 50\text{keV}$		Li-glass scintillator. Shape analysis	
1969 48	Hockenbury et al., R.P.I.	$\sigma_Y$	Natural	10 eV - 200keV	Time of flight using an electron linac as a neutron source	Large liquid scintillator. Area analysis	Scattered neutrons may be detected and enhance the capture yield. Several natural samples were used and samples of enriched isotopes were used for resonance assignment only. Many narrow resonances are seen in these data and are attributed to p-wave neutrons.
1971 50	Steglitz et al., R.P.I.	$\sigma_Y$	60	1 - 340 keV	Time of flight using an electron linac	The capture measurements used a 250 l liquid scintillator and transmission used $^{10}\text{B-NaI}$ as a neutron detector	The shape fits to the transmission data are good but the nuclear radius may be in error as a total cross-section of 4.2 b for oxygen was used whereas now a value of 3.71 b is recommended. Here again the capture may be affected by the scattered neutrons and give too high values.
		$\sigma_T$					
1970 51	Cho et al., Karlsruhe	$\sigma_T$	61	7 - 250 keV	n-sec time of flight using the p,n reaction on a pulsed Van de Graaff	$^{10}\text{B-NaI}$ at the lower energies and at high energies a proton recoil scintillator was used. Shape fitting analysis over the range 7 - 70 keV.	The statistics are very poor below 15 keV. In some energy regions the fitted curve is either systematically above or below the experimental data suggesting some discrepancies in the published parameters.
1966 52	Good et al., O.R.N.L.	$\sigma_T$	61	4 - 50 keV	fast time of flight on a pulsed Van de Graaff	Area analysis developed by K. K. Seth, ref. 64	No errors are quoted and the data does not look as good as that from ref. 51, so has been ignored.

TABLE 6(3)

Year and Reference	Authors and Laboratory	Cross-section and isotopes	Energy Range (keV)	Neutron Source	Detectors and analysis	Remarks
1972 67	Spencer et al., Karlsruhe	$\sigma_T$ 62 64	~28 - ~300 ~18 - 300	Fast time of flight on 3 MeV pulsed Van de Graaff	Li-6 glass neutron detector. Shape fit analysis using R-matrix formula	Shape fits were carried out on two metallic samples of each isotope to give the best values of the resonance parameters and nuclear reactions. This appears to be a better fit to the experimental data than that shown in ref. 51. These data give better values of the resonance parameters below 100 keV than any of the previous published data for these isotopes.
1968 49	Spitz et al. South Africa	$\sigma_\gamma$ Natural	8 - 120	Time of flight using a pulsed Van de Graaff	Moxon-Rae	The energy resolution is poor but this was one of the first sets of published data to indicate that the capture cross-section in the region 10 - 20 keV was much higher than values published previously or used in the evaluations up to that time. No corrections to the published data are made for self screening or multiple scattering.
1965 54	Grench, Lockheed	$\sigma_{act}$ 64	~200 - ~2000	Van de Graaff at spot energy points	NaI crystal used to detect decay $\gamma$ -rays. Measurements are relative to Au(n, $\gamma$ )	In the report there is no mention of corrections for multiple scattering, self screening or the effects of the plastic container. The latter would moderate the neutrons and as most capture cross-sections increase with decreasing energy, cause an increase in the observed cross-section.
1963 55	Kapehigashev and Popov, U.S.S.R.	$\sigma_\gamma$ Natural	~0.03 - ~50	Lead slowing down spectrometer	CaF <sub>2</sub> with a $\gamma$ detecting efficiency proportional to the $\gamma$ -ray energy	The data above a few keV can be ignored due to the difficulties of making corrections for self screening and multiple scattering caused by the poor energy resolution.
1960 58	Gibbons et al., ORNL	$\sigma_\gamma$ Natural	30 65	Fast time of flight on a pulsed Van de Graaff	Large liquid scintillator. The time of flight was only used to reduce the background.	These data only give an indication of the capture cross-section as neither the energy nor resolution are well defined and due to the wide resonance spacing could be either on or off a resonance at a given nominal energy.

TABLE 6(4)

-176-

Year and Reference	Authors and Laboratory	Cross-section and isotopes	Energy Range (keV)	Neutron Source	Detectors and analysis	Remarks
1960 59	Diven et al., Los Alamos	$\sigma_{\gamma}$ Natural	175 - 1000	Spot energy points using fast time of flight on a pulsed Van de Graaff	Large liquid scintillator used to detect the capture $\gamma$ -rays and time of flight used to reduce background effects. Measurements are relative to $U-235(n, \sigma_p + \sigma_{\gamma})$	The fast time of flight reduce both the effects of the background and thermalised neutrons. These data are about the best in this energy region but may suffer from the effects of self screening, multiple scattering and the prompt detection of scattered neutrons.
1960 61	Schmitt and Cook, ORNL	$\sigma_{\gamma}$ Natural	24	Shell transmission using Sb-Be neutron source		The uncertainty of $\sim 3$ keV on the energy of the Sb-Be neutrons makes comparison of these data with other data difficult due to the presence of several narrow capture p-wave resonances in the energy region of the source.
1961 60	Staviskii and Shapar, USSR	$\sigma_{\gamma}$ Natural	35 - 950	Spot energies using a Van de Graaff with a neutron energy spread of $\sim 20$ keV	CaF <sub>2</sub> $\gamma$ -ray detectors	These data are normalised to the results of Diven et al. (ref. 59) and extend these results lower in energy.
1965 40	Rayburn and Wollan, ORNL	$\sigma_T$ Natural	1.44 eV	Cadmium covered indium foils were used as neutron detectors on a collimated neutron beam from the ORNL graphite reactor		Preliminary results were reported in 1952. These are some of the most accurate total cross-sections to be published. The measurement on $^{nat}Ni$ is in good agreement with the data from ref. 47.
1958 63	Belanova, USSR	$\sigma_{\gamma}$ Natural	25, 220, 878	Shell transmission measurements using Sb-Be, Na-D <sub>2</sub> O, Na-Be neutron sources		The uncertainties in the neutron energies and the spread make comparison with other data difficult especially for the Sb-Be source.

TABLE 7

Recommended resonance parameters for Ni-58

Recommended $\ell = 0$			Recommended $\ell > 0$					
$E_R$ keV	$\Gamma_n$ keV	$\Gamma_\gamma$ eV	$E_r$ (keV)	$\Gamma_n$ (eV)	$\Gamma_\gamma$ (eV)	$E_r$ (keV)	$\Gamma_n$ (eV)	$\Gamma_\gamma$ (eV)
-28.5	7.87	2.0	6.89	0.022	1.0	509.24	(75)	1.0
- 5.5	1.081	1.87	12.6	(0.03)	1.0	513.74	(100)	1.0
15.42	1.15	2.0	13.3	0.47	1.0	531.24	422	1.0
63.2	3.58	2.0	13.6	1.08	1.0	545.24	640	1.0
108.0	1.28	2.0	16.5	(0.02)	1.0	555.74	1600	1.0
123.8	0.63	2.0	17.2	(0.02)	1.0	560.74	1260	1.0
137.5	1.76	2.0	19.0	0.067	1.0			
140.5	3.46	2.0	20.0	0.25	1.0			
159.0	5.04	2.0	21.1	1.27	1.0			
169.0	0.64	2.0	26.6	2.33	1.0			
192.0	3.62	2.0	32.4	2.56, g=2	1.0			
207.0	6.82	2.0	34.2	1.85	1.0			
232.24	6.0	2.0	36.1	6.12	1.0			
244.24	0.25	2.0	39.5	(1.3)	1.0			
271.24	6.0	2.0	47.9	3.75, g=2	1.0			
279.24	2.0	2.0	148.74	160	1.0			
304.24	0.75	2.0	184.74	227	1.0			
326.24	2.0	2.0	216.24	245	1.0			
350.24	1.5	2.0	248.74	343	1.0			
368.24	0.25	2.0	258.24	(75)	1.0			
395.24	0.75	2.0	287.74	200	1.0			
418.74	5.0	2.0	307.74	(50)	1.0			
427.24	8.0	2.0	335.74	592	1.0			
454.74	3.0	2.0	344.74	560	1.0			
462.74	0.75	2.0	358.74	426	1.0			
496.74	2.0	2.0	379.74	426	1.0			
508.24	2.0	2.0	389.74	480	1.0			
523.74	0.75	2.0	397.74	(50)	1.0			
572.24	10.0	2.0	414.24	(50)	1.0			
588.74	2.5	2.0	417.24	(20)	1.0			
601.24	6.0	2.0	427.24	1800	1.0			
			436.74	(20)	1.0			
			446.24	(20)	1.0			
			452.24	(20)	1.0			
			459.74	(75)	1.0			
			493.74	1987	1.0			

TABLE 8

Recommended resonance parameters for Ni-60

Recommended $\ell = 0$			Recommended $\ell > 0$		
$E_R$ keV	$\Gamma_n$ keV	$\Gamma_\gamma$ eV	$E_r$ keV	$\Gamma_n (g=1)$ eV	$\Gamma_\gamma$ eV
-5.50	0.0525	5.5	1.292	0.0003	1.0
12.47	2.11	3.3	2.257	0.073	1.0
28.642	0.752	1.1	5.53	0.059	1.0
43.08	0.077	1.73	12.20	0.044	1.0
65.13	0.440	2.33	13.60	0.099	1.0
			23.8	0.85 $g=2$	1.0
					1.0
86.80	0.32	2.0	30.1	0.475	1.0
98.10	0.94	2.0	32.9	0.540	1.0
107.8	0.66	2.0	33.3	0.235	1.0
156.4	0.44	2.0	39.4	1.30	1.0
162.1	1.33	2.0			1.0
186.5	5.85	2.0	47.4	0.76 $g=2$	1.0
198.0	3.28	2.0	49.6	0.345	1.0
257.8	3.62	2.0	50.8	(0.1)	1.0
279.6	0.75	2.0	51.5	0.84	1.0
316.8	3.20	2.0	52.7	(0.1)	1.0
326.3	7.37	2.0	56.3	0.60	1.0
339.5	6.05	2.0	56.9	0.71	1.0
347.24	0.25	2.0	71.3	0.66	1.0
358.44	1.0	2.0	73.2	1.56	1.0
376.74	4.0	2.0	78.2	0.875	1.0
413.54	0.75	2.0	79.9	1.75	1.0
422.24	2.0	2.0			
427.74	0.5	2.0	127.74	40	
437.24	1.0	2.0	139.74	70	
447.24	3.0	2.0	157.24	380	
454.24	1.5	2.0	207.24	110	
463.24	1.0	2.0	215.24	94	
474.24	0.5	2.0	221.24	98	
485.84	3.75	2.0	230.24	208	
499.24	5.0	2.0	253.24	870	
514.74	2.25	2.0	283.74	620	
521.54	5.0	2.0	293.74	360	
526.24	3.0	2.0	307.24	500	
534.24	0.5	2.0	359.74	1076	
557.74	0.5	2.0	379.74	220	
581.74	0.25	2.0	387.74	280	
589.74	0.5	2.0	393.24	266	
596.04	2.5	2.0	398.24	312	
			402.74	390	
			432.74	220	
			498.74	565	
			503.74	325	
			512.74	2565	
			553.74	700	
			557.24	260	

TABLE 9

Recommended resonance parameters for Ni-61

Recommended $\ell = 0$				Recommended $\ell > 0$		
$E_r$ keV	J	$\Gamma_n$ keV	$\Gamma_\gamma$ eV	$E_r$ (keV)	$\Gamma_{n_{g=1}}$ (eV)	$\Gamma_\gamma$ (eV)
7.15	1	0.074	2.5	1.354	0.315	1.0
7.55	2	0.177	2.3	2.35	(0.01)	1.0
8.74	2	0.006	2.6	3.14	0.092	1.0
12.64	2	0.075	1.7	3.30	0.92	1.0
13.63	2	0.061	1.6	6.47	0.54	1.0
14.02	1	0.017	3.1	7.12	3.54	1.0
16.70	1	0.817	2.2	7.53	(0.1)	1.0
17.86	1	0.177	1.6	8.71	1.86	1.0
18.87	2	0.069	0.9			
24.62	1	0.129	1.4			
28.21	2	0.003	3.0			
29.11	1	0.409	2.4			
30.64	2	0.013	2.0			
31.13	1	0.788	2.0			
31.83	2	0.008	2.0			
32.70	2	0.220	2.0			
33.68	1	0.058	2.8			
37.13	2	0.133	3.0			
41.34	1	0.176	2.0			
43.25	2	0.010	2.0			
43.60	2	0.030	2.0			
45.49	1	0.066	2.0			
46.16	1	0.054	2.0			
50.51	1	0.133	2.0			
53.30	2	0.141	2.0			
54.81	1	0.189	2.0			
56.49	2	0.119	2.0			
58.16	1	0.178	2.0			
64.07	2	0.535	2.0			
65.87	2	1.430	2.0			
68.77	2	1.100	2.0			

TABLE 10

Recommended resonance parameters for Ni-62

Recommended $\ell = 0$			Recommended $\ell > 0$		
$E_r$ keV	$\Gamma_n$ keV	$\Gamma_\gamma$ eV	$E_r$ keV	$\Gamma_n$ eV	$\Gamma_\gamma$ eV
4.599	2.075	2.31	138.74	113	1.0
42.872	0.34	2.0	190.74	125	1.0
77.23	0.070	2.0	217.74	175	1.0
			260.74	105	1.0
94.74	2.5	2.0	273.74	315	1.0
105.65	4.6	2.0	298.24	190	1.0
149.3	0.14	2.0	300.74	470	1.0
188.2	0.09	2.0	316.74	225	1.0
214.7	0.19	2.0	320.24	356	1.0
229.5	6.18	2.0	324.24	560	1.0
243.23	0.78	2.0	353.24	267	1.0
281.1	4.80	2.0	365.24	187	1.0
287.24	1.50	2.0	404.54	4035	1.0
305.24	0.80	2.0	421.54	800	1.0
328.24	5.5	2.0	447.74	(150)	1.0
345.44	7.5	2.0	451.04	248	1.0
357.44	2.0	2.0	451.24	231	1.0
375.74	0.25	2.0	463.04	540	1.0
383.74	1.25	2.0	481.24	318	1.0
389.74	4.5	2.0	494.24	890	1.0
402.44	1.50	2.0	516.74	140	1.0
424.24	1.5	2.0	523.24	380	1.0
434.24	6.5	2.0	530.24	1725	1.0
445.24	0.35	2.0	536.74	1600	1.0
459.24	0.5	2.0	555.24	655	1.0
476.24	1.50	2.0	569.74	825	1.0
489.74	4.0	2.0	600.74	810	1.0
499.24	1.50	2.0			
509.74	0.5	2.0			
540.24	2.0	2.0			
573.04	4.0	2.0			
582.24	0.5	2.0			
584.74	10.0	2.0			
591.74	2.0	2.0			

TABLE 11

Recommended resonance parameters for Ni-64

Recommended $\ell = 0$			Recommended $\ell > 0$		
$E_R$ keV	$\Gamma_n$ keV	$\Gamma_\gamma$ eV	$E_r$ (keV)	$\Gamma_n$ (eV)	$\Gamma_\gamma$ (eV)
14.3	2.9	2.0	9.52	6.41	1.0 g=2
33.81	8.9	2.0	106.52	110	1.0
129.32	1.34	2.0	141.97	170	1.0
148.8	0.08	2.0	191.5	160	1.0
154.96	3.89	2.0	214.7	80	1.0
163.2	0.14	2.0	237.9	320	1.0
177.7	0.47	2.0	255.7	170	1.0
205.3	0.06	2.0	275.24	310	1.0
219.8	0.03	2.0	290.24	105	1.0
226.9	0.12	2.0	321.24	(50)	1.0
231.95	3.77	2.0	327.74	585	1.0
269.68	2.21	2.0	335.24	(50)	1.0
283.5	0.35	2.0	353.24	(200)	1.0
299.24	1.0	2.0	360.54	715	1.0
309.74	1.5	2.0	366.24	1870	1.0
334.24	0.25	2.0	369.24	(200)	1.0
341.44	0.5	2.0	372.74	1365	1.0
390.24	6.0	2.0	377.24	270	1.0
422.04	8.0	2.0	384.24	1730	1.0
484.24	5.0	2.0	393.74	230	1.0
524.24	1.0	2.0	396.74	810	1.0
530.54	0.75	2.0	408.24	2030	1.0
537.74	10.0	2.0	415.24	750	1.0
553.24	2.0	2.0	456.74	470	1.0
577.24	4.0	2.0	460.74	1160	1.0
584.24	0.3	2.0	467.74	985	1.0
			471.24	530	1.0
			480.24	1130	1.0
			489.04	430	1.0
			500.74	530	1.0
			504.24	760	1.0
			520.24	475	1.0
			542.74	1700	1.0
			566.24	890	1.0

TABLE 12

Assumed average parameters for nickel isotopes

Isotope	D (keV)*	Strength function* x 10 <sup>-4</sup>				Average radiation width (eV)		
		$\ell=0$	$\ell=0$	$\ell=2N-1$ $N \geq 1$	$\ell=2N$ $N \geq 1$	$\ell=0$	$\ell=2N-1$	$\ell=2N$
58	21.6	2.8	0.07	3.0	2.0	1.0	1.0	
60	16.2	2.6	0.07	3.0	2.14	0.5	0.7	
61 J=1 J=2	3.94		0.07	3.0	2.0	1.0	1.0	
	3.83		0.07	3.0	2.0	1.0	1.0	
62	19.5	2.9	0.07	3.0	2.0	1.0	1.0	
64	29.1	2.0	0.07	3.0	2.0	0.34	0.34	

\* The level spacing for spin J and angular momentum  $\ell$  is given by  $D_{J,\ell} = D_{0,0}/(2J+1)$ .

\* The strength function is defined as the average reduced neutron width divided by the average level spacing.

TABLE 13

The average capture cross-section to be added to that calculated from the resonance parameters as explained in the text

(a)

$E_1$ keV	$E_2$ keV	$\sigma_\gamma$ (mb) p and d wave only
40	50	$15.0 \pm 3.0$
50	60	$14.6 \pm 3.2$
60	70	$14.2 \pm 3.5$
70	80	$14.0 \pm 3.5$
80	90	$13.7 \pm 3.7$
90	100	$13.5 \pm 4.0$

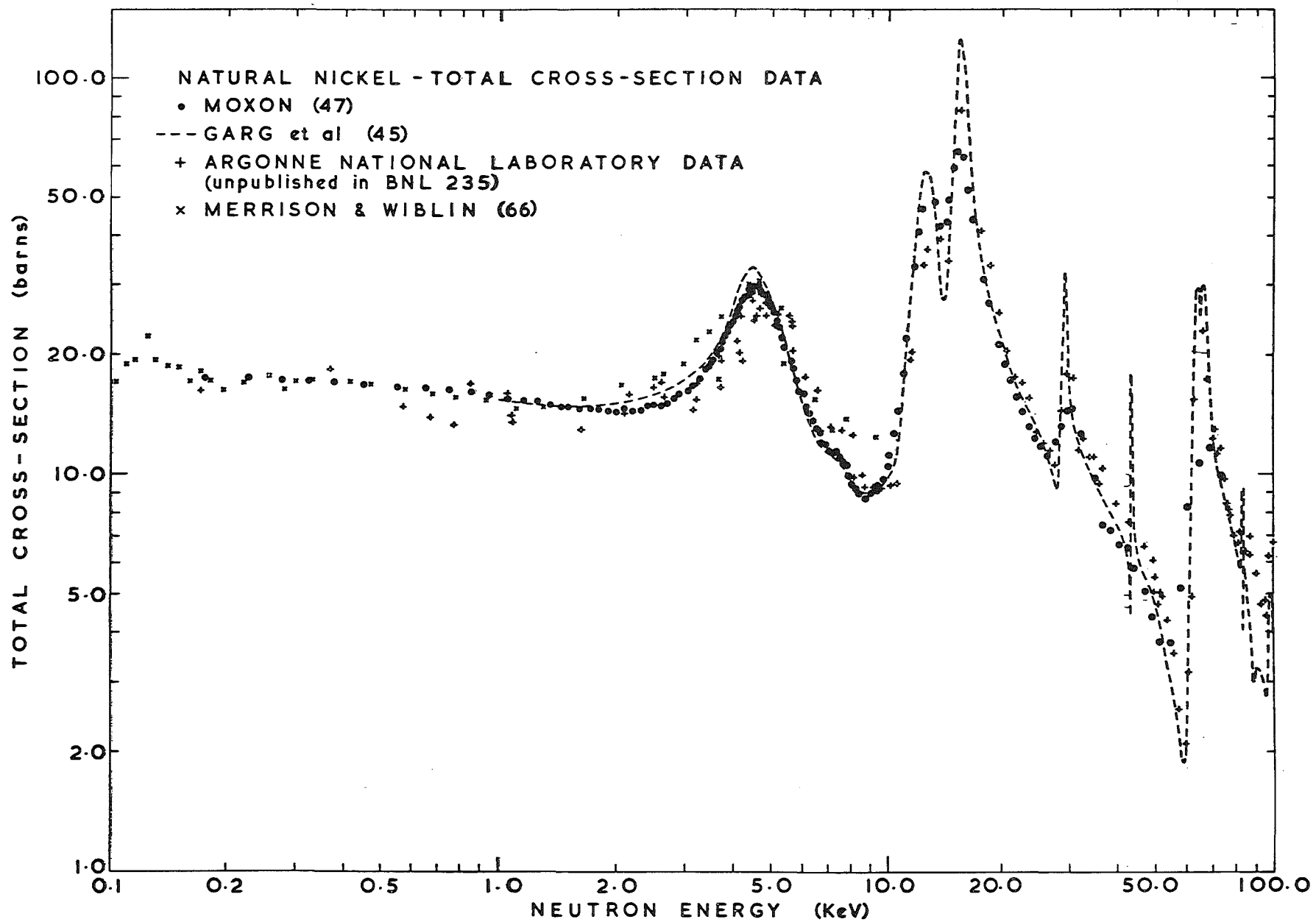
(b)

		Total capture (mb)
100	150	$14.0 \pm 3.0$
150	200	$13.0 \pm 3.0$
200	300	$8.7 \pm 1.0$
300	400	$8.3 \pm 1.0$
400	500	$8.2 \pm 0.9$
500	600	$8.0 \pm 0.8$
600	700	$7.7 \pm 0.7$
700	800	$7.4 \pm 0.6$
800	900	$7.3 \pm 0.6$
900	1000	$7.2 \pm 0.5$

Figures

- 1 Measured total cross-section of natural nickel in the energy range 0.1 to 100 keV.
- 2 Calculated total cross-section of natural nickel covering the energy range 0.1 to 100 keV.
- 3 Measured capture cross-section of natural nickel.
- 4 Calculated capture cross-section of natural nickel
- 5 Average capture cross-section of Ni-60.

FIGURE 1



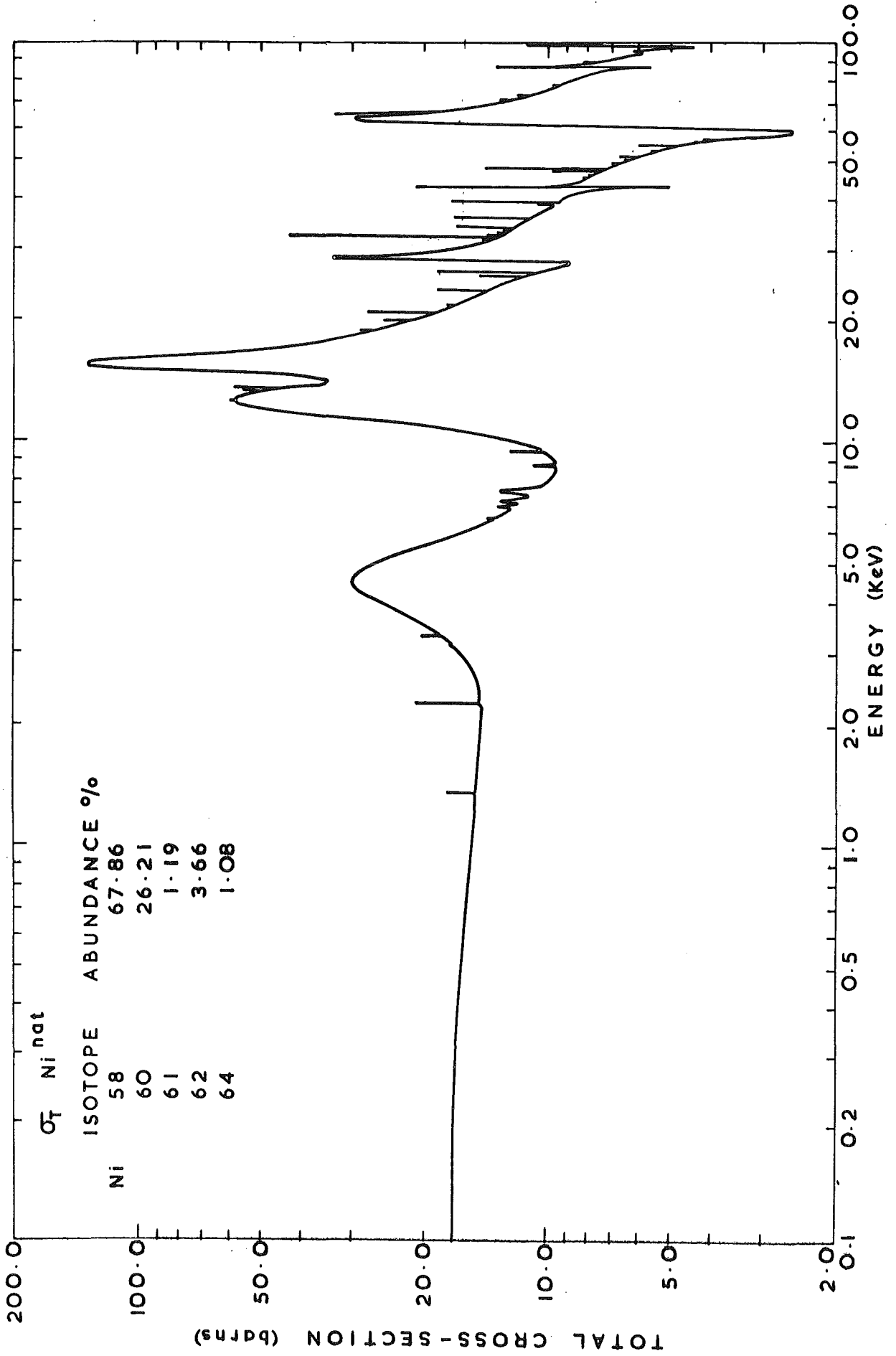


FIGURE 3

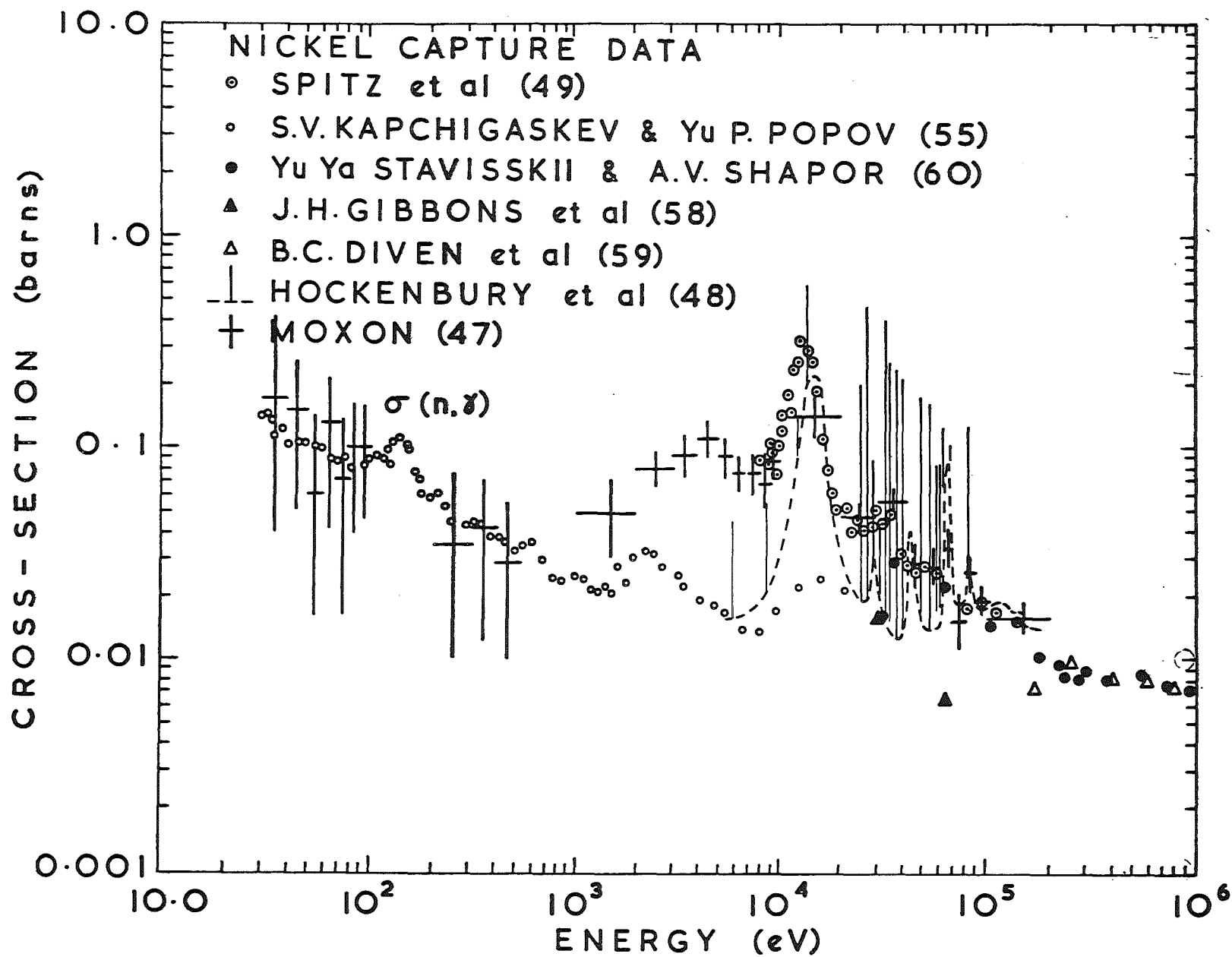


FIGURE 4

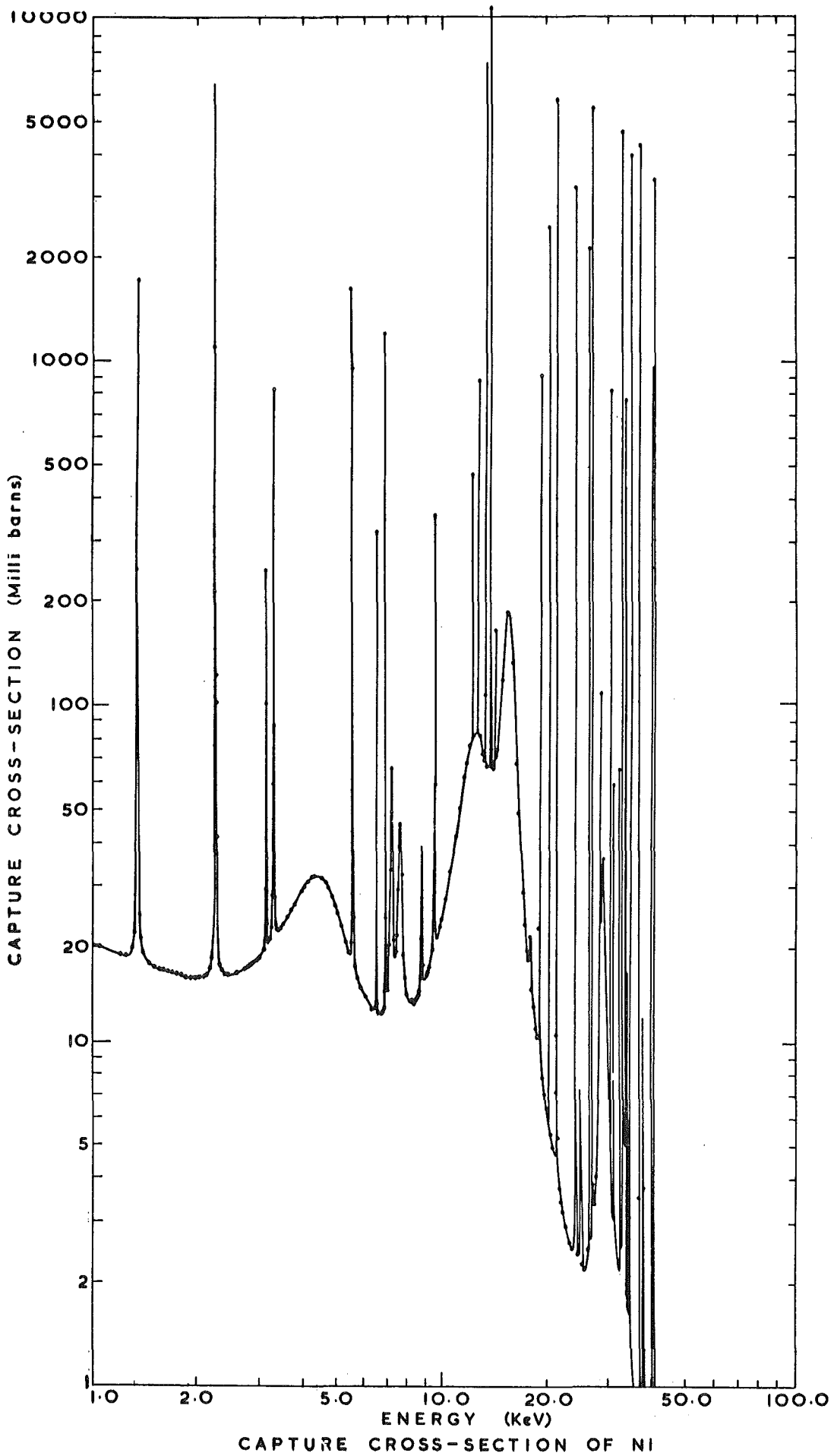
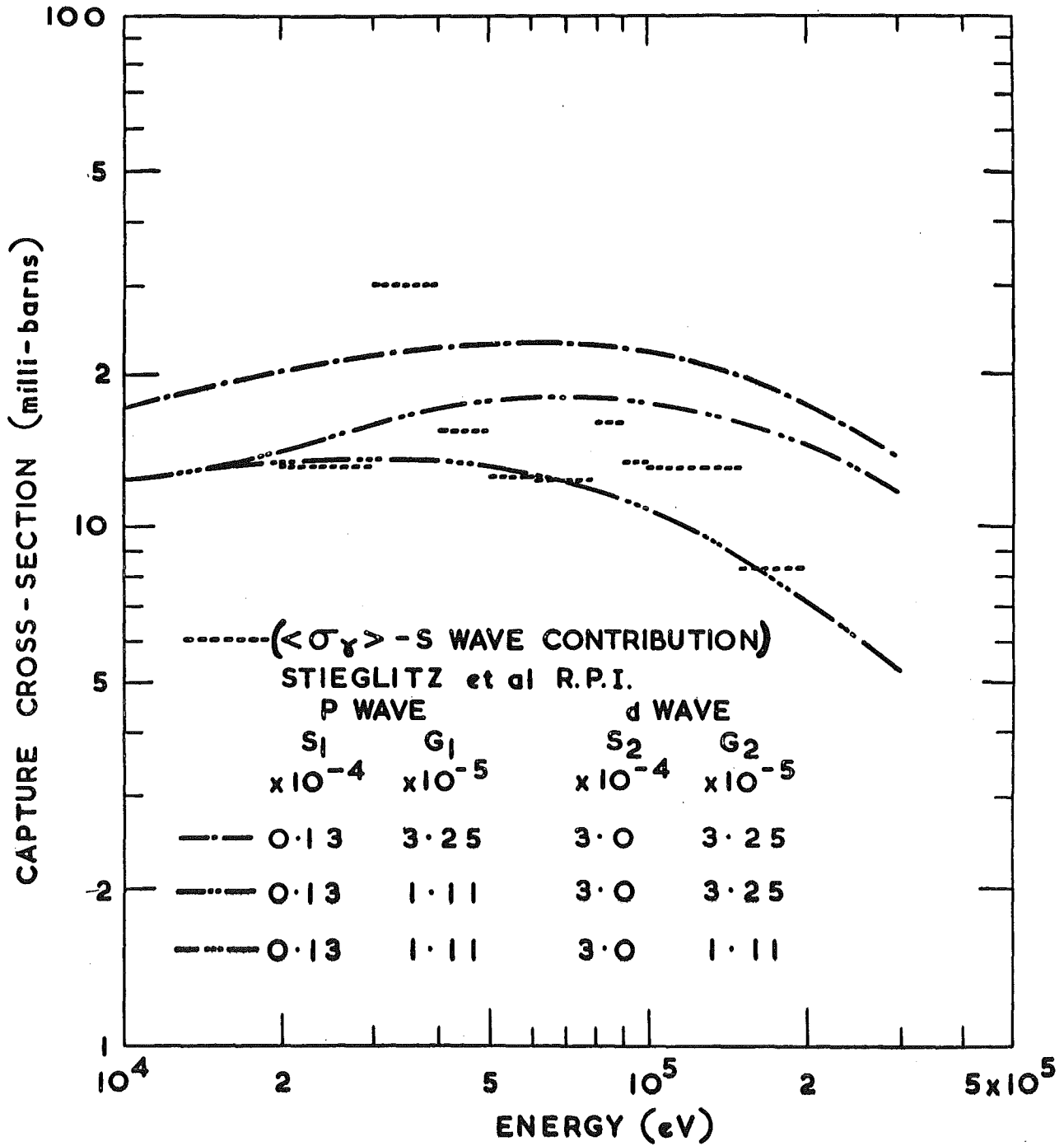


FIGURE 5



Thermal cross sections and resonance  
parameters recommended in the new BNL 325  
vol. I for Cr

S. Pearlstein  
N.N.C.S.C. Brookhaven

17 12-APR-73 16:02

THERMAL CROSS SECTIONS

<sup>24</sup>Cr

$$\begin{aligned} \sigma_T &= 3.1 \pm 0.2 \text{ b} \\ \bar{\sigma}_a &= 3.8 \pm 0.3 \text{ b} \\ \sigma_c &= 6.9 \pm 0.3 \text{ b} \\ \lambda_{coh} &= 3.532 \pm 0.010 \text{ fm} \end{aligned}$$

RESONANCE PROPERTIES

$$I_\gamma = 1.7 \pm 0.2 \text{ b}$$

THERMAL CROSS SECTIONS

<sup>50</sup>Cr

$$\sigma_T = 15.9 \pm 0.2 \text{ b}$$

RESONANCE PROPERTIES

$$\begin{aligned} I_\gamma &= 7.6 \pm 0.4 \text{ b} \\ R^2 &= 5.4 \pm 0.4 \text{ fm} \\ S_0 &= 2.2 \pm 0.8 \\ S_1 &= 0.26 \pm 0.15 \end{aligned}$$

RESONANCE PARAMETERS

$$I^a = 0^a$$

$$\lambda_{Abn} = 4.35$$

$$S_n = 9262.0 \pm 1.0 \text{ keV}$$

$E_0$ (keV)	$g\Gamma_n$ (eV)	J	$\ell$	$\Gamma_\gamma$ (eV)	$g\Gamma_n^0$ (eV)	$g\Gamma_n^1$ (eV)
Bound level		1/2	0			
5.49 ± 0.02			1	<sup>a</sup> 0.014 ± 0.003		
5.64 ± 0.03	1665 ± 50	1/2	0	3.10 ± 0.25	22.17 ± .67	
9.30 ± 0.03			1	<sup>a</sup> 0.053 ± 0.01		
18.60 ± 0.08			1	<sup>a</sup> 0.66 ± 0.11		
19.2 ± 0.08			1	<sup>a</sup> 0.437 ± 0.073		
24.0 ± 0.1			1	<sup>a</sup> 0.058 ± 0.013		
24.8 ± 0.1			1	<sup>a</sup> 0.365 ± 0.060		
28.426 ± 0.006	415 ± 6	1/2	0	<sup>a</sup> 0.57 ± 0.07	2.46 ± .04	
33.40 ± 0.12		[3/2]	1	<sup>a</sup> 0.99 ± 0.15		
35.30 ± 0.13		[3/2]	1	1.65 ± 0.23		
37.3 ± 0.2	2250 ± 20	1/2	0	2.50 ± 0.3	11.65 ± .10	
40.6 ± 0.2			1	<sup>a</sup> 0.88 ± 0.12		
50.1 ± 0.3		[1/2]	1	<sup>a</sup> 0.60 ± 0.08		
53.7 ± 0.3			1	<sup>a</sup> 0.72 ± 0.13		
54.99 ± 0.01	281 ± 8	1/2	0	0.88 ± 0.10	1.20 ± .03	
59.7 ± 0.3		[3/2]	1	<sup>a</sup> 1.12 ± 0.17		
63.4 ± 0.4			1			
64.79 ± 0.03	43 ± 6	1/2	0		.16 ± .02	
64.9 ± .4			1			
65.0 ± 0.43			1			
69.2 ± .5			1			
70.5 ± .5			1			
73.5 ± .5			1			

<sup>50</sup>Cr

E <sub>0</sub> (keV)	g <sub>n</sub> <sup>0</sup> (eV)	J	ℓ	Γ <sub>γ</sub> (eV)	g <sub>n</sub> <sup>0</sup> (eV)	g <sub>n</sub> <sup>1</sup> (eV)
77.8 ± .5			1			
79.4 ± .5			1			
88.9 ± .6			1			
90.7 ± .6			1			
94.75 ± 0.03	1800 ± 100	1/2	0		5.85 ± .32	
111.80 ± 0.08	90 ± 20	1/2	0		.27 ± .06	
113.0			>0			
114.78 ± 0.08	120 ± 20	1/2	0		.35 ± .05	
116.5	168 ± 30		>0			
122.0			>0			
129.01 ± 0.07	520 ± 50	1/2	0		1.45 ± .14	
142.0	240 ± 50		>0			
156.63 ± 0.07	1230 ± 70	1/2	0		3.11 ± .18	
162.45 ± 0.07	700 ± 50	1/2	0		1.74 ± .12	
165.21 ± 0.07	3300 ± 200	1/2	0		7.67 ± .46	
218.3 ± 0.3	170 ± 40				.364 ± .09	
231.7 ± 0.3	750 ± 100	1/2	0		1.56 ± .21	
245.6 ± 0.4	200 ± 50	1/2	0		.40 ± .10	
276.8 ± 0.4	1800 ± 100	1/2	0		3.42 ± .19	
283.5			>0			
293.0 ± 3.0	3700 ± 400	1/2	0		6.84 ± .74	
313.5	1060 ± 480	3/2	1			6.2
328.6 ± 3.3	4500 ± 1000	1/2	0		7.85 ± 1.74	
341.0			>0			
348.0			>0			
356.6 ± 3.9	4500 ± 1000	1/2	0		7.54 ± 1.67	
359.5 ± 4.0	1750 ± 350	1/2	0		2.92 ± .58	
370.0 ± 4.0	10000 ± 3000	1/2	0		16.44 ± 4.93	
381.0	684 ± 70		>0			
388.5 ± 4.0	4000 ± 800	1/2	0		6.42 ± 1.28	
395.0	0.250	1/2	0		0.415	
405.0	1110 ± 220	3/2	1			4.8
413.7	1.750	1/2	0		2.841	
416.5	14.000	1/2	0		22.655	
431.5	1090 ± 180	3/2	1			4.4
433.5	10.000	1/2	0		15.889	
442.0			>0			
454.5	.250	1/2	0		0.389	
459.5	733 ± 50	1/2	1			2.8
467.5	6.500	1/2	0		9.980	
472.0	875 ± 125	1/2	1			3.2
478.0	2.500	1/2	0		3.800	
489.0	1.750	1/2	0		2.633	
502.5	4.000	1/2	0		5.945	
509.0			>0			
515.0	2.000	1/2	0		2.940	
523.0	0.500	1/2	0		0.730	
536.0			>0			
538.5	3.000	1/2	0		4.323	
547.0	2.500	1/2	0		3.577	
553.8	6.000	1/2	0		8.538	
560.5	3.000	1/2	0		4.246	
578.0	2.700	1/2	0		3.770	
580.5	7.000	1/2	0		9.755	
590.7	1.500	1/2	0		2.074	

18 12-APR-73, 16.02

<sup>a</sup> g<sub>n</sub><sup>0</sup>Γ<sub>γ</sub>/Γ

THERMAL CROSS SECTIONS

$\sigma_T = 0.76 \pm 0.06$  b  
 $r_{coh} = 4.9$  fm

RESONANCE PROPERTIES

$I_T = 0.60 \pm 0.05$  b  
 $R_T^2 = 5.7 \pm 0.3$  fm  
 $S_0 = 2.1 \pm 1.1$   
 $S_1 = 0.30 \pm 0.15$

RESONANCE PARAMETERS

$I^{\pi} = 0^+$

$\chi_{abn} = 83.79$

$S_n = 7940.5 \pm 0.9$  keV

$E_0$ (keV)	$g_n^2$ (eV)	J	$l$	$\Gamma_T$ (eV)	$g_n^0$ (eV)	$g_n^1$ (eV)
Bound level						
1.626 ± 0.005	0.080 ± 0.012		1		.0020 ± .0003	0.84
22.92 ± 0.01	4 ± 1		1	<sup>a</sup> 0.55 ± 0.09	.026 ± .007	1.1
27.60 ± 0.11			1	<sup>a</sup> 0.46 ± 0.08		
31.62 ± 0.01	15 ± 1		0	0.31 ± 0.05	.084 ± .006	
33.90 ± 0.13			1	<sup>a</sup> 0.34 ± 0.06		
34.30 ± 0.13			1	<sup>a</sup> 0.26 ± 0.05		
48.30 ± 0.21		[3/2]	1	0.47 ± 0.08		
50.19 ± 0.01	1710 ± 20	1/2	0	1.16 ± 0.20	7.63 ± .09	
57.58 ± 0.01	75 ± 10	[3/2]	1	0.36 ± 0.16	.31 ± .04	4.0
79.2 ± 0.6			1	<sup>a</sup> 0.38 ± 0.07		
96.23 ± 0.03	6800 ± 100	1/2	0	4.80 ± 0.80	21.92 ± .32	
106.0 ± 0.1	60 ± 20	3/2	1	0.43 ± 0.07	.18 ± .06	1.3
111.6 ± 0.1	60 ± 20	3/2	1	0.31 ± 0.05	.18 ± .06	1.3
113.0 ± 0.4		3/2	1	0.7 ± 0.1		
117.6 ± 0.4	30 ± 10	1/2	0		.088 ± .029	
121.38 ± 0.02	610 ± 20	1/2	0		1.75 ± .06	
124.0 ± 1.0		[3/2]	1	0.73 ± 0.13		
130.10 ± 0.05	220 ± 20	3/2	1	0.67 ± 0.11	.61 ± .05	3.8
139.71 ± 0.07	5400 ± 200	1/2	0		14.45 ± .54	
141.3 ± 0.2	700 ± 200	1/2	0		1.86 ± .532	
155.0 ± 1.2		1/2	1	<sup>a</sup> 0.62 ± 0.11		
168.0 ± 1.3			1	<sup>a</sup> 0.84 ± 0.15		
205.0 ± 1.5	130 ± 60	3/2	1		.29 ± .13	1.4
224 ± 1.5	<100					
234.0 ± 0.6	300 ± 100		>0		.62 ± .21	

RC

19 12-APR-73 16.02

$E_0$ (keV)	$g_n^0$ (eV)	J	$\ell$	$\Gamma_\gamma$ (eV)	$g_n^0$ (eV)	$g_n^1$ (eV)
235.8 ± 0.2	1100 ± 100	1/2	0		2.27 ± .21	
242.6 ± 0.4	220 ± 50		>0		.45 ± .10	
246.3 ± 0.2	1010 ± 60	1/2	1		2.04 ± .12	7.7
249.3 ± 0.2	550 ± 50				1.10 ± .10	
252.0 ± 1.0	810 ± 70	3/2	1		1.52 ± .14	6.0
256.7 ± 0.3	310 ± 50		1		.612 ± .10	2.2
281.9 ± 0.3	550 ± 80	1/2	0		1.04 ± .15	
288.0 ± 1.0	<100	3/2	1			
331.1 ± 3.5	6700 ± 1000	1/2	0		11.72 ± 1.75	
349.0 ± 3.5	152		>0			
363.5 ± 3.5	3500 ± 1000	1/2	0		5.81 ± 1.66	
401.0 ± 3.5	18000 ± 4000	1/2	0		28.43 ± 6.32	
418.0 ± 3.5	1000 ± 300	1/2	0		1.55 ± 4.64	
442.0 ± 3.5	813		>0			
460.5 ± 4.0	12000 ± 4000	1/2	0		17.68 ± 5.89	
530.0 ± 5.0	8000 ± 2400	1/2	0		10.98 ± 3.30	

•  $g_n^0 \Gamma_\gamma / \Gamma$

•  $g_n^1$

330

21 12-RR-73 16.02

<sup>52</sup>Cr

22-12-RR-73, 16.02

THERMAL CROSS SECTIONS

$\sigma_{\gamma} = 18.2 \pm 1.5 \text{ b}$

RESONANCE PROPERTIES

$I_{\gamma} = 8.85 \pm 1.00 \text{ b}$   
 $R^{\dagger} = 6.9 \pm 0.3 \text{ fm}$   
 $\langle D \rangle = 4.1 \pm 0.7 \text{ keV}$   
 $S_0 = 5.0 \pm 2.1$   
 $S_1 = 0.074 \pm 0.050$

RESONANCE PARAMETERS

$J^{\pi} = 3/2^{-}$

$\%Abn = 9.50$

$S_n = 9720.2 \pm 0.7 \text{ keV}$

$E_D$ (keV)	$2g\Gamma_n$ (eV)	J	$\ell$	$\Gamma_{\gamma}$ (eV)	$2g\Gamma_n^0$ (eV)
Bound level		1			
4.185 ± 0.015	1140 ± 60	1	0	3.23 ± 0.45	17.62 ± .93
5.67 ± 0.025	260 ± 20	2	0	1.33 ± 0.20	3.45 ± .27
6.74 ± 0.04	900 ± 75	1	0	5.28 ± 0.80	10.96 ± .91
8.18 ± 0.04	1230 ± 110	2	0	3.25 ± 0.4	13.60 ± 1.22
12.10 ± 0.04			1	<sup>a</sup> 0.36 ± 0.06	
12.90 ± 0.04			1	<sup>a</sup> 0.22 ± 0.04	
14.60 ± 0.05			1	<sup>a</sup> 0.26 ± 0.05	
19.60 ± 0.06	133 ± 19	2	0		.95 ± .14
20.20 ± 0.08			1	<sup>a</sup> 0.77 ± 0.14	
22.40 ± 0.10			1	<sup>a</sup> 0.29 ± 0.05	
25.90 ± 0.08	280 ± 25	2	0	0.61 ± 0.07	1.74 ± .16
27.00 ± 0.09	550 ± 50	1	0	1.57 ± 0.17	3.35 ± .30
28.80 ± 0.11			1	<sup>a</sup> 0.65 ± 0.12	
29.30 ± 0.12	430 ± 40	2	0	1.21 ± 0.14	2.51 ± .23
31.50 ± 0.13			1	<sup>a</sup> 0.31 ± 0.06	
32.00 ± 0.14			1	<sup>a</sup> 0.23 ± 0.05	
34.90 ± 0.15			1	<sup>a</sup> 0.32 ± 0.07	
37.70 ± 0.17			1	<sup>a</sup> 0.35 ± 0.07	
42.40 ± 0.19			1	<sup>a</sup> 0.21 ± 0.04	
43.20 ± 0.20			1	<sup>a</sup> 0.20 ± 0.04	
47.1 ± 0.2			1	<sup>a</sup> 0.37 ± 0.07	
49.8 ± 0.2			1		
51.0 ± 0.3			1		
53.5 ± 0.3			1	0.40 ± 0.08	
64.8 ± 0.3			1	0.60 ± 0.08	
65.7 ± 0.3	5700 ± 150	2	0		22.23 ± .59
69.7 ± 0.3			1	1.25 ± 0.24	
73.1 ± 0.3	800 ± 200	1			2.95 ± .74
74.1 ± 0.3	1400 ± 100	2	0		5.14 ± .37
87.2 ± 0.3	5500 ± 750	1	0		18.63 ± 2.54
94.5 ± 0.4	750 ± 125	(2)	0		2.44 ± .41
99.7 ± 0.4	300 ± 75	1	0		.95 ± .24
107.8 ± 0.4	1700 ± 200	2	0		5.18 ± .61
123.6 ± 0.4	3000 ± 750	1			8.53 ± 2.13
124.5 ± 0.4	600 ± 250	2			1.70 ± .71
127.6 ± 0.4	500 ± 250	2			1.40 ± .70

$^{53}_{24}\text{Cr}$					
$E_0$ (keV)	$2g_n^0$ (eV)	J	$\ell$	$\Gamma_\gamma$ (eV)	$2g_n^0$ (eV)
129.5 ± 0.5	300 ± 150	2			.83 ± .42
135.0 ± 0.5	18000 ± 3750	1	0		48.99 ± 10.20
145.9 ± 0.5	800 ± 125	2			2.09 ± .33
157.8 ± 0.5	1100 ± 125	2			2.77 ± .32
159.5 ± 0.5	2600 ± 375	2			6.51 ± .94
172.7 ± 0.6	1500 ± 250	2			3.61 ± .60
175.7 ± 0.6	3000 ± 600	1	0		7.156 ± 1.4
183.0 ± 0.7	2600 ± 525	1			6.08 ± 1.22
186.0 ± 0.7	600 ± 250	2			1.39 ± .58
195.7 ± 0.7	800 ± 125	2			1.80 ± .28
201.7 ± 0.7	700 ± 125	2			1.55 ± .28
221.6 ± 0.7	5200 ± 1000	2			11.04 ± 2.12
227.5 ± 0.7	400 ± 125	2			.84 ± .26
239.0 ± 0.8	3750 ± 750	2			7.67 ± 1.53
244.5 ± 0.8	3000 ± 750	1			6.07 ± 1.51
246.0 ± 0.8	600 ± 375	2			1.20 ± .76

• Positive energy resonances contribute about 11 b to the thermal absorption cross section. Support for spin 1 assignment is based on ratio of thermal capture of spin 2 state to spin 1 state.

•  $2g_n^0 \Gamma_\gamma / \Gamma$

23 12-APR-73, 16-02

$^{54}\text{Cr}$

24 12-APR-73, 16.02

THERMAL CROSS SECTIONS

$\sigma_T = 0.36 \pm 0.04 \text{ b}$

RESONANCE PROPERTIES

$I_\gamma = 0.18 \pm 0.04 \text{ b}$

$R_\gamma = 4.8 \pm 0.2 \text{ fm}$

$S_0 = 1.8 \pm 1.0$

$S_1 = 0.042 \pm 0.024$

RESONANCE PARAMETERS

$I^\pi = 0^+$

$\% \text{Abn} = 2.36$

$S_n = 6246.3 \pm 0.4 \text{ keV}$

$E_0$ (keV)	$g\Gamma_n$ (eV)	J	$\ell$	$\Gamma_\gamma$ (eV)	$g\Gamma_n^0$ (eV)
10.30±0.04			1	<sup>a</sup> 0.14±0.02	
14.40±0.05			1	<sup>a</sup> 0.28±0.04	
19.10±0.08			1	<sup>a</sup> 0.25±0.04	
23.1 ±0.1	550 ± 35		0	0.19±0.05	3.62± .23
51.1 ±0.3			1	<sup>a</sup> 0.34±0.05	
54.9 ±0.3			1	<sup>a</sup> 0.36±0.06	
67.5 ±0.3		[3/2]	1	<sup>a</sup> 0.94±0.18	
76.4 ±0.5			1		
90.1 ±0.6			1		
120.1 ±0.8	5600 ± 400	1/2	0		16.16±1.2
129.0	250	1/2	0		.70
169.8	500		>0		
179.1 ±1.4	1900 ± 170	1/2	0		4.49± .40
189.3	255		>0		
228.0			>0		
233.0			>0		
247.5	1255	1/2	1		
264.0			>0		
279.5	9000	1/2	0		17.02
282.5	3000	1/2	0		5.70
285.0	300		>0		
290.5	600	1/2	0		1.12
300.5	500	1/2	0		0.92
314.0			>0		
325.0	16000	1/2	0		28.33
330 ±3	13000 ±1500	1/2	0		22.63±2.61
332.0	810		>0		
342.0	200	1/2	0		.34
351.5	500	1/2	0		.84
355.5	300	1/2	0		.50
358.7	400		>0		
362.0	500	1/2	0		.83
387.5	1040		>0		
393.5	4000	1/2	0		6.38

<sup>a</sup>  $g\Gamma_n\Gamma_\gamma/\Gamma$

25 12-APR-73 16.02

THERMAL CROSS SECTIONS

Isotope	Measurement	Reference	Author
$Cr^{54}$	$\sigma_{\gamma}$ (spectra) (thermal)	NP/A,187,12(72)	White
$Cr$	Christiansen filter	ZN/A,26,391(71)	Koester
$Cr^{50}$	activation	JIN,30,349(68)	Sims
$Cr^{53}$	$\sigma_{\gamma}$ (spectra) (thermal)	CJP,43,1128(65)	Bartholomev
$Cr^{53}$	$\sigma_{\gamma}$ (spectra) (thermal)	PR,131,777(63)	White
$Cr^{52}$	diffraction	ARN,11,303(61)	Wilkinson
$Cr^{50}$	activation	NSE,8,378(60)	Lyon
$Cr^{54}$	activation	PR,95,781(54)	Bazorgan
$Cr$	$\sigma_t$	PR,92,702(53)	Melkonian
$Cr^{50,52,53,54}$	pile osci.	PR,88,412(52)	Pomerance
$Cr$	pile osci.	CR,232,2089(51)	Grimeland
$Cr$	pile osci.	PR,83,641(51)	Pomerance
$Cr$	$\bar{\sigma}_s$ diffraction	PR,81,527(51)	Shull
$Cr$	pile osci.	PPS/A,63,1175(50)	Colmer
$Cr$	$\bar{\sigma}_s$ diffraction	PR,80,342(50)	Harris
$Cr$		PR,69,411(46)	Coltman
$Cr$	$\bar{\sigma}_s$	PRS/A,162,127(37)	Goldhaber
$Cr$	$\bar{\sigma}_s$	PR,50,133(36)	Mitchell
$Cr$	$\sigma_t$	PR,48,265(35)	Dunning

RESONANCE PARAMETERS

Isotope	Measurement	Energy Range (keV)	Reference	Author
$Cr^{50}$	$\sigma_t$	28.4-290	KFK-1517(72)	Spencer
$Cr^{52}$	$\sigma_t$	22.9-282	KFK-1517(72)	Spencer
$Cr^{53}$	$\sigma(\gamma,n)$	23-543	PR/C,3,672(71)	Baglan
$Cr^{53}$	$\sigma(\gamma,n)$	50.2-364	PR/C,4,1314(71)	Jackson
$Cr^{53}$	$\sigma_t$	19.5-246	NP/A,164,97(71)	Mueller
$Cr^{50}$	$\sigma_t \sigma_{\gamma}$	5.6-357	NP/A,163,592(71)	Stieglitz
$Cr^{52}$	$\sigma_t \sigma_{\gamma}$	1.6-331	NP/A,163,592(71)	Stieglitz
$Cr^{53}$	$\sigma_t \sigma_{\gamma}$	4.2-176	NP/A,163,592(71)	Stieglitz
$Cr^{54}$	$\sigma_t \sigma_{\gamma}$	23.1-355	NP/A,163,592(71)	Stieglitz
$Cr, Cr^{52}$	$\sigma_t$	755-902	CEA-R-3279(67)	Cabe
$Cr^{50}$	$\sigma_t$	95.5-591	AP,37,367(66)	Farrell
$Cr^{54}$	$\sigma_t$	116-394	AP,37,367(66)	Farrell
$Cr^{53}$	$\sigma_t$	3.6-28.6	PR,151,912(66)	Good
$Cr^{50}$	$\sigma_{\gamma}$	5.5	AE,16,256(64)	Kapchigashev
$Cr^{52}$	$\sigma_{\gamma}$	1.7	AE,16,256(64)	Kapchigashev
$Cr^{53}$	$\sigma_t$	19-39	BAP,8,556(63)	Kim
$Cr^{52}$	$\sigma_t$	51-636	AP,17,319(62)	Bowman
$Cr^{50}$	$\sigma_t$	6.6-95	AP,14,387(61)	Bilpuch
$Cr^{52}$	$\sigma_t$	51-140	AP,14,387(61)	Bilpuch
$Cr^{54}$	$\sigma_t$	23.5-119	AP,14,387(61)	Bilpuch
$Cr, Cr^{52}$	$\bar{\sigma}_s$	30-115	PR,109,1620(58)	Block
$Cr^{50}$	$\sigma_t$	5.5	PR,111,288(58)	Cote
$Cr^{52}$	$\sigma_t$	51-406	PR,108,414(57)	Hibdon
$Cr$	$\sigma_t$	102-342	ANL-5554,55(56)	Hibdon
$Cr^{53}$	$\sigma_t$	69.0-396	ANL-5554,55(56)	Hibdon
$Cr$	$\sigma_t$	3.8	PR,92,702(53)	Melkonian

Thermal cross sections and resonance  
parameters recommended in the new BNL 325  
vol. I for Fe



$^{54}_{26}\text{Fe}$					
$E_0$ (keV)	$g\Gamma_n$ (eV)	J	$\ell$	$\Gamma_\gamma$ (eV)	$g\Gamma_n^0$ (eV)
173.0 ± 1.0	4800 ± 1200	1/2	0		11.54 ± 2.89
188.5 ± 1.0	38000 ± 10000.	1/2	0		87.52 ± 23.03
223.0 ± 1.5	1900 ± 380	1/2	0		4.023 ± .80
230.0 ± 1.5	500 ± 100	1/2	0		1.04 ± .21
244.5 ± 2.0	1300 ± 260	1/2	0		2.63 ± .53
245	240		>0		
262	200		>0		
277	265		>0		
280	110		>0		
282	250		>0		
293	450		>0		
305.5 ± 3.0	7000 ± 1400	1/2	0		12.66 ± 2.53
317.0 ± 3.0	14000 ± 2800	1/2	0		24.87 ± 4.97
329.5 ± 3.0	2750 ± 550	1/2	0		4.79 ± .96
369 ± 3.0	3000	1/2	0		4.9
399	250		>0		
403	110		>0		
411	600		>0		
415	120		>0		
416 ± 4	19000 ± 5000	1/2	0		29.46 ± 7.75
419	<100	(1/2)	>0		
431.0 ± 4.0	7500 ± 1800	1/2	0		11.42 ± 2.74
435.5 ± 4.0	1750 ± 350	1/2	0		2.65 ± .53
438	<100	(1/2)	>0		
441	<100	(1/2)	>0		
445	<100	(1/2)	>0		
449	905		>0		
453	2060		>0		
462	<100	(1/2)	>0		
464	<100	(1/2)	>0		
471	<100	(1/2)	>0		
489.0 ± 5.0	10000 ± 2000	1/2	0		14.30 ± 2.86
491	215		>0		
494	680		>0		
496	435		>0		
503	650		>0		
506.5	750	1/2	0		1.1

<sup>a</sup>  $g\Gamma_n\Gamma_\gamma/\Gamma$

<sup>b</sup> Calculated

31 12-APR-73, 16.02



$^{56}\text{Fe}$							
$E_0$ (keV)	$g_n^{\Gamma}$ (eV)		J	$\ell$	$\Gamma_{\gamma}$ (eV)	$g_n^{\Gamma_0}$ (eV)	$g_n^{\Gamma_1}$ (eV)
290	<100			>0			
315.0 ±1.0	5500 ±1100		1/2	0		9.80 ±1.96	
337	130			>0			
350	670			>0			
357	260			>0			
360.5 ±1.0	9300 ±2000		1/2	0		15.48 ±3.33	
382.0 ±1.0	10000 ±3000		1/2	0		16.18 ±4.85	
404	610			>0			
406.0 ±1.0	2500 ± 500		1/2	0		3.92 ± .78	
418	800		[3/2]	>0			
428	<100		(1/2)	>0			
438.0 ±1.0	1500 ± 300		1/2	0		2.27 ± .45	
442	<100		(1/2)	>0			
448	1000		[1/2]	1			3.3
465	115			>0			
469.5 ±1.0	1500 ± 300		1/2	0		2.19 ± .44	
481	385			>0			
491	1300		[1/2]	1			4.1
496	<100		(1/2)	>0			
501.0 ±0.4	2000		1/2	0			
503.5 ±0.2	600						
512.1 ±0.2	770						
513.1 ±0.4	700						
527.2 ±0.4	365			>0			
531.9 ±0.4	395			>0			
536.2 ±0.4	235			>0			
538.7 ±0.4	925			>0			
544.5 ±0.4	600			>0			
545.6 ±0.4	1100			>0			
552.3 ±0.4	450			>0			
558.7 ±0.4	465			>0			
561.5 ±0.4	1230		1/2	0			
562.8 ±0.8	~600						
565.4 ±0.5							
569.3 ±0.5							
577.5 ±0.5	2000		[3/2]	1			5.5
578.8 ±0.5	~700						
590.4 ±0.5							
595.0 ±0.5							
604.2 ±0.6							
615.0 ±0.6	2500		1/2	0		3.19	
623.7 ±0.6							
631.1 ±0.6							
633.3 ±0.6							
637.0 ±0.6	385			>0			
641.0 ±0.6	330						
646.4 ±0.6	2000		[3/2]	>0			

\*  $g_n^{\Gamma} \Gamma_{\gamma} / \Gamma$

33 12-APR-73 16.02

<sup>57</sup><sub>26</sub>Fe

34 12-APR-73, 16.02

THERMAL CROSS SECTIONS

$\sigma_y = 2.48 \pm 0.30$  b  
 $a_{coh} = 2.3 \pm 0.1$  fm

RESONANCE PROPERTIES

$I_\gamma^c = 1.3 \pm 0.2$  b  
 $R^{\frac{1}{2}} = 6.5 \pm 0.7$  fm  
 $S_0 = 5.4 \pm 1.6$

RESONANCE PARAMETERS

$I^p = 1/2^-$                        $\Sigma \Gamma_{bn} = 2.19$                        $S_n = 10043.0 \pm 1.0$  keV

$E_0$ (keV)	$2g\Gamma_n$ (eV)	J	$\ell$	$\Gamma_\gamma$ (eV)	$2g\Gamma_n^0$ (eV)
1.63 ± 0.01				<sup>a</sup> 0.10 ± 0.02	
3.92 ± 0.05	100 ± 20	0	0	1.14 ± 0.06	1.60 ± .32
4.75 ± 0.06				<sup>a</sup> 0.10 ± 0.02	
6.21 ± 0.07	615 ± 75	1	0	1.32 ± 0.12	7.80 ± .95
7.22 ± 0.08				<sup>a</sup> 0.72 ± 0.18	
7.90 ± 0.08				<sup>a</sup> 0.36 ± 0.06	
12.8 ± 0.1				<sup>a</sup> 0.86 ± 0.20	
13.9 ± 0.1				<sup>a</sup> 1.4 ± 0.4	
17.7 ± 0.3				<sup>a</sup> 1.17 ± 0.32	
21.3 ± 0.4				<sup>a</sup> 2.18 ± 0.56	
<sup>a</sup> 29.0 ± 0.4	4870 ± 400	1	0	4 ± 1	28.60 ± 2.35
41.0 ± 0.5	1350 ± 150	1			6.67 ± .74
45.5 ± 0.5	525 ± 150	1			2.46 ± .70
55.81	5000 ± 750	0			21.16 ± 3.17
61.0	5550 ± 750	1			22.47 ± 3.04
77.2	2925 ± 300	1			10.53 ± 1.08
93.7	300 ± 75	1			9.80 ± .25
109.6	3450 ± 450	1			10.42 ± 1.36
110.15	1800 ± 150	1			5.42 ± .45
125.0	2250 ± 300	1			6.36 ± .85
126.0	1250 ± 250	0			3.52 ± .70
129.5	6300 ± 1050	1			17.51 ± 2.92
134.5	4950 ± 750	1			13.50 ± 2.05
141.0	2250 ± 450	1			5.99 ± 1.20
167.3	1650 ± 150	1			4.03 ± .37
169.0	2550 ± 300	1			6.20 ± .73
176.3	350 ± 50	0			.83 ± .12
185.5	5250 ± 600	1			12.19 ± 1.39
189.5	1600 ± 200	0			3.68 ± .46

<sup>a</sup>  $2g\Gamma_n\Gamma_\gamma/\Gamma$

<sup>b</sup> Rohr et al reported also inelastic widths in the energy range from 29.15 to 189.5 keV.

<sup>58</sup>Fe

THERMAL CROSS SECTIONS

$\sigma_T = 1.15 \pm 0.02 \text{ b}$

RESONANCE PROPERTIES

$I_\gamma = 1.19 \pm 0.07 \text{ b}$

RESONANCE PARAMETERS

$I^n = 0^*$

$\%Abn = 0.31$

$S_n = 6586.6 \pm 3.5 \text{ keV}$

$E_0$ (keV)	$\Gamma_\gamma$ (eV)
0.230	$^a 0.0065 \pm 0.0014$
0.359	$^a 0.017 \pm 0.005$
2.82	
6.16	
10.5	
19.2	

$^a g_n^2 \Gamma_\gamma / \Gamma$

35 12-APR-73 16.02

THERMAL CROSS SECTIONS

Isotope	Measurement	Reference	Author
Fe <sup>58</sup>	activation	JIN,34,2699(72)	Steinnes
Fe	activation	JNE,24,35(70)	Ryves
Fe <sup>58</sup>	activation	PRIVATE COMM.(67)	Fabry
Fe	pile osci.	66PARIS,1,479(66)	Carre
Fe <sup>58</sup>	activation	66BERKLEY,331(66)	Carter
Fe	$\sigma_t$ 1.44 ev	NP,61,381(65)	Rayburn
Fe	pile osci.	CEA-2485(64)	Carre
Fe <sup>58</sup>	activation	AC,36,1588(64)	Girardi
Fe <sup>58</sup>	activation	PRIVATE COMM.(63)	Girardi
Fe	reflection	RSI,33,916(62)	Bally
Fe	diffraction	JPJ,17,(B111),1(62)	Shull
Fe	pile osci.	61BUCHAR,623(61)	Bouzyk
Fe	pulsed n	ZET,41,1037(61)	Isakov
Fe <sup>54</sup>	activation	NSE,8,378(60)	Lyon
Fe <sup>58</sup>	activation	NSE,8,378(60)-	Lyon
Fe	pile osci.	JNE,12,32(60)	Tattersall
Fe	reactivity	DP-207(57)	Wade
Fe <sup>58</sup>	activation	PRIVATE COMM.(56)	Grimeland
Fe	$\sigma_t$	PR,91,451(53)	Goldberg
Fe	$\sigma_a$	HPA,25,521(52)	Haenni
Fe <sup>56</sup>	$\sigma_a$	JPR,13,333(52)	Longchamp
Fe <sup>54,56,57,58</sup>	pile osci.	PR,88,412(52)	Pomerance
Fe	pile osci.	CR,232,2089(51)	Grimeland
Fe	$\sigma_t$	PR,83,1123(51)	Havens
Fe	local osci.	PR,83,641(51)	Pomerance
Fe,Fe <sup>54,56,57</sup>	diffraction	PR,81,527(51)	Shull
Fe	pile osci.	PPS/A,63,1175(50)	Colmer
Fe	$\sigma_a$	CR,231,1475(50)	Faraggi
Fe	$\sigma_a$	HPA,23,513(50)	Haenni
Fe	pile osci.	PR,80,342(50)	Harris
Fe	reflection	PR,71,666(47)	Fermi
Fe <sup>58</sup>	activation	PR,72,888(47)	Seren
Fe	capture	PR,69,411(46)	Coltman
Fe	$\sigma_t \bar{\sigma}_s$	PR,60,155(41)	Whitaker
Fe	$\sigma_t$	PR,57,976(40)	Beyer
Fe	$\bar{\sigma}_s$	PRS/A,162,127(37)	Goldhaber

36-12-MPR-73, 16-02

## RESONANCE PARAMETERS

Isotope	Measurement	Energy Range (keV)	Reference	Author
Fe <sup>54</sup>	$\sigma_t \sigma_\gamma$	3.1-39.0	PRIVATE COMM.(72)	Block
Fe <sup>56</sup>	$\sigma_t \sigma_\gamma$	0.23-19.2	PRIVATE COMM.(72)	Block
Fe <sup>56</sup>	analysis	27.9-435.5	PRIVATE COMM.(72)	Hynchank
Fe <sup>56</sup>	$\sigma(\gamma, n)$	27-410	PR/C, 3, 2475(71)	Baglan
Fe, Fe <sup>54, 56, 57</sup>	$\sigma_t$	0-187	PR/C, 3, 2447(71)	Garg
Fe <sup>57</sup>	$\sigma(\gamma, n)$	27.7-269	PR/C, 4, 1314(71)	Jackson
Fe <sup>54</sup>	$\sigma_\gamma(\text{spectra})$	7.8-52	AUJ, 24, 805(71)	Kenny
Fe <sup>56</sup>	$\sigma_\gamma(\text{spectra})$	11-73	AUJ, 24, 805(71)	Kenny
Fe	$\sigma_t$	500-2500	NSE, 42, 28(70)	Carlson
Fe, Fe <sup>56</sup>	$\sigma_\gamma(\text{spectra})$	1.17	PR/C, 1, 973(70)	Chrien
Fe, Fe <sup>56</sup>	$\bar{\sigma}_t$	1.15	PL/B, 28, 656(69)	Asami
Fe, Fe <sup>54, 56, 57</sup>	$\sigma_\gamma$	10.2-129	70MELSINKI, 1, 633(70)	Ernst
Fe, Fe <sup>54, 56, 57, 58</sup>	$\sigma_\gamma$	0.23-102	70MELSINKI, 2, 815(70)	Moxon
Fe <sup>54</sup>	$\sigma_\gamma$	7.82-52	PR, 178, 1746(69)	Hockenbury
Fe <sup>56</sup>	$\sigma_\gamma$	1.15-129	PR, 178, 1746(69)	Hockenbury
Fe <sup>57</sup>	$\sigma_\gamma$	1.63-40	PR, 178, 1746(69)	Hockenbury
Fe <sup>58</sup>	$\sigma_\gamma$	0.23-10.4	PR, 178, 1746(69)	Hockenbury
Fe, Fe <sup>56</sup>	$\sigma_t$	1.15	NP/A, 132, 129(69)	Julien
Fe <sup>57</sup>	$\sigma_t$	29.2-189.5	ZP, 227, 1(69)	Rohr
Fe <sup>56</sup>	analysis	512-1442	CHP, 6, 15(68)	Chien
Fe	$\sigma_t$	500-646.4	KFK-1000(68)	Cierjaks
Fe <sup>57</sup>	$\sigma_t$	3.9-45.5	PR, 151, 912(66)	Good
Fe <sup>56</sup>	$\sigma_t$	74-242.7	66PARIS, 1, 137(66)	Rohr
Fe, Fe <sup>54, 56, 57</sup>	$\sigma_\gamma$	1.15-28	65ANTWERP, 88(65)	Moxon
Fe, Fe <sup>56</sup>	$\sigma_t$ moving sample	1.2	PL, 14, 123(65)	Muradyan
Fe, Fe <sup>56</sup>	$\sigma_t$	1.15	PL, 13, 234(64)	Block
Fe <sup>56</sup>	$\sigma_\gamma(\text{spectra})$	1.15	ORNL-3778, 64(64)	Block
Fe, Fe <sup>54, 56, 57</sup>	$\sigma_t$	1.17-221	CR-1860(64)	Garg
Fe <sup>56</sup>	$\sigma_t \sigma_\gamma$	22-50	PR/B, 136, 695(64)	Macklin
Fe <sup>57</sup>	$\sigma_t \sigma_\gamma$	12.7-27	PR/B, 136, 695(64)	Macklin
Fe, Fe <sup>56</sup>	$\sigma_t$	0-1.2	PR, 132, 801(63)	Moore
Fe, Fe <sup>56</sup>	$\sigma_\gamma$	1.18	AERE-PR/NP-6, 15(63)+	Moxon
Fe <sup>54</sup>	$\sigma_t$	8-507	AP, 17, 319(62)	Bowman
Fe <sup>56</sup>	$\sigma_t$	28-645	AP, 17, 319(62)	Bowman
Fe	$\sigma_\gamma$	1.15	RP1-(ATR), 8(62)	Russell
Fe <sup>54</sup>	$\sigma_t$	7.25-147	AP, 14, 387(61)	Bilpuch
Fe <sup>56</sup>	$\sigma_t$	28.3-189	AP, 14, 387(61)	Bilpuch
Fe <sup>57</sup>	$\sigma_t$	6	AP, 14, 387(61)	Bilpuch
Fe	$\sigma_\gamma$	1.18-10	ZET, 38, 989(60)	Isakov
Fe <sup>57</sup>	$\sigma_t$	3.9-6.1	ORNL-2610, 19(58)	Miller
Fe, Fe <sup>56</sup>	$\sigma_t$	29-406	PR, 108, 414(57)	Hibdon
Fe <sup>56</sup>	$\sigma_t$	8-85	PR, 102, 1574(56)	Gibbons
Fe, Fe <sup>54</sup>	$\sigma_t$	92-401	ANL-5554, 55(56)	Hibdon
Fe, Fe <sup>57</sup>	$\sigma_t$	143-149	ANL-5554, 55(56)	Hibdon

37 12-APR-73 16.02

Thermal cross sections and resonance  
parameters recommended in the new BNL 325  
vol. I for Ni

<sup>28</sup>Ni

THERMAL CROSS SECTIONS

$$\begin{aligned} \sigma_T &= 4.43 \pm 0.16 \text{ b} \\ \bar{\sigma}_n &= 17.3 \pm 0.5 \text{ b} \\ a_{coh} &= 10.3 \pm 0.1 \text{ fm} \end{aligned}$$

RESONANCE PROPERTIES

$$\begin{aligned} I_T &= 2.2 \pm 0.2 \text{ b} \\ R_T &= 7.3 \pm 0.4 \text{ fm} \\ S_0 &= 2.9 \pm 0.3 \end{aligned}$$

44 12-APR-73, 16.02

<sup>28</sup>Ni

THERMAL CROSS SECTIONS

$$\begin{aligned} \sigma_T &= 4.6 \pm 0.3 \text{ b} \\ \bar{\sigma}_n &= 26.0 \pm 0.3 \text{ b} \\ \sigma_a &= 0.68 \pm 0.36 \text{ mb} \\ \sigma_c &= 30.4 \pm 0.4 \text{ b} \\ a_{coh} &= 14.4 \pm 0.1 \text{ fm} \end{aligned}$$

RESONANCE PROPERTIES

$$\begin{aligned} I_T^c &= 2.2 \pm 0.2 \text{ b} \\ R_T^c &= 7.5 \pm 0.5 \text{ fm} \\ \langle D \rangle &= 3.0 \pm 0.3 \text{ keV} \\ S_0 &= 3.1 \pm 0.8 \end{aligned}$$

RESONANCE PARAMETERS

$I^n = 0^+$		%Abn = 67.88			$S_n = 8999.3 \pm 1.0 \text{ keV}$	
$E_0$ (keV)	$g\Gamma_n$ (eV)	J	$\ell$	$\Gamma_\gamma$ (eV)	$g\Gamma_n^0$ (eV)	$g\Gamma_n^1$ (eV)
-28.5 ± 5.0		1/2	0	9.0 ± 0.6	98.0 ± 5.4	
6.89			[1]	<sup>a</sup> 0.022 ± 0.003		
13.34 ± 0.03			[1]	<sup>a</sup> 0.39 ± 0.05		
13.66 ± 0.04			[1]	<sup>a</sup> 0.57 ± 0.05		
15.50 ± 0.04	1200 ± 100	1/2	0	2.1 ± 0.7	9.64 ± 0.80	
19.03 ± 0.05			[1]	<sup>a</sup> 0.07 ± 0.01		
20.04 ± 0.05			[1]	<sup>a</sup> 0.22 ± 0.03		
21.16 ± 0.05			[1]	<sup>a</sup> 0.56 ± 0.06		
26.08 ± 0.07			[1]	<sup>a</sup> 0.25 ± 0.05		
26.67 ± 0.07			[1]	<sup>a</sup> 0.70 ± 0.07		
32.36 ± 0.08		[3/2]	[1]	<sup>a</sup> 1.38 ± 0.15		
34.24 ± 0.08			[1]	<sup>a</sup> 0.65 ± 0.08		
36.12 ± 0.09			[1]	<sup>a</sup> 0.86 ± 0.10		
39.59 ± 0.10			[1]	<sup>a</sup> 0.66 ± 0.15		
47.8 ± 0.2		[3/2]	[1]	<sup>a</sup> 1.3 ± 0.2		
52.0 ± 0.2		[3/2]	[1]	<sup>a</sup> 1.5 ± 0.3		
54.7 ± 0.2			[1]	<sup>a</sup> 0.30 ± 0.10		
58.6 ± 0.2			[1]	<sup>a</sup> 0.52 ± 0.15		
60.1 ± 0.2			[1]	<sup>a</sup> 0.44		

<sup>68</sup>Ni

45 12-APR-73, 16.02

$E_0$ (keV)	$g\Gamma_n$ (eV)	J	$\ell$	$\Gamma_\gamma$ (eV)	$g\Gamma_n^0$ (eV)	$g\Gamma_n^1$ (eV)
61.8 ± 0.2			(1)	<sup>a</sup> 0.71 ± 0.15		
63.0 ± 0.2	3600 ± 200	1/2	0	3.2 ± 0.8	14.34 ± 0.80	
66.4 ± 0.2			(1)	<sup>a</sup> 0.36		
68.8 ± 0.2			(1)	<sup>a</sup> 0.24		
69.8 ± 0.2			(1)	<sup>a</sup> 0.46		
78.0 ± 0.2			(1)	<sup>a</sup> 0.12 ± 0.03		
81.1 ± 0.2			(1)	<sup>a</sup> 0.73		
83.1 ± 0.2	110 ± 40		0	3.5 ± 0.7	0.38 ± 0.14	
89.8 ± 0.2			(1)	<sup>a</sup> 0.45		
92.3 ± 0.2			(1)	<sup>a</sup> 0.17		
94.5 ± 0.3			(1)	<sup>a</sup> 0.9 ± 0.2		
97.0 ± 0.3			(1)	<sup>a</sup> 0.5 ± 0.1		
101.1 ± 0.3			(1)	<sup>a</sup> 1.0 ± 0.2		
105.3 ± 0.3			(1)	<sup>a</sup> 1.8 ± 0.4		
107.7 ± 0.5	1400 ± 200	1/2	0	3.5 ± 0.8	4.27 ± 0.61	
110.7 ± 0.3			(1)	<sup>a</sup> 1.3 ± 0.3		
117.5 ± 0.3			(1)	<sup>a</sup> 0.8 ± 0.3		
120.3 ± 0.3		1/2	0	3.3 ± 0.6		
125.0 ± 0.5	700 ± 200	1/2	0	3.2 ± 0.6	1.98 ± 0.57	
137.5 ± 0.7	1760 ± 200	1/2	0		4.75 ± 0.54	
140.5 ± 0.8	3460 ± 500	1/2	0		9.23 ± 1.33	
147.5 ± 0.8	175		>0			
159.5 ± 0.9	6000 ± 1000	1/2	0		15.02 ± 2.50	
169.0 ± 1.0	750 ± 220	1/2	0		1.82 ± 0.54	
183.5 ± 1.1	250		>0			
193.0 ± 1.2	3500 ± 500	1/2	0		7.97 ± 1.14	
207.0 ± 1.5	6800 ± 1200	1/2	0		14.95 ± 2.64	
215.0 ± 1.5	260		>0			
231.0 ± 1.8	6000	1/2	0		12.48	
243.0 ± 1.8	250	1/2	0		0.51	
247.5 ± 1.8	360		>0			
270.0 ± 2.0	6000	1/2	0		11.55	
278.0 ± 2.0	2000	1/2	0		3.79	
286.5 ± 2.0	215		>0			
303.0 ± 2.0	750	1/2	0		1.36	
325.0 ± 2.0	2000	1/2	0		3.51	
334.5 ± 2.5	624		>0			
343.5 ± 2.5	585		>0			
349.0	1500	1/2	0		2.54	
357.5	443		>0			
367.0	250	1/2	0		0.41	
378.5	443		>0			
387.5	500		>0			
394.0	750	1/2	0		1.20	
417.0	5000	1/2	0		7.74	
426.0	1830 ± 400	3/2	1			5.2
426.5	8000	1/2	0		12.25	
454.5	3000	1/2	0		4.45	
461.5	750	1/2	0		1.10	
492.5	2000		>0			
495.5	2000	1/2	0		2.84	
507.0	2000	1/2	0		2.81	

46 12-APR-73, 16.02

<sup>58</sup> Ni						
E <sub>0</sub> (keV)	g <sub>n</sub> <sup>Γ</sup> (eV)	J	ℓ	Γ <sub>γ</sub> (eV)	g <sub>n</sub> <sup>0</sup> (eV)	g <sub>n</sub> <sup>1</sup> (eV)
522.5	750	1/2	0		1.04	
530.0	430		>0			
544.0	640		>0			
554.5	1490 ± 300	1/2	1			3.3
559.5	1260		>0			
571.0	10000	1/2	0		13.23	
588.5	2500	1/2	0		3.26	
600.0	6000	1/2	0		7.75	

<sup>a</sup> g<sub>n</sub><sup>Γ</sup>γ/Γ

THERMAL CROSS SECTIONS

$$\begin{aligned} \sigma_{\gamma} &= 92 \pm 4 \text{ b} \\ \sigma_a &= 12 \pm 2 \text{ b} \end{aligned}$$

RESONANCE PROPERTIES

$$I_{\gamma} = 138 \pm 8 \text{ b}$$

RESONANCE PARAMETERS

$$I^{\pi} = 3/2^{-}$$

$$S_n = 11387.5 \pm 1.7 \text{ keV}$$

E <sub>0</sub> (keV)	2g <sub>n</sub> <sup>Γ</sup> (eV)	J	ℓ	Γ <sub>0</sub> (eV)	2g <sub>n</sub> <sup>0</sup> (eV)
.20310 ± .00005	7.88 ± 0.231	1	0	3.4 ± 1.0	0.548 ± 0.015

<sup>59</sup>Ni  
[8 × 10<sup>4</sup> yr]



$^{60}\text{Ni}$						
$E_0$ (keV)	$g_n^0$ (eV)	J	$\ell$	$\Gamma_\gamma$ (eV)	$g_n^0$ (eV)	$g_n^1$ (eV)
101.9 ±0.3			[1]	0.10 ±0.05		
108.3 ±0.3	700 ± 100	1/2	0	1.1 ±0.3	2.13±0.31	
111.6 ±0.3		1/2	1	2.7 ±0.6		
120.6 ±1.1		3/2	1	1.3 ±0.3		
123.8 ±1.2			1			
129.7 ±1.3			1			
136.5 ±1.4		1/2	1	4.3 ±0.9		
139.6 ±1.4		1/2	1	4.0 ±0.9		
156.4 ±1.2	440 ± 50		0		1.11±0.13	
162.0 ±0.4	1400 ± 200	1/2	0	2.2 ±0.5	3.48±0.50	
186.6 ±1.5	5800 ± 800	1/2	0		13.43±1.85	
198.0 ±1.8	3100 ± 350	1/2	0		6.97±0.79	
206.0 ±1.8	120		>0			
214.0 ±1.8	74		>0			
220.0 ±1.8	106		>0			
229.0 ±1.8	224		>0			
252.0 ±2.0	910		>0			
257.8 ±2.1	3500 ± 600	1/2	0		6.89±1.18	
279.6 ±2.3	750 ± 160	1/2	0		1.42±0.30	
282.5 ±2.4	647		>0			
292.5 ±2.4	378		>0			
306 ±2.5	525		>0			
316.0 ±2.5	3200 ± 600	1/2	0		5.69±1.07	
326.3 ±2.5	7000 ±1100	1/2	0		12.25±1.93	
339.5 ±2.5	6500 ±1500	1/2	0		11.16±2.57	
357.2 ±2.6	1000	1/2	0		1.67	
358.5 ±2.6	1113		>0			
375.5	4000	1/2	0			
378.5	226		>0			
387.5	290		>0			
392.0	225		>0			
397.0	321		>0			
401.5	400		>0			
412.3	750	1/2	0		1.17	
421.0	2000	1/2	0		3.08	
426.5	500	1/2	0		0.77	
431.5	230		>0			
446.0	3000	1/2	0		4.49	
453.0	1500	1/2	0		2.23	
462.0	1000	1/2	0		1.47	
473.0	500	1/2	0		0.73	
484.6	3750	1/2	0		5.39	
497.5	578		>0			
498.0	5000				7.63	
502.5	333		>0			
511.5	2420	3/2	1			
513.5	2250	1/2	0		3.14±6.3	
520.3	5000	1/2	0		6.93	
525.5	3000	1/2	0		4.14	
533.0	500	1/2	0		0.69	
552.5	710		>0			
556.5	500	1/2	0		0.67	

48 12-APR-73 16.02

49 12-APR-73 16.02

$^{90}_{28}\text{Ni}$						
$E_0$ (keV)	$g\Gamma_n$ (eV)	J	$\ell$	$\Gamma_\gamma$ (eV)	$g\Gamma_n^0$ (eV)	$g\Gamma_n^1$ (eV)
566.0	260		>0			
580.3	250	1/2	0		0.33	
588.5	500	1/2	0		0.65	
594.8	2500	1/2	0		3.24	

$^a g\Gamma_n\Gamma_\gamma/\Gamma$

THERMAL CROSS SECTIONS

$^{91}_{28}\text{Ni}$

- $\sigma_\gamma = 2.5 \pm 0.8$  b
- $\sigma_n = 9.6 \pm 2.0$  b
- $\sigma_a = 0.047 \pm 0.021$  b
- $\sigma_t = 12.1 \pm 0.8$  b
- $\lambda_{coh} = 7.60 \pm 0.06$  fm

RESONANCE PROPERTIES

- $I_\gamma^e = 1.6 \pm 0.4$  b
- $R^f = 6.4 \pm 0.3$  fm
- $\langle D \rangle = 0.79 \pm 0.10$  keV
- $S_0 = 3.0 \pm 0.8$

RESONANCE PARAMETERS

$I^a = 3/2^-$

$\%Abn = 1.19$

$S_n = 10596.6 \pm 1.4$  keV

$E_0$ (keV)	$2g\Gamma_n$ (eV)	J	$\ell$	$\Gamma_\gamma$ (eV)	$2g\Gamma_n^0$ (eV)
1.35±0.01				$^a 0.48 \pm 0.060$	
2.35±0.01					
3.14±0.01				$^a 0.17 \pm 0.04$	
3.30±0.01				$^a 0.96 \pm 0.12$	
6.36±0.01					
6.47±0.01				$^a 0.70 \pm 0.20$	
7.15±0.02	50 ± 6	1	0	2.5 ± 0.4	0.59 ± 0.07
7.55±0.02	225 ± 20	2	0	2.3 ± 0.6	2.59 ± 0.23
8.73±0.02	7.5 ± 2.5	2	0	2.6 ± 0.8	0.080 ± 0.027
9.91±0.02			[1]	$^a 0.18 \pm 0.06$	
10.20±0.03			[1]	$^a 0.38 \pm 0.10$	
10.90±0.03					
11.4 ± 0.03					
11.8 ± 0.03					
12.64±0.03	90 ± 10	2	0	1.7 ± 0.4	0.80 ± 0.09
13.60±0.03	76 ± 5	2	0	1.6 ± 0.4	0.65 ± 0.04
14.02±0.03	13 ± 3	1	0	3.1 ± 0.5	0.11 ± 0.03
14.45±0.04			[1]	$^a 0.60 \pm 0.06$	
15.38±0.04			[1]	$^a 0.34 \pm 0.08$	
16.70±0.05	600 ± 20	1	0	2.2 ± 0.4	4.64 ± 0.15
16.80±0.05			[1]	$^a 0.28 \pm 0.08$	
17.83±0.05	140 ± 10	1	0	1.6 ± 0.5	1.05 ± 0.08

$^{60}_{28}\text{Ni}$					
$E_0$ (keV)	$2g\Gamma_n$ (eV)	J	$\ell$	$\Gamma_\gamma$ (eV)	$2g\Gamma_n^0$ (eV)
18.83±0.05	90 ± 10	2	0	0.9 ± 0.3	0.66 ± 0.07
20.25±0.05			[1]	<sup>a</sup> 0.18±0.06	
20.50±0.05			[1]	<sup>a</sup> 0.22±0.06	
21.35±0.05			[0]	<sup>a</sup> 1.76±0.40	
24.12±0.05	97 ± 8	1	[1]	<sup>a</sup> 0.72±0.18	0.62 ± 0.05
24.62±0.06			0	1.4 ± 0.3	
25.12±0.06			[1]	<sup>a</sup> 0.50±0.12	
25.96±0.06			[1]	<sup>a</sup> 0.48±0.12	
26.45±0.06			[1]	<sup>a</sup> 0.36±0.10	
27.10±0.07			[1]	<sup>a</sup> 0.40±0.10	
27.65±0.07			[1]	<sup>a</sup> 0.80±0.20	
28.21±0.07	6.3± 5.0	2	0	3.0 ± 1.0	0.038±0.030
29.11±0.07	310 ± 20	1	0	2.4 ± 0.4	1.82 ± 0.12
30.64±0.08	19 ± 10	2	0		0.11 ± 0.06
31.13±0.08	570 ± 40	1	0		3.23 ± 0.23
31.83±0.08	12.5± 7.5	2	0		0.070±0.042
32.70±0.08	265 ± 25	2	0		1.47 ± 0.14
33.68±0.08	50 ± 10	1	0	2.8 ± 0.5	0.27 ± 0.05
37.13±0.09	180 ± 20	2	0	3.0 ± 0.5	0.93 ± 0.10
41.34±0.10	150 ± 20	1	0		0.74 ± 0.10
43.25±0.11	12.5± 10.0				0.060±0.048
43.61±0.11	37.5± 17.5	2	0		0.18 ± 0.08
45.49±0.11	50 ± 6	1	0		0.23 ± 0.03
46.16±0.12	40.5± 6.0	1	0		0.19 ± 0.03
50.51±0.12	100 ± 9	1	0		0.45 ± 0.04
53.30±0.13	176 ± 13	2	0		0.76 ± 0.06
54.81±0.14	142 ± 14	1	0		0.61 ± 0.06
56.49±0.14	149 ± 13	2	0		0.63 ± 0.06
58.16±0.15	133 ± 15	1	0		0.55 ± 0.06
64.07±0.16	68 ± 6	2	0		0.27 ± 0.02
65.87±0.16	1790 ± 225	2	0		6.97 ± 0.09
68.77±0.17	1375 ± 625	2	0		5.24 ± 2.38

<sup>a</sup>  $2g\Gamma_n\Gamma_\gamma/\Gamma$

50 12-APR-73, 16:02

$^{88}\text{Ni}$

SI 12-APR-73, 16.02

THERMAL CROSS SECTIONS

$$\begin{aligned} \sigma_y &= 14.2 \pm 0.3 \text{ b} \\ \sigma_0 &= 9.5 \pm 0.4 \text{ b} \\ \sigma_t &= 23.7 \pm 0.5 \text{ b} \\ a_{coh} &= -8.7 \pm 0.2 \text{ fm} \end{aligned}$$

RESONANCE PROPERTIES

$$\begin{aligned} I_y &= 6.8 \pm 0.2 \text{ b} \\ R' &= 6.2 \pm 0.3 \text{ fm} \\ S_0 &= 2.9 \pm 0.7 \end{aligned}$$

RESONANCE PARAMETERS

$J^\pi = 0^+$                        $\chi^2_{\text{Abn}} = 3.66$                        $S_n = 6837.7 \pm 1.0 \text{ keV}$

$E_0$ (keV)	$g\Gamma_n$ (eV)	J	$\ell$	$\Gamma_y$ (eV)	$g\Gamma_n^0$ (eV)	$g\Gamma_n^1$ (eV)
4.54±0.05	1600 ±160	1/2	0	0.76±0.12	23.75±2.29	
42.87±0.01	340 ± 10	1/2	0		1.64±0.05	
56.91±0.02	56 ± 4		[1]			2.5
77.23±0.03	70 ± 7	1/2	0		0.25±0.03	
78.42±0.04	48 ± 7		[1]			1.4
94.7 ±0.02	2500 ±100	1/2	0		8.12±0.33	
105.65±0.03	4600 ±200	1/2	0		14.15±0.62	
137.5	127		>0			
149.3 ±0.1	140 ± 20	1/2	0		0.36±0.05	
188.2 ±0.2	90 ± 20		0		0.21±0.05	
214.7 ±0.2	190 ± 20	1/2	0		0.41±0.04	
229.5 ±0.04	6250 ± 80	1/2	0		13.05±0.17	
242.2 ±0.08	780 ± 40	1/2	0		1.58±0.08	
259.5	113		>0			
272.5	333		>0			
280.5	4800 ±200	1/2	0		9.06±0.38	
286.0	1500 ±500	1/2	0		2.81±0.93	
297.0	200		>0			
299.5	500		>0			
304.0	800	1/2	0		1.45	
315.5	238		>0			
319.0	375		>0			
323.0	580		>0			
327.0	5500	1/2	0		9.62	
344.2	7500	1/2	0		12.78	
352.0	279		>0			
356.2	2000	1/2	0		3.35	
364.0	194		>0			
374.5	250	1/2	0		0.41	
382.5	1250	1/2	0		2.02	
388.5	4500	1/2	0		7.22	
401.5	1500	1/2	0		2.37	
403.3	392		>0			
420.3	813		>0			
423.0	1500	1/2	0		2.31	
433.0	6500	1/2	0		9.88	

$^{63}_{28}\text{Ni}$						
$E_0$ (keV)	$g_n^0$ (eV)	J	$\ell$	$\Gamma_\gamma$ (eV)	$g_n^0$ (eV)	$g_n^1$ (eV)
444.0	350	1/2	0		0.53	
449.8	250		>0			
450.0	236		>0			
458.0	500	1/2	0		0.74	
461.8	550		>0			
475.0	1500	1/2	0		2.18	
480.0	324		>0			
488.5	4000	1/2	0		5.72	
493.5	934	1/2	1			2.8
498.0	1500	1/2	0		2.13	
508.5	500	1/2	0		0.70	
515.5	145		>0			
522.0	390		>0			
529.0	1690	3/2	1			4.7
535.5	1390	1/2	1			
539.0	2000	1/2	0		2.72	
554.0	675		>0			
568.5	843		>0			
571.8	4000	1/2	0		5.29	
581.0	500	1/2	0		0.66	
583.5	10000	1/2	0		13.09	
590.5	2000	1/2	0		2.60	
599.5	905	1/2	1			2.2

52 12-RR-73, 16, 102

THERMAL CROSS SECTIONS

$^{63}_{28}\text{Ni}$   
[100 yr]

$$\sigma_\gamma = 23 \pm 3 \text{ b}$$

<sup>88</sup>Ni  
<sup>28</sup>Ni

THERMAL CROSS SECTIONS

$\sigma_T = 1.49 \pm 0.03 \text{ b (2.520 hr } ^{85}\text{Ni)}$   
 $a_{coh} = -0.38 \pm 0.07 \text{ fm}$

RESONANCE PROPERTIES

$I_T = 1.1 \pm 0.2 \text{ b}$   
 $R_T^1 = 6.4 \pm 0.1 \text{ fm}$   
 $S_0 = 1.3 \pm 0.1$   
 $S_1 = 0.6 \pm 0.3$

RESONANCE PARAMETERS

$I^{\pi} = 0^+$	$\%Abn = 1.08$	$S_n = 6837.7 \pm 1.0 \text{ keV}$		
$E_0 \text{ (keV)}$	$g_n^{\Gamma} \text{ (eV)}$	$J \quad \ell \quad \Gamma_T \text{ (eV)}$	$g_n^0 \text{ (eV)}$	$g_n^1 \text{ (eV)}$
9.52		<sup>a</sup> 1.7 ± 0.2		
14.3 ± 0.2	2900 ± 500	1/2 0 .76 ± .15	24.25 ± 4.18	
25.8 ± 0.1				
31.8 ± 0.1				
33.81 ± 0.04	8900 ± 500	1/2 0	48.40 ± 2.72	
62.4 ± 0.1				
82.8 ± 0.1				
106.52 ± 0.08	110 ± 30	>0		
129.32 ± 0.03	1400 ± 50	1/2 0	3.89 ± 0.14	
141.5 ± 0.1	170 ± 20	>0		
148.8 ± 0.1	80 ± 20	1/2 0	0.21 ± 0.05	
155.0 ± 0.1	3950 ± 100	1/2 0	10.04 ± 0.25	
163.2 ± 0.1	160 ± 20	1/2 0	0.40 ± 0.05	
177.7 ± 0.1	470 ± 30	1/2 0	1.12 ± 0.07	
191.0 ± 0.2	140 ± 30	[1]		
205.3 ± 0.2	60 ± 20	1/2 0	0.13 ± 0.04	
214.7 ± 0.3	90 ± 20	>0		
219.8 ± .1	30 ± 20	1/2 0	0.064 ± 0.043	
226.9 ± .3	120 ± 30	1/2 0	0.25 ± 0.06	
231.95 ± .04	3770 ± 90	1/2 0	7.83 ± 0.19	
237.9 ± 0.1	320 ± 40	>0		
255.7 ± 0.3	170 ± 40	>0		
269.7 ± 0.1	2210 ± 90	1/2 0	4.26 ± 0.17	
283.5 ± 0.4	350 ± 70	1/2 0	0.66 ± 0.13	
298.0 ± 2.5	1000	1/2 0	1.83	
308.5 ± 2.5	1500	1/2 0	2.70	
327.0 ± 2.5	597	>0		
333.0 ± 2.5	250	1/2 0	0.43	
340.2	500	1/2 0	0.86	
360.3	728	>0		
365.0	1857	[3/2] 1		7.6
371.5	1318	[3/2] 1		5.3
383.0	1597	[3/2] 1		
389.0	6000	1/2 0	9.62	
392.5	235	>0		
395.5	815	>0		
407.0	2020	[3/2] 1		7.4

53 12-APR-73 16.02

<sup>65</sup>Ni

$E_0$ (keV)	$g\Gamma_n$ (eV)	J	$\ell$	$\Gamma_\gamma$ (eV)	$g\Gamma_n^0$ (eV)	$g\Gamma_n^1$ (eV)
414.0	759		>0			
420.8	8000	1/2	0		12.33	
455.5	560	[1/2]	1			
459.5	1100	[3/2]	1			
466.5	995	[1/2]	1			
470.0	535		>0			
479.0	1090	[1/2]	1			
483.0	5000	1/2	0		7.19	
499.5	535		>0			
503.0	766		>0			
519.0	477		>0			
523.0	1000	1/2	0		1.38	
536.5	10000	1/2	0		13.65	
541.5	1670	[3/2]	1			4.5
552.0	2000	1/2	0		2.69	
565.0	900		>0			
576.0	4000	1/2	0		5.27	
583.0	300	1/2	0		0.39	

54 12-APR-73, 16.02

<sup>a</sup>  $g\Gamma_n\Gamma_\gamma/\Gamma$

<sup>65</sup>Ni  
[2.520 hr]

THERMAL CROSS SECTIONS

$\sigma_\gamma = 24.3 \pm 2.0$  b

RESONANCE PROPERTIES

$I_\gamma = 11 \pm 2$  b

THERMAL CROSS SECTIONS

Isotope	Measurement	Reference	Author
Ni <sup>59</sup>	$\sigma_a$	KAPL-3979(72)+	Eiland
Ni <sup>59</sup>	pile osci.	PRIVATE COMM.(72)	Kirouac
Ni <sup>59</sup>	pile osci.	KAPL-3980(72)	Kirouac
Ni <sup>63</sup>	radiation balance	ARI,22,777(71)	Barnes
Ni <sup>59</sup>	$\sigma_a$	ANS,14,168(71)	Kangilaski
Ni	$\sigma_\gamma$ noxon rae	NIM,86,83(70)	Malik
Ni <sup>62</sup>	activation	JNE,24,35(70)	Ryves
Ni <sup>65</sup>	activation	NAP,9,662(70)	Serment
Ni <sup>62</sup>	activation	JIN,32,2839(70)	Sims
Ni <sup>59</sup>	$\sigma_a$	ANS,13,557(70)	Weitman
Ni <sup>65</sup>	mass spectrometry	JIN,31,1241(69)	Pinajian
Ni <sup>64</sup>	activation	ORNL-4343,71(68)	Emery
Ni <sup>61,64</sup>	diffraction	PR,156,1225(67)	Sidhu
Ni <sup>61,62,64</sup>	$\sigma_t$	PRIVATE COMM.(65)	Doil'nitsyn
Ni,Ni <sup>58</sup>	$\sigma_t$ 1.44 ev	NP,61,381(65)	Rayburn
Ni <sup>62</sup>	mass spectrometry	PR,125,1619(62)	Horrocks
Ni <sup>64</sup>	activation	NSE,8,378(60)	Lyon
Ni	pile osci.	JNE,12,32(60)	Tattersall
Ni <sup>58,61</sup>	$\sigma_a$	ZP,153,106(58)	Munnich
Ni <sup>65</sup>	activation	PRIVATE COMM.(58)	Schuman
Ni <sup>62</sup>	mass spectrometry	CJC,34,1742(56)	McMullen
Ni	mirror reflections	PR,96,1297(54)	Allen
Ni	$\sigma_t$	PR,91,451(53)	Goldberg
Ni <sup>58,60,61,62,64</sup>	pile osci.	PR,88,412(52)	Pomerance
Ni	pile osci.	CR,232,2089(51)	Grimeland
Ni	local osci.	PR,83,641(51)	Pomerance
Ni,Ni <sup>58,60,62</sup>	$\sigma_t$ diffraction	PR,81,527(51)	Shull
Ni	$\bar{\sigma}_s$	PR,83,379(51)	Weiss
Ni	$\bar{\sigma}_s$	PR,77,575(50)	Bendt
Ni	pile osci.	PPS/A,63,1175(50)	Colmer
Ni	pile osci.	PR,80,342(50)	Harris
Ni,Ni <sup>58,60,62</sup>	diffraction	PR,79,395(50)	Koehler
Ni	$\bar{\sigma}_s$	PR,71,666(47)	Fermi
Ni	$\sigma_\gamma$	PR,69,411(46)	Coltman
Ni	$\bar{\sigma}_s$	JPJ,24,569(42)	Kimura
Ni	$\sigma_t$	PR,60,155(41)	Whitaker
Ni	$\sigma_t$	PR,57,976(40)	Beyer
Ni	$\sigma_t \bar{\sigma}_s$	PRS/A,162,127(37)	Goldhaber
Ni	$\bar{\sigma}_s$	PR,50,133(36)	Mitchell
Ni	$\sigma_t$	PR,48,265(35)	Dunning

SS 12-APR-73, 16.02

RESONANCE PARAMETERS

Isotope	Measurement	Energy Range (keV)	Reference	Author
Ni <sup>62</sup>	$\sigma_c$	4.6	PRIVATE COMM.(73)	Good
Ni <sup>58</sup>	$\sigma_c, \sigma_y$	15	AERE-PR/NP-18,4(72)	Axmann
Ni <sup>62</sup>	$\sigma_c, \sigma_y$	4.6	AERE-PR/NP-18,4(72)	Axmann
Ni <sup>61</sup>	$\sigma_c, \sigma_y$	1.35-21.3	PRIVATE COMM.(72)	Block
Ni <sup>64</sup>	$\sigma_c, \sigma_y$	14.3-82.8	PRIVATE COMM.(72)	Block
Ni <sup>58</sup>	$\sigma_y$	13.3-125	PRIVATE COMM.(72)	Froehner
Ni <sup>60</sup>	$\sigma_y$	12.2-162	PRIVATE COMM.(72)	Froehner
Ni <sup>61</sup>	$\sigma_y$	7.2-69	PRIVATE COMM.(72)	Froehner
Ni <sup>59</sup>	$\sigma_c$	0.203	KAPL-3980(72)	Kirouac
Ni <sup>59</sup>	$\sigma_c$	0.203	PRIVATE COMM.(72)	Kirouac
Ni <sup>62</sup>	$\sigma_c$	42.9-288	KFK-1517(72)	Spencer
Ni <sup>64</sup>	$\sigma_c$	14.3-284	KFK-1517(72)	Spencer
Ni <sup>58</sup>	$\sigma_c$	15.3-110.7	KFK-1271/3(71)	Beer
Ni <sup>60</sup>	$\sigma_c$	12.5-194.6	KFK-1271/3(71)	Beer
Ni <sup>62</sup>	$\sigma_c$	12.9-288	KFK-1271/3(71)	Beer
Ni <sup>64</sup>	$\sigma_c$	14.3-283.5	KFK-1271/3(71)	Beer
Ni	$\sigma_c$	32.2-333	PR/C,3,2447(71)	Gang
Ni <sup>58</sup>	$\sigma_c$	0-207	PR/C,3,2447(71)	Gang
Ni <sup>60</sup>	$\sigma_c$	12.4-196	PR/C,3,2447(71)	Gang
Ni <sup>62</sup>	$\sigma_c$	4.5-149	PR/C,3,2447(71)	Gang
Ni <sup>61</sup>	$b(\gamma, n)$	11.6-198	PR/C,4,1314(71)	Jackson
Ni <sup>60</sup>	$\sigma_c, \sigma_y$	1.3-340	NP/A,163,592(71)	Stieglitz
Ni <sup>61</sup>	$\sigma_c$	7.2-69	70HELSINKI,1,619(70)	Cho
Ni <sup>60</sup>	$\sigma_y$	12.5-66	70HELSINKI,1,633(70)	Ernst
Ni <sup>61</sup>	$\sigma_y$	7.2-37	70HELSINKI,1,633(70)	Ernst
Ni <sup>58</sup>	$\sigma_y$	6.9-124	PR,178,1746(69)	Hockenbury
Ni <sup>60</sup>	$\sigma_y$	1.3-97	PR,178,1746(69)	Hockenbury
Ni <sup>61</sup>	$\sigma_y$	1.4-90	PR,178,1746(69)	Hockenbury
Ni <sup>62</sup>	$\sigma_y$	2.3-4.6	PR,178,1746(69)	Hockenbury
Ni <sup>64</sup>	$\sigma_y$	9.5-83	PR,178,1746(69)	Hockenbury
Ni <sup>58</sup>	$\sigma_c$	107-600	AP,37,367(66)	Farrell
Ni <sup>60</sup>	$\sigma_c$	97-594	AP,37,367(66)	Farrell
Ni <sup>62</sup>	$\sigma_c$	94-600	AP,37,367(66)	Farrell
Ni <sup>64</sup>	$\sigma_c$	105-583	AP,37,367(66)	Farrell
Ni <sup>61</sup>	$\sigma_c$	7.0-48.4	PR,151,912(66)	Good
Ni <sup>58</sup>	$\sigma_c$	0-207	AP,14,387(61)	Bilpuch
Ni <sup>60</sup>	$\sigma_c$	14.5-199	AP,14,387(61)	Bilpuch
Ni, Ni <sup>58</sup>	$\sigma_c$	65	ANL-5498,52(55)	Hibdon
Ni <sup>62</sup>	$\sigma_c$	4.2	ORNL-1496,14(52)	Pavlicki

56 12-APR-73 16.02

Comparison of the KeV-capture cross section for  
Cr, Fe, Ni on ENDF/B, UKNDL and KEDAK

B. Schatz

Kernforschungszentrum Karlsruhe, Germany

A comparison of the KeV capture data for the structural materials on the 3 evaluated nuclear data files ENDF/B, UKNDL, KEDAK is given on Figs. 1 - 8 for Cr, Figs. 1' - 6' for Fe, Figs. 1'' - 8'' for Ni. For this comparison the ENDF/B version 3 was used, the UKNDL version available in 1971 at CCDN, the KEDAK version 2 from 1970. As far as KEDAK is concerned the version 2 contains for the structural materials the same data as version 1 from 1967 i.e. the data stem from J.J. Schmidts evaluations /1/.

The curves marked by points represent the ENDF/B3 data. They were obtained by calculating the capture cross sections with the Breit-Wigner single level or multi level formalism using the ENDF/B3 resonance parameters for the different isotopes and adding their contributions and the background cross section. This calculation was performed by J. Schepers at Mol using the code BRIGITTE which converts ENDF/B data into the KEDAK format.

The curves marked by squares are the smooth cross sections from

the UK-Nuclear Data Library. The curves marked by crosses give the smooth capture cross section stored on KEDAK. These data are in most cases different from those which would be obtained on the basis of the KEDAK resonance parameters.

As far as Chromium is concerned the KEDAK-data and the UK-data show a rather smooth behaviour with the exception of the two resonances at about 1.7 KeV and 6 KeV. The two curves agree in general well with each other, above 150 KeV the differences amount to about 10 - 20 %. The UK- and KEDAK-data have the same basis of experimental data, namely the results of the old lead pile measurements of Kapchigashev, Popov /2/. The ENDF/B3 data, however, are based below 350 KeV on the experimental results of Stieglitz /3/ and above this energy up to 650 KeV those of Bowman et.al. /4/. The incorporation of these more recent and much improved experimental data sets in the american file implies that the ENDF/B capture data show considerable structure in the whole energy range. In the lower energy range below about 50 KeV the ENDF/B curve is systematically higher than the other curves by at least a factor of two.

Concerning Iron the capture data of the UKND- and the ENDF/B3-library show in structure as well as in magnitude a completely similar behaviour over the whole energy range, whereas the KEDAK capture data are systematically higher, in general by a factor between 2 and 3, and have a considerable broader structure than the capture data on the other two files. These differences can be explained by the different experimental data basis which for KEDAK goes back to 1964 and for UKNDL and ENDF/B3 to 1969 /5/.

A comparison of the Nickel capture data shows the following: Above 200 KeV the UKNDL- and KEDAK-data show no structure at all, whereas the ENDF/B data have resonance structure up to 650 KeV. Also below 200 KeV the ENDF/B data indicate much more structure than the data on the other two files, the UKNDL-data show structure

even only up to 30 KeV. In the range below 200 KeV the KEDAK-data are considerably lower (by a factor of about 2 till 4) than the ENDF/B data. The ENDF/B capture data are below 650 KeV based on the results of the capture yield measurements of Stieglitz from 1970 /3/ and Hockenbury from 1969 /5/. The KEDAK-data go back to the measurements of Bilpuch et.al. /6/ from 1961. Since in the latter measurements very few resonances could be resolved in comparison with those resolved in the RPI-measurements and since in particular no higher l-wave resonances were detected, the differences between KEDAK and ENDF/B can be understood. For UKNDL a new evaluation for Ni has been performed and will be included in the 1973 version of UKNDL, but it could not yet been considered here.

References

- /1/ J.J. Schmidt, KFK 120 Part. I (1966)
- /2/ S.P. Kapchigashev, Y.P. Popov , Sov. J. At. En. 16 (1964) 306
- /3/ R.G. Stieglitz et.al., Nucl. Phys. A 163 (1971) 592
- /4/ C.D. Bowman et. al., Ann. Phys. 17 (1962) 319
- /5/ R.W. Hockenbury ,Phys. Rev. 178 (1969) 1746
- /6/ E.G. Bilpuch et. al., Ann. Phys. 14 (1961) 387

Fig. 1 - 8

Comparison of the kev-capture cross section  
for Chromium

on the KEDAK, UKNDL and ENDF/B3 nuclear data  
file

~~XXXX~~ - KEDAK : Version 2 (1970)

□-□-□ - UKNDL (1971)

— — — - ENDF/B3



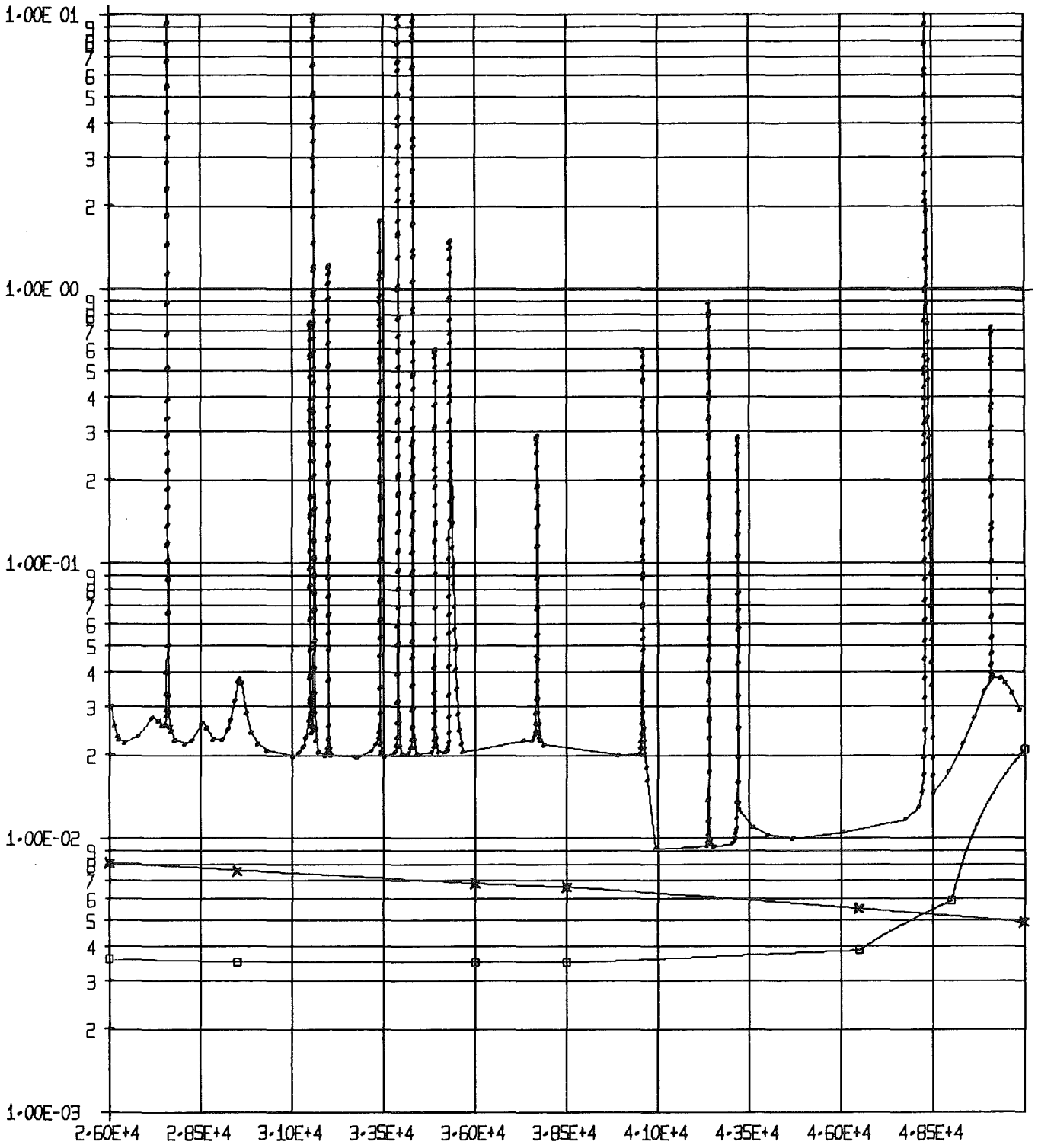


Fig. 2

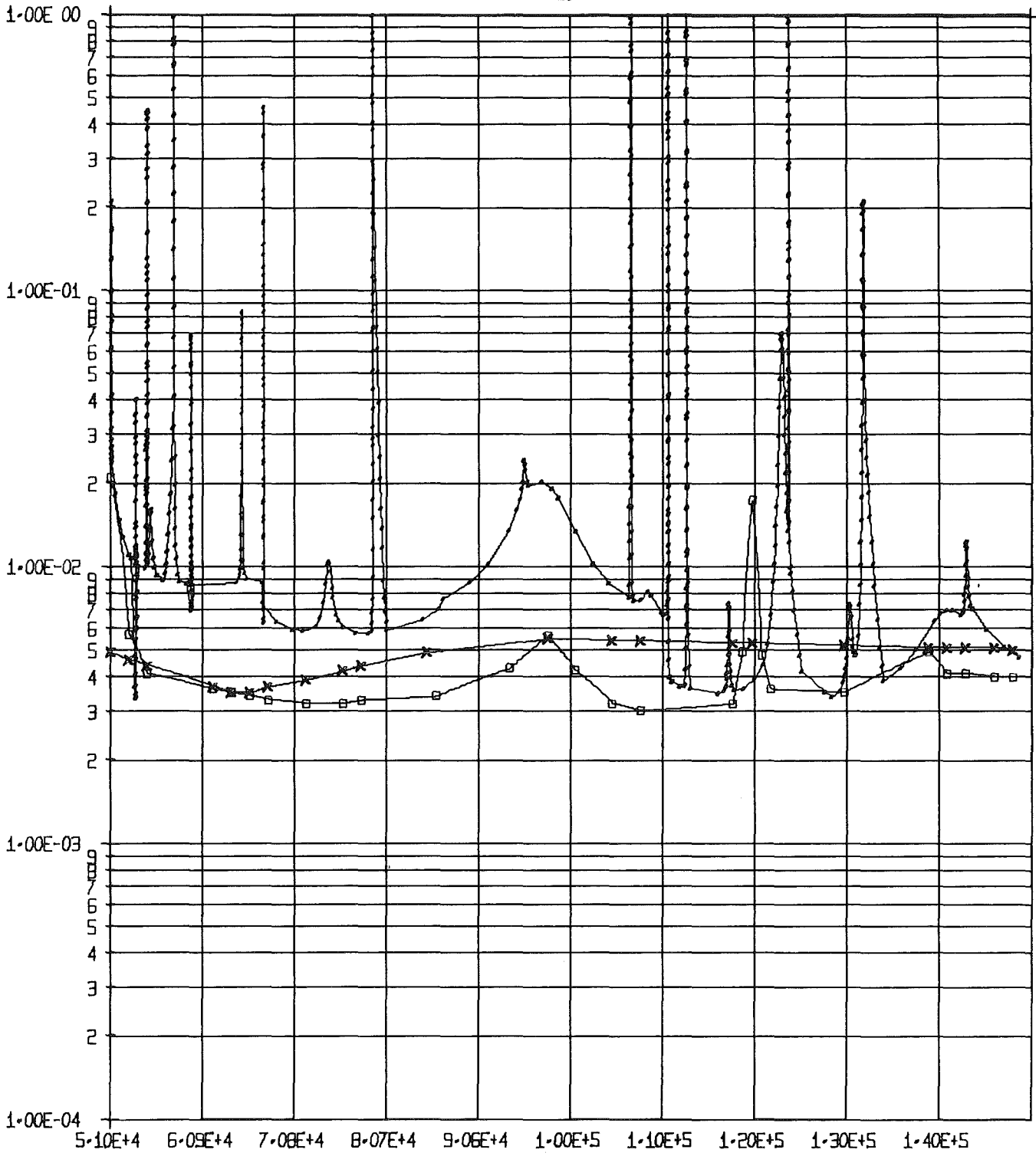


Fig. 3

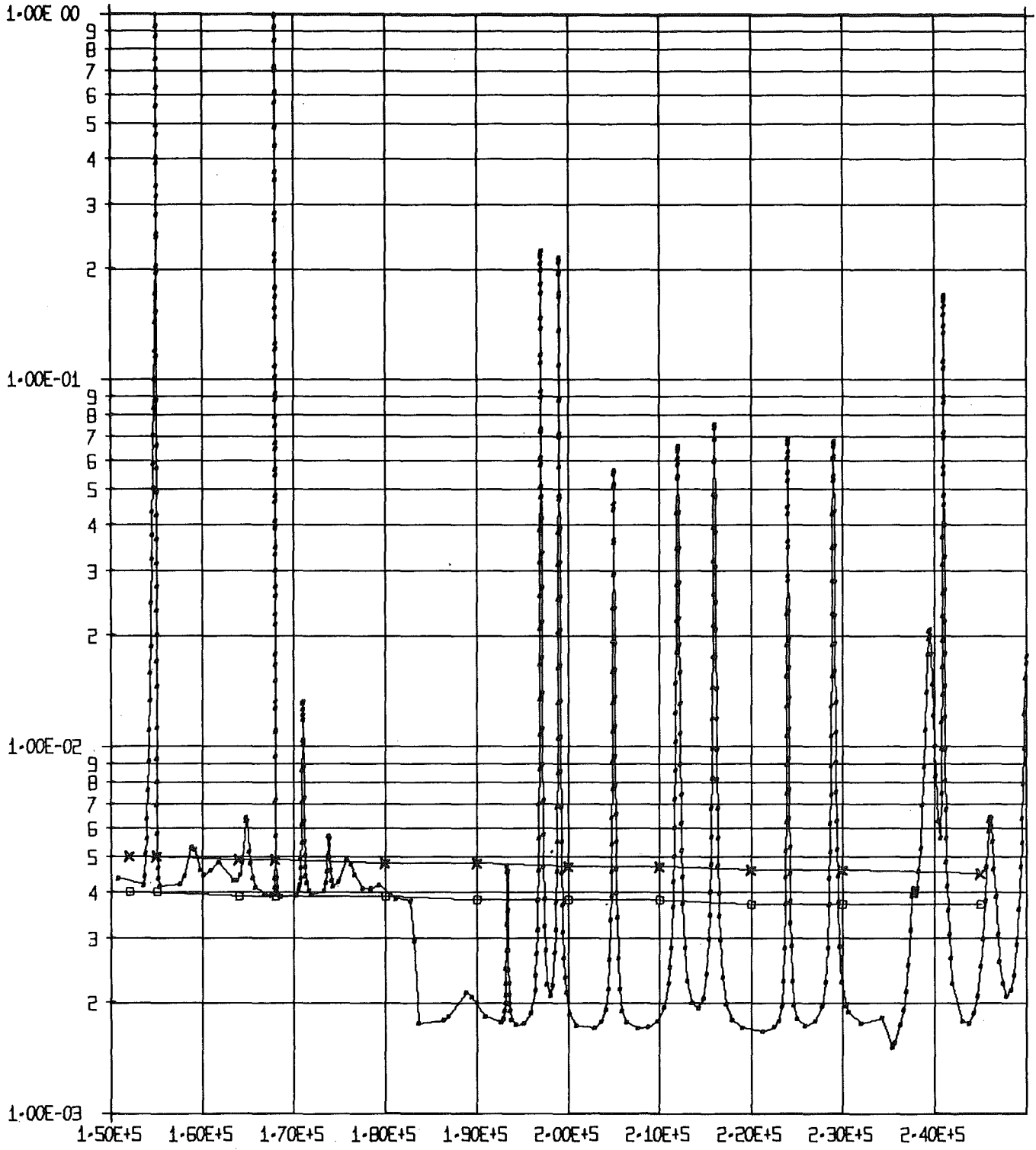


Fig. 4

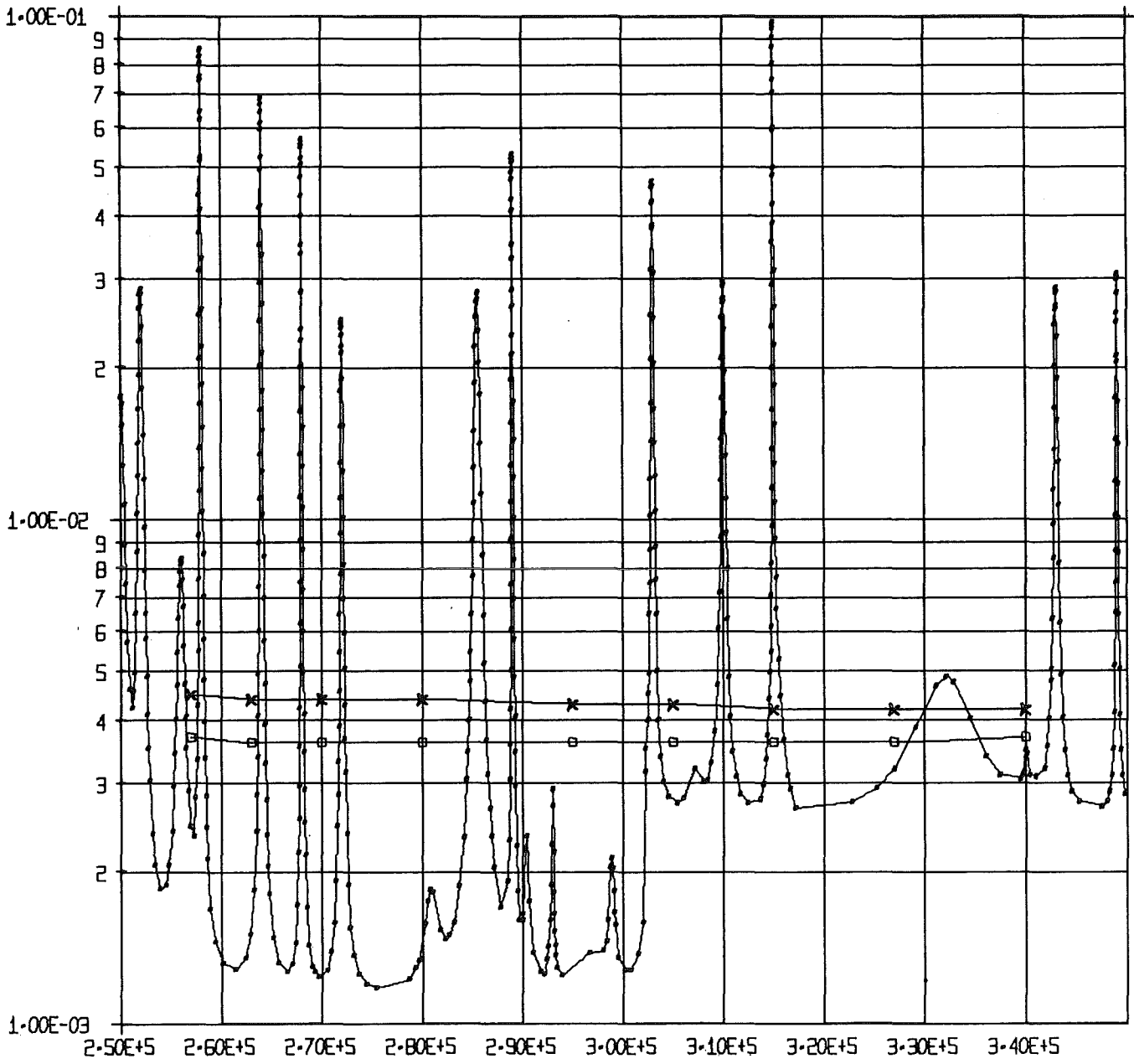
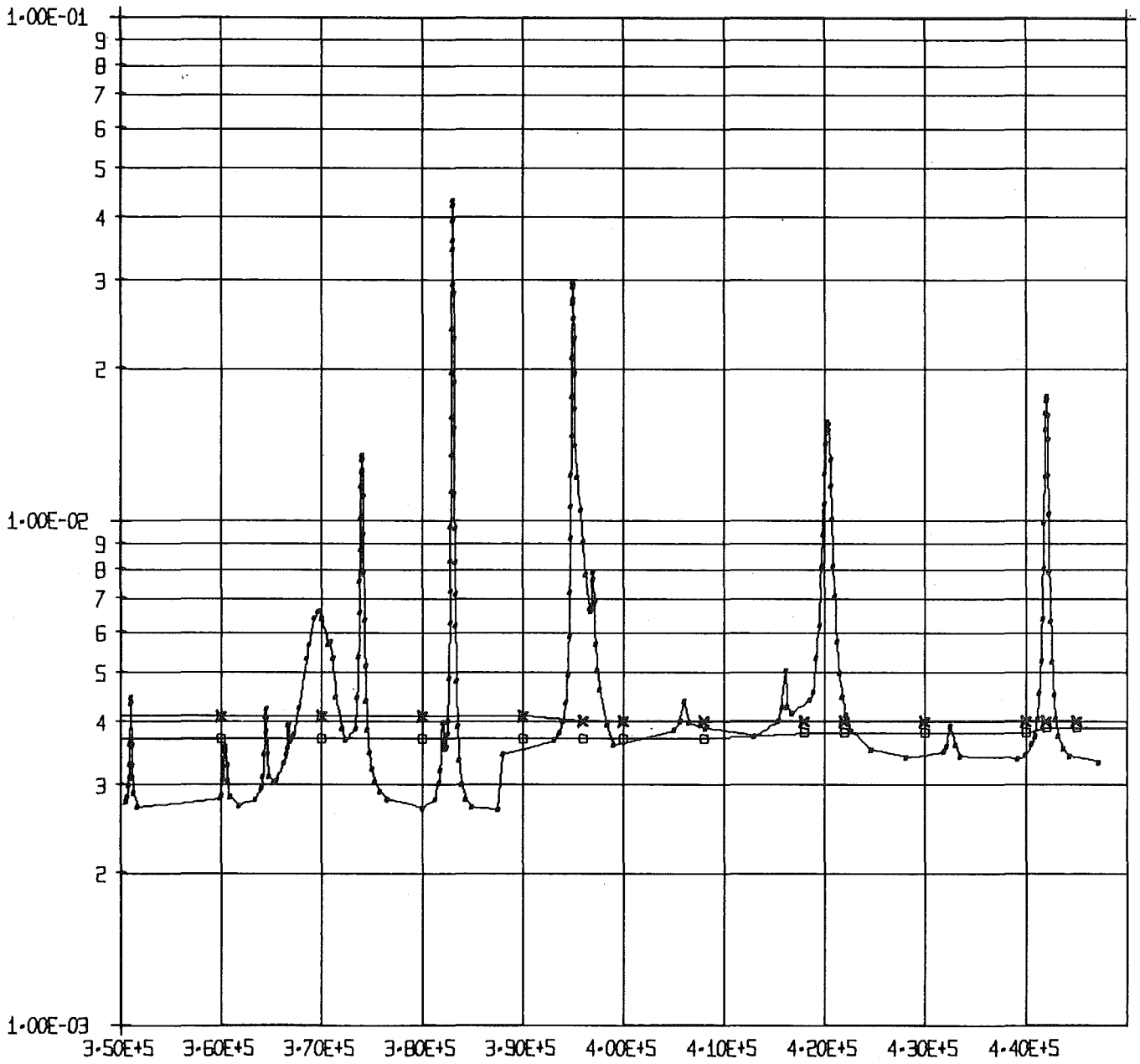


Fig. 5



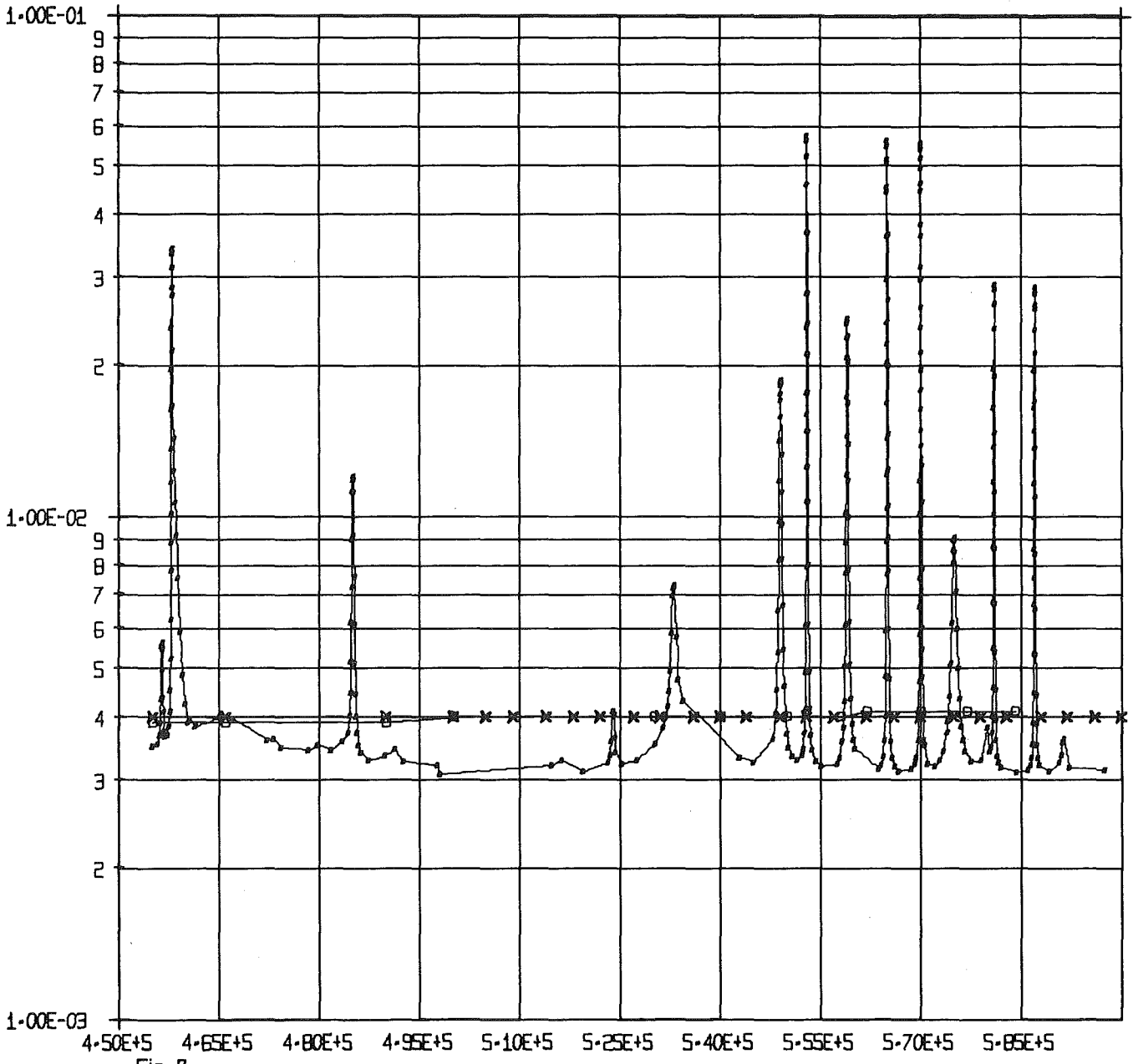


Fig. 7

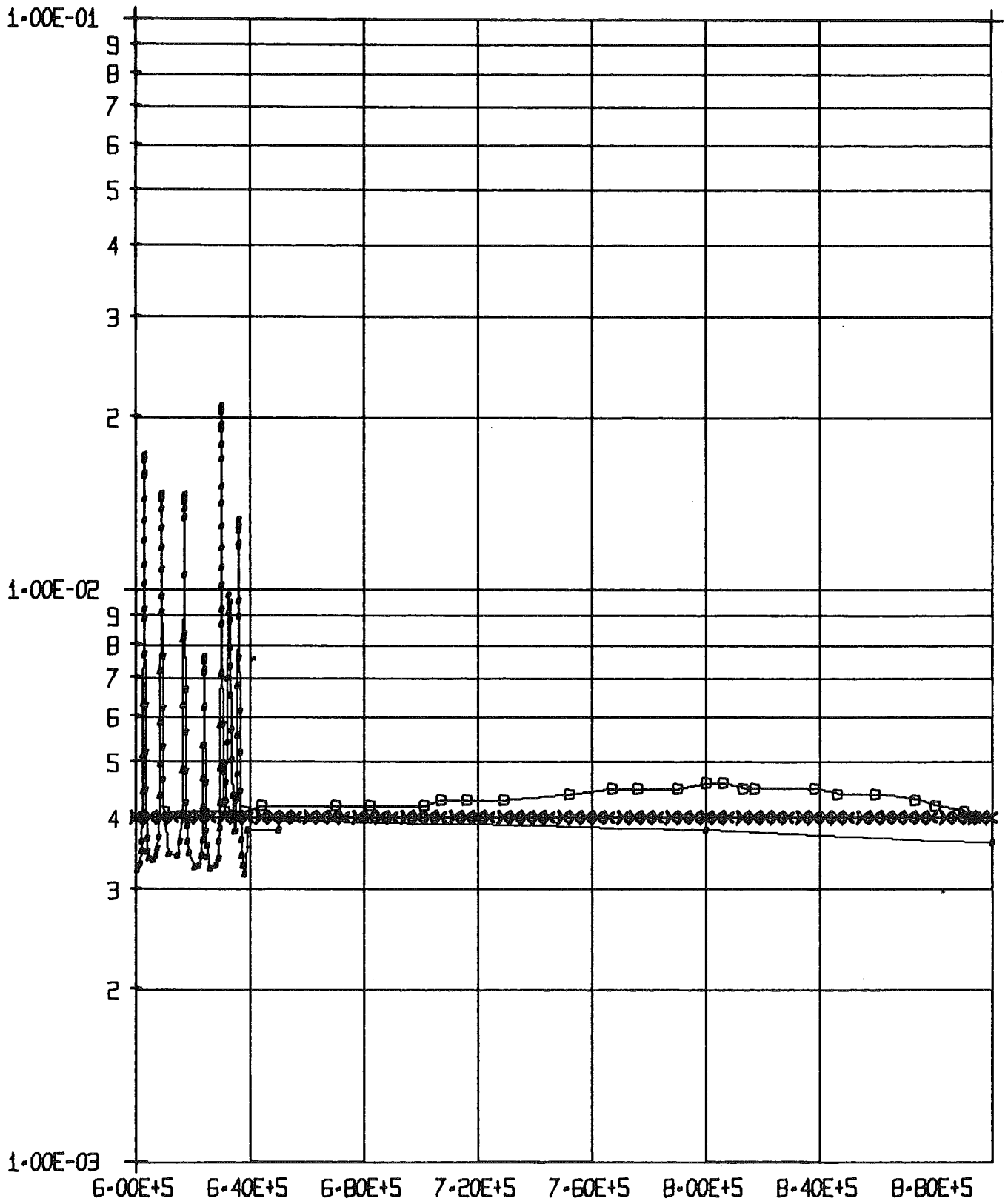


Fig. 1' - 6'

Comparison of the kev-capture cross section  
for Iron

on the KEDAK, UKNDL and ENDF/B 3 nuclear data  
file

XXXXX - KEDAK : Version 2 (1970)

□-□-□ - UKNDL (1971)

----- - ENDF/B 3

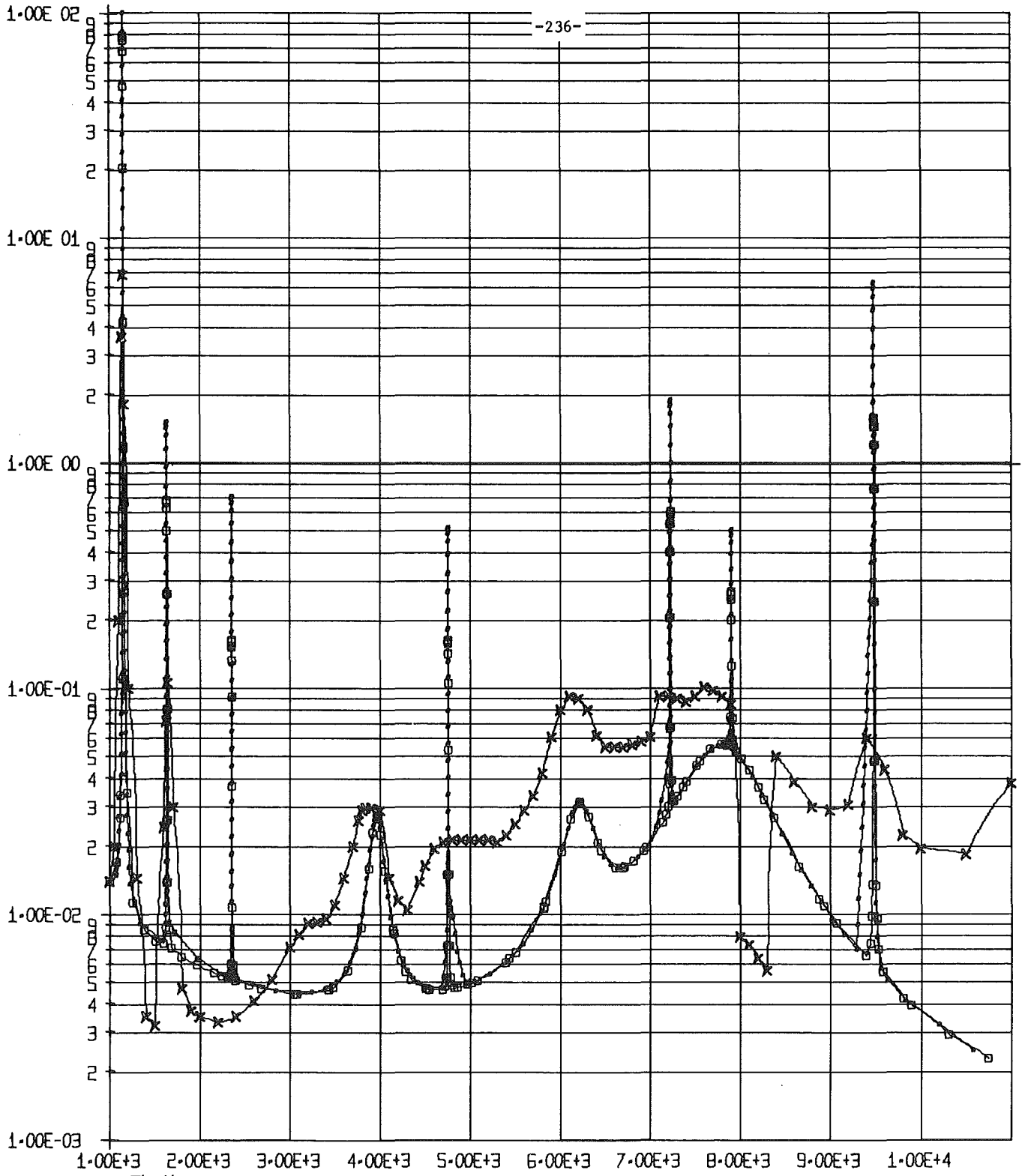


Fig.1'

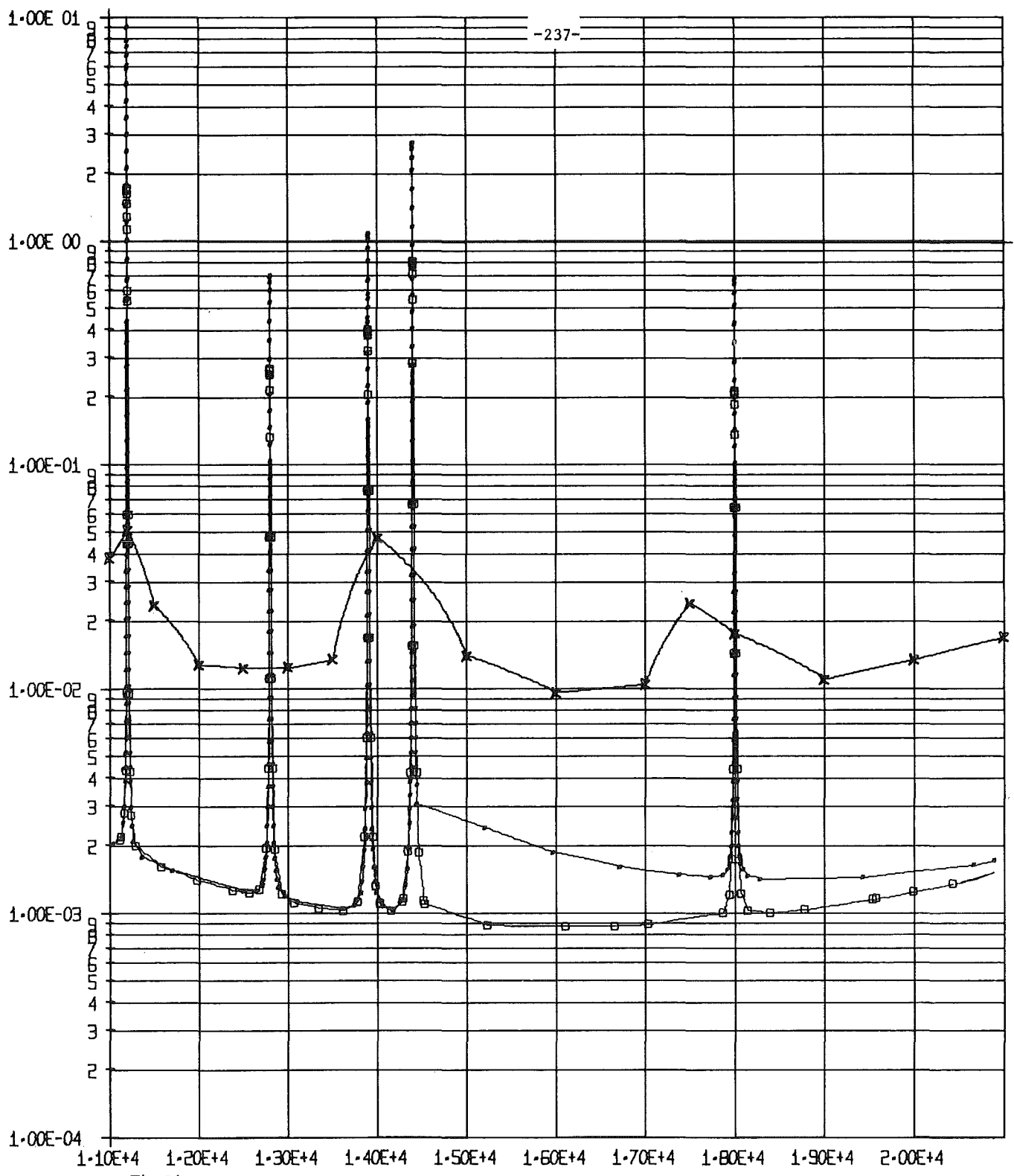


Fig. 2'

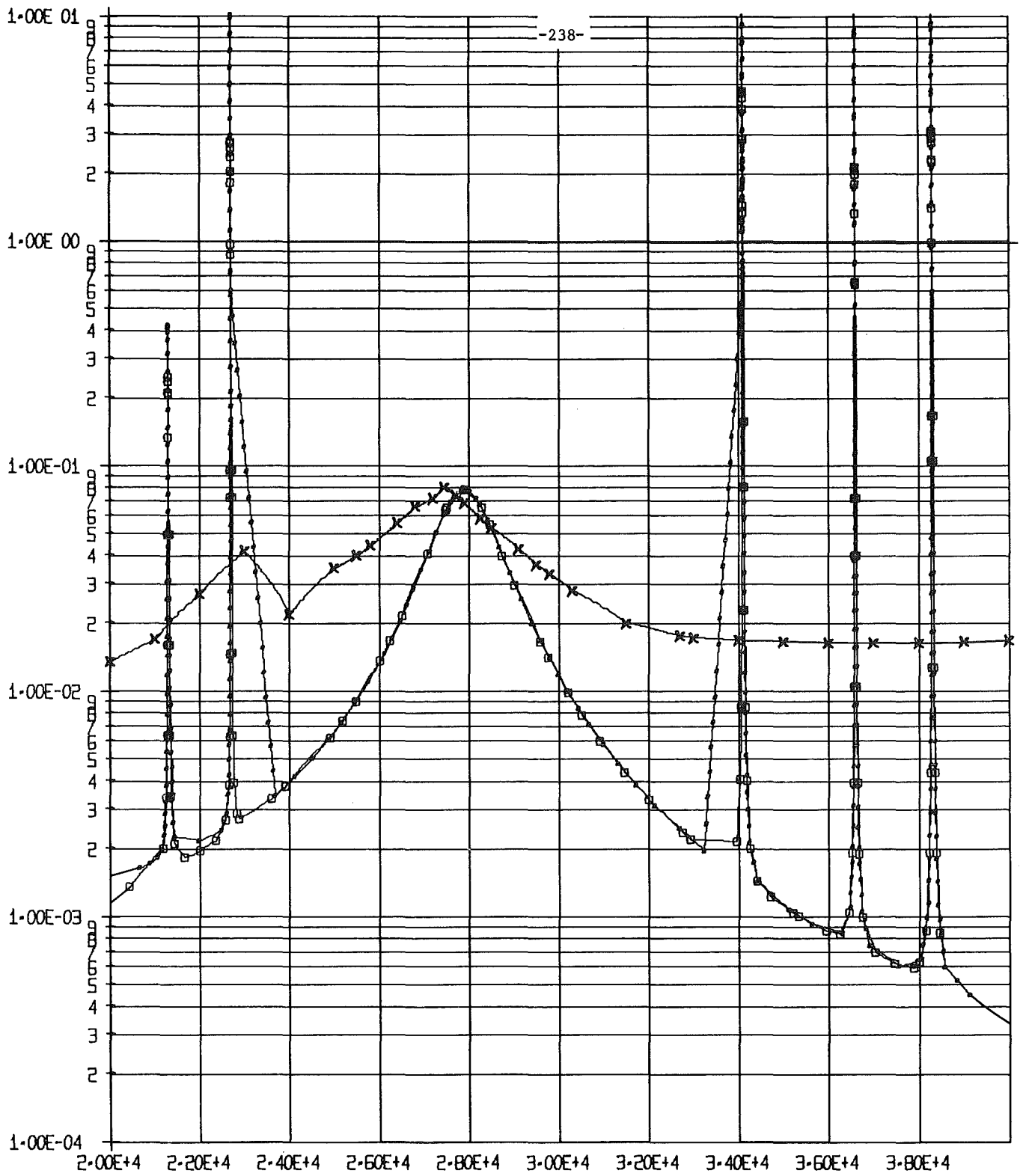


Fig. 3'

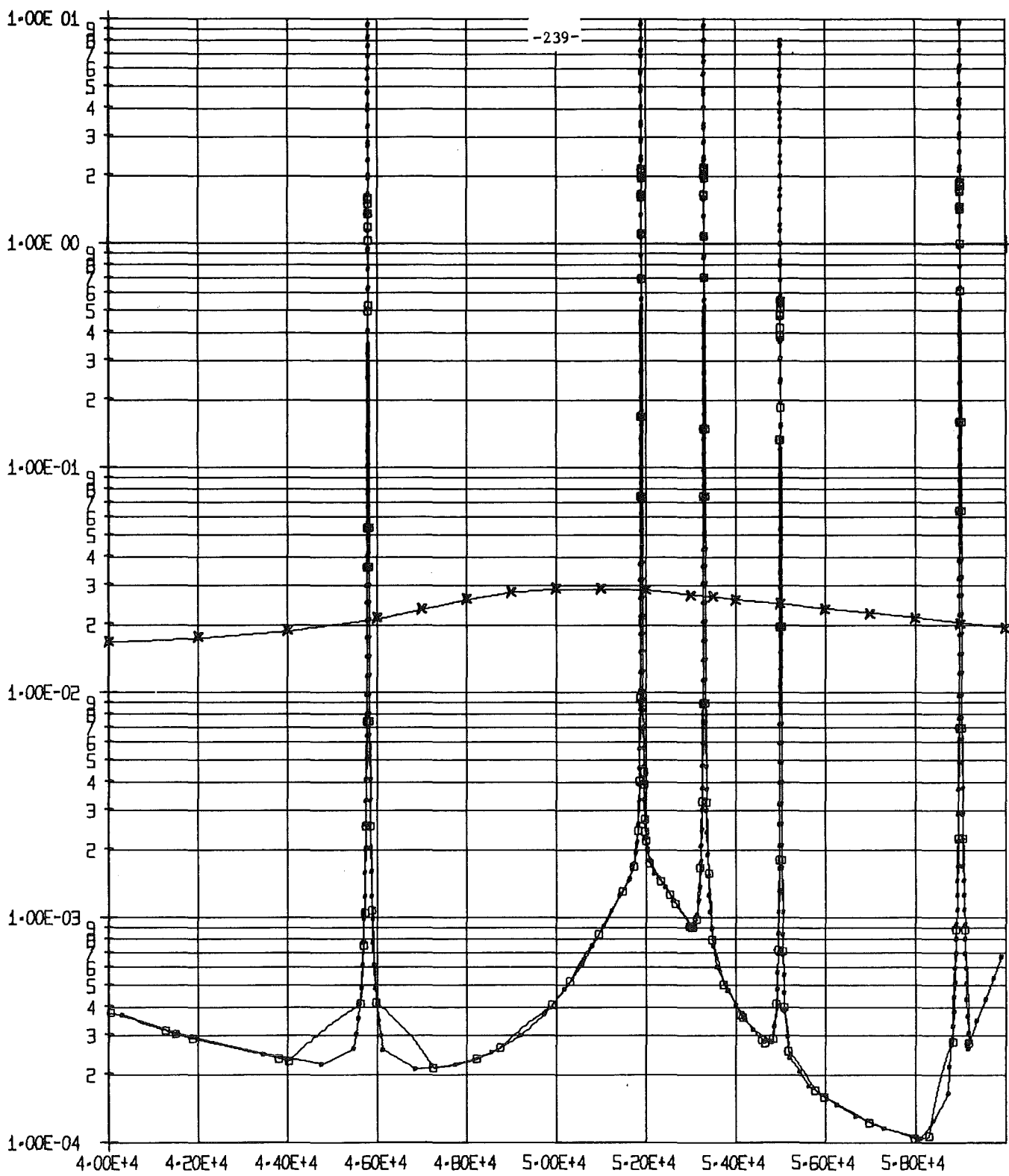


Fig. 4'

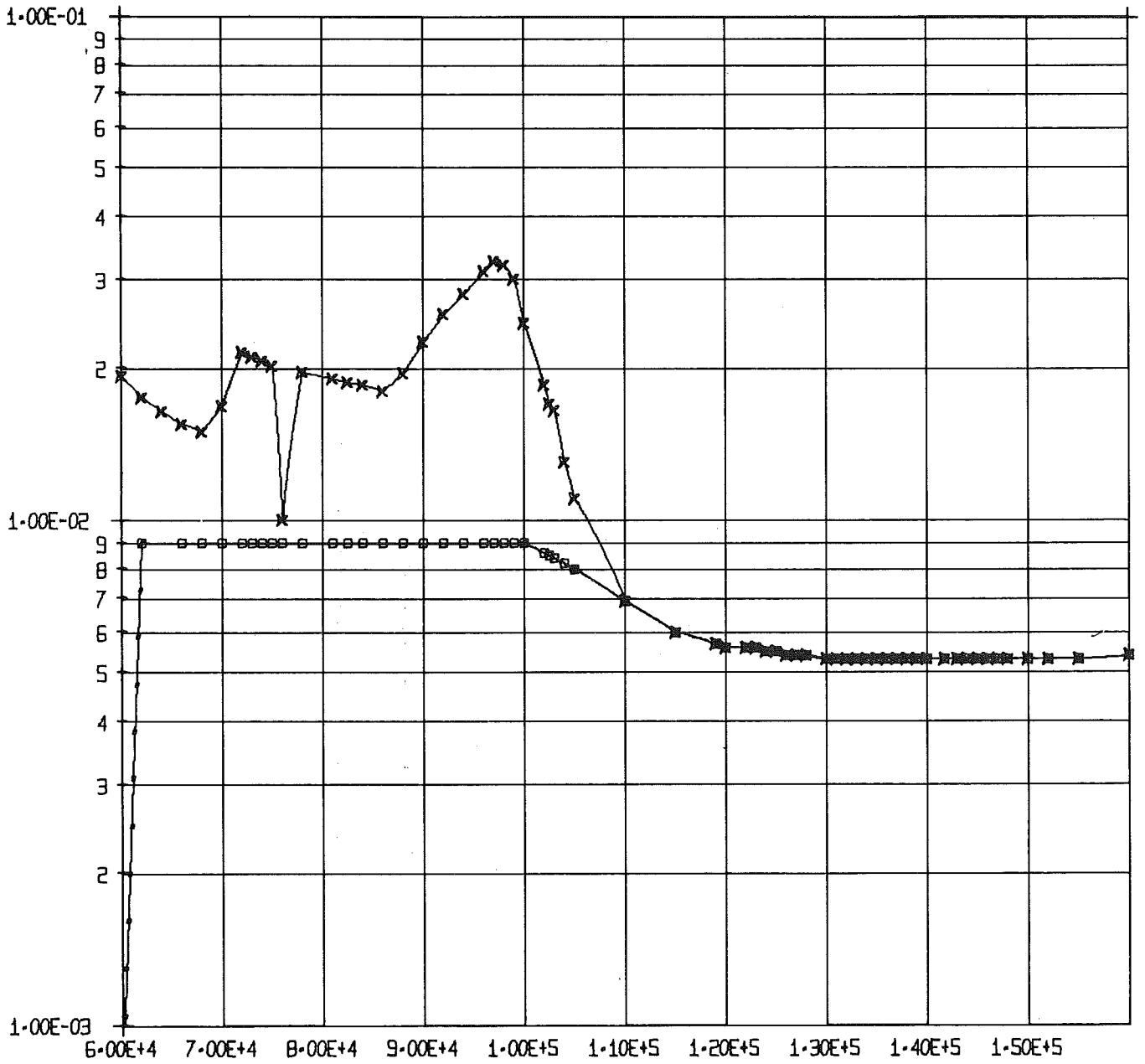


Fig. 5'

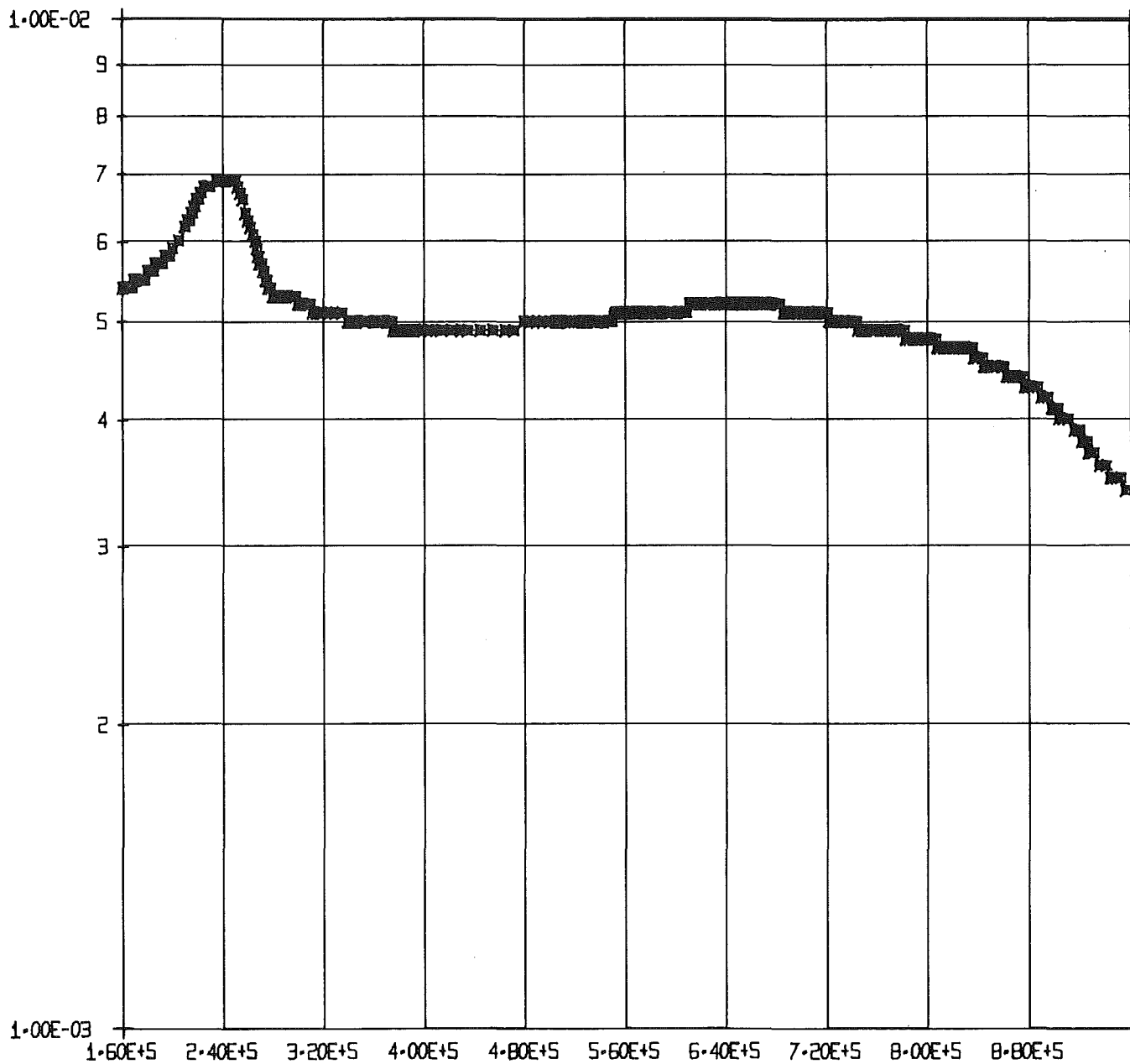


Fig. 6'

Fig. 1" - 8"

Comparison of the kev-capture cross section  
for Nickel

on the KEDAK, UKNDL and ENDF/B 3 nuclear data  
file

~~XXXX~~ - KEDAK : Version 2 (1970)

□-□-□ - UKNDL (1971)

————— - ENDF/B 3

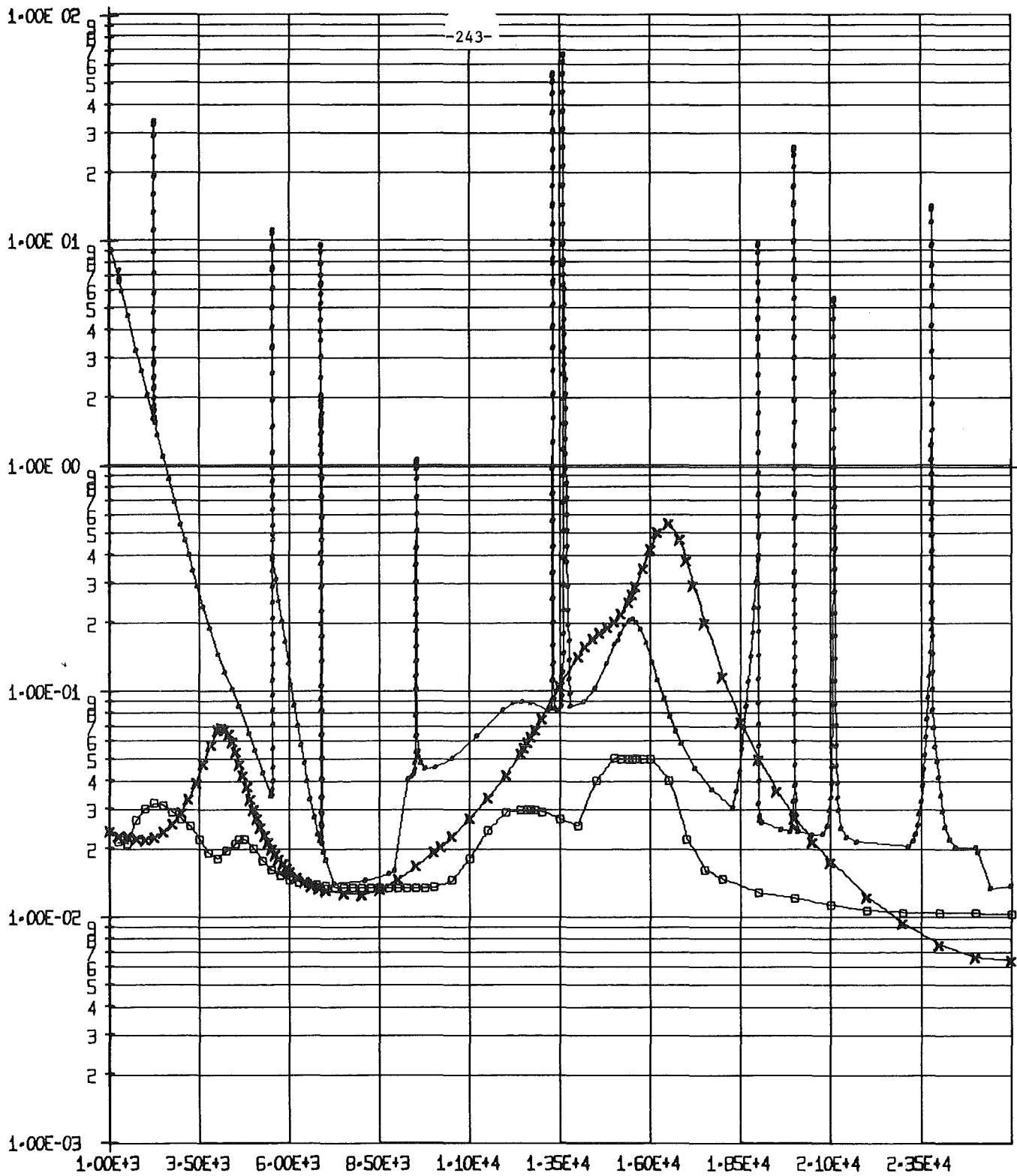


Fig.1"

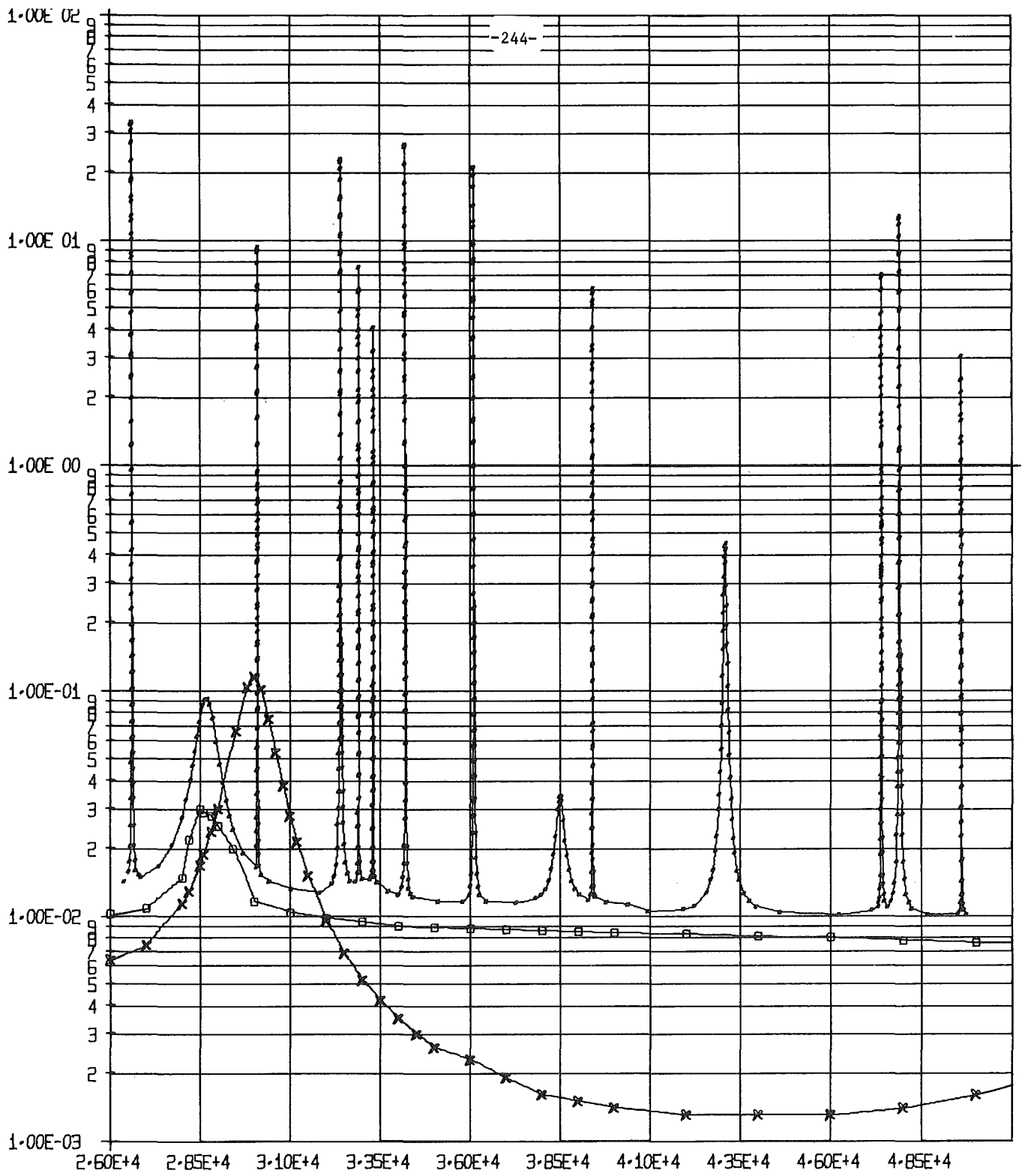


Fig. 2"

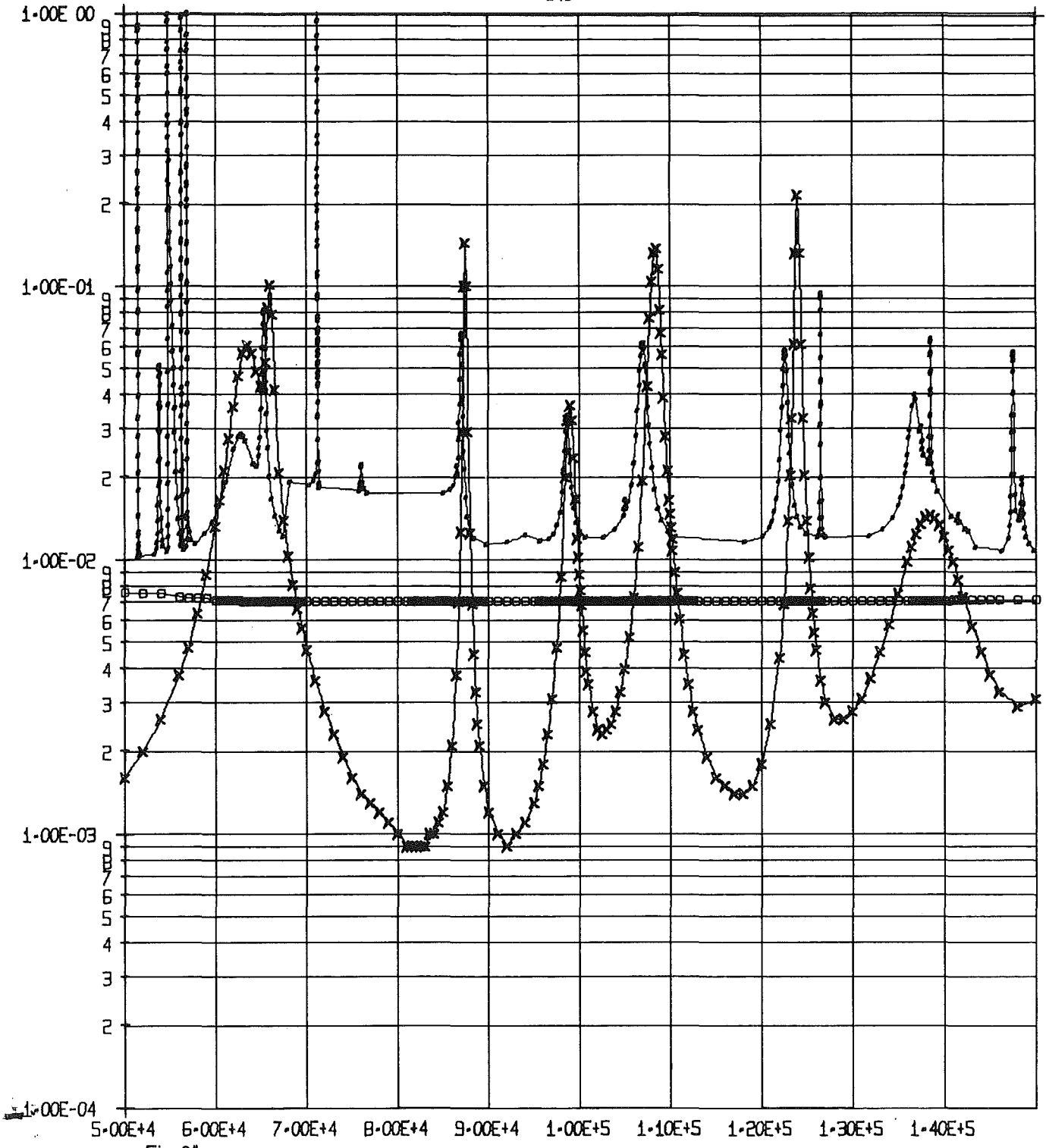


Fig. 3"

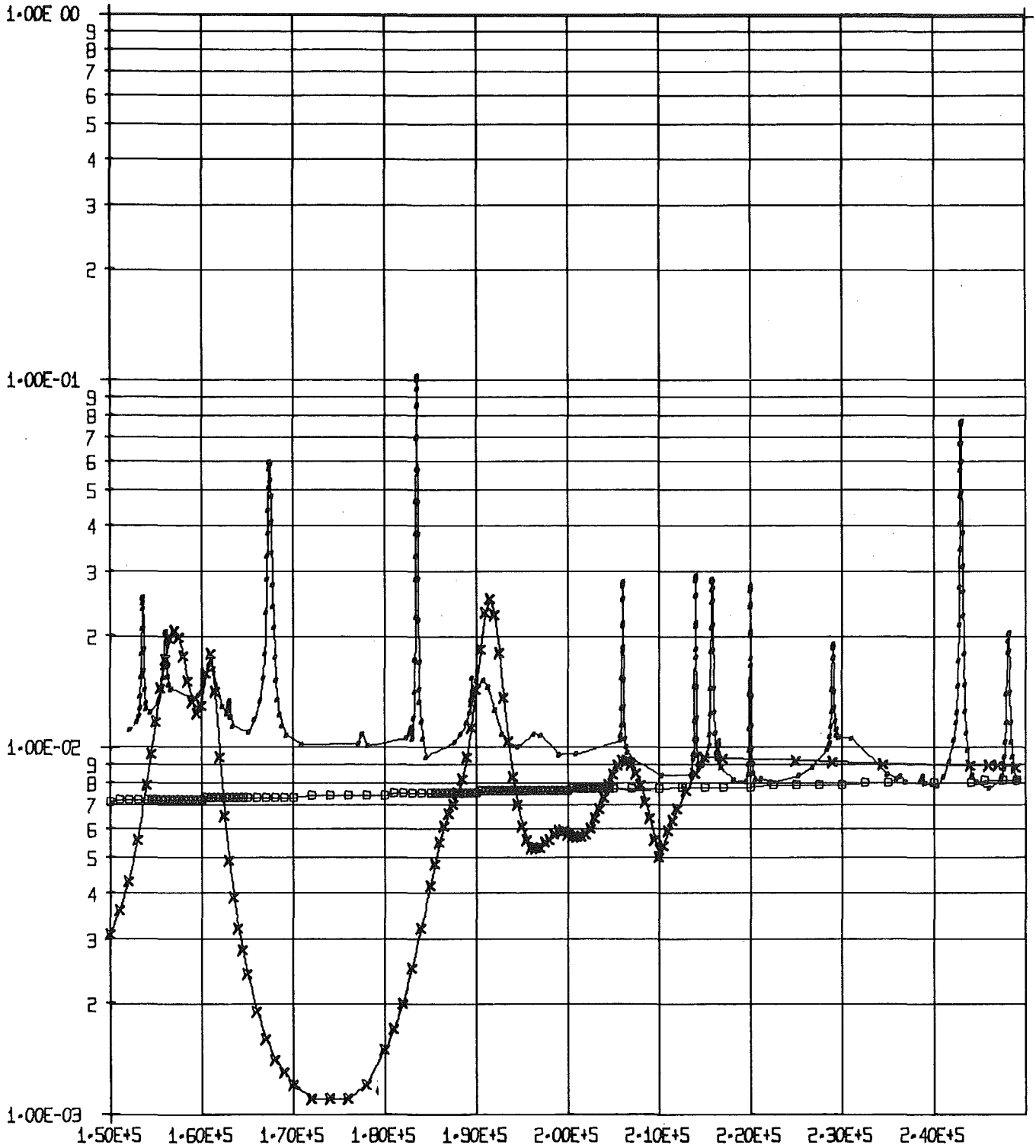


Fig. 4\*

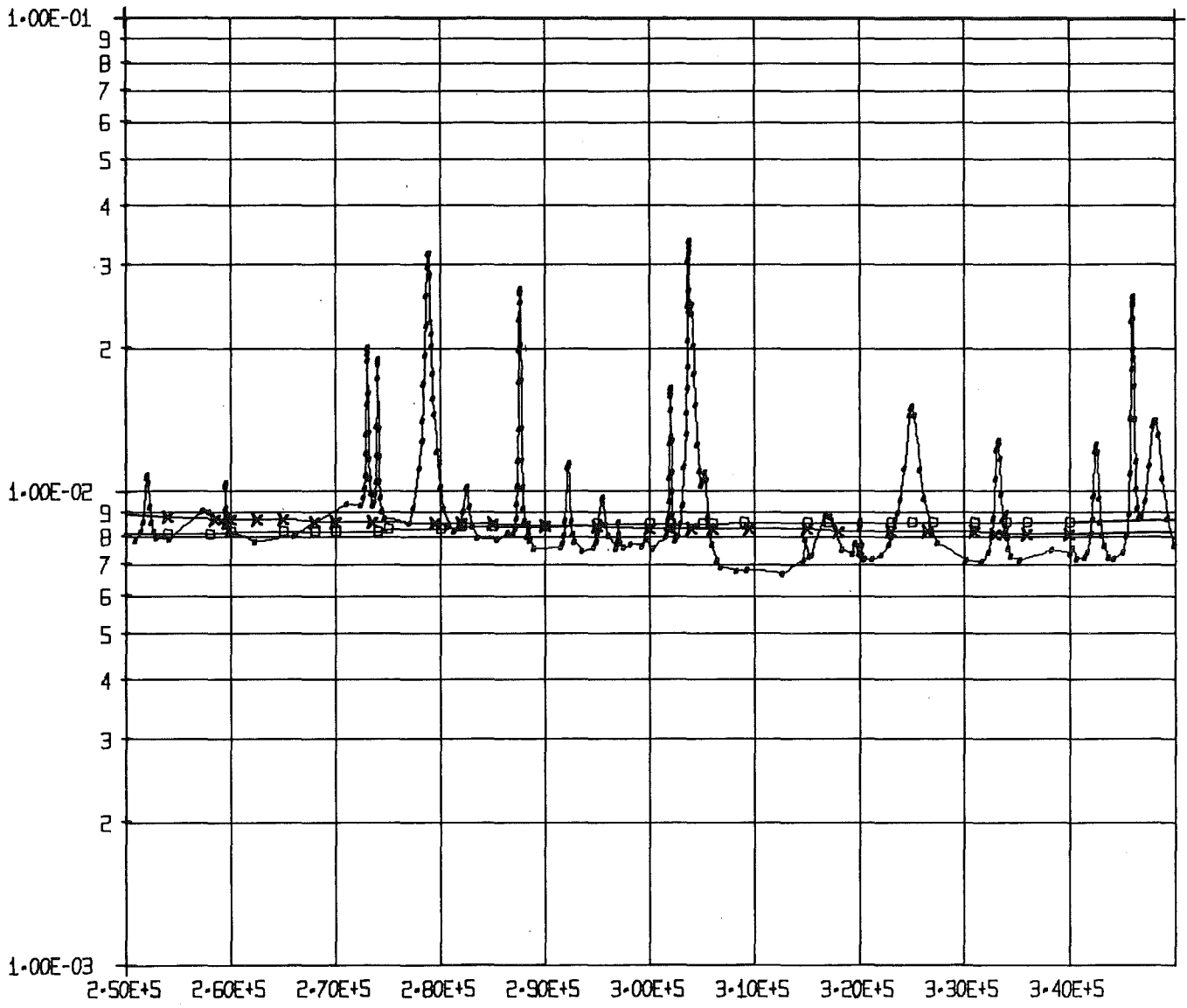


Fig.5"

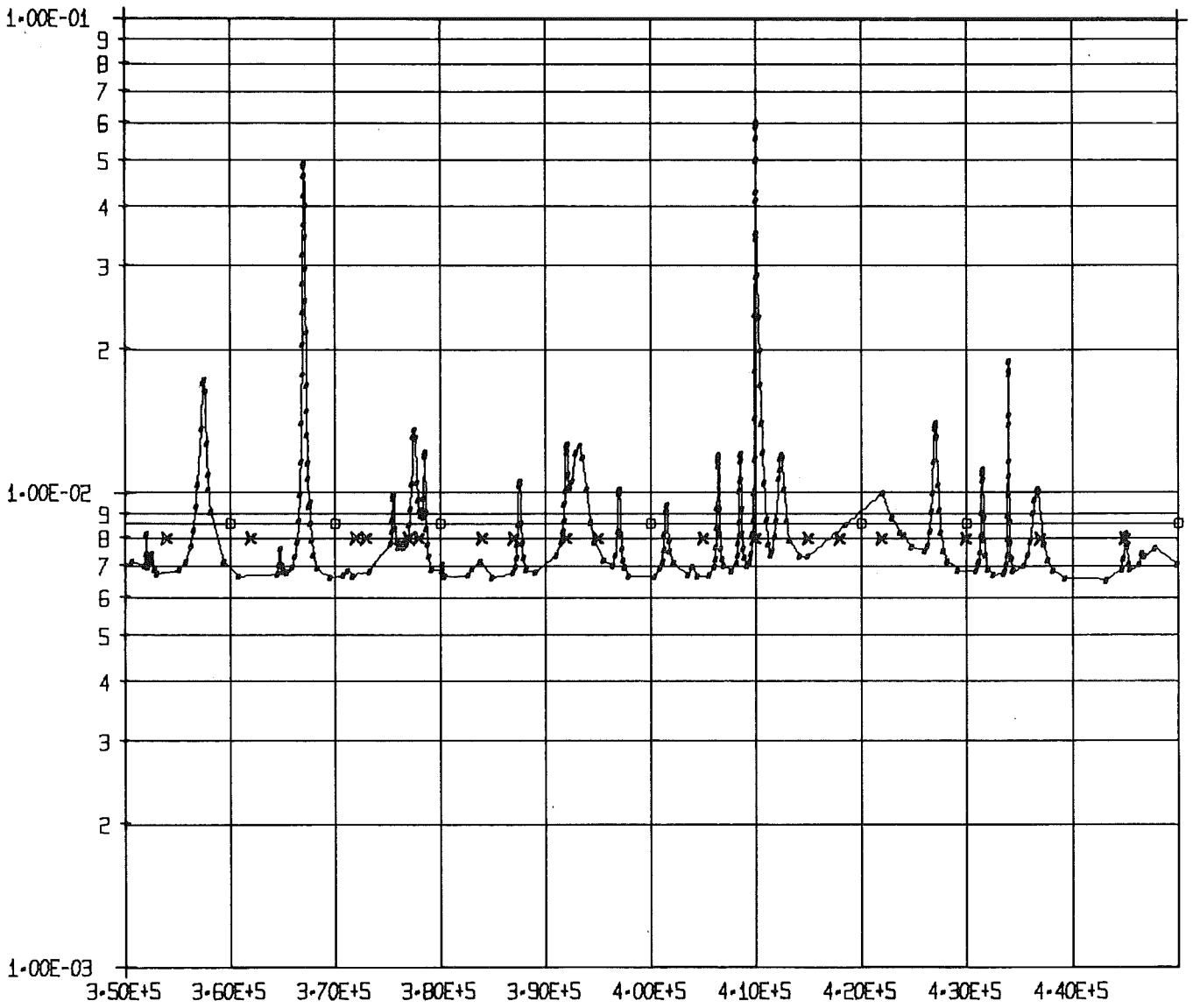


Fig. 6\*

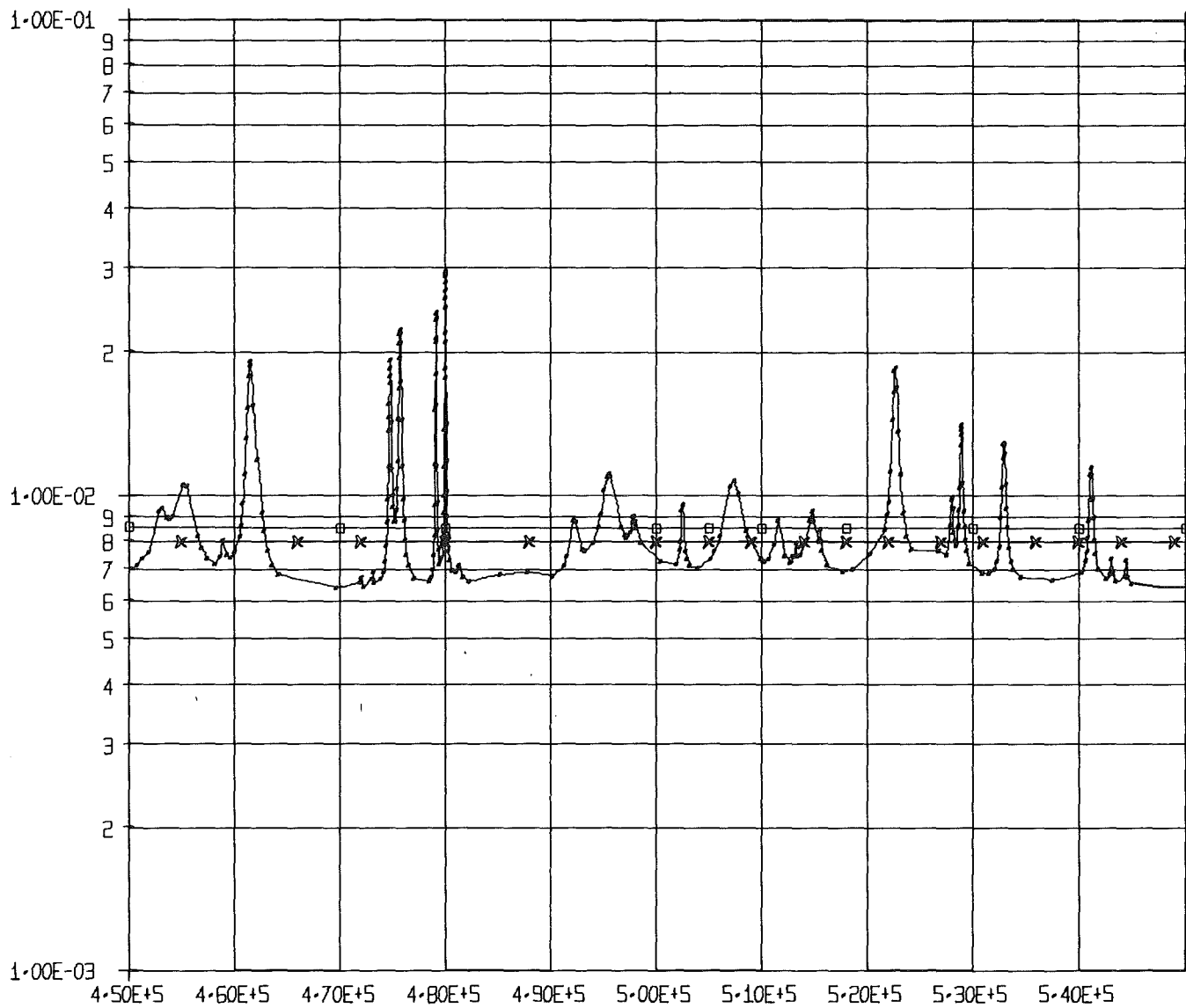


Fig. 7"

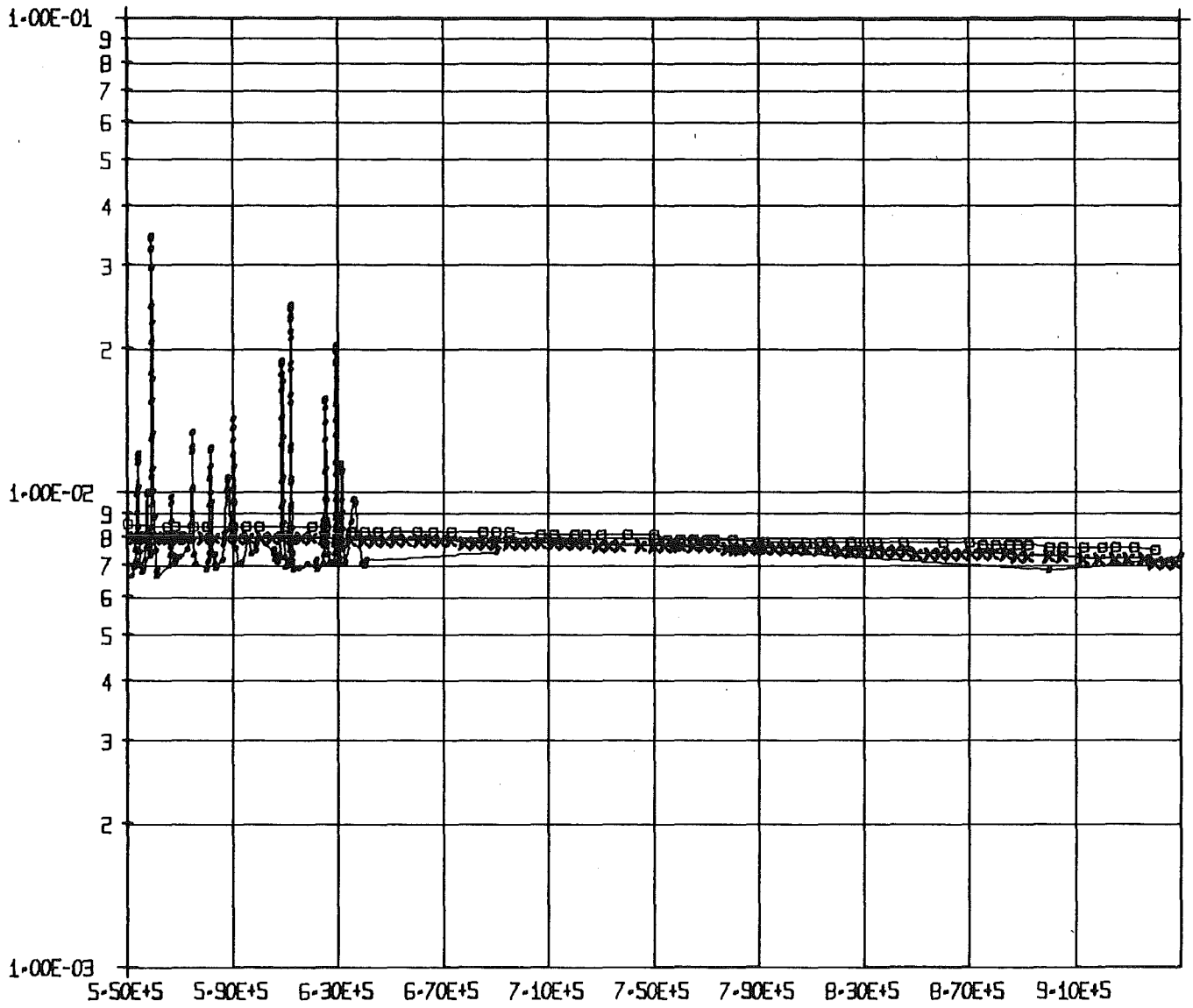


Fig. 8"

SUMMARY ON TOPIC II:

EVALUATED DATA

by

P. Ribon, C.E.N. Saclay

I - RECENT EVALUATIONS OR COMPILATIONS.

- 1) Fe - ENDF-3 - (Mat 1180) is appreciably different from ENDF-2 : the capture cross section between 2 and 200 keV is smaller and there are only a few resolved resonances :

$^{54}\text{Fe}$  : 2 ( $\ell = 0$ ) and 2 ( $\ell = 1$ ) resonances

$^{56}\text{Fe}$  : 2 ( $\ell = 0$ ) and 12 ( $\ell = 1$ ) resonances

$^{57}\text{Fe}$  : 3 ( $\ell = 0$ ) and 8 ( $\ell = 1$ ) resonances

- UKNDL - 1973 file (recent evaluation by J. Story) contains about 3500 energy points; above 360 keV the data are taken from ENDF - MAT 1124. There are parameters for 152 resolved resonances :

$^{54}\text{Fe}$  : 27 ( $\ell = 0$ ) and 25 ( $\ell = 1$ ) resonances

$^{56}\text{Fe}$  : 26 ( $\ell = 0$ ), 37 ( $\ell = 1$ ) and 6 ( $\ell = 2$ ) resonances

$^{57}\text{Fe}$  : 25 ( $\ell = 0$ ) and 9 ( $\ell = 1$ ) resonances

$^{58}\text{Fe}$  : 2 ( $\ell = 0$ ) resonances

- A French evaluation, still in progress, (G. Le Coq and P. Ribon) is characterised by the inclusion of many simulated resonances; at present there are parameters for 213 resonances of  $^{56}\text{Fe}$ .

- 2) Ni - ENDF-3 - (Mat 1123). The capture cross section between 5 and 20 keV is smaller than in ENDF-2, but is slightly greater above 200 keV. There are 1480 energy points between 1 keV and 0.69 MeV, and resolved resonance parameters for 294 levels :

$^{58}\text{Ni}$  : 31 ( $\ell = 0$ ) and 36 ( $\ell = 1$ ) resonances

$^{60}\text{Ni}$  : 40 ( $\ell = 0$ ) and 49 ( $\ell = 1$ ) resonances

$^{62}\text{Ni}$  : 35 ( $\ell = 0$ ) and 35 ( $\ell = 1$ ) resonances

$^{64}\text{Ni}$  : 24 ( $\ell = 0$ ) and 44 ( $\ell = 1$ ) resonances

- UKNDL - 1973 file (recent evaluation by M. Moxon) contains about 2700 energy points; above 600 keV the data have not been revised. There

are resolved resonance parameters for 314 levels :

$^{58}\text{Ni}$  : 31 ( $\ell = 0$ ) and 42 ( $\ell \geq 1$ ) resonances

$^{60}\text{Ni}$  : 38 ( $\ell = 0$ ) and 44 ( $\ell \geq 1$ ) resonances

$^{62}\text{Ni}$  : 33 ( $\ell = 0$ ) and 27 ( $\ell \geq 1$ ) resonances

$^{64}\text{Ni}$  : 26 ( $\ell = 0$ ) and 34 ( $\ell \geq 1$ ) resonances

$^{61}\text{Ni}$  : 31 ( $\ell = 0$ ) and 8 ( $\ell \geq 1$ ) resonances

- 3) Cr - ENDF-3 - (Mat 1121) is only slightly different from ENDF 2 from 10 to 20 keV and above 200 keV. It has 1244 energy points between 1 keV and 0.65 MeV, and gives parameters for 183 resonances :

$^{50}\text{Cr}$  : 38 ( $\ell = 0$ ) and 20 ( $\ell = 1$ ) resonances

$^{52}\text{Cr}$  : 14 ( $\ell = 0$ ) and 59 ( $\ell = 1$ ) resonances

$^{53}\text{Cr}$  : 15 ( $\ell = 0$ ) and 10 ( $\ell = 1$ ) resonances

$^{54}\text{Cr}$  : 14 ( $\ell = 0$ ) and 13 ( $\ell = 1$ ) resonances

- 4) Resonance parameters - We also notice the "Atlas of resolved neutron resonance parameters", edited by "Lawrence Livermore Laboratory", which is a computerised compilation of all available resonance parameters (energy, widths and quantum numbers) and gives "selected values". For example, there are 47 resonances for  $^{54}\text{Fe}$  up to 506.5 keV, 114 for  $^{56}\text{Fe}$  up to 1.442 MeV, 13 for  $^{57}\text{Fe}$  up to 45.5 keV and 7 for  $^{58}\text{Fe}$  up to 10.4 keV.

## II - GENERAL COMMENTS ON RECENT EVALUATIONS.

They include more details on the fluctuations of cross sections with energy than the previous ones. More precisely, they introduce more resolved resonances.

The old evaluations are based on the lead spectrometer between 5 and

50 keV mainly for Ni and Cr. The new ones, based on other experiments, give much higher capture cross sections in certain energy regions.

There is no explanation for this fact.

In the  $1/v$  energy range, the estimated accuracy of the recent UKNDL evaluations on Fe and Ni is 10%; this accuracy is about 30% between 10 and 100 keV (accuracy for an average over a 2 lethargy unit interval). The importance of the small resonances (p- and d-wave resonances) is emphasised because their contribution to the total capture cross section is predominant above 10 - 20 keV.

The values of the total radiative widths,  $\Gamma_\gamma$ , are badly known, although for some resonances the capture areas have been measured. There is an agreement that, for even target nuclides,  $\Gamma_\gamma$  depends strongly on the parity of the compound state, i.e. from theoretical consideration it is felt that for negative parity states ( $\ell = 1$  or  $\ell = 3$ ) the  $\Gamma_\gamma$  value could be less than half the values for positive parity states ( $\ell = 0$  or  $2$ ). This conclusion is supported by a few experimental results on resolved resonances, or by analysis of average cross-sections in the 100 keV energy range.

The value of  $\Gamma_\gamma$  may fluctuate noticeably from one level to another, but no definite figure is advanced for the dispersion. According to British results on Co (not corrected for experimental conditions) the fluctuations have an effective  $\nu$ -value of 7 to 12.

The parameters for the 1.15 keV resonance of  $^{56}\text{Fe}$  appear to be well-known.

Two independent evaluations give :

	<u>Story</u>	<u>Ribon</u>
E (eV)	1154 $\pm$ 4	1149
$\Gamma_n$ (eV)	0.0592 $\pm$ 0.0032	0.060 $\pm$ 0.003
$\Gamma_\gamma$ (eV)	0.581 $\pm$ 0.051	0.605 $\pm$ 0.040
$\ell, J$	1, 1/2 $^-$	1, 1/2 $^-$

III - RECOMMENDATIONS AND SUGGESTIONS.

- 1) Resonance interferences - For s-wave resonances it is necessary to take into account the resonance interferences when calculating the cross sections; to avoid the use of heavy multilevel codes for reactor calculations, the point-wise cross section representation is useful. For the description of narrow resonances, it is necessary to define energies by 6-figure numbers.
- 2) Negative energy resonances - At least one negative energy resonance must be introduced for each of the main isotopes; this is adjusted in order to describe the available thermal and low energy data (capture, scattering, coherent scattering, total).

Furthermore, the effects of distant resonances should be taken into account in the formalism. One way of doing this is by the introduction of fictitious strong resonances at a large negative energy and high positive energy.

- 3) Experimental results - The analysis of small resonances which are resolved in total cross section measurements is useful for they are generally p- or d-wave resonances, and contribute to most of the capture.

The consequences of parasitic neutron scattering in the strong s-wave resonances on the results of capture cross section measurements have to be clarified.

Generally the capture area  $A_\gamma$  of resonances resolved in capture cross-section measurement are interpreted as  $g \Gamma_n \Gamma_\gamma / \Gamma_t$  for one resonance; but in fact an s-wave peak may have p- and d-wave resonances superimposed which give capture contributions of the same order of magnitude even though their neutron widths are very different.

- 4) Values of average parameters - We need better information on average level spacing and radiation width versus spin, parity and energy; information on the fluctuations of radiation widths are also required.

It is recommended that the total width  $\Gamma$ , of a few resonances is measured by transmission techniques with cooled samples of natural iron and nickel below 10 keV in order to determine the radiation width of p-wave resonances. (Note - Below 10 keV, for p-wave resonances,  $\Gamma_n \ll \Gamma_\gamma$ , while the Doppler width is of the same order of magnitude as  $\Gamma_\gamma$ .)

- 5) Information from other sources - It was remarked, but only very briefly discussed, that other experiments can provide useful information. In the case of the ( $\gamma$ , n) experiment, with gamma-rays just above the neutron threshold, a study of the angular distribution, using time of flight techniques to resolve the levels, can give their spins. Similar conclusions can be drawn from studies of the capture gamma-ray spectra, but this may be more difficult owing to the low capture and high scattering cross-sections.

TOPIC III

USER ASPECTS

Cadarache April 24<sup>th</sup>, 1973

E A C R P WORKING GROUP MEETING

"The KeV capture of structural materials Ni, Fe, Cr".

KARLSRUHE May 8-9<sup>th</sup>, 1973

ORAL PRESENTATION

IMPORTANCE OF THE CAPTURE CROSS SECTION OF  
STRUCTURAL MATERIALS FOR FAST POWER REACTORS

J.V. BARRE

I - INTRODUCTION

I/1. It is a pleasure to try to explain you as shortly and simply as possible the influence of structural material nuclear data on fast power reactor performances.

First of all, this presentation will deal only with mixed plutonium oxide fuelled, sodium cooled and uranium oxide-sodium reflected fast reactors. Power range lies between 200 and 2000 MWe.

.../...

At the present stage of fast reactor physics improvement at CEA, it is considered that stainless steel capture effective cross sections, mainly Fe, Ni and Cr data, represent, together with fission product capture cross sections, the two first priorities to be requested in the next WRENDA list /1/. This is the reason why the conclusions of this meeting are impatiently waited for.

The main power reactor parameters sensitive to capture cross section of structural materials (Fe, Cr, Ni) are firstly considered : they define the requested accuracy on the capture data. Secondly the relative importance of isotopes, the main important multigroup constants and the main energy range are mentioned. Thirdly, the present knowledge of these data from reactor physics and integral experiments is discussed on the basis of the Cadarache multigroup cross section set Version 3, available from March 1973 and the CEA fast reactor physics programme.

Finally, the influence of other structural material data on core parameters and the general aspects of structural material data on reactor performances are briefly described.

## II- POWER REACTOR PARAMETERS SENSITIVE TO Fe-Cr-Ni CAPTURE RATES

II/1. At the present stage of the Version 3 Cadarache cross section set, the Fe - Cr - Ni capture cross sections are the main unknown variables of the macroscopic absorption law used to predict the characteristics of a clean power reactor core. This is due to two new aspects of fast reactor physics at CEA : improvement of the knowledge and evolution of the requested performances.

The programme of fast reactor physics, completed during the last years, give the waited results ( 2 ) ( 3 ). The accuracy reached on the predictions from integral experiments put in evidence new sources of possible errors previously negligible : it is typically the case for stainless steel capture rates.

At CEA, the requests from the design group move from 250 MWe reactor to the 1200 MWe plant . At this step, an improvement on the predictions of the critical enrichments is hoped, due to the important Plutonium inventory and the better accuracy needed for the fuel cycle optimisation. Furthermore, the impact of the load factor could lead to consider the possibility of an increase of the stainless steel volumic percentage for the first cores.

II/2. Two main power reactor parameters are sensitive to structural material capture rate :

- . critical enrichment
- . global breeding gain

a) Critical enrichment :

The usual "four factors" formula is currently used in fast reactor field to decompose the main parameters important for reactivity :

$$K^* = \eta \epsilon p f$$

The parameter  $f$  represents the useless capture rates, :

$$f = \frac{\sum A_{\text{Fertile}} + \sum A_{\text{Fissile}}}{\sum A_{\text{Total}}}$$

For reactivity, this capture rate corresponds to the quantity  $(1 - f)$  :

$$\frac{dK}{K} = \frac{1-f}{K^*} \approx - \left( \frac{1}{f} - 1 \right) \frac{1}{K^*} \quad (1)$$

The magnitude of this effect is given in table 1 for three enrichments and 22 % stainless steel volumic composition. It varies between 1.7 and 3.4% according to the enrichment. For other design plants, a 5 % effect in reactivity can be obtained.

b) Breeding gain : ( G B G )

In fact, the effect of capture cross sections of structural material on breeding gain is directly related to their effect on reactivity. It can be easily demonstrated that the absolute variation of G B G is closely proportional to the reactivity variation by the relation :

$$\Delta \text{GBG} \approx \sqrt{\frac{dK}{K}} \approx -\sqrt{\frac{1-f}{K^*}} \approx -\frac{\sqrt{1-f}}{K^*}$$

- 1 % in  $K_{eff}$  corresponds to - 0.03 in G B G.

**II/3.** Looking to the orders of magnitude of the requests, the more stringent constraint comes in any case from reactivity :

+ 1 % for  $K_{eff}$  for all sources, that means

+ 0,5 % for the neutronic sources in the clean core

+ 0,03 for G B G

In conclusion, taking into account all possible sources of errors, it comes from these figures that the requested accuracy on the capture cross section of structural materials must be better than 10 %, in the range + 5 % + 7 %.

### III - MAIN NUCLEAR DATA

#### III/1. Relative importance of isotopes

For the design reactors at CEA, the structural materials consist of stainless steel. In any case, for reactor physicists point of view, the volumic composition remains almost constant :

Fe  $\approx$  70 %

Cr  $\approx$  18 %

Ni  $\approx$  10 %

The quantity  $(\frac{1}{f} - 1)$  equal to the capture rate of structural material over the absorption rate in fertile and fissile elements allows to decompose the effect on reactivity of the various isotopes (see equation 1). Table 1 gives the effect on reactivity for Fe Cr and Ni.

The relative importance does not vary largely with enrichment :

Fe  $\approx$  40 to 50 %

Ni  $\approx$  16 to 22 %

Cr  $\approx$  10 to 12 %

#### III/2. Main multigroup constants

The main difficulties on these structural material capture cross sections come from the definition of the resonance parameters used to calculate the self shielding factors. As it is well known from everywhere, most of fast reactor calculations are performed now in the multigroup approximation. Self-shielding effect is taken into account by factors  $f_g$  calculated from resonance parameters and tabulated versus the well-known parameter called dilution: the dilution of the isotope self-shielded represents, in a way, the importance of this isotope in the definition of the flux fine structure. I just recall you that the self-shielding factor  $f_g$  is the ratio of the real dilution cross section to the infinite dilution cross section and so varies between 0 and 1.

For Fe, Cr, Ni element capture reaction, the problem of the definition of these factors (or of the determination of resonance parameters) is complicated by the two approximatively equal contributions

.../...

to capture cross section, in a simple presentation, from large s wave resonance (strongly self-shielded) and narrow p wave ones (weakly self-shielded).

Hopefully, for most power reactors, the Fe - Cr - Ni dilutions do not vary too much :

Fe  $\approx$  10 to 20 barns     $f_{g\_minimum} \approx$  0.5 to 0.6  
 Ni  $\approx$  150 barns            "             $\approx$  0.95  
 Cr  $\approx$  100 barns            "             $\approx$  0.90

The corresponding self shielding factors, estimated from the present available data, show the problem is mainly important for Fe. The following table decomposes the Fe self-shielding factor versus energy for a typical 1200 MWe reactor :

E KeV	$f_g$	E KeV	$f_g$
498 - 302	0.90	67 - 41	0.98
302 - 183	0.89	41 - 25	0.59
183 - 111	0.87	25 - 15	0.99
111 - 67	0.75		

Average over the whole spectrum, the Fe self shielding factor is 0.90, independently of the spectra in the 200-2000MWe range. However,

it must be claimed these present factors have to be considered cautiously. From my point of view, this problem is probably more difficult to solve than the knowledge of the infinite dilution capture cross section.

### III/3. Main energy range

For the three isotopes considered, the most important energy range is located between 1 and 300 KeV independently of the enrichment (Fig. 1 - Fig. 2). The following table gives the percentage of capture between these energies for Fe and Ni and three Pu enrichments EN :

.../...

	Fe	Ni
EN = 25 %	62 %	28 %
18 %	64 %	35 %
12 %	66 %	43 %

For stainless steel capture probability, 60 % of capture rate take place also in the same energy range. Notice however the high level of Nickel capture above 1 MeV.

The capture probability law for a standard stainless steel differs largely from the total macroscopic capture law (FIG.3) and is more similar to the total macroscopic absorption probability law.

Looking to the capture average microscopic cross sections it can be seen that small variations exist as a function of enrichment, specially for stainless steel :

EN%	Fe mb	Ni mb	Cr mb	Stainless steel mb
25	6.5	23	5.8	8.0
18	6.8	20	6.4	8.1
12	7.8	18	7.7	8.8

#### IV - PRESENT KNOWLEDGE FROM INTEGRAL EXPERIMENTS

IV/1. The new Cadarache multigroup cross section set Version 3, available from March 1973, has been adjusted on a lot of integral experiments, mainly cell parameters: material buckling,  $K_{\infty}$ , spectral indices.

Among structural material captures, only the infinite dilution Fe capture cross section has been adjusted.

The stainless steel volumic percentage in the lattices used in the adjustment varies between 10 and 22 % for the majority of the cores : that correspond to 1 to 3.5 % in Keff according to the enrichment. For all these cases, there are no discrepancy between calculated and measured values larger than an equivalent of 0.6 % in reactivity.

For two cores, one "K<sub>∞</sub> = 1" experiment (ZEBRA 8 C) and one material buckling experiment (ZEBRA 9), the volumic percentages of stainless steel are respectively 60 % and 50 %. This corresponds to 10 % and 5.3 % in Keff. In the two lattices, after adjustment of Fe capture cross sections, the agreement between calculated and experimental values is about the same one that for other lattices with 20 % stainless steel. From these results, it is concluded that in the range of stainless steel volumic percentage of power reactor, the effective capture cross section of standard stainless steel in the Version 3 cross section set is accurate enough compared to the requests. But Fe capture cross section adjustments are defined by these two lattices.

IV/2. That conclusion does not mean necessarily that Fe, Cr, Ni infinite dilution capture cross section and self shielding factors in this Version 3 are corrected : compensations can exist.

Looking to reactivity worth measurements of stainless steel, mild steel, Nickel and Chromium relative to Pu 239 and U 235 performed in several lattices, particularly at ERMINE, general trends can be observed on the ratio calculation over experiment :

Stainless steel	:	$\frac{C}{E}$	≈	0.9 to 1.10
Mild steel or Fe	:	$\frac{C}{E}$	≈	1.5 to 1.80
Nickel	:	$\frac{C}{E}$	≈	0.5 to 0.60
Chromium	:	$\frac{C}{E}$	≈	0.7

Considering the well-known difficulties of analysis of such experiments and the contribution of the slowing down term to reactivity worth, it is tentatively concluded that in the Version 3 cross section set :

- Fe effective capture cross sections are too high: ≈ 40<sup>+</sup> - 30 %
- Cr effective capture cross sections are too low : ≈ 35<sup>+</sup> - 20 %
- Ni effective capture cross sections are too low : ≈ 50<sup>+</sup> - 30 %

Standard 304 stainless steel capture cross sections are corrected

- 0  $\pm$  15 %

- Two remarks must be done :

a) Even taking into account an uncertainty of  $\pm$  30 % on the slowing down effect in the reactivity worth, these trends remain significant

b) No self shielding factors are used presently for Cr and Ni. That means that infinite dilution capture cross section for these two isotopes are too low by about 48 and 48 % respectively.

IV/3. When microscopic cross sections used in the Version 3 cross section set are compared to differential measurements and evaluations, it appears that for Cr (Fig. 5) and Ni (Fig. 6) a large increase of microscopic capture in the range 1 - 100 KeV can be done. Preliminary evaluations by LECOQ et al based on SPITZ measurements lead to the following results for infinite dilution :

	Fe <sub>mb</sub>	Ni <sub>mb</sub>	Cr <sub>mb</sub>	Stainless Steel <sub>mb</sub>
Standard	7.9	19	7.4	9.4
LECOQ 71	14	38	15	17.4

These results are confirmed by the recent measurements of LERIGOLEUR at CADARACHE presented to this meeting.

However for Fe, the differential measurements suggest also a large increase of capture cross section (Fig. 4), in contradiction with the results of integral experiments for mild steel or stainless steel.

IV/4. In conclusion, it appears clearly that the agreement obtained for stainless steel in Version 3 is due to compensations between Fe, Ni, Cr infinite dilution cross sections and self shielding factors. To transpose results from integral experiments to design plant with possible different dilutions or compositions, it is unsatisfactory to work with such compensation. That is a reason of the first priority given to the knowledge of infinite dilution capture cross sections of Fe, Cr and Ni to  $\pm 5\%$  and self shielding factors to about  $\pm 3\%$ .

#### V - IMPORTANCE OF OTHER STRUCTURAL MATERIAL DATA

- Only some brief remarks will be done.

- In standard stainless steel, volumic percentage of Mn and Mo can reach 2%. Considering the average microscopic capture cross section of these isotopes ( $Mn \approx 140 \text{ mb}$  -  $Mo \approx 65 \text{ mb}$ ), it is necessary to know these cross sections to about  $\pm 20\%$ .

- Inelastic cross section of stainless steel represents between 30% and 45% of the total inelastic cross section above 1 MeV. These cross sections are requested to  $\pm 5\%$  for Fe,  $\pm 20\%$  for Chromium and  $\pm 30\%$  for Nickel.

- For  $\gamma$  heating and shielding purpose, spectra of secondary  $\gamma$  radiation are requested with better accuracy ( $\approx 10\%$ ).

- No better accuracies on capture cross section are requested from shielding purposes than from core parameters. But Fe, Ni and Cr total cross section must be known to about  $\pm 3\%$ ; angular distribution for elastic scattering has to be known accurately, for example 2% on  $\mu$ .

- Finally cross sections (n, p), (n,  $\alpha$ ) must be defined to about  $\pm 20\%$  for swelling and damage problems.

BIBLIOGRAPHY

- /1/ BARRE J.Y. et al - Rôles respectifs des évaluations et des expériences intégrales pour la physique des réacteurs rapides SM 170/69  
Symposium IAEA sur les applications des constantes nucléaires dans la science et la technologie PARIS 12-16 Mars (1973)
- /2/ BOUCHARD J. et al - Experimental study of burn-up in fast breeder reactors - New developments in reactor physics and shielding II (ANS National meeting, KIAMESHA LAKE) Conf 720901 (1972) 868
- /3/ BARRE J.Y. et al - Reactor physics and fast power breeders : MASURCA core R-Z programme, idem (1972) 822

TABLE I

STRUCTURAL MATERIALS : REACTIVITY BALANCE

Enrichment	25 %			18 %			12 %		
f	0,967			0,963			0,957		
$\frac{dK}{K}$ (%)	1,7			2,3			3,4		
Isotope	Fe	Cr	Ni	Fe	Cr	Ni	Fe	Cr	Ni
$\frac{1}{f} - 1$	0,017	0,004	0,007	0,019	0,005	0,008	0,024	0,006	0,008
$\frac{dK}{K}$ (%)	0,8	0,2	0,4	1,2	0,3	0,5	1,8	0,5	0,6

Fig.1 - FER ; CAPTURE PERCENTAGE  
BELOW THE ENERGY E

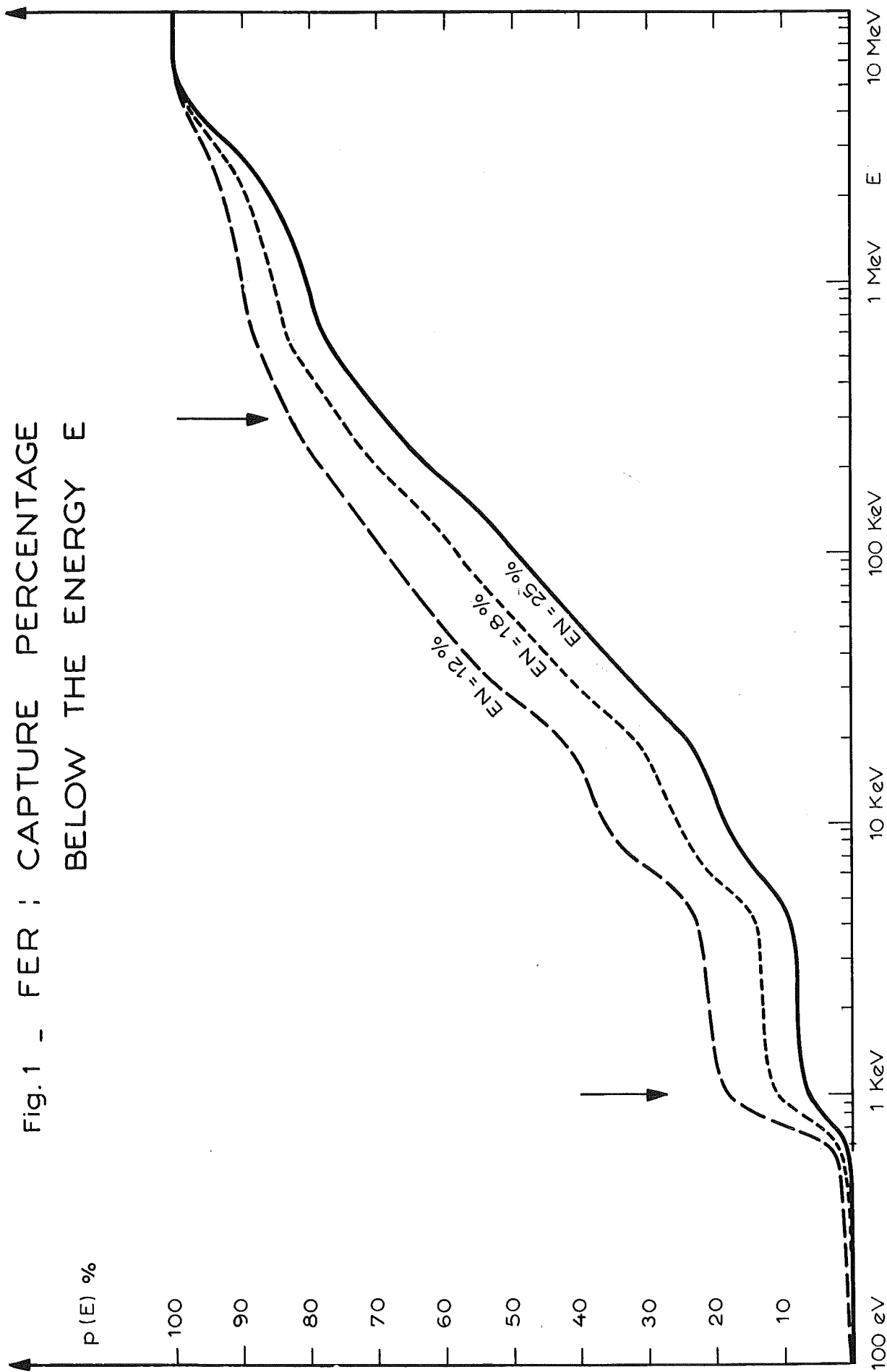


Fig.2 - NICKEL : CAPTURE PERCENTAGE BELOW THE ENERGY E

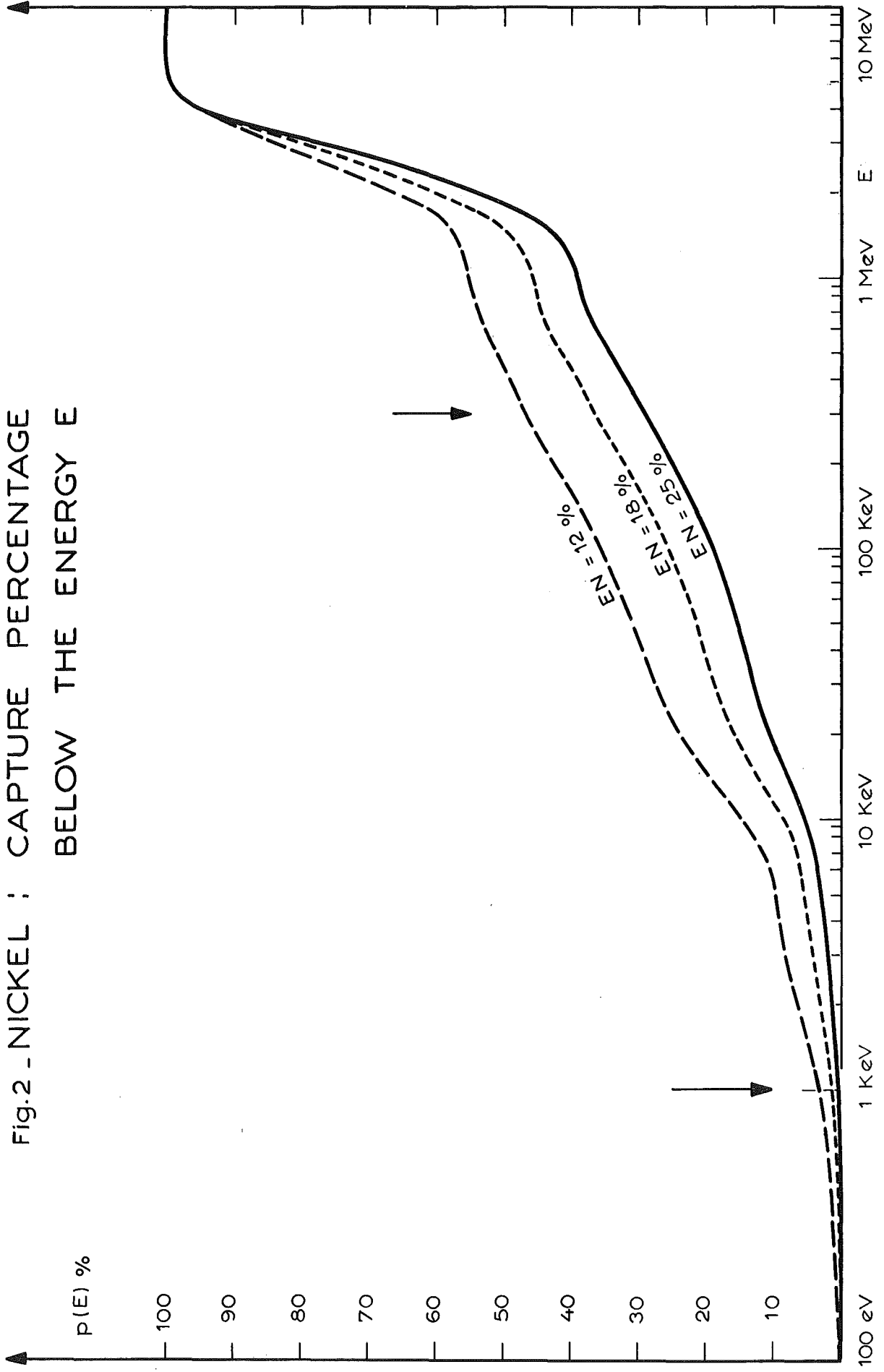


Fig. 3 - REACTION RATE PERCENTAGE  
BELOW THE ENERGY E

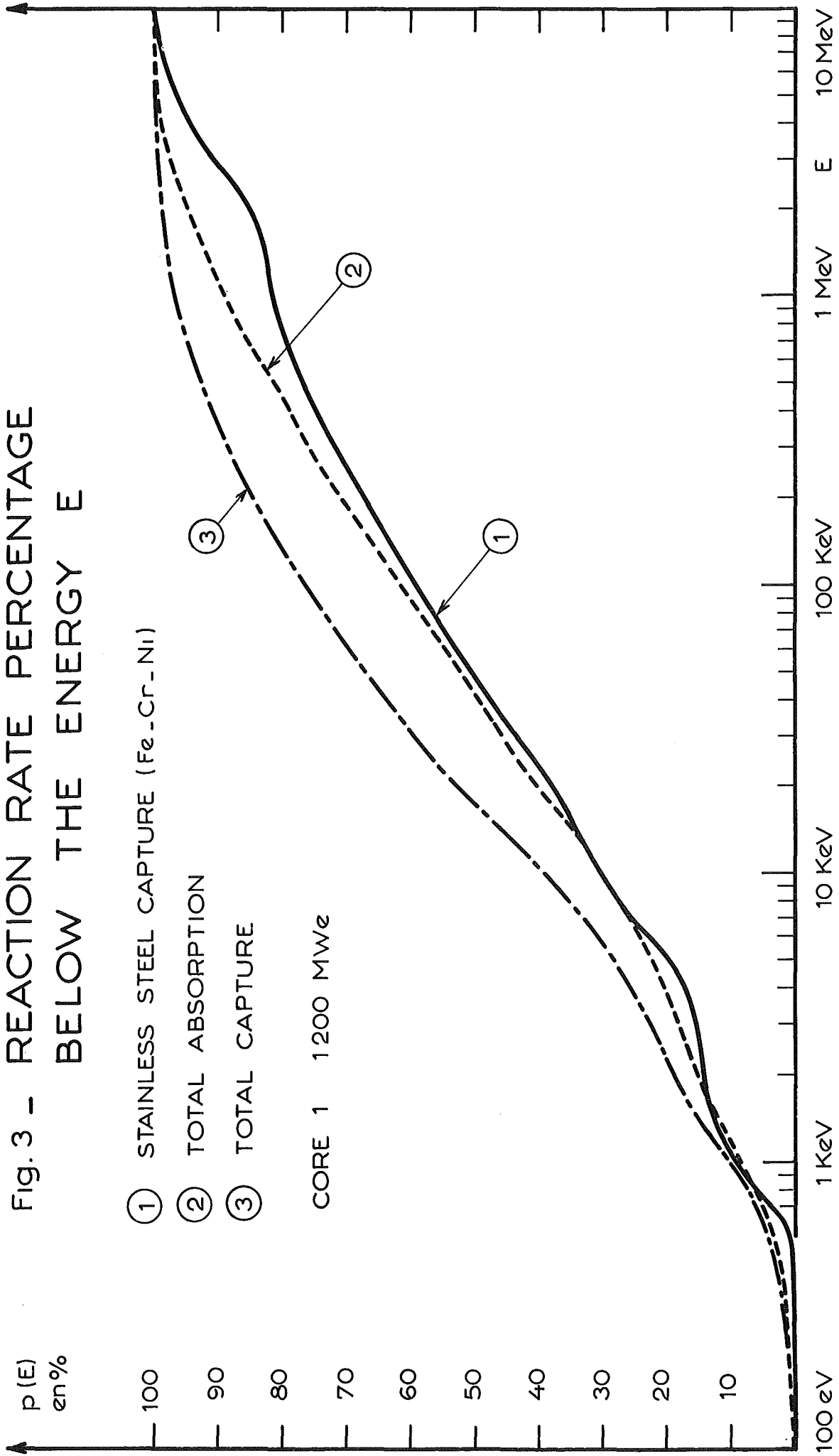
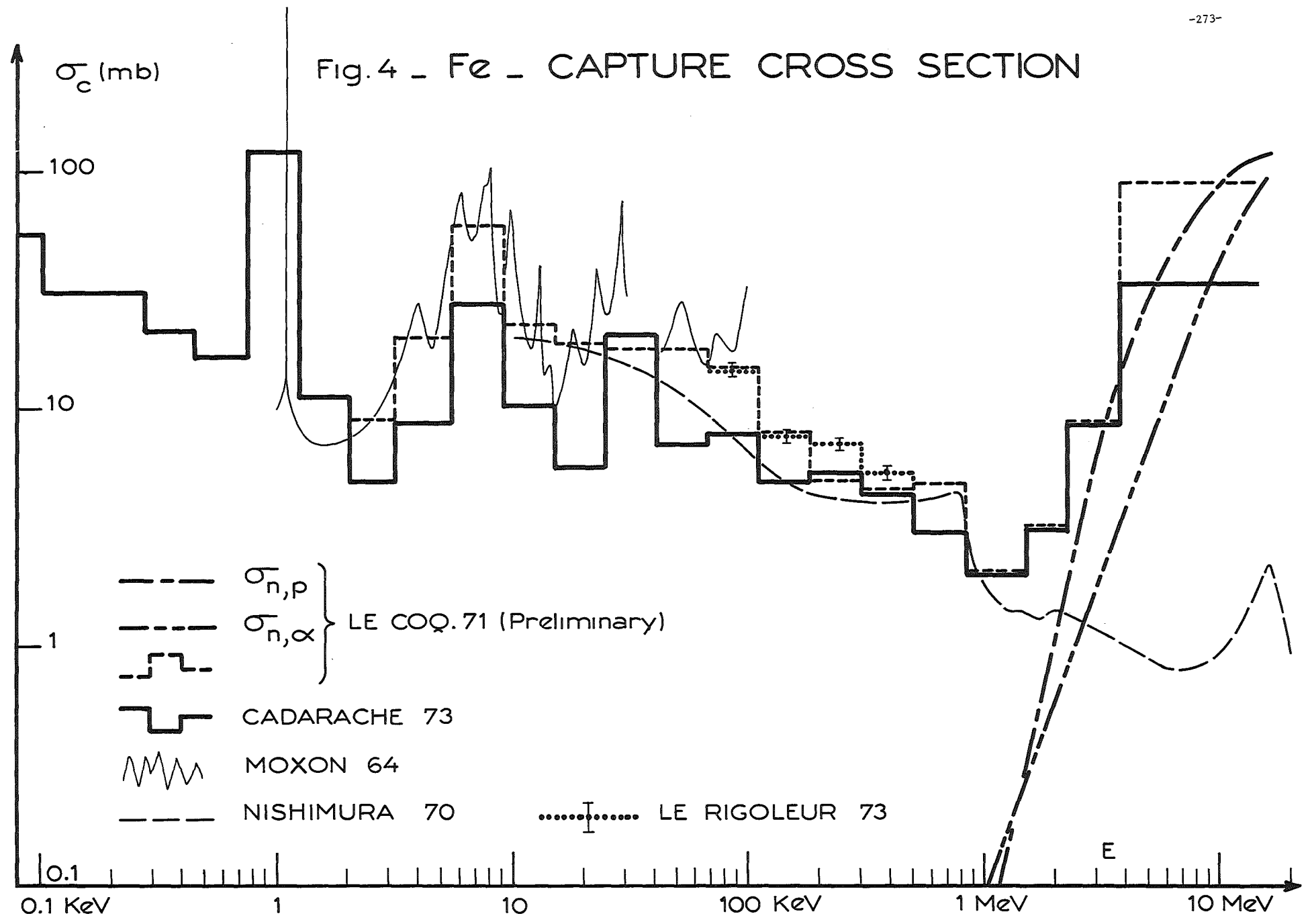
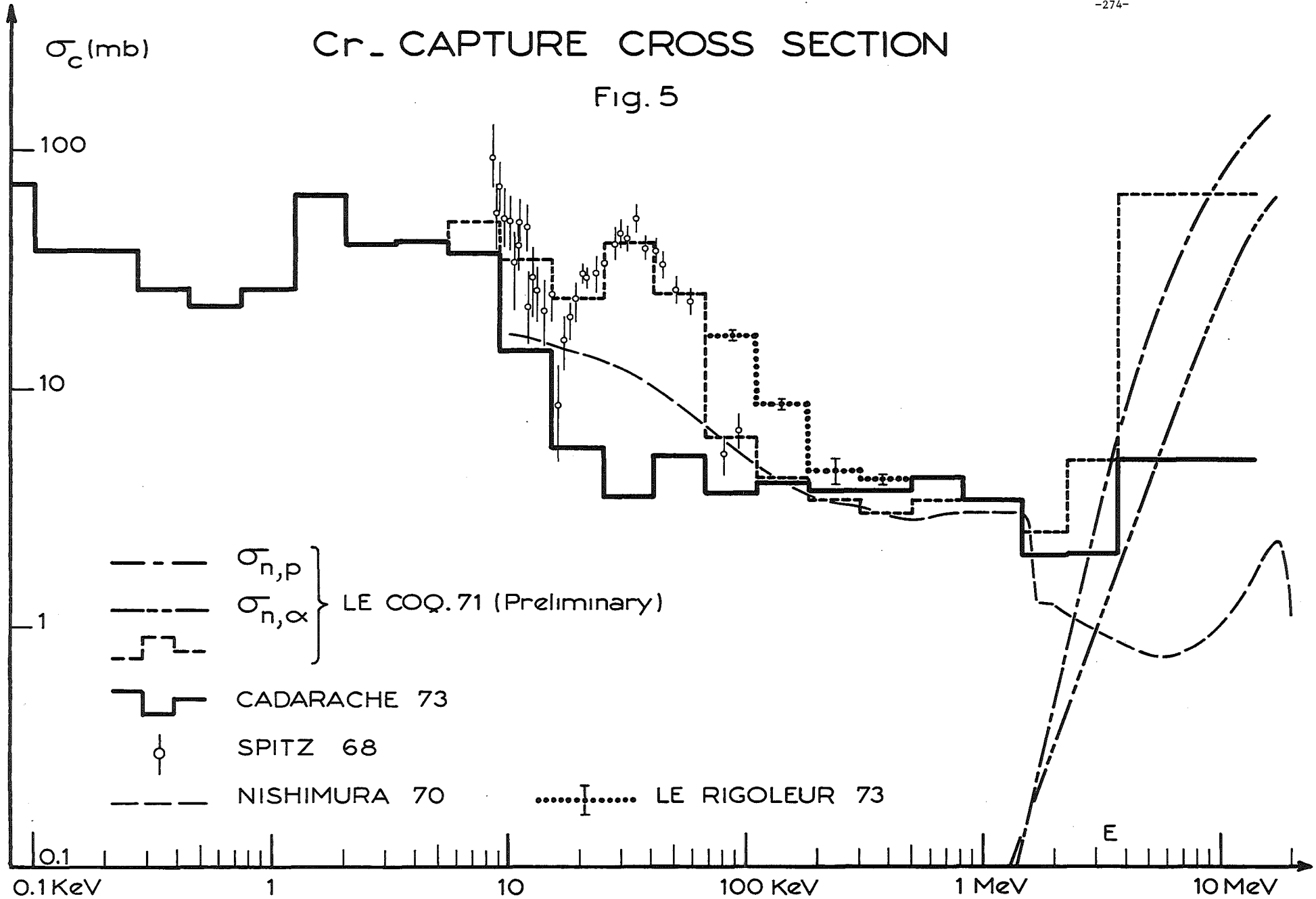


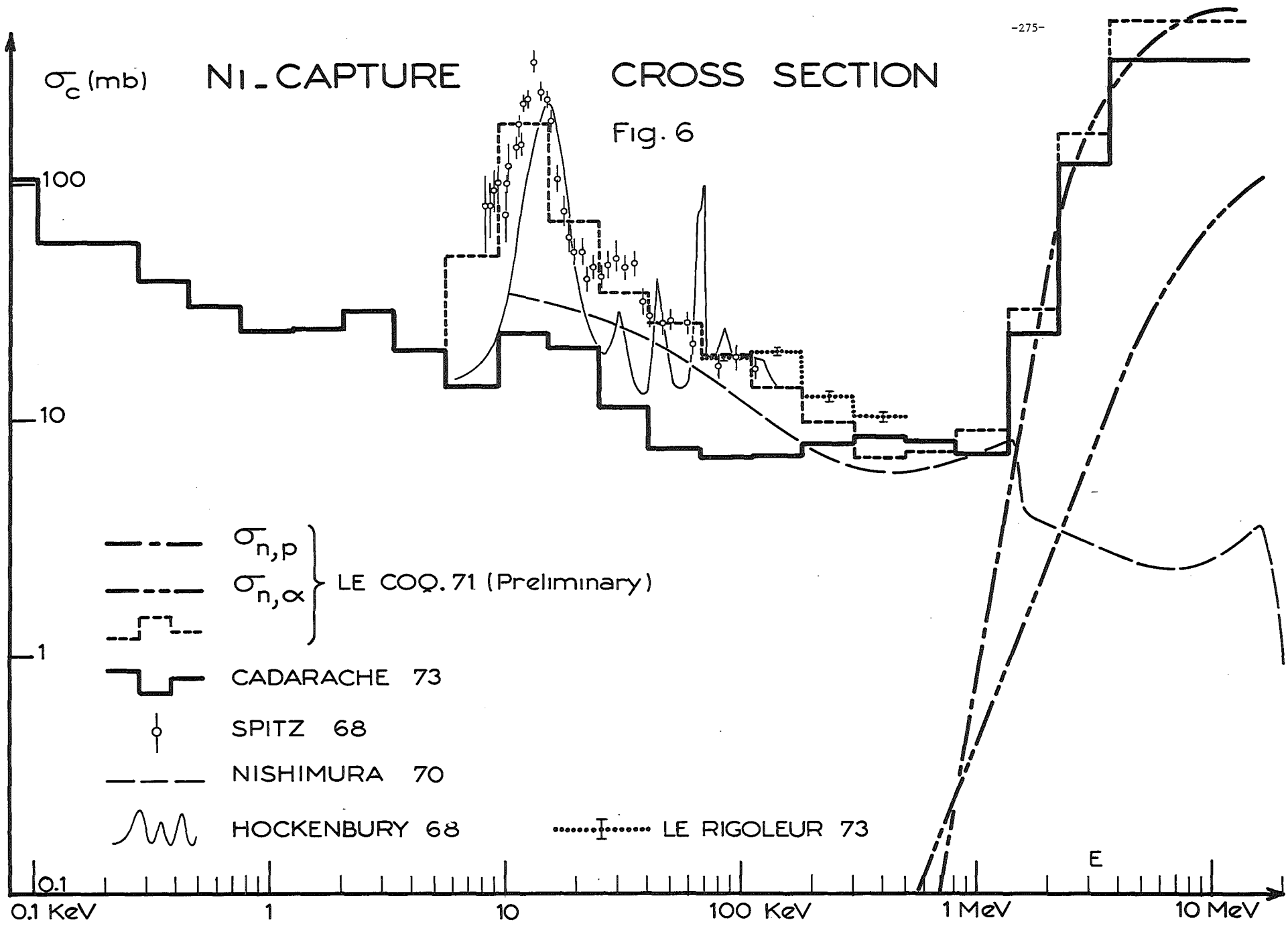
Fig.4 - Fe - CAPTURE CROSS SECTION



# Cr CAPTURE CROSS SECTION

Fig. 5





ON THE INFLUENCE OF THE CAPTURE CROSS SECTION  
OF IRON ON THE INTEGRAL PROPERTIES OF  
SOME FAST REACTOR CRITICAL ASSEMBLIES

by

H. Häggblom

AB Atomenergi, Studsvik, Fack, S-611 01 Nyköping, Sweden

Abstract

Calculations have been made on the sensitivities of fast reactor data to changes in the capture cross section of iron. ENDF/B-III neutron data library has been used for calculations on the FRO assembly, 10 on ZPR-III/32 and on the inner core of ZPPR-2. The SPENG library has been used for the ZPR-III cores 29, 35, 48, 53 and 55.

Contribution to the EACRP/EANDC working group meeting in  
Karlsruhe, May 8-9, 1973

## 1. Introduction

The atomic density of iron is in a large fast sodium cooled breeder of the order of 20 per cent. The parasitic absorption is 5-10 per cent of the total absorption. Because of the large uncertainties in the capture data [1, 2], it is important to investigate the effect of these uncertainties on fast reactor integral data. Extensive studies have been made by Rowlands et al. [2]. The iron cross sections in the UKNDL and ENDF/B-III are in many respects similar but it is important to note that the integral data are also dependent upon the neutron spectrum. Calculations using ENDF/B may therefore give results which differ from those obtained with the UKNDL.

The methods for calculating sensitivities to changes in neutron data are necessarily approximate. This is because there is need for calculations on a large number of nuclides, neutron reactions, and energy ranges. In the present work perturbation theory is used. The computer programme PERSEN calculates changes in  $k_{\text{eff}}$  using a spherical reactor model with one or two regions. The programme FUGUE [3] calculates changes in  $k_{\text{eff}}$ , reaction rate ratios, and reactivity worths using a fundamental mode approximation. Thus, the calculations on multi-zoned reactors were only concerned with the inner zone. They may still be of value because of the small flux gradients in the inner zones. Thus central reaction rate ratios are not essentially affected by the surrounding regions. For ZPPR-2 the change in  $k_{\text{eff}}$  has been calculated with FUGUE using the composition of the inner core zone only. The result is of course different from what it would be for the right composition, but it still gives an estimation of the requested accuracy of the cross sections concerned.

The assemblies considered in this work are mostly small and they have therefore a relatively hard neutron spectrum. The extrapolation of the sensitivities to a large reactor is very uncertain, but the iron content of the assemblies varies between very large limits. The result for a power reactor is therefore supposed not to be very far away from the range of the results obtained here.

## 2. Compositions and other fundamental data

The compositions of the uranium fuelled cores are given in Table 1 and the plutonium fuelled cores in Table 2. For ZPR-III/55 and ZPPR-2 only the innermost zones were considered. This is quite sufficient in the first case because  $B_m^2 = 0$  and there is virtually no influence from the outer zones. For ZPPR-2 the calculated  $B_m^2$  was also rather small. The other ZPR-III assemblies and the FRO assemblies had only one core zone. The reflector compositions are given elsewhere, e.g. in ref. 4. Table 3 gives the geometrical dimensions, the mass of fissile material, the cross section library used in the calculations, and the calculated  $k_{eff}$ . A short description of the data in the SPENG library is given in ref. 4. It is worth mentioning here that the iron data follow the J.J. Schmidt evaluation [5] up to 10 MeV. Thus, the capture cross section is in average much larger than in ENDF/B-III. The methods for obtaining  $k_{eff}$  with different corrections for heterogeneity etc are also given in ref. 4. No values for ZPPR-2 are given in Table 3 because only fundamental-mode evaluations were made. For this assembly ENDF/B-III data were used. The material buckling obtained was  $6.13 \cdot 10^{-4} \text{ cm}^{-2}$

For some central reaction rate ratios in ZPPR-2 the following values were obtained

$$\frac{\sigma_f^{28}}{\sigma_f^{49}} = 0.0217 \quad , \quad \frac{\sigma_f^{25}}{\sigma_f^{49}} = 1.110 \quad , \quad \frac{\sigma_c^{28}}{\sigma_f^{49}} = 0.1652 \quad , \quad \frac{\sigma_c^{49}}{\sigma_f^{49}} = 0.302$$

$$\frac{\sigma_c(\text{Fe})}{\sigma_f^{49}} = 0.0070$$

A figure which is important for the breeding ratio is the capture rate in  $^{238}\text{U}$  to the absorption in  $^{239}\text{Pu}$ . This value was 0.836 for the central material with the critical buckling value.

A remarkable result was the large value of  $k_{eff}$  for ZPR-III/32 using ENDF/B-III. This assembly has the highest iron content of all. The result indicates that the capture cross section of iron may be too low.

For comparison with the work by Takano and Ishiguro, published for this meeting, calculations of the iron capture cross section have been made for different values of the background cross section,  $\sigma_0$ . The cross sections are obtained in the following way. Starting from ENDF/B-III an intermediate library was produced. This library contains both point-by-point and self-shielded group cross sections. The latter type of data were produced for iron in the region 35-60 keV, using the single-level resonance formula. J-functions were calculated using the intermediate resonance approximation. For infinite background cross section the contribution from each resonance was assumed to be confined to the energy group considered. For finite values of  $\sigma_0$  the tails of the resonances were allowed to contribute to the cross sections of adjacent groups. Therefore, shielding factors cannot be correctly calculated for this region. In the rest of the resonance region point-by-point cross sections were calculated using the multilevel formalism. Then, having obtained an intermediate library, group cross sections were calculated for the whole energy region of interest. This was done by considering homogeneous mixtures of iron and a fictitious atom with unit atomic weight and the potential cross section was then given by the atomic ratio between the two nuclides. The weighting function in the group cross section calculation was inversely proportional to the total macroscopic cross section. The capture cross sections obtained are given in Table 7.

### 3. Sensitivity calculations

The sensitivity of an integral quantity  $I_i$  to a change in a neutron data  $\sigma_n$  is defined by the expression

$$S_{i,n} = \frac{\sigma_n}{I_i} \frac{\partial I_i}{\partial \sigma_n}$$

$I_i$  may also include data describing the neutron spectrum. In the present work only  $k_{\text{eff}}$  and reaction rate ratios were included. Changes in  $k_{\text{eff}}$  were obtained by the usual first order perturbation theory. Hereby the computer programme PERSEN was normally used. It is limited to spherical geometry and two regions. Changes in reaction rate ratios were obtained by general perturbation theory, developed by Usachef [6] and by Gandini [7]. The corresponding computer code FUGUE [3] is zero-dimensional.

The index  $n$  defines a given reaction and a given energy group. In order to limit the size of the matrix  $S_{i,n}$  the number of energy groups were limited to six. When using the SPENG library the energy boundaries were: 10 MeV, 0.82 MeV, 0.183 MeV, 41 keV, 9.1 keV, 0.75 keV and 0.04 eV. In the later calculations with the ENDF/B library the two lowest boundaries were changed to 2.03 keV and 1.5 eV.

The sensitivities of  $k_{\text{eff}}$  to a 1 % change in the iron capture cross sections are given in Table 4. It is important to note that the values for ZPPR-2 are about as large as those for ZPR-III/29 and ZPR-III/32 which have much larger iron contents. Thus, the size of the assembly is very important. Further, the contribution is largest in the lowest energy group for the plutonium fuelled assemblies and for FRO/10. The total sensitivities are for three of the assemblies of the order of  $2 \cdot 10^{-4}$ . That means that a 100 per cent change in the iron capture cross section changes  $k_{\text{eff}}$  by about 2 %.

Tables 5 and 6 give the sensitivities of some central reaction rate ratios for FRO/10 and ZPPR-2. It is seen that they are of the same order as the sensitivities of  $k_{\text{eff}}$ . The sensitivity of the ratio (capture rate in  $^{238}\text{U}$ /absorption in  $^{239}\text{Pu}$ ) was  $2.44 \cdot 10^{-4}$  for ZPPR-2.

#### 4. Conclusions

The requested accuracy of the capture cross section of iron is of course dependent upon the accepted uncertainty in the integral data. For  $k_{\text{eff}}$  a usually accepted uncertainty is 1 %. To this error there are, however, contributions from a large number of sources. It seems reasonable to assume that the contribution from  $\sigma_c(\text{Fe})$  should not be larger than 0.1 or 0.2 %. Then the allowed error is about 10 %. The contributions from different energy regions are of course not coherent. If the correlation between errors in different energy ranges is small the allowed partial errors can be several times larger.

The influence from uncertainties in  $\sigma_c(\text{Fe})$  upon uncertainties in reaction rate ratios including the breeding ratio is not of major importance. The uncertainties in  $\sigma_c(^{238}\text{U})$  and  $\alpha(^{239}\text{Pu})$  are still overwhelming the influences from errors in other data.

#### 5. References

1. Moxon, M.C.: Capture cross sections of structural materials. Sec. International Conference on Nuclear Data for Reactors, Helsinki, June 1970. Proc. IAEA, Vol. II, p. 815 (1970)
2. Campbell, C.G. and Rowlands, J.L.: The relationship of microscopic and integral data. Op.cit. Vol. II, p. 391
3. Häggblom, H.: Adjustment of neutron cross section data by a least square fit of calculated quantities to experimental results. Part I: Theory. AE-422 (1971)
4. Häggblom, H.: Adjustment of neutron cross section data by a least square fit of calculated quantities to experimental results. Part II: Numerical results. AE-439 (1971)

5. Langner, I., Schmidt, J.J. and Woll, D.: Tables of evaluated neutron cross sections for fast reactor materials.  
KFK 750 (1968)
6. Usachef, N.: Perturbation theory for the breeding factor, and other ratios of a number of different processes in a reactor.  
Atomn. En. 15, p. 472 (1963)  
J. Nucl. En., 18, p. 571 (1964)
7. Gandini, A.: A generalized perturbation method for bi-linear functionals of the real and adjoint neutron fluxes.  
J. Nucl. En., 21, p. 755 (1967)

Table 1: Atomic densities times  $10^{-22}$  for the uranium fuelled cores

Core No.	$^{238}\text{U}$	$^{235}\text{U}$	Ni	Fe	Cr	Al	Na	O	C	H
FR0/10	1.963	0.498	0.048	1.489	0.096			1.619	0.187	0.374
ZPR-III 29	0.479	0.2386	0.227	1.499	0.380	1.471		1.392		
32	0.032	0.4445	0.747	4.917	1.245					
35	0.014	0.1949	0.456	3.009	0.761		0.782	0.398		

Table 2: Atomic densities times  $10^{-22}$  for the plutonium fuelled cores

Core No.	$^{242}\text{Pu}$	$^{241}\text{Pu}$	$^{240}\text{Pu}$	$^{239}\text{Pu}$	$^{238}\text{U}$	$^{235}\text{U}$	Mo	Ni	Fe	Mn	Cr	Si	Al	Na	C
ZPR-III 48		.0010	.0106	.1649	.7406		.0206	.1308	.9899		.2658		.0110	.6230	2.0765
53		.0011	.0107	.1661	.2610	.0006	.0208	.0814	.7474	.0078	.1859	.0091	.0111		5.5811
55 <sup>x)</sup>		.0005	.0051	.1069	1.5380	.0003		.0839	.6177		.1896		.0111		3.7269
ZPPR-2 <sup>x)</sup>	.00018	.00154	.01117	.08433	.55549	.00123	.0231	.1221	1.2576	.0209	.2702	.0137	.0003	.8796	.0030

x) inner zone

Table 3: Geometrical dimensions, mass of fissile material, cross section library used and calculated  $k_{eff}$  for the assemblies considered

Core No.	Cyl.rad. cm	Cyl.height cm	Rad.blank. cm	Ax.blank. cm	Sph.rad. cm	Mass kg	X-sect. library	$k_{eff}$
FRO/10	20.30	38.70	30	39		112.2	ENDF/B-III	0.9982
ZPR-III			30	30				
29			30	30	46.89	402	SPENG	0.9971
32			30	30	30.84	213	ENDF/B-III	1.0516
35			30	30	53.50	485	SPENG	1.0089
48	41.71	76.35	30	30	46.70	277.3	SPENG	1.0029
53	34.37	60.96	30	30		149.15	SPENG	1.0207
55							SPENG	0.970 <sup>x)</sup>

<sup>x)</sup>  $k_{\infty}$  for the inner zone

Table 4: Sensitivity  $S \cdot 10^5$  of  $k_{\text{eff}}$  to a 1 % change in the iron capture cross sections

Energy group	FR0/10	ZPR-III/29	ZPR-III/32	ZPR-III/35	ZPR-III/48	ZPR-III/53	ZPR-III/55	ZPPR-2 inner core
1	-0.97	- 1.92	- 3.90	- 0.95	-0.68	- 0.89	- 0.72	- 1.93
2	-1.19	- 3.42	- 7.40	- 4.23	-1.51	- 0.85	- 0.77	- 3.30
3	-0.89	- 3.83	- 5.56	- 2.68	-1.37	- 1.09	- 1.03	- 3.43
4	-0.62	- 8.71	- 2.40	- 2.30	-0.90	- 3.34	- 3.04	- 2.52
5	-0.40	- 1.69	- 0.74	- 0.18	-0.39	- 2.06	- 1.55	- 1.22
6	-3.27	- 1.09	- 1.29	- 0.84	-4.60	- 7.52	- 4.64	- 7.79
Total	-7.34	-20.66	-21.29	-11.18	-9.46	-15.75	-11.75	-19.91

Table 5: Sensitivity  $S \cdot 10^5$  of central reaction rate ratios in FRO/10 to a 1 % change in the iron capture cross sections

Energy group	Changes in	
	$\sigma_f^{28}/\sigma_f^{25}$	$\sigma_c^{28}/\sigma_c^{25}$
1	-0.59	0.05
2	1.38	-0.13
3	1.03	-0.27
4	0.75	-0.29
5	0.52	-0.16
6	2.94	-0.32
Total	6.03	-1.12

Table 6: Sensitivity  $S \cdot 10^5$  of central reaction rate ratios in ZPPR-2 to a 1 % change in the iron capture cross sections

Energy group	Changes in the following rrr:s			
	$\sigma_f^{28}/\sigma_f^{49}$	$\sigma_f^{25}/\sigma_f^{49}$	$\sigma_c^{28}/\sigma_f^{49}$	$\sigma_c^{49}/\sigma_f^{49}$
1	- 0.98	-0.047	0.10	0.12
2	3.51	-0.292	- 0.54	- 0.68
3	3.97	-0.975	- 2.10	- 2.86
4	2.90	-1.175	- 2.81	- 4.59
5	1.39	-0.695	- 1.40	- 3.20
6	8.90	-4.588	- 6.47	-22.86
Total	19.69	-7.772	-13.22	-34.07

Table 7: Capture Cross Sections at Different  $\sigma_0$  and at 300 °K

ABBN Group No.	Energy Range (keV)	$\sigma_c$ (mb)			
		$\sigma_0 = \infty$	1000 b	100 b	10 b
6	400 - 800	5.00	5.00	5.00	5.00
7	200 - 400	5.70	5.70	5.70	5.69
8	100 - 200	5.83	5.83	5.84	5.83
9	46.5 - 100	8.98	8.97	8.91	8.65
10	21.5 - 46.5	16.43	16.49	15.22	12.41
11	10.0 - 21.5	4.94	4.94	4.90	4.65
12	4.65 - 10.0	21.31	21.24	20.71	18.70
13	2.15 - 4.65	6.72	6.72	6.71	6.62
14	1.0 - 2.15	298.28	283.42	208.89	111.61

E A C R P W O R K I N G G R O U P M E E T I N G

on

The keV capture of the structural materials Ni, Fe, Cr

Karlsruhe, May 8-9th, 1973

The Reliability of Calculated Central  
Reactivity Coefficients of Structural Materials.

The Sensitivity of Ni, Fe, Cr Material Worths  
to Uncertainties in the Cross Section Data.

M.HEINDLER

Institut für Theoretische Physik und  
Reaktorphysik, Technische Hochschule  
in G r a z

Reaktorinstitut des Forschungszentrums  
G r a z  
(Austria)

## Abstract

Central reactivity coefficients (CRCs) of structural materials Cr, Fe, Ni and stainless steel are studied for a number of fast reactor assemblies. The discrepancies between measured and calculated material worths are discussed. In order to localize possible sources of error, the relative contribution of absorption, elastic and inelastic scattering as well as the sensitivity of the material worths to errors in cross section data is brought in relation to the amount of disagreement between theory and measurement.

## 1. Introduction and conclusions

The accuracy requested for integral reactor parameters such as global breeding gain,  $k_{eff}$ , critical enrichment etc. contrasts with the actual uncertainties with respect to the keV absorption cross section data of structural materials. There is strong evidence that the fairly good agreement between measured and calculated integral reactor parameters specific for stainless steel 72/18/10 (SS 304) is due to compensation of errors and somewhat artificial, since it is the result of a cross section data adjustment based on these very parameters.

This paper deals with this problem by presenting the results of a study of central reactivity coefficients (CRCs) for a number of fast reactor assemblies of the ZPR III, VERA, MASURCA and ERMINE type. Most of this work was performed in 1969 and 1970 with the support of the CEA Cadarache. Since a very careful investigation of systematic errors has been performed, the main conclusions drawn in this paper should not have lost their weight although theoretical and experimental methods involved in CRC measurement and calculation have been improved in the meantime.

In 1969 J. Ravier suggested /1/ a modification of the absorption cross section data of Fe, Cr and Ni in the Cadarache cross section set Version 2. On the one hand this was done in view of

recent measurements of absorption cross sections of structural materials by Spitz et al. /2/, Moxon /3/ and Hockenbury /4/, on the other hand in view of the discrepancies between measured and calculated CRCs /5/. The extent of these modifications suggests that uncertainties regarding the basic data of structural materials have been so far assessed too optimistically (e.g. /6/).

In this paper we shall discuss briefly what is the influence of this modification on the calculated CRCs and, as a consequence, on the discrepancies between calculated and measured material worths.

After a detailed study of all possible sources of error due to the method of calculation, we draw the following conclusions:

- The uncertainties attached to the calculated CRCs (due to errors in cross section data) largely exceed the experimental errors.
- A fairly good agreement for stainless steel is in contrast to very poor results for Cr, Fe and Ni taken separately.
- The predictions of reactor parameters (as obtained with the actually available cross section data) should not be trusted if steel with a composition different from the usual one (72/18/10) is used and/or if cores having a volumic percentage of structural materials departing the usual range (~10 to 22 %) are considered.
- The adjustment of absorption cross sections alone will not permit one to obtain good agreement between calculated and measured CRCs in all types of real and adjoint spectra studied; scattering cross section data and/or the adjoint spectra are thought to contribute significantly to the discrepancies between theory and experiment.

As a consequence, we make the following suggestions:

- High priority should be given to improvements of keV absorption cross section data of structural materials, both of infinite dilute cross sections and of resonance self-shielding factors.
- The reliability of calculation procedures used for the calculation of the adjoint spectra should be checked.

- The influence of errors in the scattering cross section data of structural materials on the discrepancies between calculated and measured reactivity coefficients should be investigated.

## 2. Calculation of the Material Worths

In table 1 we have listed the essential characteristics of the reactor assemblies in the centre of which the reactivity coefficients of Cr, Fe, Ni and stainless steel (SS) are studied. This table shows, for each assembly, the nature of the fuel, the fuel enrichment, the central fission rate ratio U-238 to U-235 and the number of structural material atoms in the core material. In addition, it shows the ratio  $\phi_5^+$  to  $\phi_1^+$ , i.e. the importance of neutrons in the 5th energy group (ranging from  $\sim 500$  to  $\sim 800$  keV) relative to that of neutrons with energies exceeding  $\sim 3.7$  MeV. This last parameter is closely related to the shape of the neutron importance function vs. energy and it turns out to be an excellent classification parameter for the various reactor assemblies with respect to the objective of this study.

We performed our calculations on the basis of version 2 of the Cadarache cross section set (referred to as "standard version") and on the "modified" or "capturing" version of this set as defined by J.Ravier /1/. The transition leading from the standard to the modified (capturing) version is performed by multiplying the standard group constants by the factors given in table 2.

The effective equivalent cross sections of the various assemblies are computed in a cell calculation. In general, these cells are supposed to be geometrically homogeneous ("homogeneous cross sections"), whereas the resonance heterogeneity is always taken into account. Both the homogeneous and the heterogeneous cross sections were available only for Masurca 1 B at that time.

These flux weighted group constants are used for determining the space dependence of the real and the adjoint neutron spectra in the S4-approximation to the neutron transport theory.

The average of the perturbed neutron flux in the sample (a detailed

description of the structural material samples can be found in /5/) is calculated by means of a computer programme described in /7/, which is based upon a formulation of the transport equation in terms of collision probabilities and which assumes the incident neutron current to be isotropic and unperturbed.

Using the standard formulae for perturbation calculations, the CRCs of the structural materials Fe, Cr, Ni and SS are calculated and compared to measured worths.

### 3. Error Analysis

Before discussing the discrepancies between measured and calculated reactivity worths, we should emphasize that a very careful error estimation has been performed regarding errors due to imperfect calculation procedures. In the following, we shall briefly discuss these error sources. More details can be found in ref./5/.

#### 3.1 Sample Size Effects

For a few assemblies and a few samples we have checked our second order perturbation (SOP) theory by a straight forward calculation of the perturbed neutron flux with transport theory. Though we found SOP and direct calculation in fairly good agreement, an empirical correction procedure was established and applied to all SOP results.

#### 3.2 Self Shielding Factors

In the Cadarache cross section set, no resonance self shielding factors are defined for the absorption cross sections of Cr and Ni, and only a few (from 15 to 500 keV) for Fe.

On the assumption that for a given dilution the effect of absorption self-shielding is about the same for Cr and Ni as it is for Fe, the range of uncertainty due to partial or total absence of absorption resonance self-shielding is estimated.

#### 3.3 Correct Dilution of the Cross Sections of the Sample Material

The reactivity effect per gramme of a sample depends not only

on the size of the sample, but also on the concentration of the sample material in the vicinity of the sample.

At the time this study was performed, there were no computer programmes available for a calculation of the exact "mean dilution" of the sample cross sections in the case of structural materials. Therefore we used for the perturbation calculations the group constants of the sample material at the dilution of this very material in the core surrounding the sample. This is referred to as "core dilution".

A very conservative error estimate is then obtained by doing the perturbation calculations once again, this time with the sample group constants at zero dilution.

For the reference material (U-235 in uranium samples), the SOP calculations could be done with the correct dilution which was calculated by a computer programme by A.Khairallah /8/. In all instances, the difference between SOP results based on group constants at the exact dilution and on those at the core dilution, did not exceed significantly 1 % for U-235. In most instances the errors due to self-shielding and dilution of the sample (§ 3.2 and § 3.3 resp.) do not exceed 5 % for Fe, 10 % for Cr and 20 % for Ni.

#### 3.4 Heterogeneity Effects Caused by the Heterogeneous Structures of the Region Surrounding the Sample

In Masurca 1B all materials worths are calculated twice: once with "homogeneous" and once with "heterogeneous" cross sections, ie. with cross sections defined in a homogenized cell and in a cell with the actual heterogeneous structure taken into account, respectively.

The discrepancies between the "homogeneous" and "heterogeneous" results for CRCs did not exceed a few percent in any case.

#### 3.5 Space dependence of neutron flux

The accuracy of the space dependence of the neutron flux, in particular of the perturbed neutron flux, was checked by a straight forward neutron transport calculation. Neglecting the influence of

the sample on the incident neutron current leads in general to an error inferior to the experimental error. Nevertheless all calculated material worths given in this paper are corrected for this effect using an interpolation scheme established empirically.

### 3.6 Energy Dependence of the Neutron Importance Function

The accuracy of the energy dependence of the calculated adjoint neutron flux was not investigated at that time. We therefore refer to E.Kiefhaber who stated in a recent paper /9/ that a typical degree of uncertainty attributed to usual few-group (e.g. 25-group) CRC calculations is  $\sim 5\%$  for Cr and Fe and  $\sim 10\%$  for Ni. These values were obtained for the ZPR III-48 assembly. In the ZPR III-48 real and adjoint spectra hardly any compensations occur between the reactivity effects of absorption, elastic and inelastic scattering. The contribution of the elastic scattering to the reactivity effect is relatively small because of compensations between the energy groups. Therefore a higher degree of uncertainty than the one listed by Kiefhaber is to be expected for assemblies with adjoint spectra involving higher contribution of the elastic scattering to the CRC of the sample.

## 4. Results

In figures 1 to 4 we have compiled for Cr, Fe, Ni and stainless steel 304 (72 % Fe, 18 % Cr, 10 % Ni) respectively, the ratio C : E, i.e. calculated to measured central reactivity coefficient. The error bars indicate the experimental uncertainties as they are listed in refs. /10/ to /33/.

One observes that the ratio C : E as a function of our classification parameter has about the same shape for all materials:

- If calculated with the standard cross sections, the ratio C : E slightly decreases with increasing parameter  $\phi_5^+ : \phi_1^+$ , i.e. with increasing slope of the adjoint neutron flux at high energies.
- If calculated with the modified absorption cross sections, the ratio C : E increases with increasing classification parameter value.

Furthermore fig. 1 shows that the agreement between calculation and experiment could be improved

- for small values of the parameter  $\phi_5^+ : \phi_1^+$  by increasing the standard absorption cross sections.
- for large values of the parameter by decreasing the standard absorption cross section.

This means that by simply adjusting the absorption cross sections one can never fit experimental and calculated results in the whole range of real and adjoint spectra investigated in this paper.

This incompatibility of correction requirements is found for the other structural materials as well. Thus we are led to the conclusion that errors in the scattering cross sections and/or (much more likely) in the calculation of the neutron importance function may contribute largely to the disagreement between calculated and measure central reactivity coefficients.

Figs. 1 to 4 show a relatively good agreement between theory and experiment for stainless steel 304 as compared to a relatively poor agreement for iron, chromium and nickel taken separately.

Evidently the good agreement for stainless steel is artificial and due to a compensation of errors. We conclude therefrom that for other types of steel (i.e. for another Fe-Cr-Ni percentage) theoretical results would be much less in agreement with experimental results.

Fig.5 to 8 give again C : E as a function of the classification parameter, this time together with the uncertainties arising from calculation procedures as discussed in § 3; in particular they give

- the upper limit of the uncertainties due to the treatment of absorption resonance self-shielding (partial or total absence of shielding factors, poor knowledge of the correct dilution)
- the upper limit of the uncertainties due to the treatment of scattering resonances (poor knowledge of the correct dilution)

In the lower half of these figures one finds the ratio C : E for the sample materials Cr (fig.5), Fe (fig.6), Ni (fig.7), and stainless steel 304 (fig.8) calculated with the standard cross sections, in the upper half one finds the same ratios calculated with the modified ("capturing") cross sections.

It can be stated that uncertainties due to imperfect calculation procedures (resonance self-shielding, dilution, second order perturbation calculation, heterogeneity) are important, but do not explain the whole extent of discrepancies between calculated and measured material worths. This conclusion should be correct even if the effect of errors in the adjoint flux calculation were taken into account.

If one would like to make a more sophisticated error analysis, one has to look at the contributions of the absorption, the elastic and the inelastic scattering to the CRCs. This will also lead to a better understanding of the meaning of our classification parameter. Figs. 9 to 13 illustrate the absolute contributions of absorption, elastic and inelastic scattering to the CRCs of Cr, Fe, Ni and SS, respectively. These figures show that the classification parameter  $\phi_5^+ : \phi_1^+$  classifies the critical assemblies according to the relative contribution of the absorption effect and to the absolute contribution of the effect of elastic and inelastic scattering to the structural material worths in these assemblies.

Therefore the assemblies are arranged with respect to the amount of compensation between the three effects contributing to the danger coefficient and, consequently, with respect to the sensitivity of the reactivity effect to uncertainties regarding the group constants. This statement might be important for answering the question whether or not absorption group constants should be adjusted by minimizing the discrepancies between calculated and measured material worths.

We think that it is reasonable to adjust absorption cross section data using CRCs if a careful analysis is performed for each of the assemblies under consideration. The objective of this analysis should be to assure that discrepancies between calculation and measurement come predominantly from errors specific to absorption cross section data. As can be seen from figs. 9 to 11, the value of the classifica-

tion parameter  $\sigma_5^+$  :  $\sigma_1^+$  might be one of the criteria whether the CRCs obtained in a given assembly should be used in an adjustment procedure.

The last results we present in this paper concern the sensitivity of the calculated material worths of Cr, Fe and Ni to uncertainties in the absorption cross sections and the importance of this kind of uncertainties as compared to the experimental errors.

In Table 3 we have listed some results, in particular the relative deviation of the material worth calculated with the modified cross section set with respect to the one calculated with the standard one. We have compared these "numerical error widths" to the experimental error widths as they are reported in refs. /10/ to /33/.

If one accepts that the difference between the "standard" and the "modified" absorption cross sections of Fe, Cr and Ni is a measure for the extent of uncertainty regarding our knowledge of the cross sections of structural materials, then this table tells us that the resulting uncertainty regarding calculated material worth exceeds in all but a few assemblies the experimental error widths. Figs. 12 to 14 illustrate this statement. This leads us to the last conclusion of this paper: The error widths due to faulty cross section data and to crude approximations in the calculation procedures largely exceed the experimental error widths. Further refinements of CRC measuring techniques might be postponed to improvements of CRC analysis.

#### Acknowledgement

I acknowledge the support of the CEA that enabled me to perform this study.

R e f e r e n c e s

- /1/ J.Ravier, private communication
- /2/ L.M.Spitz et al., Nucl.Phys. A 121 (1968), 655.
- /3/ M.C.Moxon, EANDC Conference, Antwerpen 1965, p.88.
- /4/ R.W.Hockenbury et al., Phys. Rev. 178 (1969), 1746.
- /5/ M.Heindler, PNR/SETR R.040 (1970), CEA Cadarache
- /5a/ M.Heindler, PNR/SETR R.033 (1969), EURFNR 699.
- /6/ J.Y.Barré, PNR/SETR R.026 (1968), CEA Cadarache.
- /7/ M.Heindler, Act.Phys.Austr., 33, p.349 (1971).
- /8/ A.Khairallah, private communication.
- /9/ Kiefhaber, KFK 1759 (1973), Karlsruhe.
- /10/ R.L.Mc Vean, W.G.Davey, G.J.Fischer, IAEA Symposium, Amsterdam 1963, Proceedings - Vol.1, p.85.
- /11/ J.K.Long, A.R.Baker, W.Gemmel and al., IAEA-Symposium, Vienna 1961 -Physics of fast and intermediate reactors Proceedings Vol.1 -SM 18/48
- /12/ R.Böhme and al., Proceedings of a symposium, Karlsruhe 1967 - Fast reactor physics, Vol.II-SM 101/8.
- /13/ Reactor physics constants  
ANL 5800 - p.602-604.
- /14/ J.K.Long and al., 2nd U.N. Conference on the peaceful uses of atomic energy, Proceedings Vol.12, P/598.
- /15/M.H.Mc Taggart and al., AWRE Report No R5/66, July 1966.
- /16/ P.I.Amundson and al., ANL 6337 (May 1961).
- /17/ J.M.Gasldo, J.K.Long, Mc Vean R.L., ANL 6338 (October 1961).
- /18/ P.I.Amundson, W.Gemmel, J.K.Long, ANL 6690 (1963)
- /19/ R.J.Huber, J.K.Long, R.L.Mc Vean, ANL 6401 (May 1961).
- /20/ T.A.Doyle, A.L.Hess, ANL 6669 (February 1963).
- /21/ Idaho division summary report october 1961 through september 1962, ANL 6706.
- /22/ R.M.Adams, Reactor development Program, Progress report, October 1966, ANL 7267.

- /23/ A.L.Hess, W.P.Keeney, P.Caumette, ANL 7044 (March 1966).
- /24/ P.Caumette, T.Lacapelle, J.Boyer, Rapport PNR/SETR 65/046, December 1965, CEA Cadarache.
- /25/ R.L.Mc Vean, A.Weitzberg, J.A.Kremser, ANL 7248 (March 1967).
- /26/ R.M.Adams, Reactor development program, Progress report February 1966, ANL 7176.
- /27/ A.M.Broomfield and al., Proceedings of the International Conference on Fast critical experiments and their analysis, October 1966, Argonne.
- /28/ J.Y.Barré, private communication.
- /29/ Reactor development program, Progress report, July 1967, ANL 7357.
- /30/ Reactor development program, Progress report, September 1967, ANL 7302.
- /31/ Reactor development program, Progress report, November 1967, ANL 7399.
- /32/ Reactor development program, Progress report, September 1968, ANL 7500.
  
- /33/ A.L.Hess, J.M.Gasidlo, American Nuclear Society 9th Annual Meeting, Salt Lake City 1963.

Table 1

CHARACTERISTICS OF THE ASSEMBLIES

Assembly	(1)	(2)	(3)	(4)	(5)
ZPR III - 5	U 235	17.9	.07055	.01039	.8196
11	U 235	11.7	.03852	.00779	.6152
12	U 235	20.9	.04619	.00779	.7301
25	U 235	8.8	.03109	.00779	.5993
30	U 235	39.5	.04225	.02089	.8920
ZPR III - 31	U 235	38.8	.04443	.02091	.8664
32	U 235	93.3	.04332	.06909	.9514
33	U 235	93.1	.04867	.05 24	.9568
34	U 235	31.2	.03408	.02097	.8847
35	U 235	93.3	.02907	.04226	1.0210
ZPR III - 41	U 235	17.0	.03921	.01193	.7135
44	U + Pu		.07297	.01697	.9221
47	Pu	17.2	.02366	.01424	.8105
48 A	Pu	19.2	.03015	.01383	.8167
48 B	Pu	19.7		.01388	.8113
ZPR III - 49	Pu	19.2	.03312	.01371	.8014
50	Pu	19.2	.02632	.00991	.8285
VERA - 1 B	U 235	92.9	.0701	.00851	1.0263
5 A	U 235	92.9	.0455	.00851	1.1453
MASURCA - 1 B	U 235	30.3	.03432	.00581	.9607
ERMINE II U2 Bloc G	U 235	30.3	.0175 <sup>+</sup>	.006127	1.4469 <sup>+</sup>
Bloc de graphite	U 235	30.3	.0144 <sup>++</sup>		.9233 <sup>++</sup>

- (1) ... fissile material
- (2) ... enrichment (a/o)
- (3) ... fission ratio U8:U5
- (4) ... number of Cr-, Ni- and Fe atoms per ccm of core material
- (5) ... classification parameter  $\phi_5^+$ :  $\phi_1^+$
- + ... in the middle of the bloc G (reduced density graphite)
- ++ ... in the middle of the graphite bloc

TABLE 2

CORRECTION APPLIED BY / 1/ TO THE GROUP CONSTANTS OF THE STANDARD VERSION "2" OF THE CADARACHE CROSS SECTION SET (Standard version multiplied by given correction factors leads to the reviewed version)

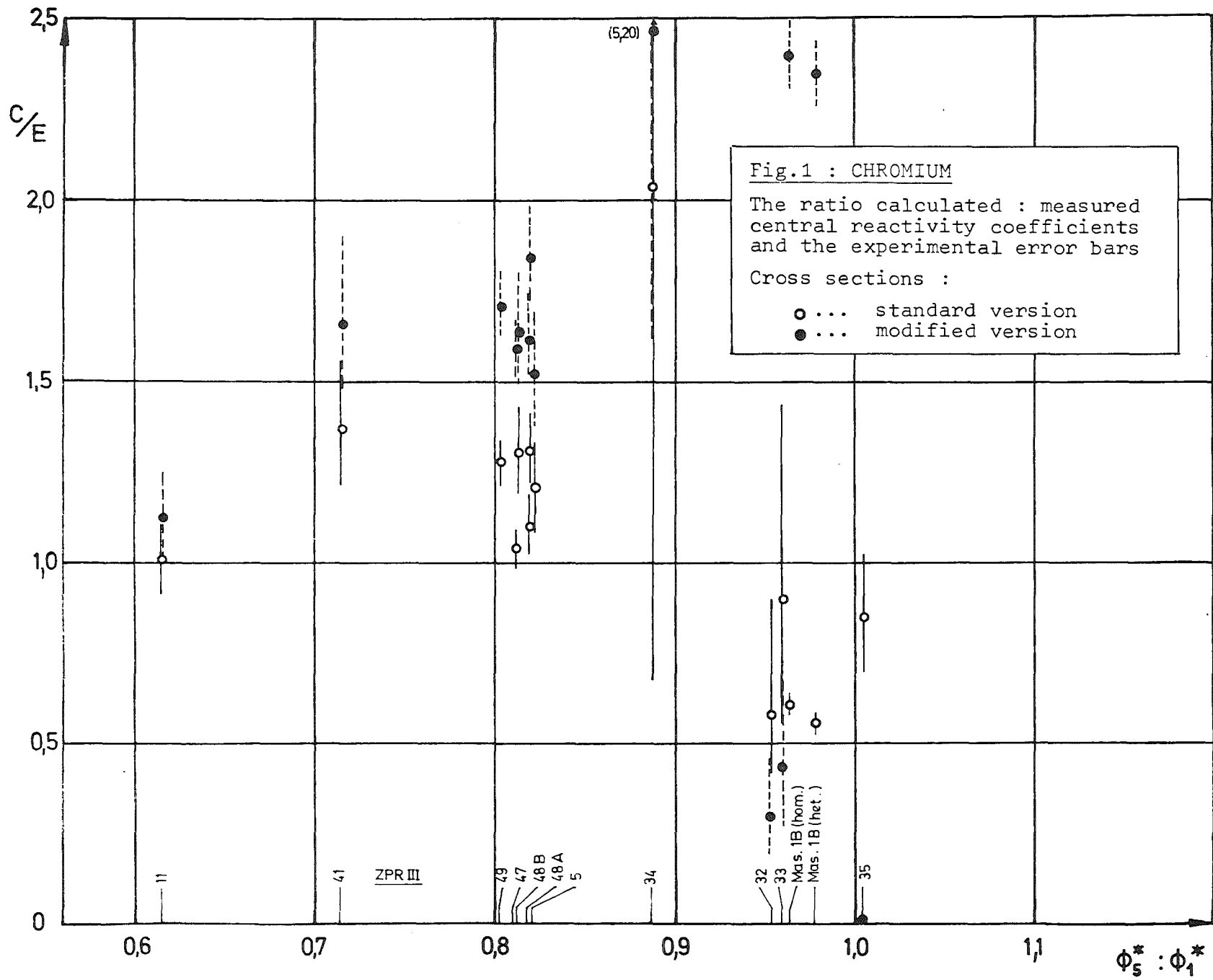
ENERGY GROUP	Fe	Cr	Ni
4		1.2	
5		1.1	
6		1.25	
7	1.18	1.35	1.2
8	2.0	1.45	1.65
9	2.58	2.05	2.62
10	3.28	4.8	2.92
11	3.6	12.5	2.75
12	3.45	3.8	1.7
13	7.6	2.8	2.24
14	1.72	2.5	1.
15	1.36	1.7	1.
16	1.3	1.6	3.
17		1.6	.25
18		1.5	1.56

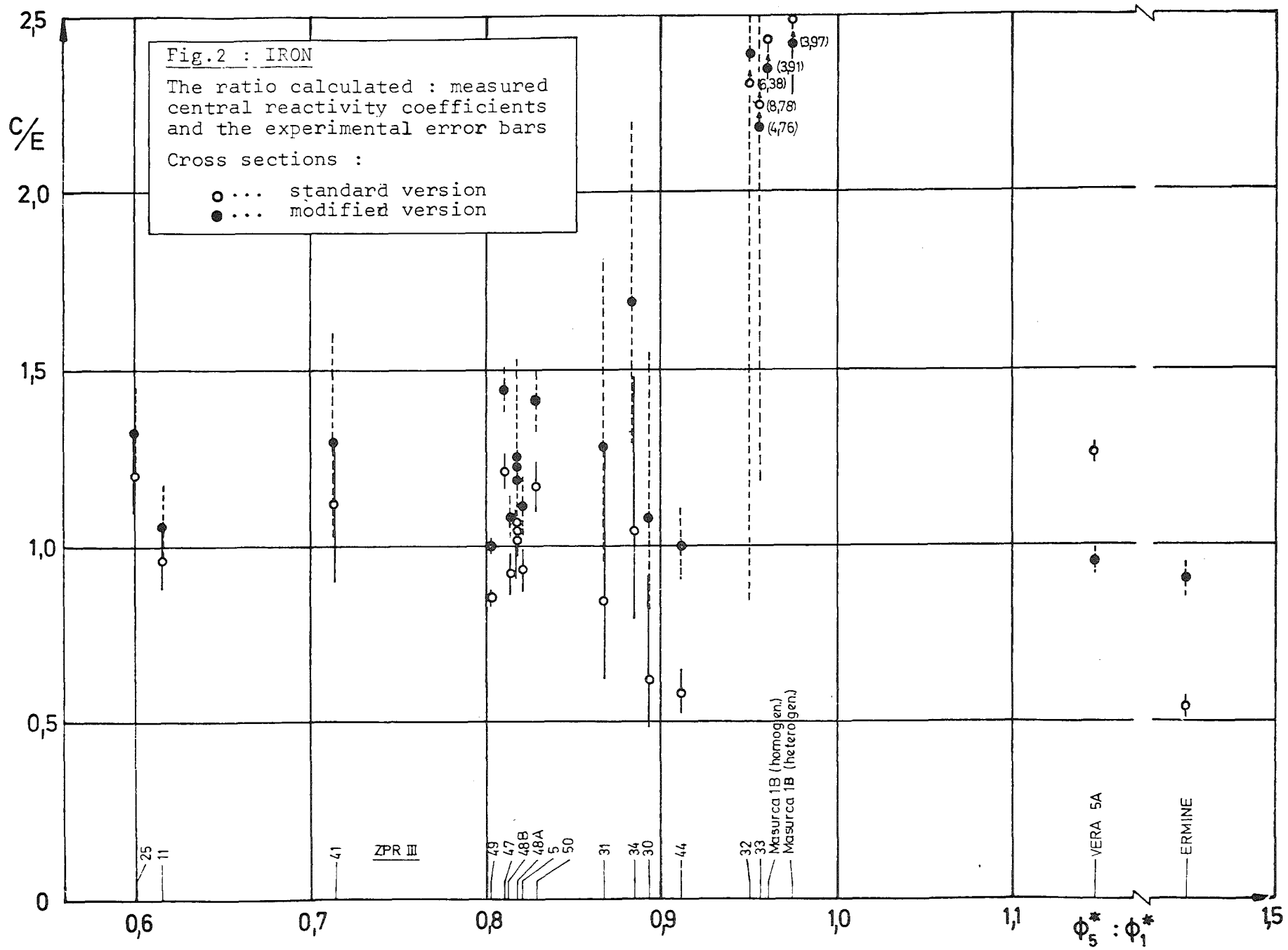
TABLE 3

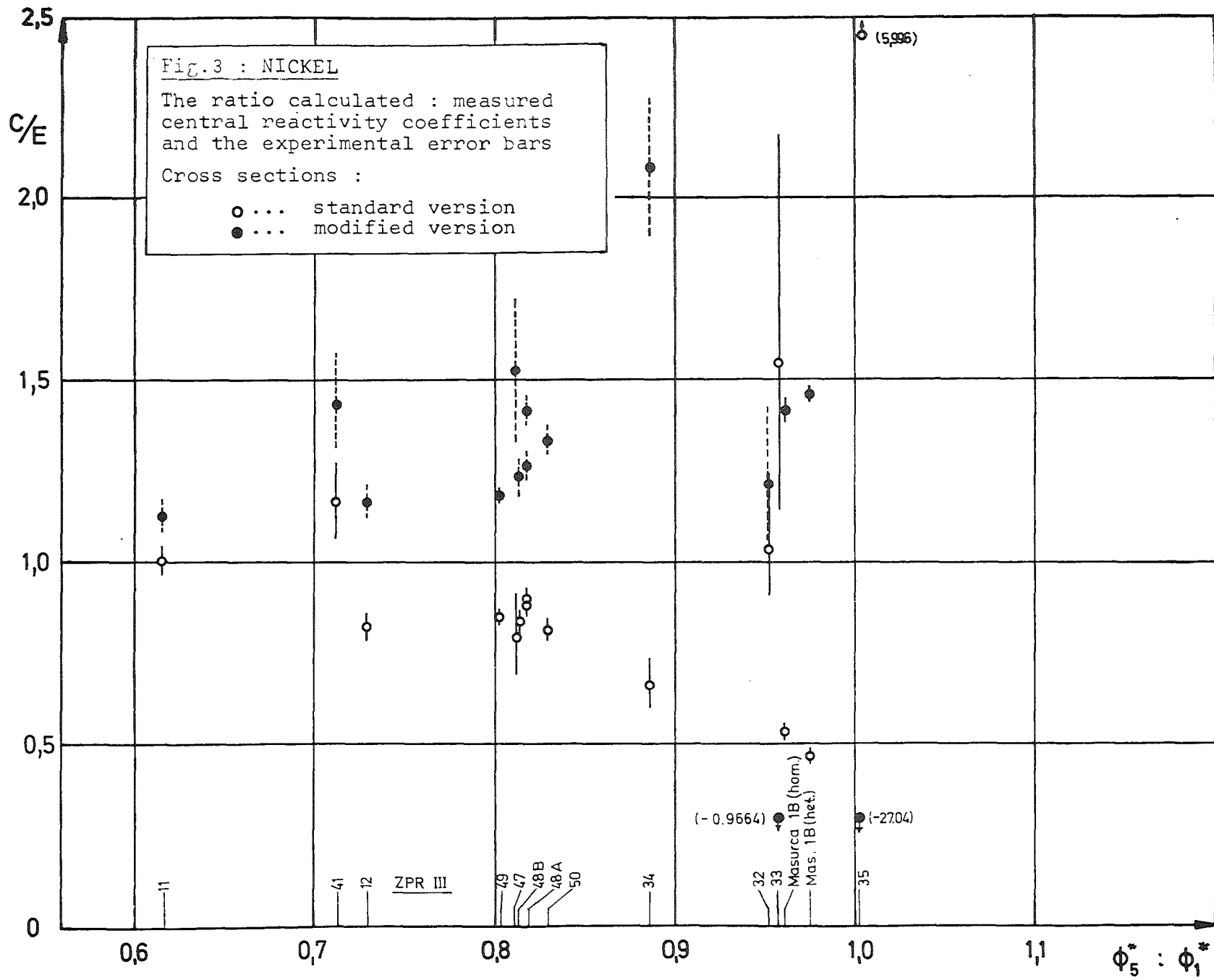
SENSITIVITY OF MATERIAL WORTHS TO VARIATIONS  
 IN ABSORPTION CROSS SECTIONS (as given in  
 Table 5) COMPARED TO EXPERIMENTAL UNCERTAINTIES  
 (as given in/10/ through /33/)

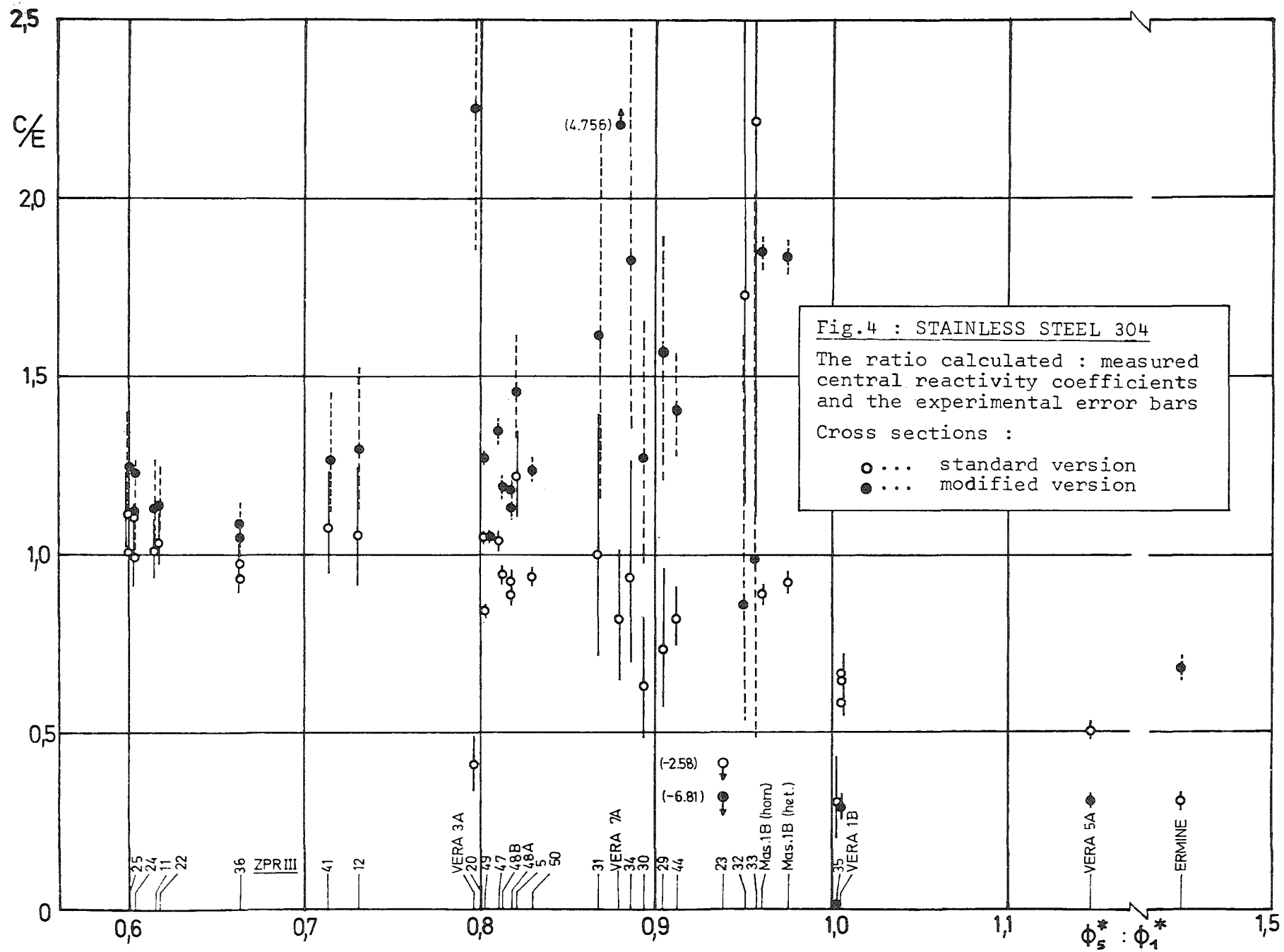
ASSEMBLY	Fe		Cr		Ni	
	theor. (%)	exp. (%)	theor. (%)	exp. (%)	theor. (%)	exp. (%)
ZPR III - 25	10.0	9	-	-	-	-
11	10.1	6	11.7	6	13.1	5-
41	15.2	31	21.2	-	23.4	-
12	-	-	-	-	41.7	-
49	17.1	.4	34.0	4	39.0	1
ZPR III - 47	19.3	2	52.9	5	93.1	5
48 B	17.6	5	25.5	8	48.2	2
48 A	17.9	2	46.4	6	61.0	1
5	19.4	-	25.7	-	-	-
50	20.3	4	-	-	63.7	2
ZPR III - 31	52.0	33	-	-	-	-
34	62.5	37	150.0	-	216.0	9
30	75.0	25	-	-	-	-
44	72.0	8	-	-	-	-
ERMINE II U2 Bloc de graphite	-	-	-	-	211.9	-
ZPR III - 32	-62.0	125	-49.1	12	16.9	14
33	-45.8	250	-52.4	23	-162.6	36
MASURCA 1 B	60.9	7	293.0	-	164.4	1
ZPR III - 35	-85.9	45	176.7	-	-551.0	-
VERA 1 B	279.4	13	-57.9	13	-783.4	13
VERA 5 A	-24.9	2	-	-	-	11
ERMINE II U2 Bloc G	66.2	4	-	-	420.4	2

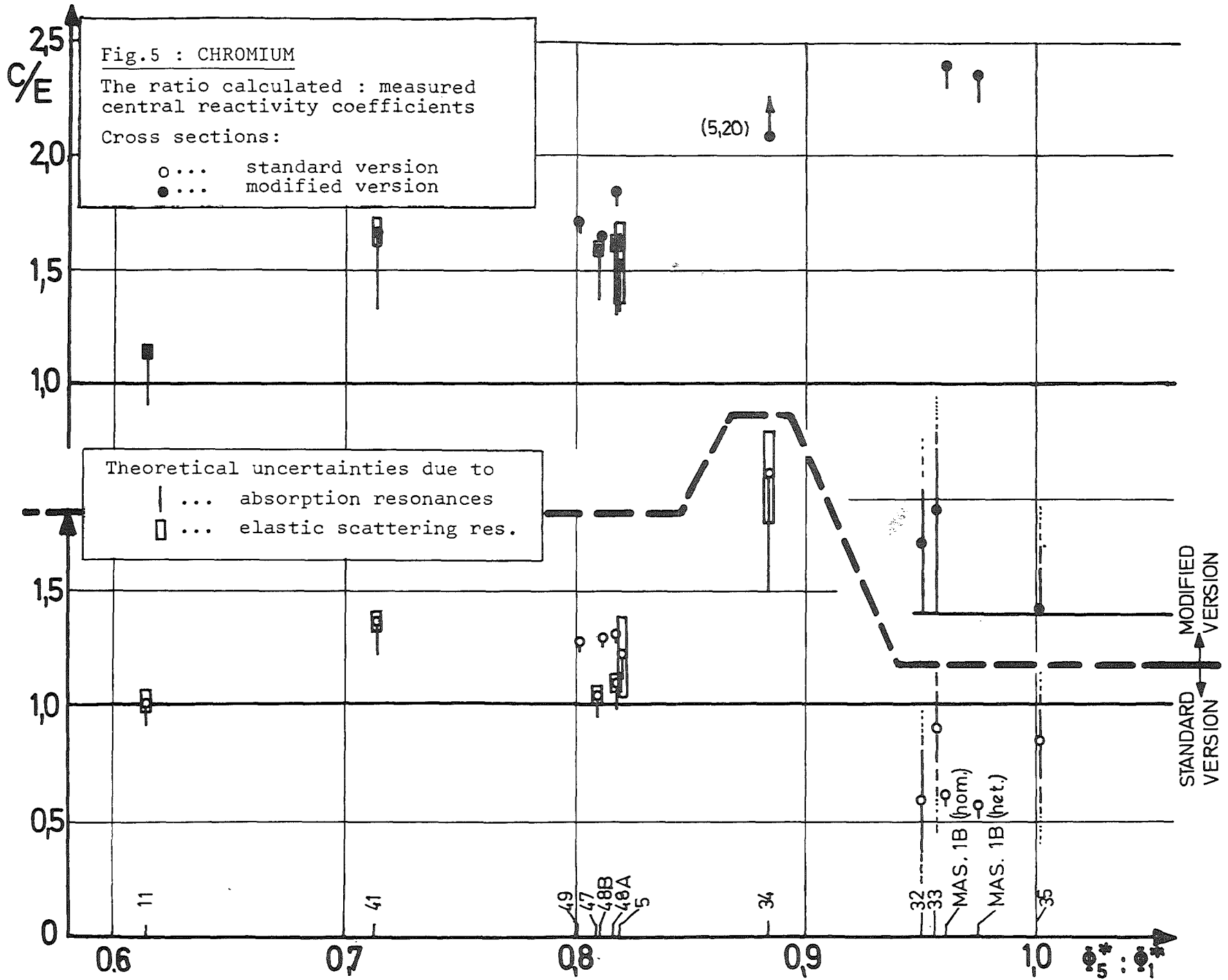
"theor." ... [(CRC)<sub>modif.</sub> - (CRC)<sub>standard</sub>] : (CRC)<sub>standard</sub> [%]

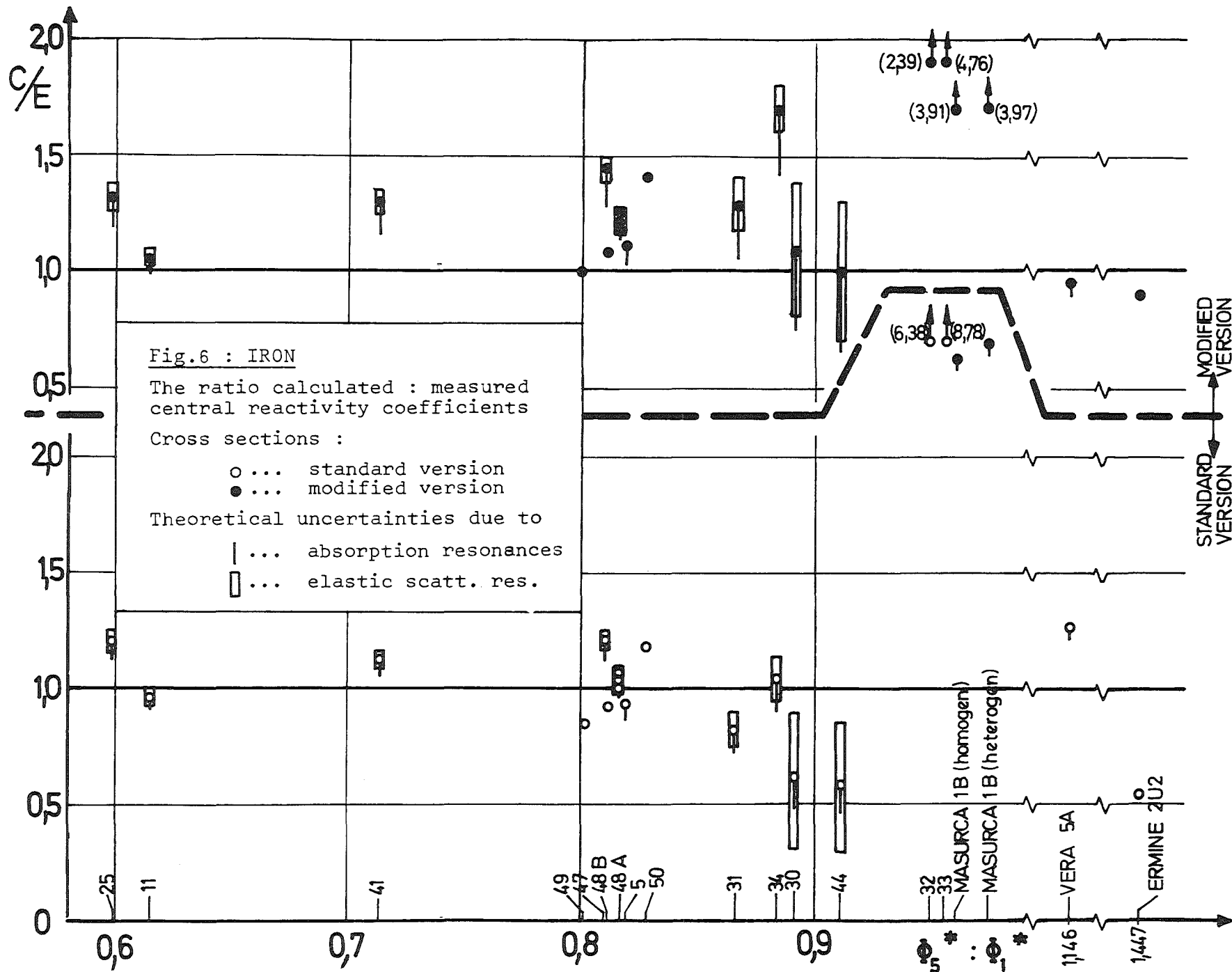


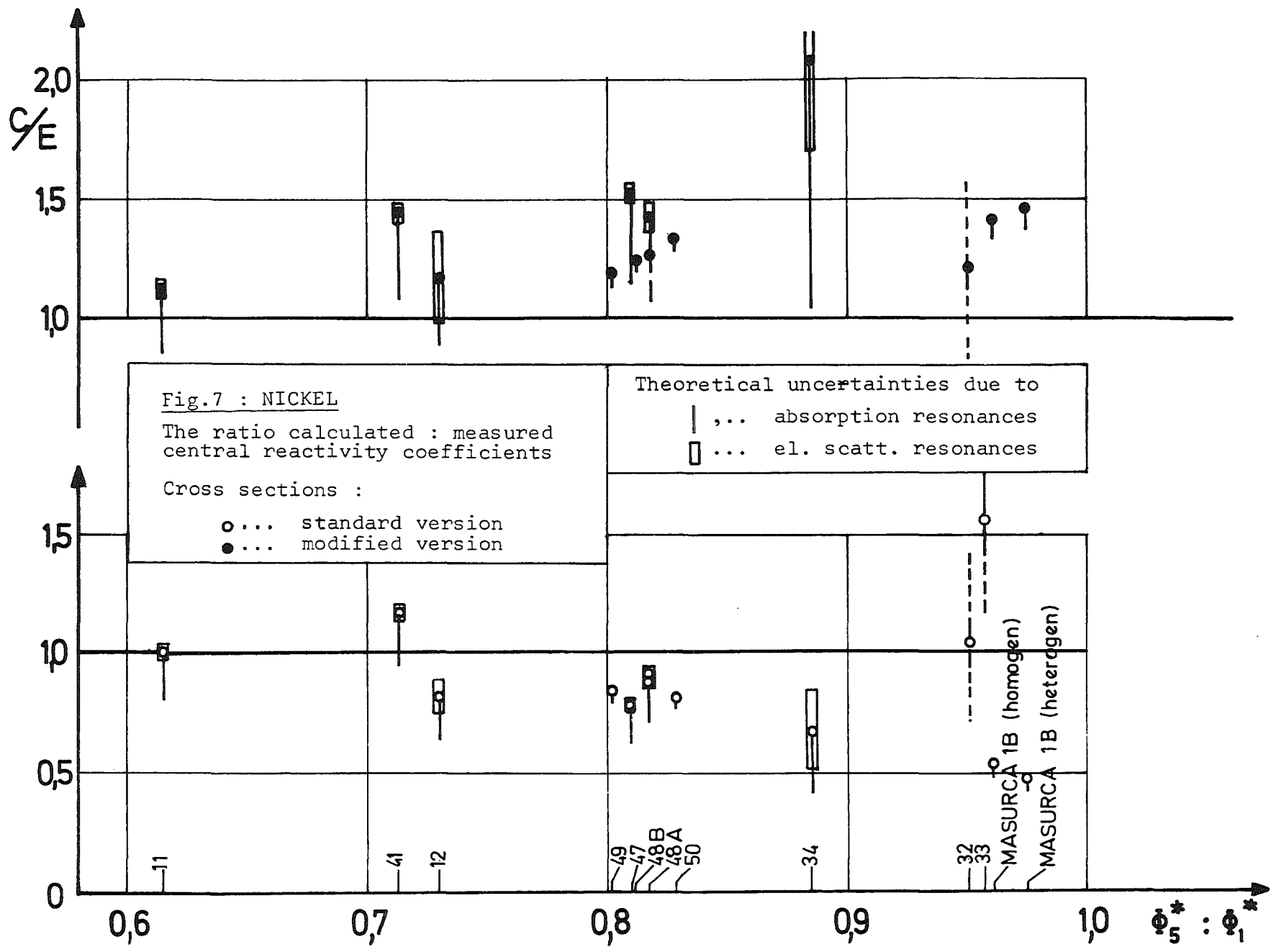


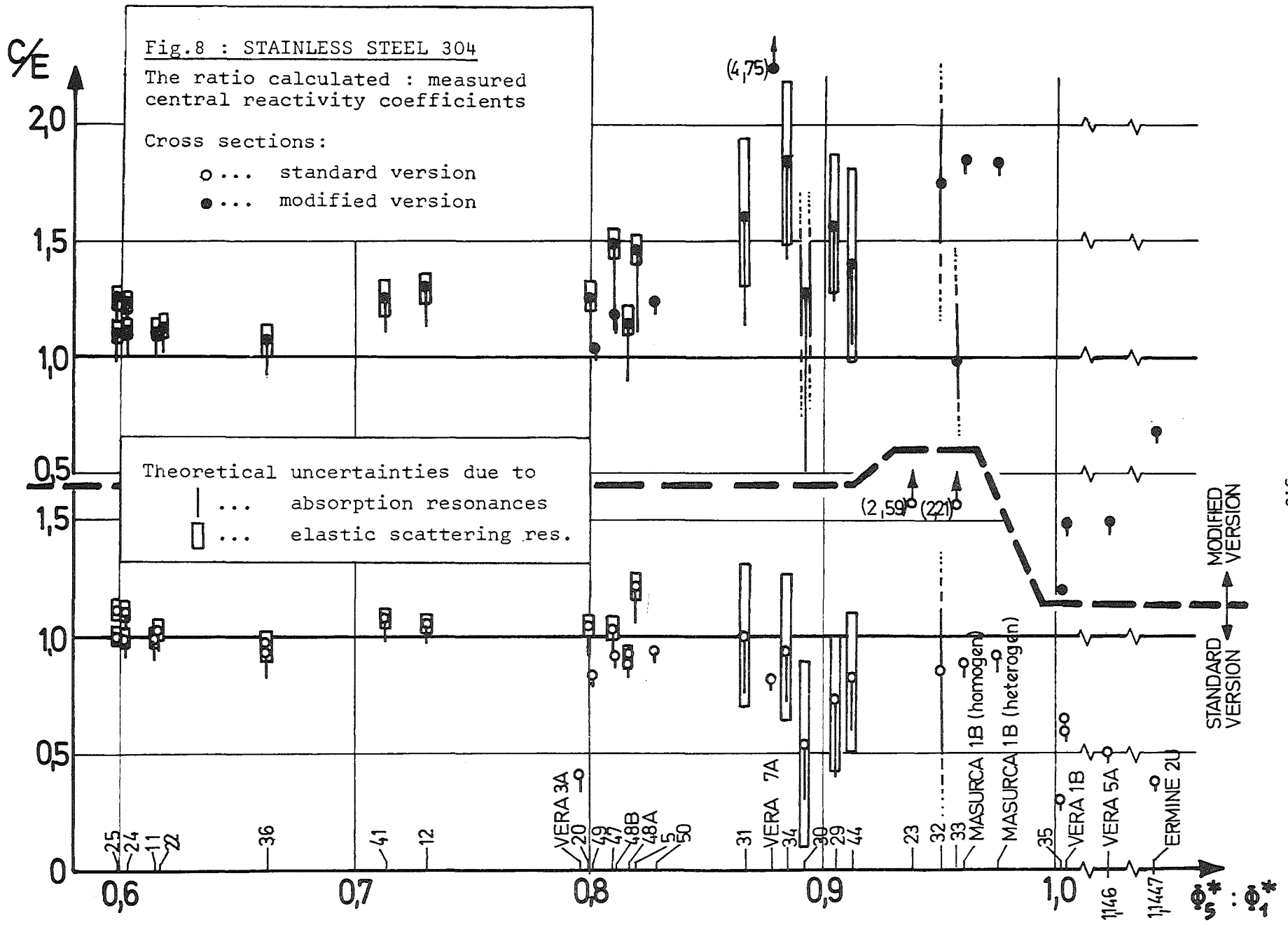












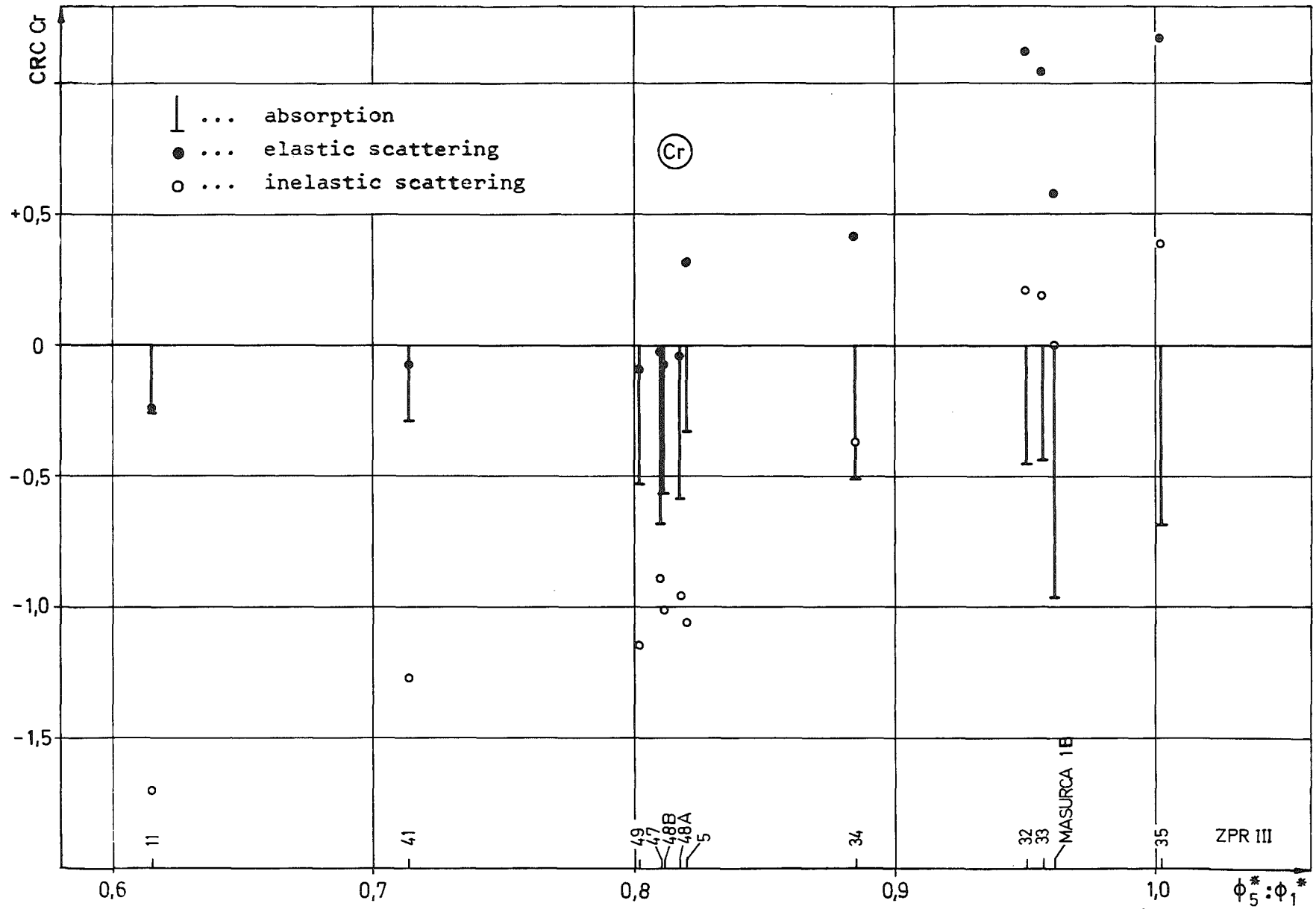


Fig.9 : CHROMIUM. Contributions to the central reactivity coefficient ( $\times 10^3$ )



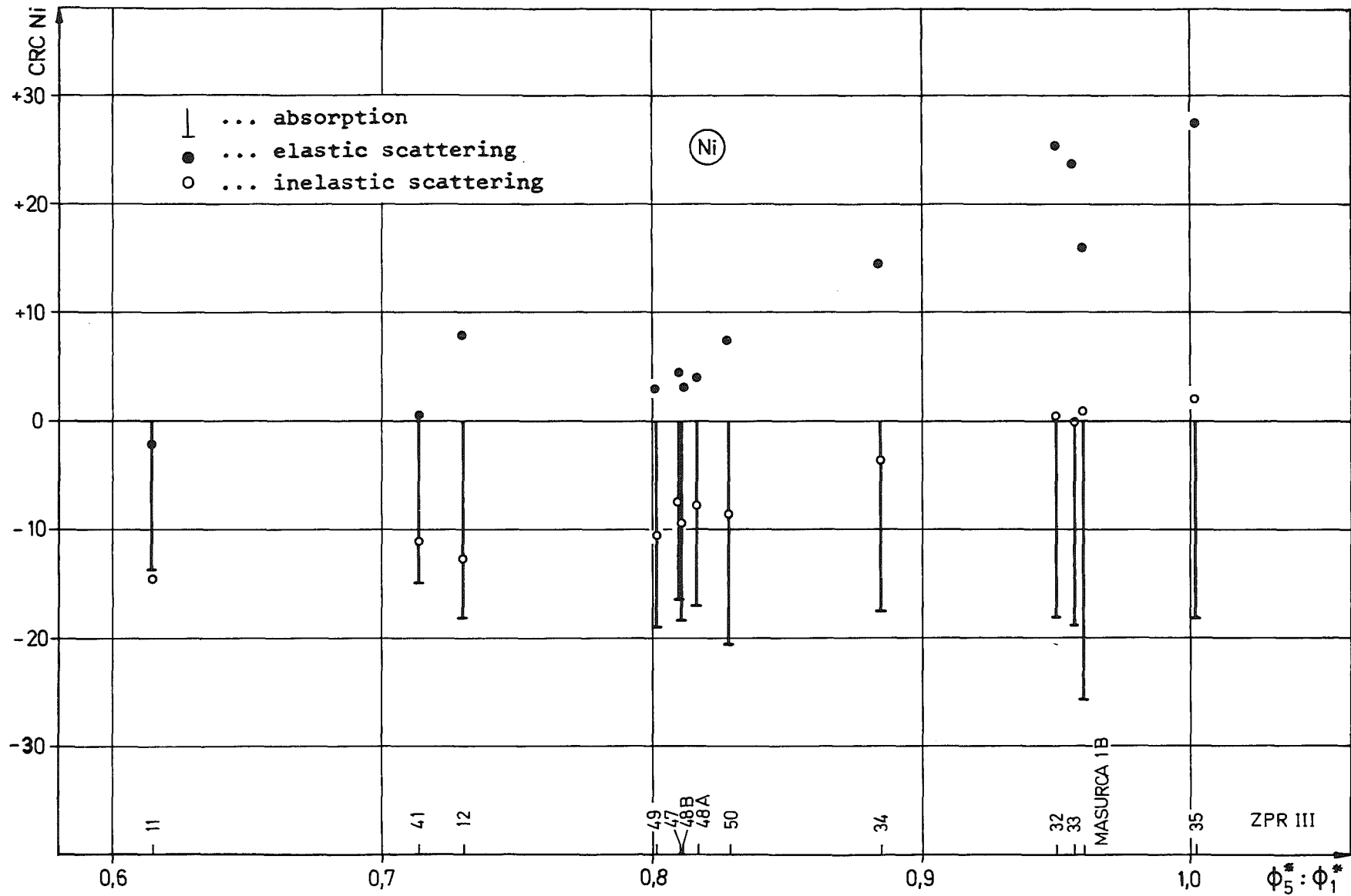


Fig.11 : NICKEL. Contributions to the central reactivity coefficient (  $\times 10^3$  )

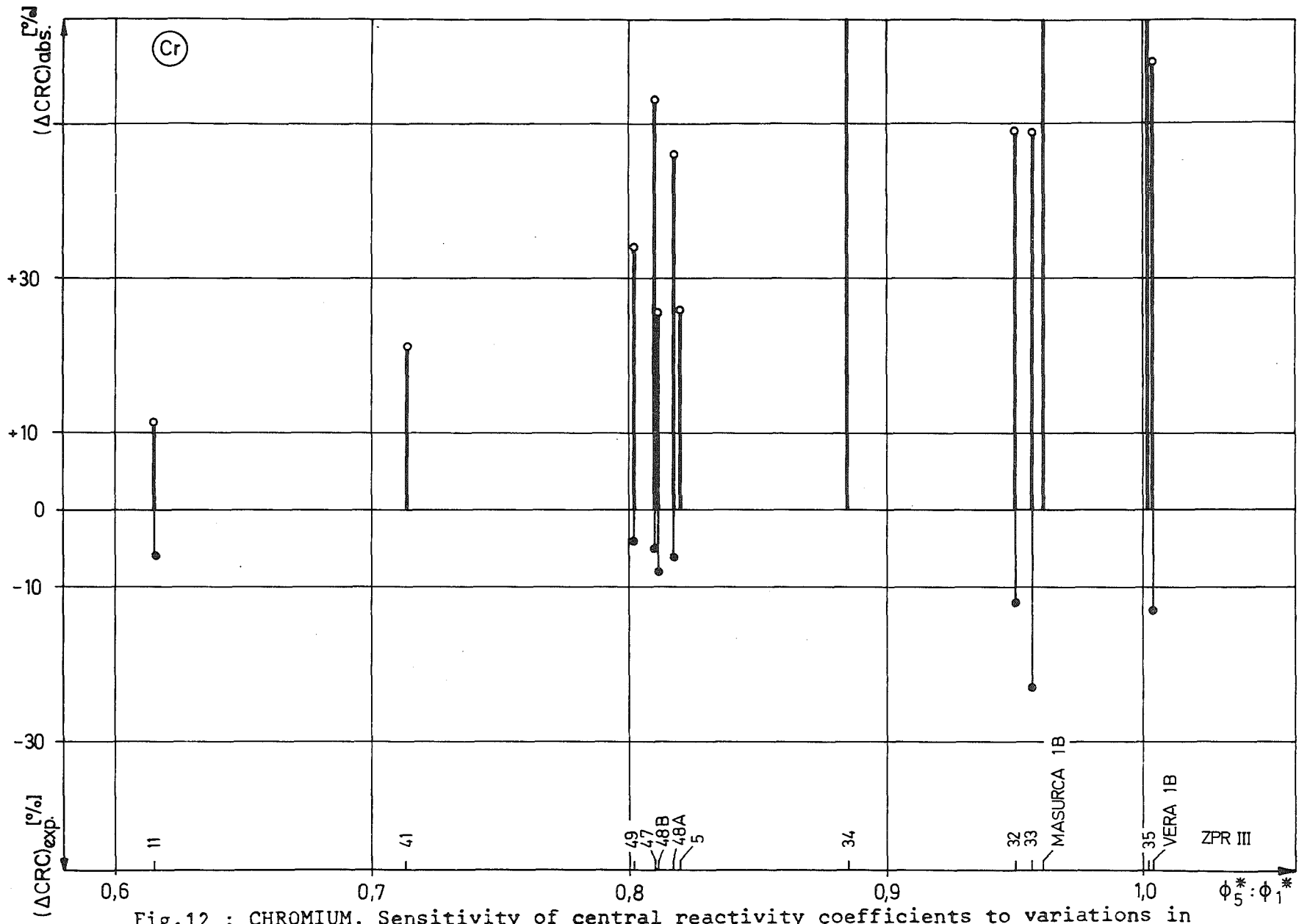


Fig.12 : CHROMIUM. Sensitivity of central reactivity coefficients to variations in absorption cross sections as compared to experimental uncertainties.

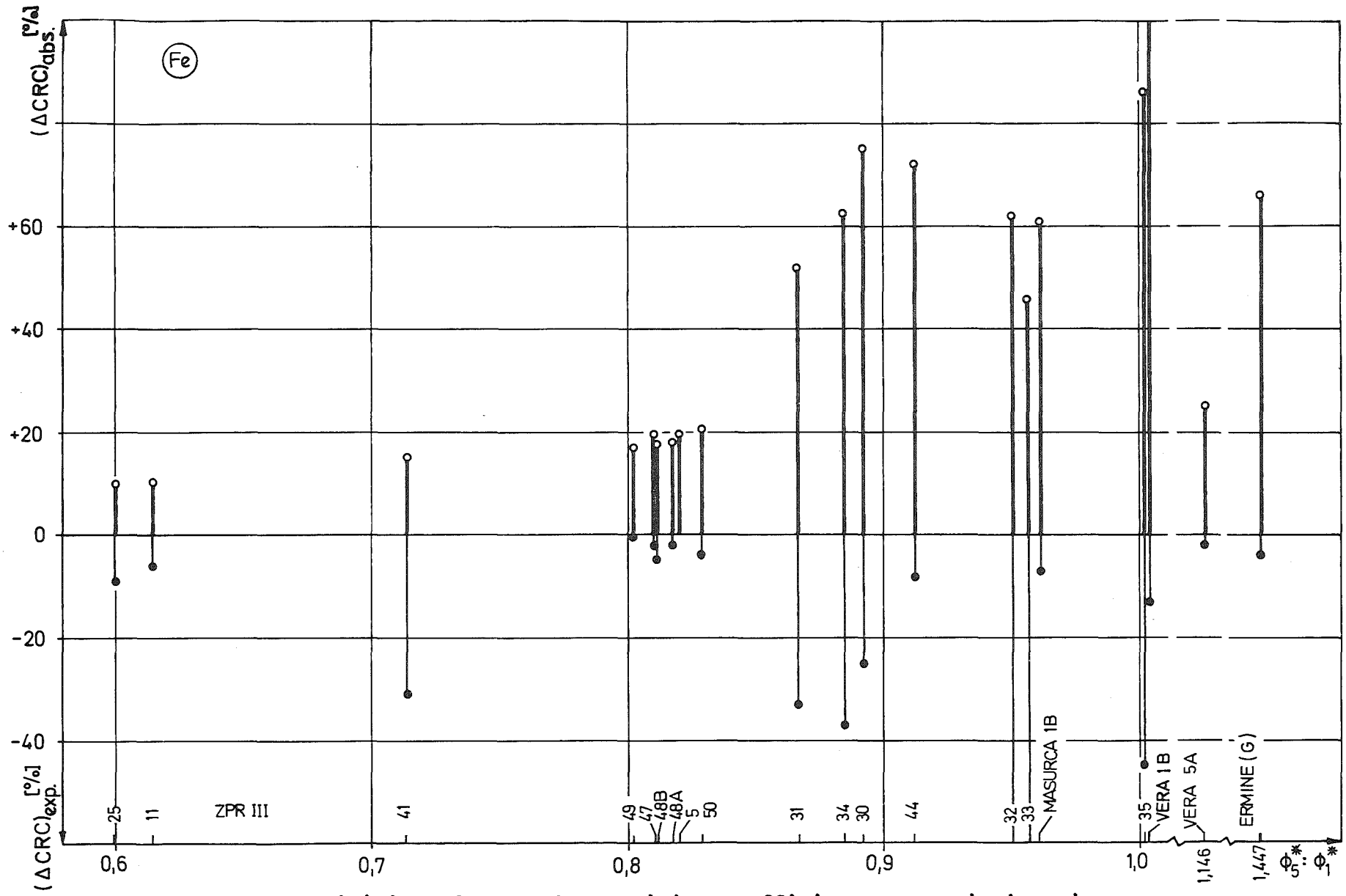


Fig.13: IRON. Sensitivity of central reactivity coefficients to variations in absorption cross sections as compared to experimental uncertainties.

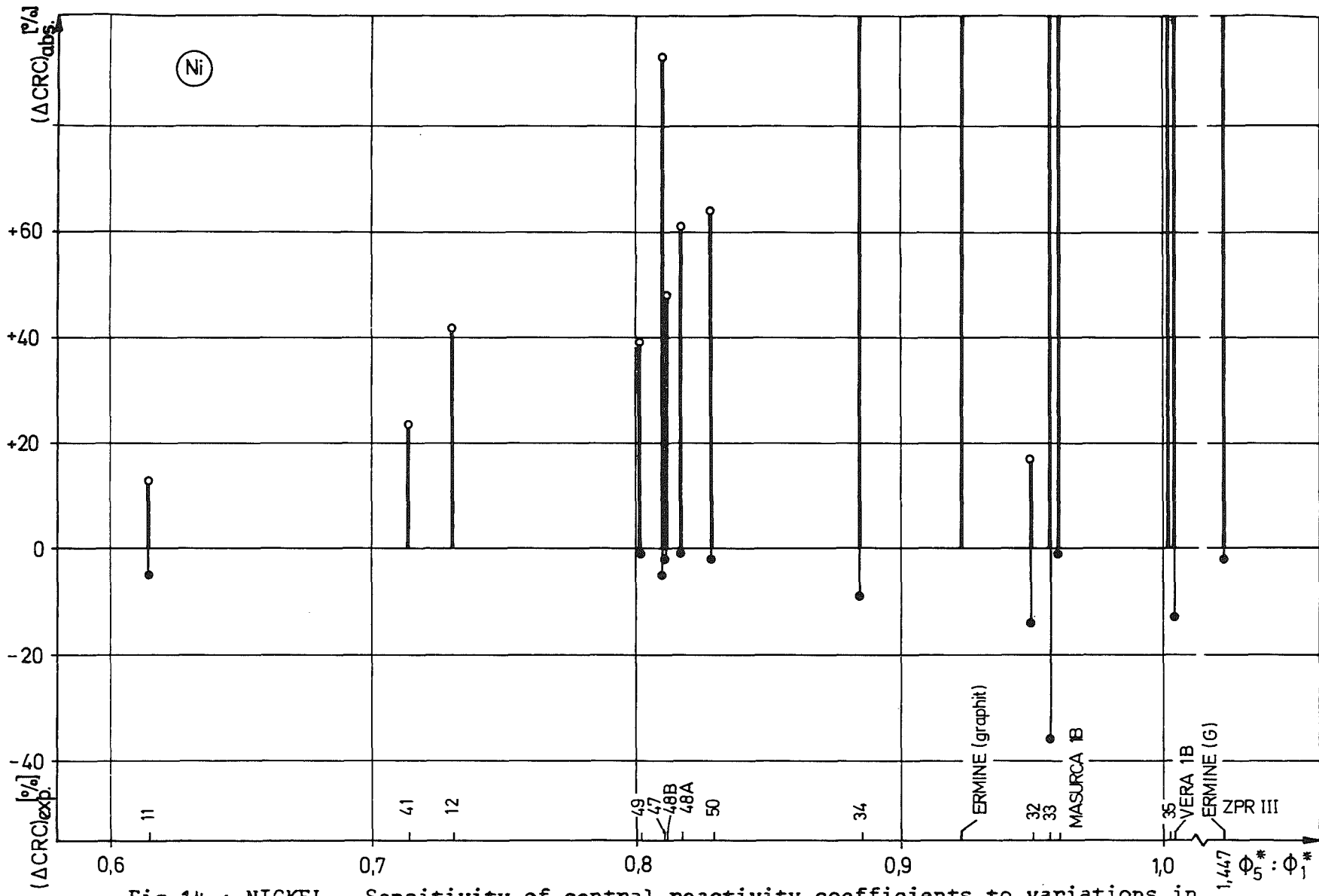


Fig.14 : NICKEL. Sensitivity of central reactivity coefficients to variations in absorption cross sections as compared to experimental uncertainties.

WORKING GROUP MEETING ON "THE KEV CAPTURE OF THE STRUCTURAL  
MATERIALS Ni, Fe, Cr" TO BE HELD IN KARLSRUHE, WEST GERMANY

FROM THE 8-9 MAY 1973 INCLUSIVE

Comparison of Effective Capture Cross Sections and Doppler Coefficients  
for Structural Materials Calculated by Three Evaluated Nuclear Data Files

Hideki Takano and Yukio Ishiguro

Japan Atomic Energy Research Institute  
Tokai-mura, Naka-gun, Ibaraki-ken, Japan

## ABSTRACT

From the viewpoint of the Doppler effect calculation of structural materials, a study is made to grasp the present situation of the nuclear data in the keV energy region. The resonance shielding factors for the effective capture cross sections of Cr, Fe and Ni are calculated by using the resonance parameters sets from the evaluated files, ENDF/B-II and -III, and Story's evaluation data. Using these shielding factors, the Doppler coefficients for stainless steel and natural iron are calculated by one dimensional simple perturbation method and are compared with the experimental values measured in the JAERI-FCA assembly V-1 and -2 cores.

The differences among the Doppler coefficients obtained from three evaluated data are very large and are mainly caused by the uncertainties in the 1.15 keV resonance parameter of  $^{56}\text{Fe}$  and in the smooth capture cross section near the resonance energy.

## 1. Introduction

The Doppler effect of structural materials has recently been noticed in fast nuclear reactors. The Doppler experiments for the stainless steel and natural iron samples performed in the Fast Critical Assembly (FCA) of the Japan Atomic Energy Institute show the possibility of playing an important role in fast reactor safety <sup>(1), (2)</sup>. That is, the Doppler effect of the structural materials is more significant than those due to fissionable materials ( $^{235}\text{U}$  and  $^{239}\text{Pu}$ ). An analysis of the experiment in the FCA core was done using a simple multigroup perturbation theory by Ishiguro <sup>(3)</sup>. The resonance shielding factors for the effective capture cross sections were calculated on the base of the narrow-resonance approximation, using the resonance parameters in the ENDF/B-II data file.

In this report, a comparison is made for the effective capture cross sections for Cr, Fe and Ni calculated by using three resonance parameter sets, ENDF/B-II, ENDF/B-III and Story's data <sup>(4)</sup>, and the influence of the changed nuclear data on Doppler coefficient are investigated. As the results, the important energy region for the evaluation of the nuclear data of the structural materials are discussed.

## 2. Calculation of the resonance shielding factors

The Doppler energy region for the structural materials exists between about 1 to 500 keV, where the resonances are considered to be isolated. The narrow resonance approximation was assumed for the calculation of the effective capture cross sections, while the total and scattering cross sections are not much shielded in this energy range so that the shielding effect can be neglected for the Doppler effect calculation.

The shielding factors for Cr, Fe and Ni were calculated by using the nuclear data files, ENDF/B-II and -III, and the resonance parameters evaluated by Story <sup>(4)</sup>. At the first stage of the present study, the KEDAK nuclear data file <sup>(5)</sup> was to be used for the purpose. Since none of the resonance parameters of the structural materials in the KEDAK file could be broadened by the Doppler effect, except for the 1.15 keV resonance of  $^{56}\text{Fe}$ , the KEDAK data was not used for the present work. Moreover, the resonance parameters for Cr had not so far evaluated by Story <sup>(4)</sup> and hence the shielding factors could not be prepared for the evaluated data by Story.

The energy region considered was from 1 to 800 keV and the region was divided into the 9 or 27 groups following the ABBN-25 <sup>(6)</sup> or JAERI-70 <sup>(7)</sup> group structure.

The results are given only for the 25 group structure in Tables 1~8. For the Story's data, the calculation for the higher energy range than 100 keV was not carried out, since the negative contribution from the interference scattering terms of the artificial resonances assumed at higher energies was unreasonably large.

In Figs. 1~3 are shown the comparison of the infinitely dilute capture cross sections for Cr, Fe and Ni. The Cr capture cross sections were not different except for the energy range 200 to 800 keV between ENDF/B-II and -III data. The iron capture cross sections show large difference among three data of ENDF/B-II and -III and of Story. In the most important energy region including the 1.15 keV resonance of  $^{56}\text{Fe}$  the difference between the capture cross sections for ENDF/B-II and -III is about 2 in factor. For Ni, the difference is seen for the range from 50 to 200 keV between ENDF/B-II and -III. The small value of Story for the range 50 to 100 keV is caused by the negative contribution from the interference scattering terms of the resonances at higher energies.

In Table 9 are shown the temperature coefficients of the shielding factors of iron for the important energy regions of the Doppler effect calculation. The temperature coefficients differ also largely among the three data. These differences between the effective cross section and their temperature coefficients have very important significance for the calculation of Doppler effect of stainless steel and iron samples. In the next section, the Doppler effects are calculated and compared with the experiments.

### 3. Comparison of Doppler coefficients calculated from three nuclear data with the experiments

The Doppler experiment of the structural materials was performed in JAERI-FCA assembly V-1 and 2<sup>(1)</sup> and recently, also in FCA VI-1<sup>(2)</sup> which is larger core than the former assemblies. The experimental results show that the Doppler coefficients observed for stainless steel and natural iron are more than 20% of negative ones of  $^{238}\text{U}$ . This means greater importance of Doppler effect due to structural materials than those for higher isotopes  $^{235}\text{U}$ ,  $^{239}\text{Pu}$  and  $^{240}\text{Pu}$  etc. in fast reactor safety.

The experiment is based on measuring the reactivity changes caused by heating a small Doppler sample (2.6 cm<sup>in</sup> diameter and 15.8 cm in length) by using oscillating technique. The analysis of the Doppler experiments were done by using one-dimensional simple perturbation method. The heterogeneous effect was considered by the usual

equivalent relation and the Doppler sample was treated as an isolated and infinitely long cylinder. A influence of the heterogeneity on the Doppler coefficient can be seen from Fig. 4. This figure shows that the exact choice of the heterogeneity effect,  $\alpha/\rho$  ( $C \equiv 0$ ), is not very important as compared with the experimental error (about  $\pm 20\%$ ). The following calculations were made by accounting the heterogeneity effect  $\alpha/\rho = 0.5$  ( $\alpha=1.3$ ).

The Doppler calculation for the stainless steel and iron samples were carried out using three sets of resonance shielding factors of Cr, Fe and Ni shown in Tables 1~8. The results are compared with the experiments in Fig. 5<sup>a)</sup>. As the Story's data did not contain Cr, the evaluated Cr data of ENDF/B-III was used when the Doppler coefficient of the stainless steel was calculated. The difference among the calculating results is quite large and 10~40%. The 25 group calculations overestimate the Doppler effect as compared with the results of the 70 group calculation. This may be understood by comparing the contribution of the Doppler coefficients from each energy group shown in Figs. 6~9. The difference between the 25 and 70 group calculations comes mainly from the energy range 1 to 2.15 keV.

The 1.15 keV resonance of  $^{56}\text{Fe}$  have large contribution of about 50 and 60% to the total Doppler effect of stainless steel and natural iron, respectively. It can be seen from Figs. 6~9 that 90% of the uncertainty in the Doppler coefficients comes from the that in this resonance parameter. This fact becomes more clear by observing the results of the 70 group calculation. Therefore, the evaluation of the 1.15 keV resonance parameter and of the smooth capture cross section near this resonance energy is very important for the analysis of Doppler effect of the structural materials.

The another result obtained by using the resonance shielding factors of ENDF/B-III and the infinitely dilute capture cross sections of ENDF/B-II are shown in Figs. 6 and 7. The result shows a different group contribution to the Doppler coefficients, compared with those obtained by the other three sets. This fact shows that a consistent evaluation for both of the resonance parameters and the background capture cross section is very important for the calculation of the Doppler coefficient of the structural materials.

a) A trivial error was found in Ishiguro's paper <sup>(2)</sup> on the present study, that is, the heterogeneity effect  $\alpha(1-C)/(N\lambda)$  was erroneously estimated. When the error was corrected, the contribution to the total Doppler effect from the energy region above 10 keV was twice larger than that of the previous paper.

#### 4. Conclusion

The effective capture cross sections of Cr, Fe and Ni were calculated by using three nuclear data of ENDF/B-II and -III and of Story for the energy range from 1 to 800 keV, and the analysis of Doppler experiments for the stainless steel and natural iron samples were made by a simple perturbation method. The results were not always satisfactory and moreover the differences among the Doppler coefficients obtained from three nuclear data were very large. This is mainly caused by the uncertainty in the nuclear data of iron. Especially, the about ninety percentage of the differences among three nuclear data comes from the uncertainty in the 1.15 keV resonance parameter of  $^{56}\text{Fe}$ . Therefore, for the analysis of Doppler effects for stainless steel and natural iron, firstly, the strict evaluation of the 1.15 keV resonance parameter and the background cross section will be most necessary and, secondly, the evaluation of iron resonance parameters and smooth cross sections will be important for the energy range from 20 to 60 keV. This means that the cross section fit is poor between the resonances also in the energy range from 20 to 100 keV.

### References

1. T. Iijima et al., "Doppler Experiment in FCA," paper submitted to the 14th EACRP Meeting, Stockholm, June (1971).
2. T. Iijima and T. Mukaiyama (JAERI), private Communication (1973).
3. Y. Ishiguro., Nucl. Sci. Eng., 49, 228 (1972) and "Shielding Factors of Capture Cross Sections with Temperature Dependence for Cr, Fe and Ni", JAERI-M-4660 (1971).
4. J.S. Story (Winfrith), Private Communication (1973).
5. D. Woll, "Card Image Format of the Karlsruhe Evaluated Nuclear Data File"; KFK-880 (1968).
6. L.P. Abagjian et al., "Group Constant for Nuclear Reactor Calculations", Consultant Bureau, New York (1969).
7. S. Katsuragi et al., "JAERI Fast Reactor Group Constants Systems: Part I," JAERI-1199 (1970) and : Part II, JAERI-1195 (1970).

TABLE 1. Capture Cross Section and Shielding Factor of Cr Obtained from ENDFB-III

ABBN Group No.	Energy Range (KeV)	$\sigma_c$ (barns)	T (°K)	Shielding factor				
				$\sigma_o = 0$	$\sigma_o = 1.0$	$\sigma_o = 10$	$\sigma_o = 10^2$	$\sigma_o = 10^3$
6	400-800	0.00316	300	1.0796	1.0591	1.0198	1.0026	1.0002
			600	1.0800	1.0595	1.0201	1.0026	1.0001
			900	1.0803	1.0598	1.0203	1.0027	1.0002
			2100	1.0813	1.0608	1.0210	1.0028	1.0002
7	200-400	0.00397	300	0.7587	0.7735	0.8676	0.9728	0.9967
			600	0.7591	0.7740	0.8684	0.9731	0.9968
			900	0.7595	0.7746	0.8692	0.9734	0.9967
			2100	0.7608	0.7764	0.8714	0.9742	0.9967
8	100-200	0.00723	300	0.7613	0.7924	0.8867	0.9766	0.9973
			600	0.7646	0.7959	0.8895	0.9773	0.9974
			900	0.7664	0.7978	0.8911	0.9778	0.9975
			2100	0.7698	0.8016	0.8945	0.9789	0.9977
9	46.5-100	0.01317	300	0.6890	0.7307	0.8471	0.9635	0.9955
			600	0.6970	0.7395	0.8542	0.9654	0.9958
			900	0.7019	0.7447	0.8583	0.9665	0.9959
			2100	0.7121	0.7557	0.8666	0.9685	0.9960
10	21.5-46.5	0.03189	300	0.7064	0.7596	0.8807	0.9763	0.9970
			600	0.7208	0.7752	0.8955	0.9809	0.9977
			900	0.7296	0.7847	0.9039	0.9833	0.9980
			2100	0.7485	0.8047	0.9201	0.9873	0.9985
11	10.0-21.5	0.02853	300	0.9626	0.9689	0.9871	0.9979	0.9997
			600	0.9645	0.9704	0.9877	0.9981	0.9997
			900	0.9654	0.9711	0.9880	0.9981	0.9997
			2100	0.9669	0.9724	0.9885	0.9982	0.9997
12	4.65-10.0	0.07790	300	0.8695	0.8760	0.9119	0.9738	0.9959
			600	0.8695	0.8760	0.9119	0.9738	0.9959
			900	0.8695	0.8760	0.9119	0.9738	0.9959
			2100	0.8695	0.8760	0.9119	0.9738	0.9959
13	2.15-4.65	0.03888	300	0.8092	0.8197	0.8778	0.9700	0.9968
			600	0.8092	0.8197	0.8778	0.9700	0.9968
			900	0.8092	0.8197	0.8778	0.9700	0.9968
			2100	0.8092	0.8197	0.8778	0.9700	0.9968
14	1.0-2.15	0.15457	300	0.3190	0.3392	0.4703	0.8108	0.9734
			600	0.3461	0.3694	0.5153	0.8460	0.9794
			900	0.3664	0.3916	0.5456	0.8653	0.9824
			2100	0.4195	0.4487	0.6154	0.9010	0.9875

TABLE 2. Capture Cross Section and Shielding Factor of Fe Obtained from ENDFB-III

ABBN Group No.	Energy Range (KeV)	$\sigma_c$ (barns)	(°K)	Shielding factor				
				$\sigma_o = 0$	$\sigma_o = 1.0$	$\sigma_o = 10$	$\sigma_o = 10^2$	$\sigma_o = 10^3$
6	400-800	0.00502	300	1.0035	1.0029	1.0012	1.0002	1.0000
			600	1.0035	1.0029	1.0012	1.0002	1.0000
			900	1.0035	1.0029	1.0012	1.0002	1.0000
			2100	1.0035	1.0029	1.0012	1.0002	1.0000
7	200-400	0.00572	300	0.9923	0.9942	0.9985	0.9998	1.0000
			600	0.9923	0.9942	0.9985	0.9998	1.0000
			900	0.9923	0.9942	0.9985	0.9998	1.0000
			2100	0.9923	0.9942	0.9985	0.9998	1.0000
8	100-200	0.00590	300	0.9937	0.9953	0.9992	1.0002	1.0001
			600	0.9937	0.9953	0.9992	1.0002	1.0001
			900	0.9937	0.9953	0.9992	1.0002	1.0001
			2100	0.9937	0.9953	0.9992	1.0002	1.0001
9	46.5-100	0.00899	300	0.8534	0.8736	0.9430	0.9912	0.9990
			600	0.8751	0.8934	0.9539	0.9931	0.9992
			900	0.8866	0.9038	0.9592	0.9940	0.9993
			2100	0.9073	0.9220	0.9680	0.9954	0.9995
10	21.5-46.5	0.01712	300	0.4994	0.5449	0.6960	0.8957	0.9845
			600	0.5337	0.5781	0.7168	0.9000	0.9850
			900	0.5537	0.5966	0.7274	0.9020	0.9853
			2100	0.5934	0.6319	0.7455	0.9053	0.9857
11	10.0-21.5	0.00501	300	0.7808	0.8214	0.9307	0.9893	0.9988
			600	0.8006	0.8393	0.9397	0.9909	0.9990
			900	0.8113	0.8488	0.9442	0.9918	0.9991
			2100	0.8310	0.8658	0.9518	0.9932	0.9992
12	4.65-10.0	0.02167	300	0.7524	0.7708	0.8587	0.9682	0.9956
			600	0.7560	0.7741	0.8604	0.9685	0.9957
			900	0.7578	0.7758	0.8613	0.9687	0.9957
			2100	0.7612	0.7788	0.8629	0.9690	0.9957
13	2.15-4.65	0.00674	300	0.9611	0.9651	0.9818	0.9971	1.0000
			600	0.9612	0.9652	0.9819	0.9971	1.0000
			900	0.9613	0.9652	0.9819	0.9971	1.0000
			2100	0.9614	0.9654	0.9820	0.9972	1.0000
14	1.0-2.15	0.30122	300	0.2526	0.2656	0.3590	0.6964	0.9491
			600	0.2777	0.2924	0.3973	0.7415	0.9598
			900	0.2970	0.3129	0.4248	0.7685	0.9654
			2100	0.3492	0.3678	0.4933	0.8224	0.9753

TABLE 3. Capture Cross Section and Shielding Factor of Ni Obtained from ENDFB-III

ABBN Group No.	Energy Range (KeV)	$\sigma_c$ (barns)	T ( $^{\circ}$ K)	Shielding factor				
				$\sigma_o = 0$	$\sigma_o = 1.0$	$\sigma_o = 10$	$\sigma_o = 10^2$	$\sigma_o = 10^3$
6	400-800	0.00770	300	0.9963	0.9946	0.9966	0.9994	0.9999
			600	0.9963	0.9947	0.9967	0.9995	0.9999
			900	0.9964	0.9947	0.9967	0.9995	0.9999
			2100	0.9967	0.9950	0.9969	0.9995	0.9999
7	200-400	0.00877	300	1.0267	1.0093	0.9974	0.9991	0.9998
			600	1.0268	1.0094	0.9975	0.9992	0.9998
			900	1.0269	1.0094	0.9975	0.9992	0.9998
			2100	1.0270	1.0095	0.9975	0.9992	0.9998
8	100-200	0.01437	300	0.9452	0.9444	0.9618	0.9916	0.9991
			600	0.9453	0.9445	0.9618	0.9917	0.9991
			900	0.9454	0.9446	0.9619	0.9917	0.9991
			2100	0.9456	0.9448	0.9621	0.9918	0.9991
9	46.5-100	0.02038	300	0.8097	0.8325	0.9022	0.9773	0.9973
			600	0.8191	0.8418	0.9104	0.9803	0.9977
			900	0.8249	0.8476	0.9154	0.9819	0.9977
			2100	0.8373	0.8600	0.9257	0.9849	0.9982
10	21.5-46.5	0.03599	300	0.7283	0.7436	0.8257	0.9552	0.9942
			600	0.7516	0.7670	0.8470	0.9631	0.9954
			900	0.7657	0.7810	0.8591	0.9672	0.9960
			2100	0.7949	0.8098	0.8827	0.9743	0.9969
11	10.0-21.5	0.09685	300	0.7421	0.7492	0.7962	0.9204	0.9878
			600	0.7494	0.7566	0.8036	0.9246	0.9884
			900	0.7537	0.7609	0.8078	0.9268	0.9888
			2100	0.7625	0.7697	0.8163	0.9310	0.9895
12	4.65-10.0	0.02830	300	0.9295	0.9329	0.9528	0.9871	0.9975
			600	0.9328	0.9361	0.9551	0.9877	0.9977
			900	0.9348	0.9380	0.9563	0.9881	0.9977
			2100	0.9389	0.9418	0.9587	0.9888	0.9979
13	2.15-4.65	0.04422	300	0.9316	0.9351	0.9558	0.9898	0.9987
			600	0.9540	0.9567	0.9718	0.9942	0.9995
			900	0.9663	0.9685	0.9803	0.9964	0.9998
			2100	0.9892	0.9902	0.9954	1.0001	1.0003
14	1.0-2.15	0.02256	300	0.9975	0.9976	0.9981	0.9990	0.9992
			600	0.9975	0.9976	0.9982	0.9990	0.9992
			900	0.9976	0.9977	0.9982	0.9990	0.9992
			2100	0.9977	0.9978	0.9983	0.9990	0.9992

TABLE 4. Capture Cross Section and Shielding Factor of Cr Obtained from ENDFB-II

ABBN Group No.	Energy Range (KeV)	$\sigma_c$ (barns)	T ( $^{\circ}$ K)	Shielding factor				
				$\sigma_o = 0$	$\sigma_o = 1.0$	$\sigma_o = 10$	$\sigma_o = 10^2$	$\sigma_o = 10^3$
6	400-800	0.00333	300	0.9684	0.9735	0.9888	0.9984	0.9999
			600	0.9684	0.9735	0.9888	0.9984	0.9999
			900	0.9684	0.9735	0.9888	0.9984	0.9999
			2100	0.9684	0.9735	0.9888	0.9984	0.9999
7	200-400	0.00335	300	0.7959	0.8100	0.8818	0.9738	0.9968
			600	0.7965	0.8106	0.8825	0.9741	0.9969
			900	0.7971	0.8112	0.8832	0.9744	0.9968
			2100	0.7989	0.8131	0.8852	0.9751	0.9969
8	100-200	0.00722	300	0.8385	0.8564	0.9199	0.9838	0.9982
			600	0.8493	0.8657	0.9242	0.9846	0.9983
			900	0.8550	0.8705	0.9265	0.9851	0.9984
			2100	0.8656	0.8791	0.9306	0.9860	0.9985
9	46.5-100	0.01317	300	0.7434	0.7740	0.8736	0.9700	0.9963
			600	0.7544	0.7850	0.8806	0.9713	0.9964
			900	0.7605	0.7909	0.8840	0.9718	0.9965
			2100	0.7720	0.8018	0.8899	0.9728	0.9966
10	21.5-46.5	0.03188	300	0.7493	0.7832	0.8849	0.9764	0.9970
			600	0.7647	0.7991	0.8995	0.9811	0.9977
			900	0.7741	0.8088	0.9078	0.9834	0.9980
			2100	0.7940	0.8289	0.9237	0.9874	0.9985
11	10.0-21.5	0.02837	300	0.9695	0.9741	0.9886	0.9981	0.9997
			600	0.9711	0.9754	0.9892	0.9982	0.9997
			900	0.9719	0.9761	0.9895	0.9983	0.9997
			2100	0.9732	0.9772	0.9899	0.9984	0.9997
12	4.65-10.0	0.07789	300	0.8742	0.8801	0.9137	0.9739	0.9959
			600	0.8742	0.8802	0.9137	0.9739	0.9959
			900	0.8742	0.8802	0.9137	0.9739	0.9959
			2100	0.8742	0.8802	0.9137	0.9739	0.9959
13	2.15-4.65	0.03887	300	0.8166	0.8263	0.8806	0.9701	0.9968
			600	0.8166	0.8263	0.8806	0.9701	0.9968
			900	0.8166	0.8263	0.8806	0.9701	0.9968
			2100	0.8166	0.8263	0.8806	0.9701	0.9968
14	1.0-2.15	0.15455	300	0.3331	0.3522	0.4780	0.8117	0.9734
			600	0.3624	0.3842	0.5235	0.8468	0.9794
			900	0.3841	0.4076	0.5540	0.8660	0.9824
			2100	0.4401	0.4670	0.6240	0.9015	0.9875

TABLE 5. Capture Cross Section and Shielding Factor of Fe Obtained from ENDFB-II

ABBN Group No.	Energy Range (KeV)	$\sigma_c$ (barns)	T ( $^{\circ}$ K)	Shielding factor				
				$\sigma_o = 0$	$\sigma_o = 1.0$	$\sigma_o = 10$	$\sigma_o = 10^2$	$\sigma_o = 10^3$
6	400-800	0.00504	300	0.9361	0.9444	0.9744	0.9957	0.9994
			600	0.9363	0.9447	0.9746	0.9957	0.9994
			900	0.9365	0.9449	0.9748	0.9958	0.9994
			2100	0.9370	0.9456	0.9754	0.9959	0.9994
7	200-400	0.00559	300	0.9600	0.9694	0.9859	0.9975	0.9997
			600	0.9600	0.9696	0.9861	0.9976	0.9997
			900	0.9601	0.9697	0.9862	0.9976	0.9997
			2100	0.9603	0.9700	0.9867	0.9977	0.9997
8	100-200	0.00847	300	0.7870	0.8688	0.9574	0.9929	0.9993
			600	0.7870	0.8688	0.9574	0.9929	0.9993
			900	0.7870	0.8688	0.9574	0.9929	0.9993
			2100	0.7870	0.8688	0.9574	0.9929	0.9993
9	46.5-100	0.02035	300	0.8531	0.8762	0.9341	0.9860	0.9982
			600	0.8584	0.8822	0.9390	0.9872	0.9984
			900	0.8614	0.8856	0.9417	0.9879	0.9985
			2100	0.8674	0.8922	0.9465	0.9889	0.9987
10	21.5-46.5	0.02713	300	0.7201	0.7814	0.8721	0.9532	0.9928
			600	0.7365	0.8002	0.8816	0.9548	0.9930
			900	0.7468	0.8111	0.8864	0.9555	0.9931
			2100	0.7694	0.8323	0.8943	0.9567	0.9932
11	10.0-21.5	0.01872	300	0.9078	0.9270	0.9727	0.9960	0.9994
			600	0.9135	0.9325	0.9758	0.9965	0.9995
			900	0.9166	0.9354	0.9773	0.9968	0.9996
			2100	0.9222	0.9407	0.9800	0.9972	0.9996
12	4.65-10.0	0.05033	300	0.8255	0.8401	0.9053	0.9793	0.9968
			600	0.8272	0.8418	0.9064	0.9796	0.9969
			900	0.8283	0.8428	0.9072	0.9797	0.9969
			2100	0.8308	0.8452	0.9087	0.9800	0.9970
13	2.15-4.65	0.01214	300	0.9678	0.9709	0.9847	0.9975	1.0001
			600	0.9699	0.9728	0.9857	0.9977	1.0001
			900	0.9710	0.9738	0.9862	0.9978	1.0001
			2100	0.9728	0.9754	0.9870	0.9980	1.0001
14	1.0-2.15	0.15334	300	0.3370	0.3559	0.4825	0.8166	0.9743
			600	0.3720	0.3930	0.5293	0.8492	0.9797
			900	0.3973	0.4195	0.5604	0.8673	0.9825
			2100	0.4602	0.4845	0.6305	0.9011	0.9874

TABLE 6. Capture Cross Section and Shielding Factor of Ni Obtained from ENDFB-II

ABBN Group No.	Energy Range (KeV)	$\sigma_c$ (barns)	T ( $^{\circ}$ K)	$\sigma_o=0$	Shielding factor			
					$\sigma_o=1.0$	$\sigma_o=10$	$\sigma_o=10^2$	$\sigma_o=10^3$
6	400-800	0.00669	300	0.9943	0.9914	0.9941	0.9990	0.9999
			600	0.9943	0.9914	0.9941	0.9990	0.9999
			900	0.9943	0.9914	0.9941	0.9990	0.9999
			2100	0.9943	0.9914	0.9941	0.9990	0.9999
7	200-400	0.00801	300	0.9936	0.9916	0.9923	0.9983	0.9997
			600	0.9937	0.9917	0.9924	0.9983	0.9997
			900	0.9937	0.9917	0.9924	0.9983	0.9997
			2100	0.9938	0.9918	0.9924	0.9983	0.9998
8	100-200	0.01437	300	0.9455	0.9467	0.9635	0.9918	0.9991
			600	0.9455	0.9468	0.9636	0.9918	0.9991
			900	0.9456	0.9469	0.9637	0.9918	0.9991
			2100	0.9458	0.9471	0.9639	0.9919	0.9991
9	46.5-100	0.02037	300	0.8299	0.8458	0.9056	0.9775	0.9973
			600	0.8393	0.8550	0.9137	0.9805	0.9977
			900	0.8450	0.8607	0.9186	0.9821	0.9977
			2100	0.8575	0.8731	0.9288	0.9850	0.9982
10	21.5-46.5	0.03667	300	0.7395	0.7534	0.8300	0.9556	0.9942
			600	0.7624	0.7763	0.8506	0.9633	0.9954
			900	0.7762	0.7900	0.8623	0.9673	0.9960
			2100	0.8046	0.8178	0.8850	0.9742	0.9968
11	10.0-21.5	0.15551	300	0.8877	0.8897	0.9065	0.9647	0.9949
			600	0.8923	0.8943	0.9111	0.9672	0.9953
			900	0.8950	0.8970	0.9137	0.9686	0.9956
			2100	0.9005	0.9025	0.9190	0.9712	0.9960
12	4.65-10.0	0.04138	300	1.0765	1.0709	1.0428	1.0082	1.0000
			600	1.0787	1.0730	1.0443	1.0086	1.0001
			900	1.0800	1.0742	1.0451	1.0088	1.0002
			2100	1.0826	1.0766	1.0467	1.0092	1.0003
13	2.15-4.65	0.04421	300	0.9345	0.9377	0.9570	0.9899	0.9987
			600	0.9562	0.9586	0.9726	0.9943	0.9995
			900	0.9681	0.9700	0.9809	0.9964	0.9998
			2100	0.9900	0.9910	0.9957	1.0001	1.0003
14	1.0-2.15	0.02254	300	0.9975	0.9976	0.9981	0.9990	0.9992
			600	0.9976	0.9977	0.9982	0.9990	0.9992
			900	0.9976	0.9977	0.9982	0.9990	0.9992
			2100	0.9977	0.9978	0.9983	0.9990	0.9992

TABLE 7. Capture Cross Section and Shielding Factor of Fe Obtained from STORRY's data

ABBN Group No.	Energy Range (KeV)	$\Sigma_c$ (barns)	T (°K)	Shielding factor				
				$\sigma_o = 0$	$\sigma_o = 1.0$	$\sigma_o = 10$	$\sigma_o = 10^2$	$\sigma_o = 10^3$
9	46.5-100	0.00633	300	0.5342	0.5603	0.7103	0.9266	0.9910
			600	0.5519	0.5787	0.7266	0.9326	0.9919
			900	0.5624	0.5895	0.7362	0.9361	0.9923
			2100	0.5842	0.6121	0.7563	0.9428	0.9926
10	21.5-46.5	0.01656	300	0.4901	0.5384	0.6841	0.8882	0.9832
			600	0.5226	0.5696	0.7038	0.8926	0.9838
			900	0.5414	0.5869	0.7140	0.8947	0.9841
			2100	0.5784	0.6197	0.7317	0.8982	0.9845
11	10.0-21.5	0.00464	300	0.7633	0.8022	0.9181	0.9870	0.9983
			600	0.7846	0.8220	0.9288	0.9890	0.9986
			900	0.7961	0.8326	0.9343	0.9901	0.9988
			2100	0.8178	0.8521	0.9438	0.9919	0.9990
12	4.65-10.0	0.01596	300	0.7712	0.7880	0.8687	0.9702	0.9958
			600	0.7758	0.7922	0.8711	0.9706	0.9959
			900	0.7782	0.7944	0.8723	0.9708	0.9959
			2100	0.7825	0.7983	0.8743	0.9713	0.9960
13	2.15-4.65	0.00581	300	0.9549	0.9592	0.9785	0.9965	0.9999
			600	0.9550	0.9594	0.9786	0.9965	0.9999
			900	0.9551	0.9595	0.9786	0.9965	0.9999
			2100	0.9552	0.9596	0.9787	0.9965	1.0000
14	1.0-2.15	0.21445	300	0.2929	0.3079	0.4143	0.7562	0.9628
			600	0.3242	0.3411	0.4583	0.7963	0.9707
			900	0.3473	0.3654	0.4885	0.8192	0.9748
			2100	0.4069	0.4272	0.5597	0.8632	0.9818

TABLE 8. Capture Cross Section and Shielding Factor of Ni Obtained from STORRY's data

ABBN Group No.	Energy Range (KeV)	$\sigma_c$ (barns)	T (°K)	Shielding factor				
				$\sigma_o = 0$	$\sigma_o = 1.0$	$\sigma_o = 10$	$\sigma_o = 10^2$	$\sigma_o = 10^3$
9	46.5-100	0.00400	300	0.7290	0.7370	0.8012	0.9433	0.9930
			600	0.7292	0.7372	0.8014	0.9433	0.9930
			900	0.7239	0.7373	0.8014	0.9433	0.9930
			2100	0.7295	0.7374	0.8015	0.9434	0.9930
10	21.5-46.5	0.02388	300	0.7200	0.7361	0.8227	0.9562	0.9945
			600	0.7582	0.7734	0.8531	0.9658	0.9956
			900	0.7806	0.7952	0.8699	0.9708	0.9961
			2100	0.8252	0.8382	0.9018	0.9793	0.9974
11	10.0-21.5	0.08527	300	0.6532	0.6636	0.7298	0.8965	0.9840
			600	0.6627	0.6730	0.7384	0.9005	0.9848
			900	0.6680	0.6782	0.7431	0.9025	0.9850
			2100	0.6780	0.6881	0.7517	0.9062	0.9856
12	4.65-10.0	0.02579	300	0.9411	0.9452	0.9656	0.9915	0.9981
			600	0.9439	0.9478	0.9674	0.9920	0.9983
			900	0.9454	0.9493	0.9684	0.9923	0.9983
			2100	0.9485	0.9522	0.9702	0.9926	0.9984
13	2.15-4.65	0.04384	300	0.9506	0.9537	0.9710	0.9946	0.9989
			600	0.9713	0.9736	0.9854	0.9984	0.9998
			900	0.9834	0.9851	0.9936	1.0005	1.0001
			2100	1.0069	1.0074	1.0089	1.0041	1.0007
14	1.0-2.15	0.02614	300	0.9590	0.9612	0.9735	0.9930	0.9978
			600	0.9638	0.9657	0.9767	0.9939	0.9982
			900	0.9668	0.9686	0.9787	0.9944	0.9984
			2100	0.9732	0.9747	0.9830	0.9955	0.9987

TABLE 9 Comparison of temperature coefficients for shielding factors of iron,  $\sigma_0 = 10(b)$

ABBN GROUP NO.	Nuclear data	$\delta f_c = (f_c(T) - f_c(300^\circ \text{K})) / (T - 300) \times 10^4$	
		T = 900°K	T = 2100°K
9	ENDF/B-II	0.127	0.0689
	ENDF/B-III	0.270	0.139
	STORY	0.432	0.2556
10	ENDF/B-II	0.238	0.123
	ENDF/B-III	0.523	0.275
	STORY	0.498	0.264
14	ENDF/B-II	1.30	0.822
	ENDF/B-III	1.097	0.746
	STORY	1.237	0.808

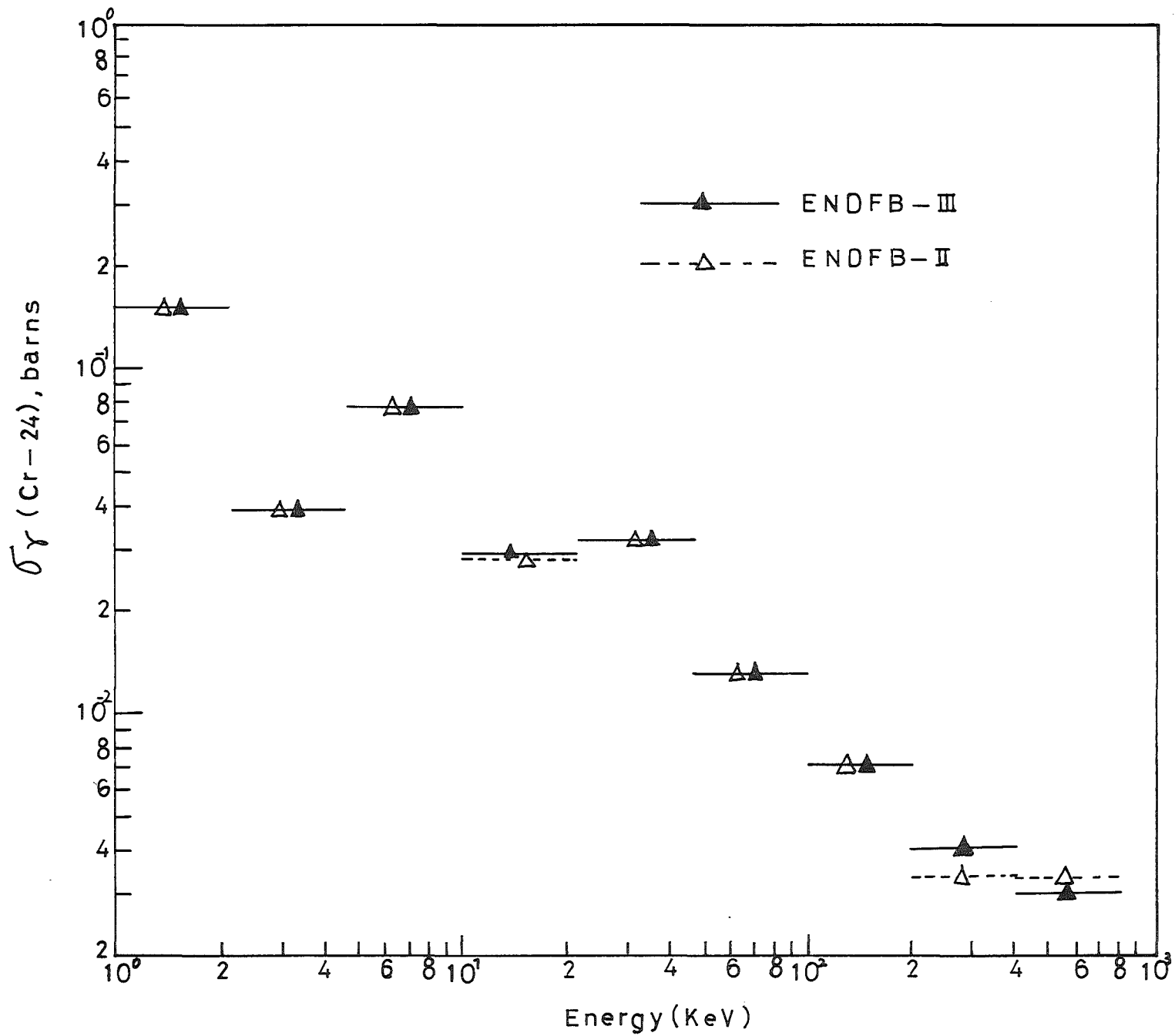


Fig 1. Comparison of infinitely dilute capture cross sections of Cr

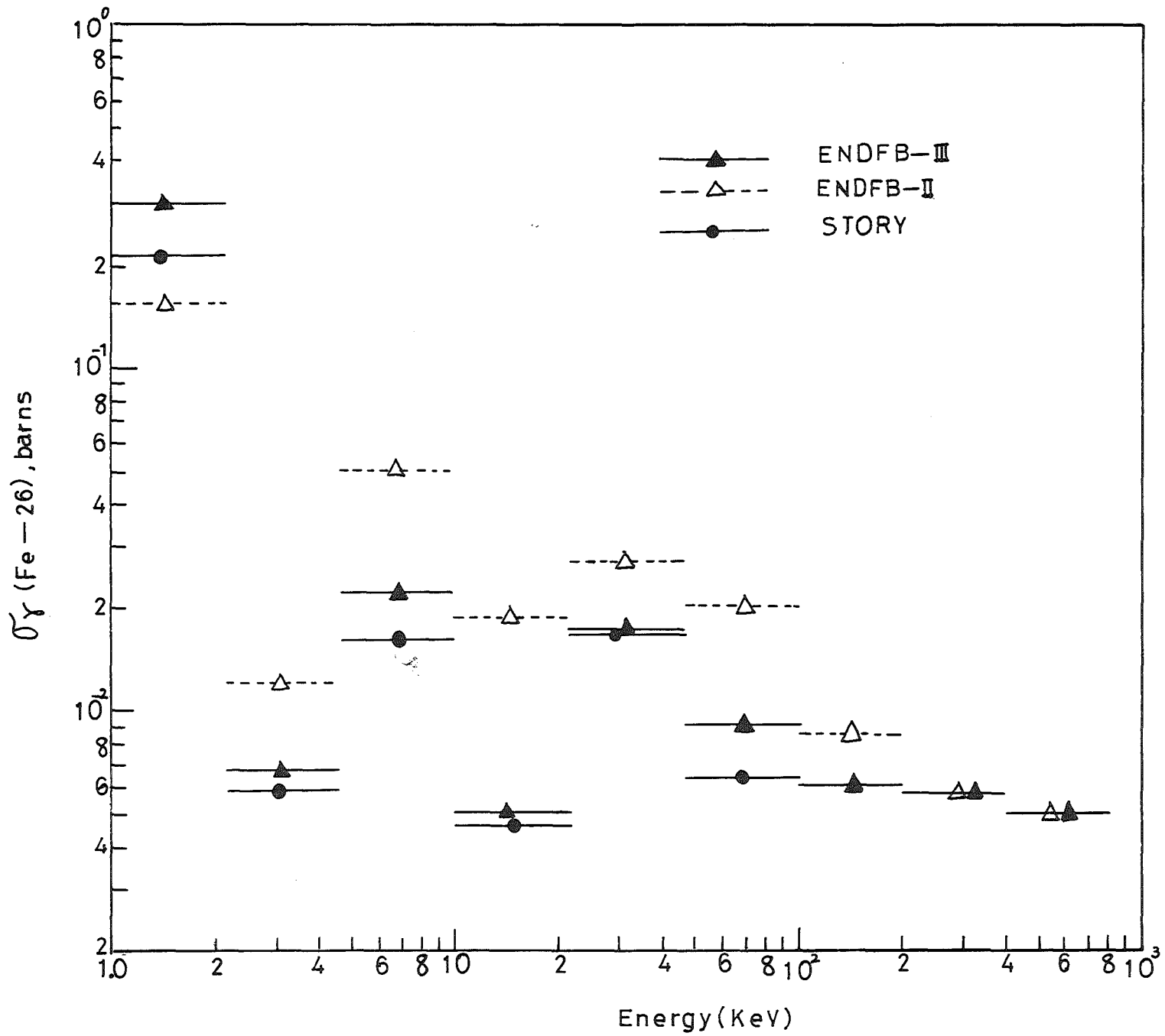


Fig 2. Comparison of infinitely dilute capture cross sections of Fe

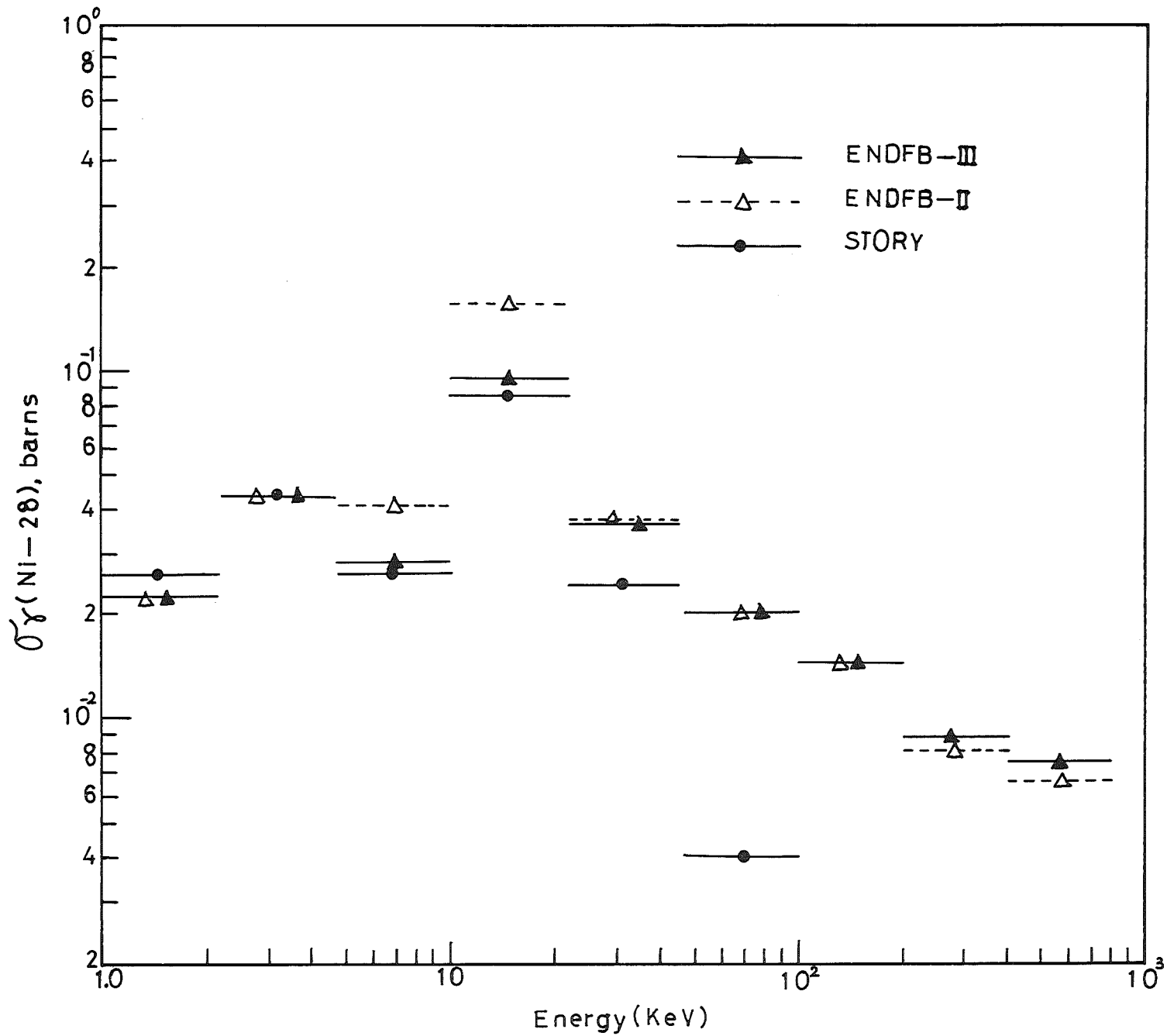


Fig 3. Comparison of infinitely dilute capture cross sections of Ni

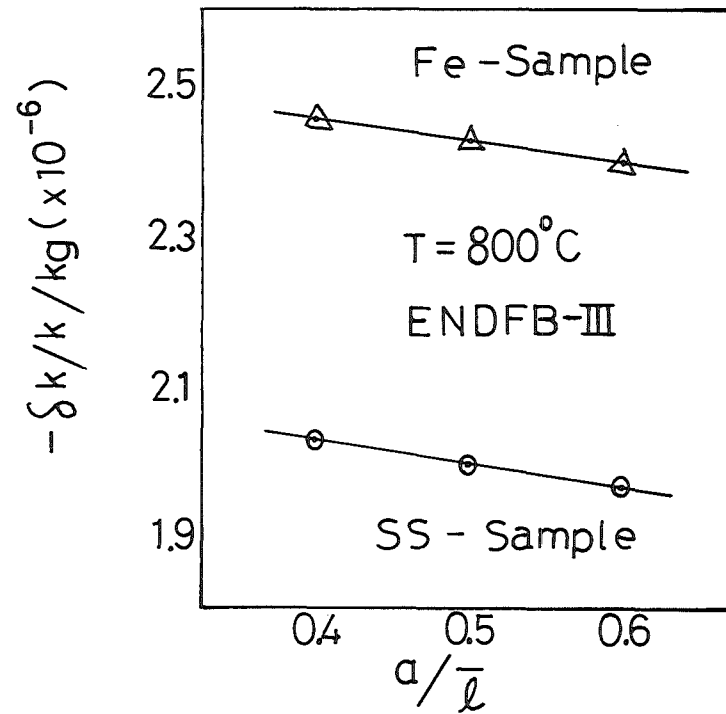


Fig 4. Influence of heterogeneous effect on Doppler coefficient

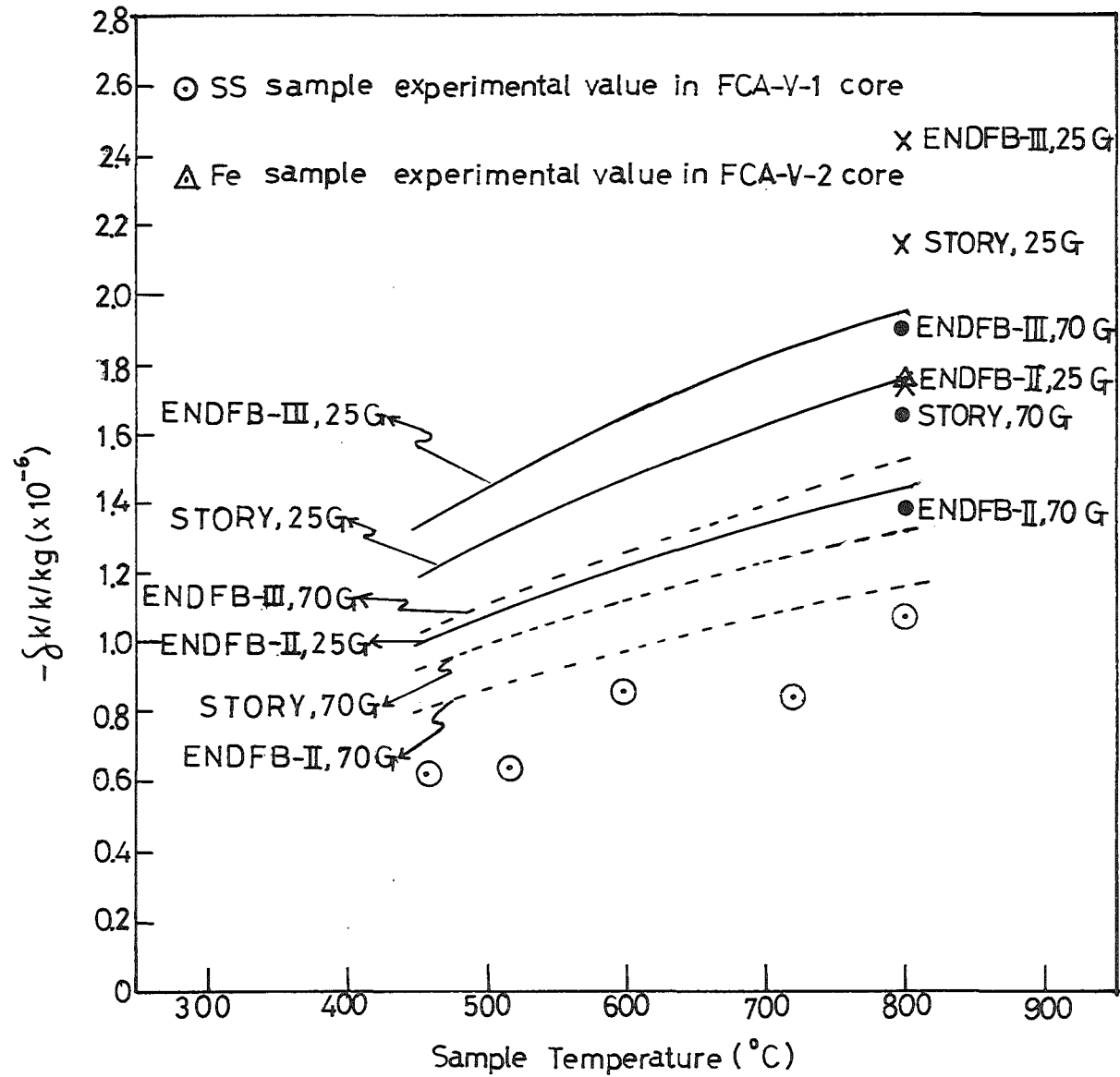


Fig 5. Comparison of Doppler effects for iron and stainless steel samples obtained from various nuclear data

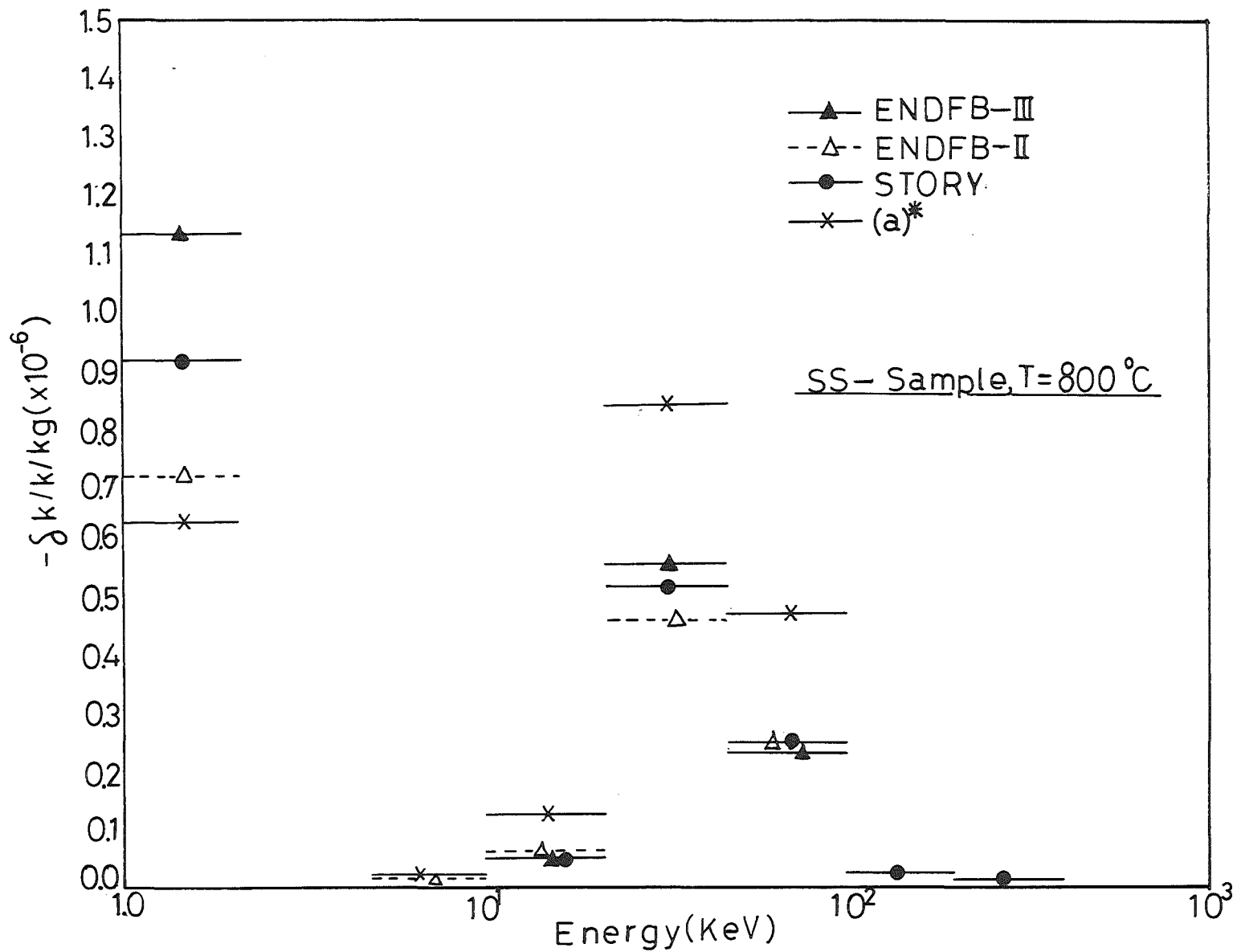


Fig 6. Contribution to Doppler coefficient from each energy group calculated by one dimensional simple perturbation code with 25 group structure

(a)\* shows the results calculated from using the self-shielding factors for ENDFB-III data and the infinitely dilute cross sections for ENDFB-II data.

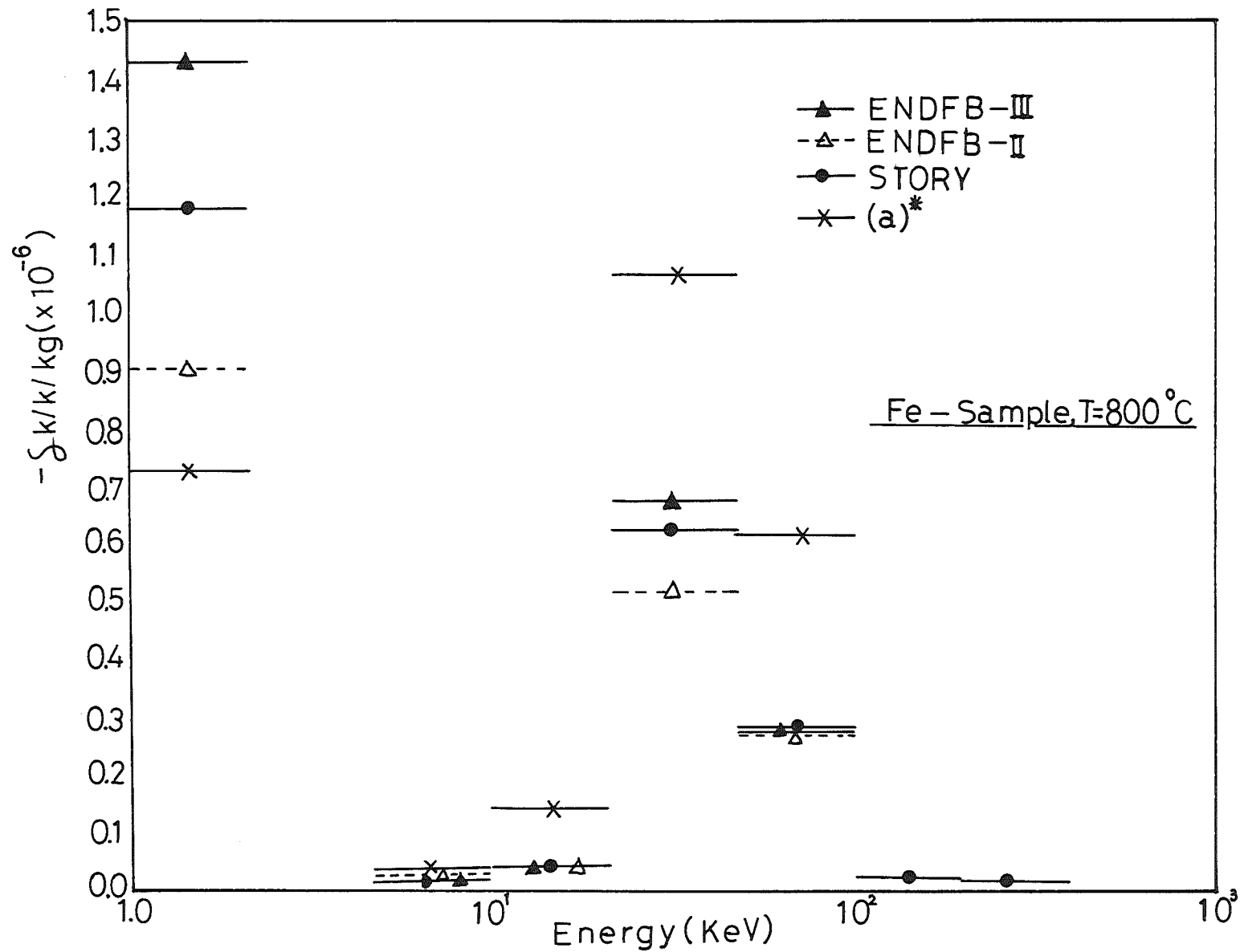


Fig 7. Contribution to Doppler coefficient from each energy group calculated by one dimensional simple perturbation code with 25 group structure

(a)\* shows the results calculated from using the self-shielding factors for ENDFB-III data and the infinitely dilute cross sections for ENDFB-II data.

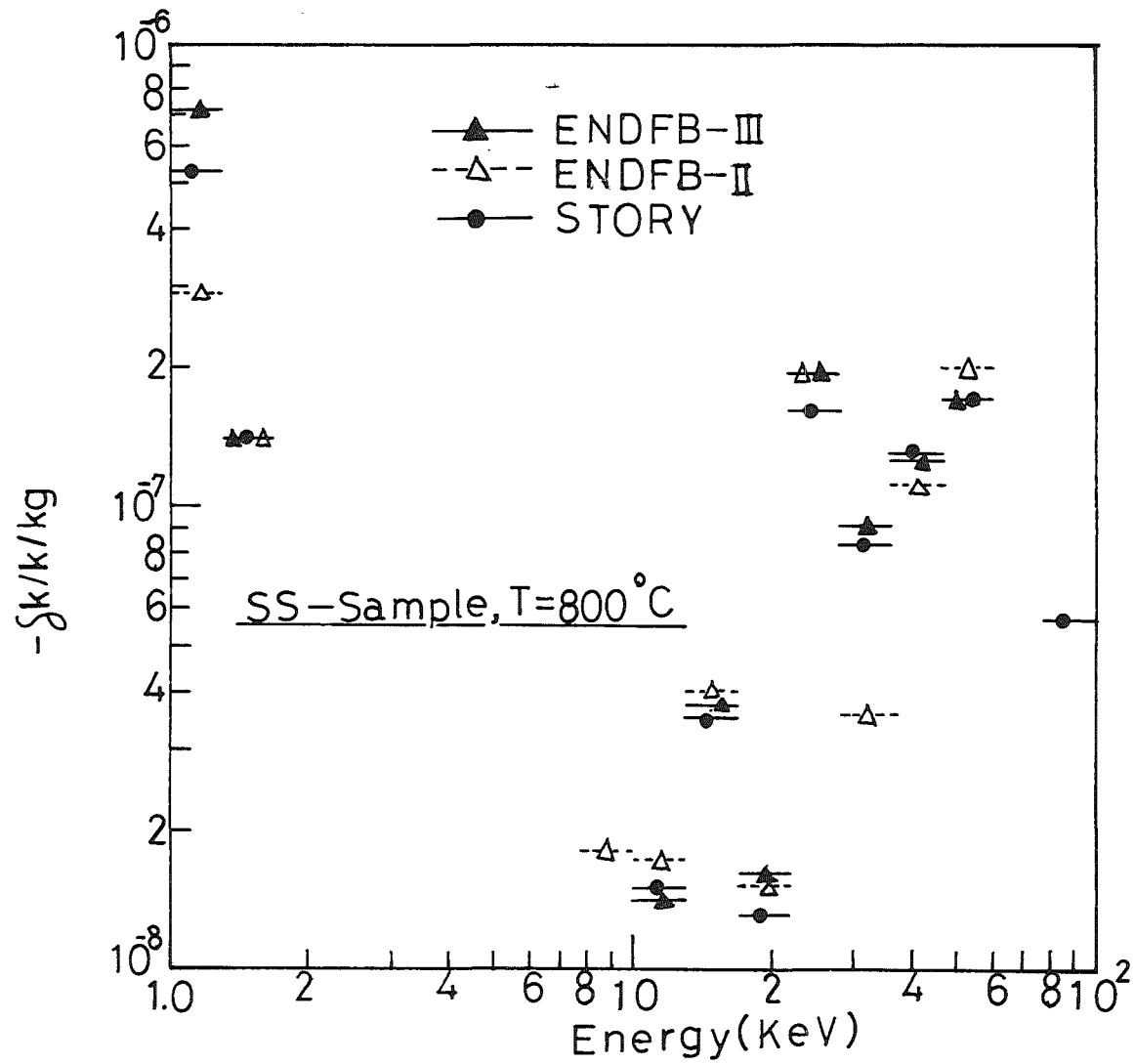


Fig 8. Contribution to Doppler coefficient from each energy group calculated by one dimensional simple perturbation code with 70 group structure

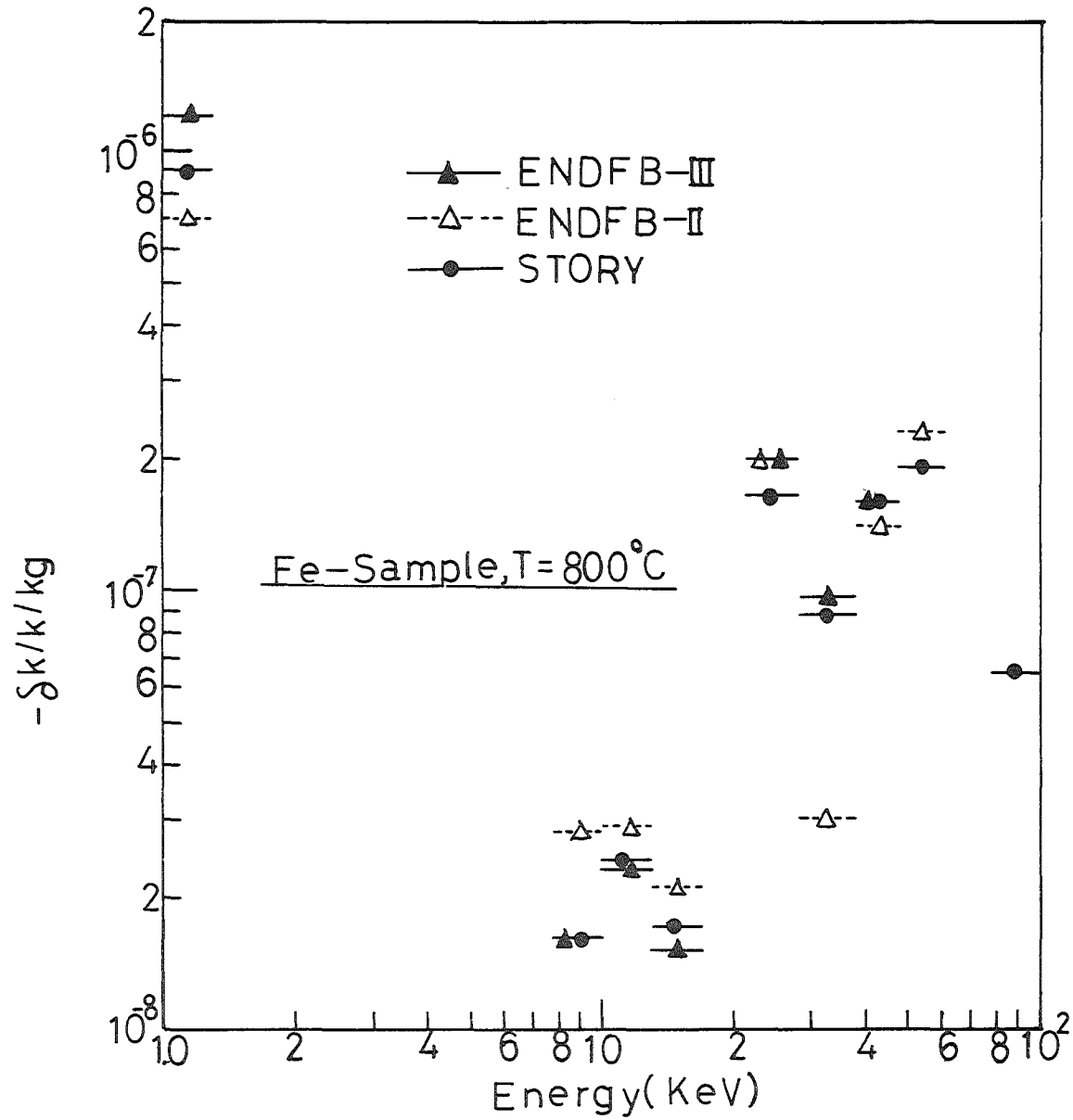


Fig 9. Contribution to Doppler coefficient from each energy group calculated by one dimensional simple perturbation code with 70 group structure

Commission of the European Communities  
EURATOM JRC Ispra  
Nuclear Studies Division

SENSITIVITY CALCULATIONS IN AN IRON SHIELD WITH  
CAPTURE CROSS SECTIONS CHANGED IN THE KEV RANGE

H. PENKUHN

Abstract

It is discussed whether a better knowledge of the absorption cross sections for the intermediate neutrons is of importance in steel shield. Calculations done with the transport code CINNA show that even in a very thick iron shield these capture cross sections do not change critically the neutron transmission.

Paper presented at the Specialists' Panel on Capture  
Cross Sections of Structural Materials.  
Karlsruhe, 8-9.5.1973

## Introduction

It is well known that core calculations -especially those for fast reactors- depend critically on the precision of the capture cross sections of the structure materials. The question was raised whether the same is true for shielding calculations -since some structure materials occur in both core and shield, especially iron and the other steel components as chromium and nickel.

We limited our calculations to the iron case. The reason was: our transport code CINNA uses the cross section library of O5R, and for Cr and Ni these data are inconsistent. In the KeV range sometimes even the trivial condition  $\sigma_{\text{tot}} > \sigma_{\text{el}}$  is hurt, and this means a negative capture cross section, in other words a slightly neutron-reproducing medium!\* Under these conditions an artificial change of the absorption cross-section cannot yield significant results. -But for iron the O5R data are consistent.

## The sensitivity calculations

The calculations were done for an iron slab of 2 meter thickness, in plane geometry. The source was isotropic and located in a second iron slab of 1 cm thickness. The dependence from the source emission spectrum was negligible. The upper energy limit was 100 KeV, the lower one 0.5 KeV. This energy range is subdivided into 5 energy groups of equal lethargy width  $\Delta u$  (here  $\Delta u \cong 1.06$ , which means a factor near 2.9 between lower and upper energy limits of each group). If the absorption cross section is halved in the critical range 20-30 KeV

\*F.i.: at 15 KeV O5R says that  $\sigma_{\text{tot}} = 3.0\text{b}$ , but  $\sigma_{\text{el}} = 3.1\text{b}$   
for Cr!

-there, at 25 KeV, is the most important minimum ("window") in the total cross section- the effect in each group including and below this energy range is near 6% at 1 m and near 10-11% at 2 m penetration depth. Table I shows details of this case. The flux increases are about linear with the penetration  $x$  and rather flat versus energy. But these variations are well below the errors tolerated in shielding calculations; after some meter penetration one is lucky if the errors are only below or near a factor two! (In our case the highest group is attenuated by about 11 decades, all others "only" by 5 decades).

In order to see whether a variation of the capture cross section in the whole considered energy range has a more pronounced effect, similar calculations were done with  $\sigma_c$  decreased and increased by 50% from 0.5 to 100 KeV. Table II and III show the results. The variations of the total flux and total heat deposition rate are only slightly higher than in the case of the variation restricted to the range 20 - 30 KeV: at  $x = 2$  m the total flux changes by 11% in table I, by 14.2% in table II, and by -12.3% in table III. But now the flux changes are no longer a flat function versus energy; they increase from  $\pm 6\%$  (highest energy group) to  $\approx \pm 30\%$  (lowest one). The fact that in all three cases the changes averaged over all energies differ only slightly (11%, 12.3%, 14.2%) is explained by the great contribution -about 83%!- of the second energy group (that which includes the "window" at 25 KeV) to the total flux. Moreover one sees that in the last group (0.5 - 1.44 KeV) the changes are markedly higher than in each other group- this is due to the strong absorption resonance at 1.15 KeV (in our library 0.169 barn).

## Conclusions

The final result of these calculations is that the capture cross section of iron in the KeV range is known with sufficient precision for shielding purposes. But is the same true for the other two important steel components, Cr and Ni? On one hand the thermal absorption cross sections of Fe, Cr, and Ni do not differ much (by a factor below two), on the other hand any steel contains considerably more Fe than Cr and Ni. Moreover Cr and Ni show resonance structures in the KeV range which seem less marked than that of Fe; at most they can have the same importance. (This conclusion can be drawn comparing the absorption cross sections of the 99-GAM-group structure for Fe, Cr and Ni). Therefore a steel containing Cr and Ni should behave roughly as Fe, if the absorption cross sections of the components are changed. But the situation is no longer necessarily the same for Mn which has high capture resonances and a great thermal absorption (about 11 barn)!

One can ask whether we do not get qualitatively the same results by the simple reasoning: At the 25-KeV-window we have  $\delta_a = 0.011$  barn; changing  $\delta_a$  by 50% means varying  $\delta_{tot}$  by 0.0055 barn ( $\delta_{el}$  unchanged), and the macroscopic total cross section then varies by  $0.6 \times 7.8 \times 0.0055 / 56 / \text{cm} = 0.047 / \text{m}$ ; this means an effect of about 5% change per meter penetration depth. This single-energy model certainly gives the right order of magnitude; but in order to know how such variations change the different energy groups (the energy spectrum) more detailed calculations are necessary.

Table I

Flux increase (in %) if  $\lambda_a$  decreased by 50% from 20 to 30 KeV

Energy limits (KeV)	8 cm	52 cm	100 cm	148 cm	164 cm	200 cm (boundary)
12 - 34.7	1.32	3.8	6.4	8.9	9.8	11.1
4.1 - 12	1.14	3.9	6.1	9	9.8	9.9
1.44- 4.1	0.96	3.8	6.1	8.7	9.6	10.6
0.5 - 1.44	1.09	3.6	5.9	8.5	9.3	10.3
0.5 -100	0.87	3.7	6.2	8.8	9.7	11
Total heating	0.28	3.5	6.4	9	9.8	11.1

\* x = distance from source slab

Table II

Flux increase (in %), if  $\lambda_a$  decreased by 50% from 0.5 to 100 KeV

Energy limits (KeV) \ x	8 cm	52 cm	100 cm	148 cm	164cm	200 cm (boundary)
34.7 -100	0.85	2.3	3.6	5	5.5	6
12 - 34.7	2.5	5.7	8.3	10.9	11.8	12.9
4.1 - 12	4.0	8.5	11	13.8	14.8	16
1.44- 4.1	5.0	10.8	13.5	16.4	17.2	18.4
0.5 - 1.44	18.0	25	28	31	32	33.5
0.5 -100	3.1	9.6	13	15.8	16.5	14.2
Total heating	1.5	7.4	10.7	13.3	14.2	13.9

Table III

Flux decrease (in %), if  $\lambda_a$  increased by 50% from 0.5 to 100 KeV

Energy x limits (KeV)	8 cm	52 cm	100 cm	148 cm	164 cm	200 cm (boundary)
34.7 -100	0.83	2.3	3.7	4.8	5.1	5.8
12 - 34.7	2.4	5.4	7.8	10	10.5	11
4.1 - 12	3.5	7.7	11.1	12	12.8	13.8
1.44- 4.1	5	9.8	11.9	13.8	14.5	15.3
0.5 - 1.44	14.4	19.8	22	23.5	23.8	25
0.5 -100	3.1	8.7	11.1	13.2	13.9	12.3
Total heating	1.4	6.8	9.7	11.6	12.3	12.1

UNCLASSIFIED

Working Group Meeting on the keV Capture of the  
Structural Materials, Ni, Fe, Cr  
Karlsruhe, May 1973

Capture Cross-Sections of Structural Materials  
of Importance in Fast Reactors

J. L. Rowlands

Introduction

The capture cross-sections of structural materials have a significant effect on the economics of fast reactors. About 10% of the neutron captures are in structural materials and this has a marked effect on the breeding performance of a fast reactor.

There is also a small but significant Doppler effect arising from the 1 keV capture resonance in iron.

The accuracy required for the capture cross-sections of the main structural materials is  $\pm 10\%$  in the energy range 1 Kev-1 Mev, with a relaxation of the accuracy requirements outside this range. (See Table 2 for an energy group breakdown.)

Information about the resonance structure of the cross-sections is also required to enable the shielded cross-sections to be calculated to this accuracy. Shielding in the 1 keV resonance in iron is particularly important. Resonance information is also required to enable Doppler effects to be estimated.

Results of the Analysis of Integral Experiments

We have analysed integral experiments using the FGL4 cross-section set (produced early in 1968) and the FGL5 set (produced in unadjusted form, FGL5U, towards the end of 1971).

The evaluations used in FGL4 were:

Fe	Schmidt	(1967)
Ni	Ravier	(1965)
Cr	Ravier and Vastel	(1966)

In FGL5U the evaluations for Fe and Ni made by Moxon, Pope and Story (1971) were used. The Fe and Ni evaluations are compared in Figs. 1 to 4.

The types of integral experiment used to obtain information about the capture cross-sections of structural materials are:

- (a) Null-reactivity test zones consisting of Pu, U and a diluent material. The reaction rates Pu239 (n,f), U238 (n,f) and (n, $\gamma$ ) are measured. From studies with test zones containing non-absorbent diluents (carbon and oxygen) Pu239 alpha is deduced from the neutron balance. The capture rate in absorbing diluents can then be derived. The Zebra 8

series of null-reactivity test zones included a test zone, Zebra 8C, in which the diluent was stainless steel.

- (b) Small sample reactivity perturbation measurements. These give information about the combined reactivity effects of absorption and scattering.

These measurements are combined with other integral measurements and spectrum measurements to obtain cross-section adjustments by a least squares fitting procedure. Irradiation of samples in the Dounreay Fast Reactor, followed by mass spectrographic analysis, has also provided data on the capture cross-sections of structural materials, but these measurements have not been included in the cross-section adjustment studies.

The integral measurements which relate to the capture cross-sections of structural materials are few and were made in similar spectra. Consequently, the energy discrimination in the cross-section adjustments is poor. Because iron is present in Zebra 8C (and in other assemblies) in a much higher proportion than chromium and nickel the adjustment to the iron capture cross-section is more accurate than the adjustments for nickel and chromium (which are determined mainly by the central reactivity perturbation measurements).

In Table 1 the adjustments indicated for iron are tabulated. The adjustments to the FGL4 and FGL5U sets are compared with the percentage differences between FGL5U and FGL4. The adjustments indicated for the FGL4 iron data are broadly similar to the differences between the FGL5U and FGL4 data. The large adjustment in the group containing the 1 keV iron resonance is probably a consequence of the inadequate treatment of the shielding of this resonance in the FGL4 set. Also, there is a tendency for capture cross-sections above 25 keV to be increased and those below 25 keV to be decreased, as is shown by the adjustments indicated for the FGL5U set. This tendency results from fitting to spectrum measurements. Since all cross-sections are changed in this way this adjustment to the iron capture cross-section cannot be regarded as significant. It can be concluded that the latest evaluation of the iron capture cross-section is consistent with the integral measurements.

The adjustments for nickel and chromium are only broadly indicative, because the only integral measurements relating specifically to these substances are the small sample reactivity perturbation measurements. An increase of about 15% in the FGL4 nickel capture cross-section is indicated. The FGL5U data is on average (in a typical sodium cooled fast reactor spectrum) 50% higher than FGL4. (It is about a factor of 3 higher in the energy range 10 to 70 keV.) The adjustment indicated for the FGL5U data is a reduction of about 15%. This suggests that a cross-section intermediate between the FGL4 and FGL5U data would be most consistent with the integral data.

For chromium capture no net change is indicated for the average value in a fast reactor spectrum, but there is a small increase above 25 keV and reduction at lower energies to give a better fit to spectrum measurements. These changes are not significant.

Fast Reactor Physics Division  
Building A32  
AEE Winfrith

25 April 1973

Table 1

Adjustments to the Iron Capture Cross-Section

Group	Lower Energy (keV)	FGL4 Standard Deviation (percent)	FGL4 Adjustment (percent)	FGL5U/FGL4 Difference (percent)	FGL5U Standard Deviation (percent)	FGL5U Adjustment (percent)
1	1,350	40	- 1	- 0.3	40	9
2	498	40	- 5	- 0.6	40	1
3	183	40	- 10	- 16.1	40	7
4	67.4	40	- 16	- 26.7	30	16
5	24.8	40	- 27	- 54.1	30	40
6	9.12	40	- 51	- 69.7	30	3
7	3.35	40	- 63	- 65.2	20	- 9
8	1.23	40	- 71	- 24.0	10	- 1
9	0.454	40	- 84	- 31.7	10	- 8
10	Thermal	40	- 64	- 0.8	10	- 1

TABLE 2

Energy Group Breakdown of Absorption in Iron in a typical  
fast reactor spectrum (FGL5U data)

<u>Group</u>	<u>Lower Energy</u>	<u>Percentage of Absorptions</u>
1	10 Mev	0.4
2	6.07	2.0
3	3.68	2.8
4	2.23	1.6
5	1.35	1.0
6	821 Kev	1.8
7	498	5.0
8	302	4.4
9	183	5.5
10	111	8.4
11	67.4	10.6
12	40.9	5.8
13	24.8	10.2
14	15.0	3.0
15	9.12	3.6
16	5.53	4.6
17	3.35	1.0
18	2.03	2.4
19	1.23	1.5
20	749 eV	22.8
21	454	0.7
22	275	0.5
23	167	0.2
24	101	0.1

Fig 1 IRON CAPTURE ( $0.4 \text{ eV} - 10^3 \text{ eV}$ )

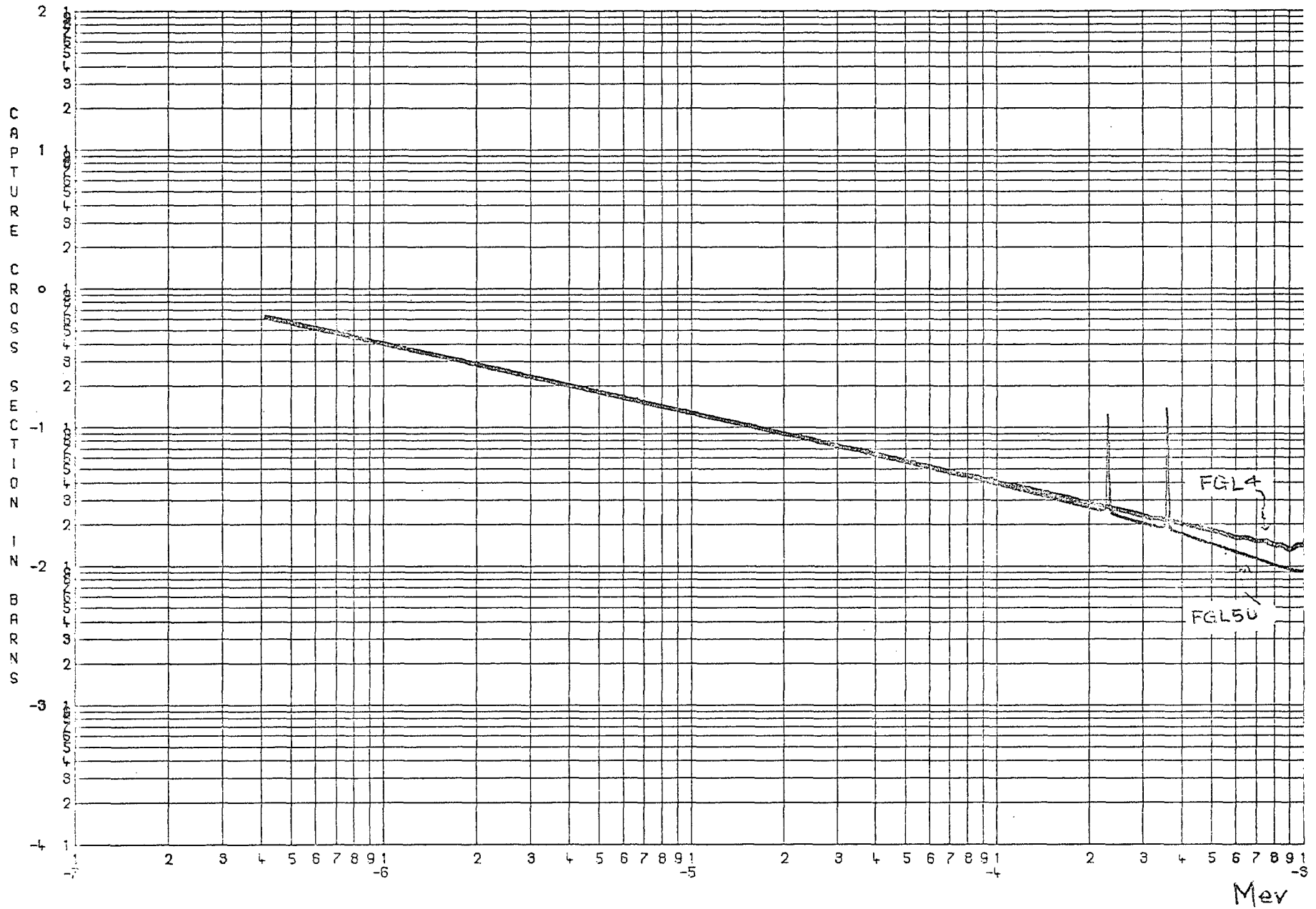


Fig 2 IRON CAPTURE (1kes - 20Mev)

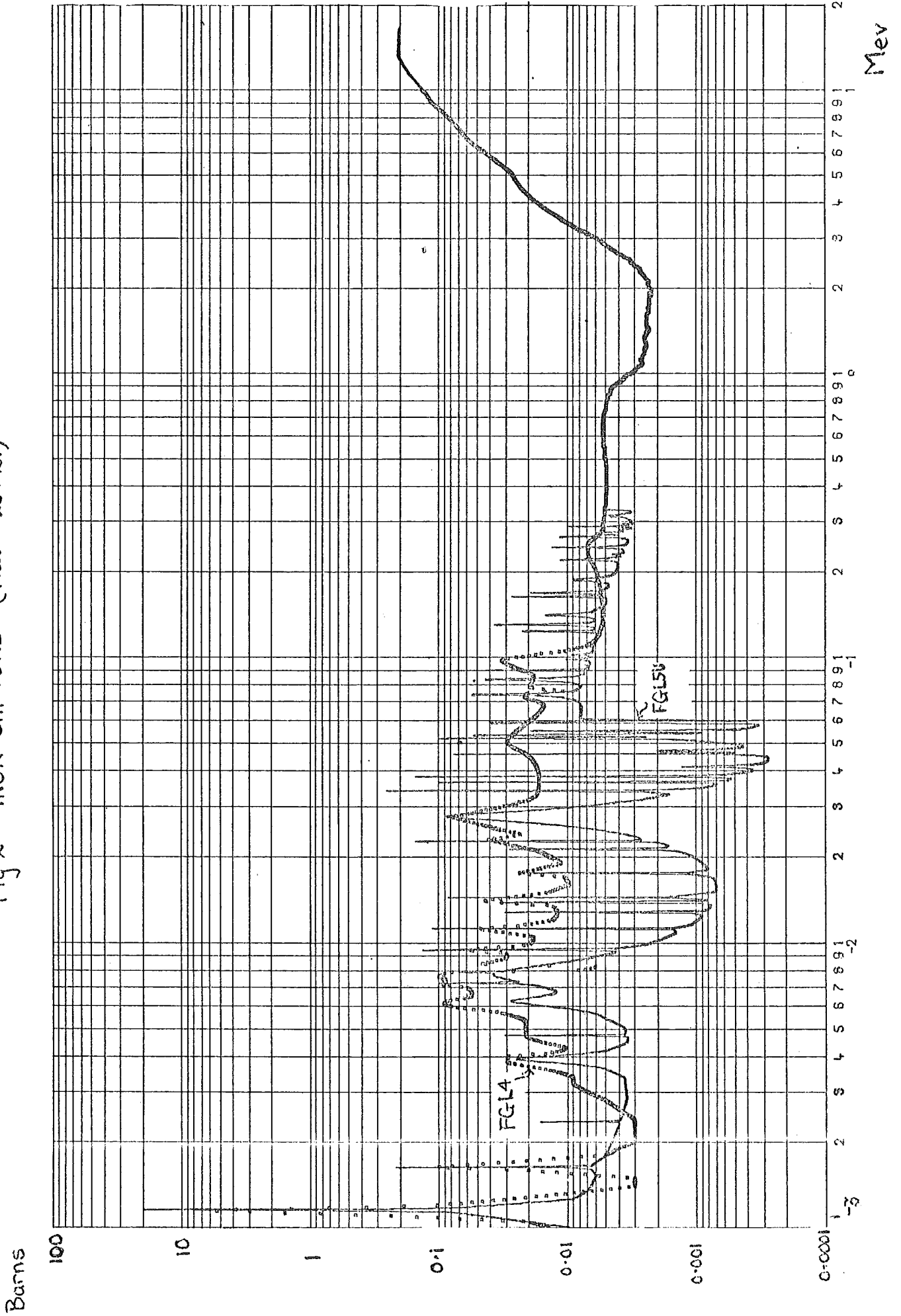


Fig 3. NICKEL CAPTURE (0.4 eV - 10<sup>3</sup> eV)

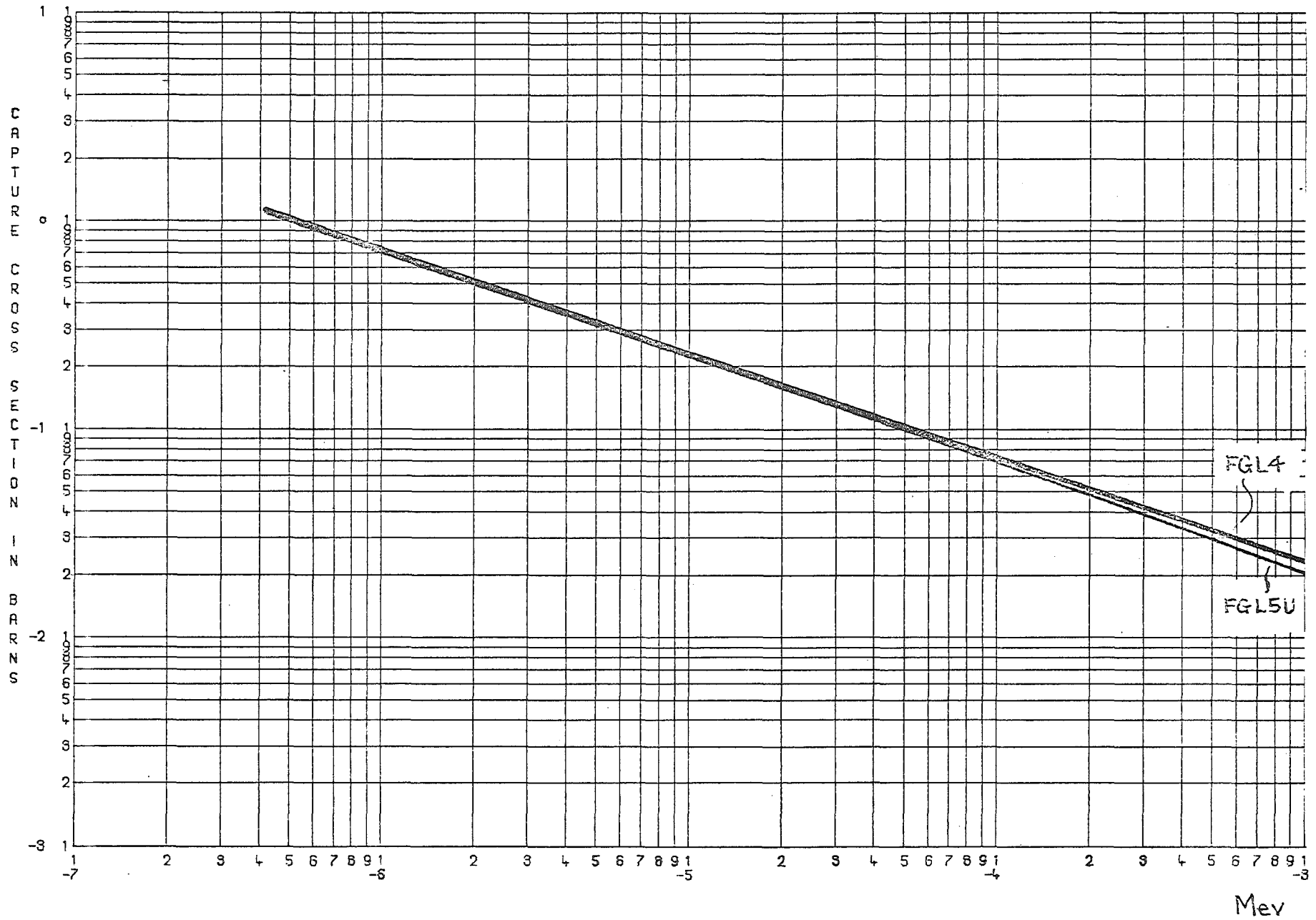
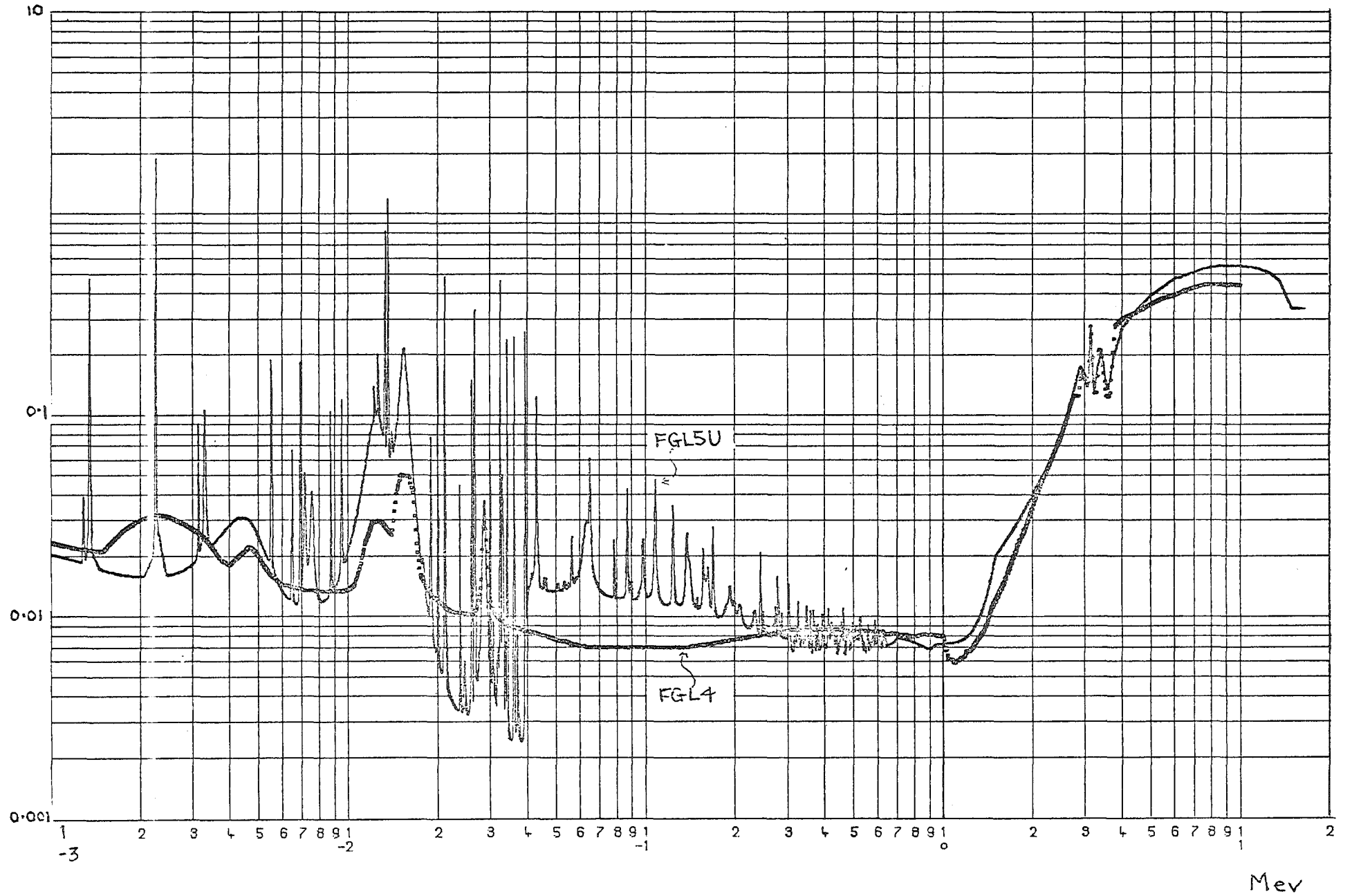


Fig 4 NICKEL CAPTURE (1 kev - 20 Mev)

Barns



SUMMARY ON TOPIC III: USER ASPECTS

by

H. Küsters

Kernforschungszentrum Karlsruhe

The impact of capture cross sections of structural materials on physics quantities in fast reactors has been discussed under various aspects: critical enrichment, breeding gain, reactivity worth, Doppler coefficient and shielding. The results and recommendations are briefly summarized.

1. Sensitivity of physics quantities on capture data of structural materials

It was shown that a change of 10 % in the capture data of Fe causes a change in criticality of about 0,2 % for ZPPR-2. For large commercial LMFBR systems this impact is slightly higher. For these reactor systems economically the breeding gain is of greater importance than initial enrichment. Though a true cost-benefit analysis has not been presented, a sound feeling leads to an accuracy of better than 0.05 for this quantity. A 10 % uncertainty in the capture data of Fe or stainless steel might change the breeding gain by less than or about 0.01.

If an accuracy of the criticality by less than or about 1 % and the breeding gain by less then or about 0.05 can be tolerated for commercial systems, the accuracy for the capture data of structural materials should be requested accordingly to the percentage of structural materials (about 25 %) in the core composition.

A further point of investigation was the influence of the capture data of Fe to the Doppler coefficient. It was stated that the difference between the numbers for the Doppler coefficients obtained from the data for Fe, Cr, Ni in the files ENDF/BII, ENDF/BIII and Story's 1972 data

was very large. Especially, about 90 % of the differences stem from the uncertainty in the nuclear data of the 1.15 keV resonance of Fe 56. The effect of these uncertainties on the total Doppler coefficient of a large LMFBR is moderate to small.

In shielding investigations, the magnitude of the capture data of structural materials is not of importance.

## 2. Target accuracy for the capture data of structural materials

There was agreement on the requested accuracy for the data under discussion according to the sensitivity studies: the capture in stainless steel in the energy range between 1 keV to 1 MeV should be accurate to better or about  $\pm 10\%$ , mainly because of a reliable prediction of breeding. This in conclusion means about the same accuracy for the Fe-capture data, while the request for Ni and Cr is more relaxed. An accuracy of about  $\pm 20\%$  seems sufficient from the present point of view.

## 3. Check of capture data in integral experiments

Some checks of the capture data in critical experiments were presented. These checks can only be indicative, because compensating effects among the contributions of these data from various energy regions and isotopes as well as the presently dominating uncertainties of the data for fertile and fissile materials may not allow to draw too firm conclusions with regard to the capture data accuracy of structural materials. One of the important investigations by the Cadarache group shows that by adjusting the capture data of Cr and Ni to the recently measured high capture values, then a decrease of Fe-capture cross section only can fit integral experiments in ZEBRA (with a high steel content) and ERMINE. This is in contradiction to recent results of differential measurements of Fe-neutron-capture-cross sections (Le Rigoleur). The new evaluation of Fe data by the UK group seems to be in accordance with integral data, at least not in contradiction to them.

#### 4. Recommendations

- a) As long as the difficulties exist in interpreting critical experiments with large steel contents, the capture data especially of Fe need to be re-investigated very carefully by experimenters and evaluators.
- b) In order to draw more firm conclusions, a thorough study should clarify the importance of resonance selfshielding of structural resonances. Due to the fact that there exists a clear tendency for larger selfshielding in the relevant resonance groups, the request for reliable resonance parameters is being expressed strongly.
- c) To determine the proper contribution of structural materials to the Dopplercoefficient, it is necessary to improve the reliability of the 1.15 keV Fe-resonance data.
- d) The check of the UK-evaluations for Fe and Ni in sensitive experimental investigations is recommended. Users should repeat their sensitivity studies with more modern resonance parameters and resonance self-shielding factors, although larger discrepancies between theory and integral experiments are not felt to be caused dominantly by uncertainties in resonance selfshielding factors.
- e) For use in the adjustment procedures error bars should be attributed to evaluated data.
- f) A New evaluation for capture data of Cr to an accuracy of  $\pm 20\%$  is requested.

IV. APPENDIX

List of Participants

J.Y. Barre'	CEN , Cadarache
H. Beer	KFZ Khe
G. De Leeuw	CEN/SCK (Mol)
S. De Leeuw	" "
A. Ernst	KFZ Khe
F.H. Fröhner	CCDN Saclay (KFK)
D.B. Gayther	AERE Harwell UK
H.Hägglom	Studsvik/Sweden
M. Heindler	Reaktorinst.Graz
F. Käppeler	KFZ Khe
E. Kiefhaber	KFZ Khe
H. Küsters	KFZ Khe
T. Lemley	IAEA Nuclear Data Section
M. Motta	CNEN, Bologna, Italy
M.C. Moxon	AERE Harwell UK
K. Okamoto	CCDN Saclay (NEA/OECD)
D. Paya	CEN Saclay
P. Ribon	CEN Saclay
C. Le Rigoleur	CEN, Cadarache
G. Rohr	BCMN/EURATOM GEEL
B. Schatz	KFZ Khe
M.G. Sowerby	AERE Harwell UK
R.R. Spencer	KFZ Khe
J.S. Story	AEE Winfrith UK
H. Penkuhn	CCR Euratom Ispra, Italy